frontiers | Research Topics

Revolutions in human biospecimen study: Leveraging new technologies to explore the pathology, therapeutics and biomarkers for atherosclerotic disease

Edited by
Ying Wang, Michal Mokry and Kathryn L. Howe

Published in
Frontiers in Cardiovascular Medicine

ISSN 1664-8714
ISBN 978-2-8325-3935-4
DOI 10.3389/978-2-8325-3935-4

About Frontiers

Frontiers is more than just an open access publisher of scholarly articles: it is a pioneering approach to the world of academia, radically improving the way scholarly research is managed. The grand vision of Frontiers is a world where all people have an equal opportunity to seek, share and generate knowledge. Frontiers provides immediate and permanent online open access to all its publications, but this alone is not enough to realize our grand goals.

Frontiers journal series

The Frontiers journal series is a multi-tier and interdisciplinary set of open-access, online journals, promising a paradigm shift from the current review, selection and dissemination processes in academic publishing. All Frontiers journals are driven by researchers for researchers; therefore, they constitute a service to the scholarly community. At the same time, the *Frontiers journal series* operates on a revolutionary invention, the tiered publishing system, initially addressing specific communities of scholars, and gradually climbing up to broader public understanding, thus serving the interests of the lay society, too.

Dedication to quality

Each Frontiers article is a landmark of the highest quality, thanks to genuinely collaborative interactions between authors and review editors, who include some of the world's best academicians. Research must be certified by peers before entering a stream of knowledge that may eventually reach the public - and shape society; therefore, Frontiers only applies the most rigorous and unbiased reviews. Frontiers revolutionizes research publishing by freely delivering the most outstanding research, evaluated with no bias from both the academic and social point of view. By applying the most advanced information technologies, Frontiers is catapulting scholarly publishing into a new generation.

What are Frontiers Research Topics?

Frontiers Research Topics are very popular trademarks of the *Frontiers journals series*: they are collections of at least ten articles, all centered on a particular subject. With their unique mix of varied contributions from Original Research to Review Articles, Frontiers Research Topics unify the most influential researchers, the latest key findings and historical advances in a hot research area.

Find out more on how to host your own Frontiers Research Topic or contribute to one as an author by contacting the Frontiers editorial office: frontiersin.org/about/contact

Revolutions in human biospecimen study: Leveraging new technologies to explore the pathology, therapeutics and biomarkers for atherosclerotic disease

Topic editors

Ying Wang — University of British Columbia, Canada

Michal Mokry — University Medical Center Utrecht, Netherlands

Kathryn L. Howe — University of Toronto, Canada

Citation

Wang, Y., Mokry, M., Howe, K. L., eds. (2023). *Revolutions in human biospecimen study: Leveraging new technologies to explore the pathology, therapeutics and biomarkers for atherosclerotic disease*. Lausanne: Frontiers Media SA.

doi: 10.3389/978-2-8325-3935-4

Table of contents

frontiers in Cardiovascular Medicine

ORIGINAL RESEARCH
published: 17 March 2022
doi: 10.3389/fcvm.2022.843426

Identification of Potential Diagnostic Biomarkers From Circulating Cells During the Course of Sleep Deprivation-Related Myocardial Infarction Based on Bioinformatics Analyses

Xiang Chen[1,2], *Qian Li*[1], *Zhong Zhang*[1], *Minjing Yang*[1] *and E. Wang*[1,2]*

[1] *Department of Anesthesiology, Xiangya Hospital Central South University, Changsha, China,* [2] *National Clinical Research Center for Geriatric Disorders (Xiangya Hospital), Xiangya Hospital Central South University, Changsha, China*

OPEN ACCESS

Edited by:
Michal Mokry,
University Medical Center Utrecht, Netherlands

Reviewed by:
Dao Wen Wang,
Huazhong University of Science and Technology, China
Ender Coskunpinar,
University of Health Sciences, Turkey

***Correspondence:**
E. Wang
ewang324@csu.edu.cn

Specialty section:
This article was submitted to Atherosclerosis and Vascular Medicine, a section of the journal Frontiers in Cardiovascular Medicine

Received: *25 December 2021*
Accepted: *22 February 2022*
Published: *17 March 2022*

Citation:
Chen X, Li Q, Zhang Z, Yang M and Wang E (2022) Identification of Potential Diagnostic Biomarkers From Circulating Cells During the Course of Sleep Deprivation-Related Myocardial Infarction Based on Bioinformatics Analyses. Front. Cardiovasc. Med. 9:843426. doi: 10.3389/fcvm.2022.843426

Background: Myocardial infarction (MI) is the leading cause of death from non-infectious diseases worldwide and results in rapid deterioration due to the sudden rupture of plaques associated with atherosclerosis, a chronic inflammatory disease. Sleep is a key factor that regulates immune homeostasis of the body. The imbalance in circulating immune cells caused by sleep deprivation (SD) may represent a risk factor leading to the rapid deterioration of plaques and MI. Therefore, it is of profound significance to identify diagnostic biomarkers for preventing SD-related MI.

Methods: In the present study, we identified coexpressed differentially expressed genes (co-DEGs) between peripheral blood mononuclear cells from MI and SD samples (compared to controls) from a public database. LASSO regression analysis was applied to identify significant diagnostic biomarkers from co-DEGs. Moreover, receiver operating characteristic (ROC) curve analysis was performed to test biomarker accuracy and diagnostic ability. We further analyzed immune cell enrichment in MI and SD samples using the CIBERSORT algorithm, and the correlation between biomarkers and immune cell composition was assessed. We also investigated whether diagnostic biomarkers are involved in immune cell signaling pathways in SD-related MI processes.

Results: A total of 10 downregulated co-DEGs from the sets of MI-DEGs and SD-DEGs were overlapped. After applying LASSO regression analysis, SYTL2, KLRD1, and C12orf75 were selected and validated as diagnostic biomarkers using ROC analysis. Next, we found that resting NK cells were downregulated in both the MI samples and SD samples, which is similar to the changes noted for SYTL2. Importantly, SYTL2 was strongly positively correlated not only with resting NK cells but also with most genes related to NK cell markers in the MI and SD datasets. Moreover, SYTL2 was highly associated with genes in NK cell signaling pathways, including the MAPK signaling pathway, cytotoxic granule movement and exocytosis, and NK cell activation. Furthermore, GSEA and KEGG analyses provided evidence that the DEGs identified from

MI samples with low vs. high SYTL2 expression exhibited a strong association with the regulation of the immune response and NK cell-mediated cytotoxicity.

Conclusion: In conclusion, SYTL2, KLRD1, and C12orf75 represent potential diagnostic biomarkers of MI. The association between SYTL2 and resting NK cells may be critically involved in SD-related MI development and occurrence.

Keywords: myocardial infarction, sleep deprivation, diagnostic biomarker, immune cells, bioinformatic analysis

INTRODUCTION

Myocardial infarction (MI) has become one of the major causes of death and disability worldwide (1, 2). MI mainly occurs in patients with coronary artery disease (CAD), especially coronary atherosclerosis, who experience unstable periods with activated inflammation in the vascular wall (2, 3). Although the exact cause of MI remains unknown, traditional risk factors, including hypertension, smoking, diabetes, obesity and unhealthy diet, might greatly increase the incidence of MI. In addition, up to 5% of elderly people (>75 years old) develop silent MI with no history of established heart disease (4). Once MI occurs, heart failure, heart attack, and cardiac arrest might follow if not treated in a timely and effective manner, ultimately leading to death. Many epidemiological studies and randomized controlled clinical trials have suggested that promoting a healthy lifestyle and diet can help manage hypertriglyceridemia for the prevention of atherosclerotic cardiovascular disease and MI (5, 6).

A short duration of sleep and sleep deprivation (SD) show secular trends alongside changes in modern society that require longer hours of work, which has been considered a global health epidemic (7, 8). Studies from many countries have indicated that SD is correlated with overall health and mortality as well as specific cardiovascular and/or metabolic disorders (9). In a prospective observational study including 461,347 participants free of relevant cardiovascular disease, the researchers found that cases with habitual self-reported short (<6 h) sleep duration had a 20% increased multivariable-adjusted risk of incident for MI compared to cases who sleep 6–9 h/night (7). Healthy sleep duration mitigated MI risk even among individuals at high genetic risk (7). SD contributes to a greater risk of MI, which might result in metabolic and endocrine dysfunction, an imbalanced immune system, and endothelial dysfunction caused by the lack of sleep (10–13). Given the global burden of MI, it is vital to identify novel molecular biomarkers involved in the mechanism of SD-related MI for early detection and continuous monitoring to guide health care professionals, which might help to ensure formulation of the correct therapeutic regimen.

With the remarkable evolution of bioinformatics, microarray gene expression data can be used to identify hub genes and differentially involved signaling pathways in the course of MI, which promotes a comprehensive perspective on key cellular and molecular mechanisms. Research based on bioinformatics methods found that IL1R2, IRAK3, and THBD expression levels were notably higher in peripheral blood mononuclear cells (PBMCs) of patients with acute MI (AMI) and were identified as diagnostic markers of AMI (14). These genes were also significantly associated with various subtypes of immune cells within the AMI samples (14). The occurrence of MI is accompanied by composition changes in T cells and natural killer cells (NK cells) as well as monocyte and macrophage infiltration (15). Of note, long-term SD leads to elevated markers of inflammatory activity and an abnormal number of immune cells, which are in the same range as that observed in individuals at risk for developing cardiovascular disease in the future (16). For the mentioned reasons, evaluating and ascertaining the distinctions within the proportion of immune cells are important in clarifying the potential mechanisms of SD-related MI.

The present study obtained PBMC whole-genome microarray datasets from a public database to identify co-expressed differentially expressed genes (co-DEGs) within SD and MI samples. Then, least absolute shrinkage and selection operator (LASSO) regression analysis was applied to screen and identify diagnostic biomarkers of MI based on the co-DEGs. Next, the correlation between diagnostic markers and the composition of immune cells was analyzed using CIBERSORT algorithms. Gene set enrichment analysis (GSEA) and Kyoto Encyclopedia of Genes and Genomes (KEGG) analysis were performed to increase our understanding of the underlying immune mechanisms involved in the development of MI.

METHODS

Microarray Data

Two peripheral-blood whole-genome microarray datasets related to MI, GSE59867 and GSE62646, were selected and obtained from the Gene Expression Omnibus (GEO) database (https://www.ncbi.nlm.nih.gov/GEO/). Both datasets were based on the GPL6244 platform of Affymetrix Human Gene 1.0 ST Array. The GSE59867 dataset contains data from PBMC samples from patients ($n = 111$) with ST-segment elevation myocardial infarction (STEMI) and stable CAD patients ($n = 46$) without a history of MI. The expression profiles of 28 patients with STEMI and 14 stable CAD patients without a history of MI were included in the GSE62646 dataset. These two datasets were combined by batch correction with the "combat" function of the "sva" package of R using empirical Bayes frameworks (17), and then used to identify the co-DEGs of MI. The GSE48060 dataset was obtained from the PBMC samples of 31 patients with MI and 21 controls based on the GPL570 platform of Affymetrix Human Genome U133 Plus 2.0 Array and were downloaded as a validation dataset for the co-DEGs of MI. To identify the DEGs of SD, the GSE37667 dataset based on the GPL570 platform of Affymetrix Human Genome U133 Plus 2.0 Array was

downloaded. PBMC gene expression profiles of nine healthy male volunteers at baseline at night and after 60 h of prolonged SD were collected.

Gene symbols were transformed from the probes in each dataset based on their probe annotation files. The final expression value of the gene corresponding to multiple probes was obtained by calculating the average expression value. Then, we applied background correction and quartile normalization for all gene expression values to obtain normally distributed expression values using the "limma" package in R.

Screening of DEGs

DEGs between MI and CAD samples as well as SD and control samples were identified using Wilcoxon test *via* the "limma" package in R. Because alterations of RNA expression levels in PBMCs are generally lower than that in other human tissues (18), we set the fold change (FC) > 1.3 and original $P < 0.05$ as significance cut-offs to screen the DEGs based on the recommended methods from studies that designed and uploaded the GSE59867 and GSE62646 datasets (19–21). Volcano plots were used to visualize the distribution of the DEGs. Co-DEGs between MI-DEGs (GSE59867 and GSE62646 datasets) and SD-DEGs (GSE37667 dataset) were identified as the genes overlapping in these three gene sets and were visualized using a Venn diagram.

Identification of Diagnostic Biomarkers

To identify significant diagnostic biomarkers for the discrimination of MI and CAD cases, we performed LASSO regression analysis using the "glmnet" package in R. As a type of shrinkage method for linear regression models, LASSO regression analysis identifies the subset of predictors from the best fitting model by k-fold cross validation, which effectively reduces the prediction error. With a constraint imposed on the model parameters, the shrinkage process is conducted to shrink the regression coefficients of some variables toward zero. Variables with a regression coefficient unequal to zero are included in the final model. Thus, the risk score of each case was calculated using the following formula: Risk score $= \Sigma$expgenei* βi, where expgenei represents the gene expression value, and βi represents the regression coefficient of gene i extracted from the LASSO regression analysis for the GSE59867 dataset.

Evaluation of Diagnostic Value of MI Biomarkers

To evaluate the accuracy and diagnostic ability of the biomarkers and risk score, receiver operating characteristic (ROC) curve analysis was applied for the GSE59867 dataset using the "pROC" package in R. In addition, we also used the GSE62646 and GSE48060 datasets as external validation datasets to verify the diagnostic value of the identified biomarkers. The area under the curve (AUC) of the ROC curve was calculated with sensitivity and specificity values and visualized using the "pROC" package in R.

Discovery of Immune Cell Subtypes

To quantify the relative population-specific immune cell enrichment for each sample, the CIBERSORT algorithm was performed with 1,000 permutations to calculate the normalized enrichment scores of 22 types of immune cells using the "cibersort" package in R (22). The CIBERSORT algorithm improves deconvolution performance to obtain normalized enrichment scores based on support vector regression, which is a machine learning approach. The CIBERSORT gene signature matrix, termed LM22, contains 547 genes and distinguishes 22 types of immune cell subtypes. Therefore, the enrichment scores can be inferred from the eigenmatrix, such as LM22, and gene expression in each sample within a given dataset. In addition, we further classified the 22 immune cell types into 4 aggregated immune cell types, including total lymphocytes, total dendritic cells (sum of activated and resting dendritic cell percentages), total macrophages (sum of M0, M1, and M2 macrophage percentages) and total mast cells (sum of activated and resting mast cell percentages) (23). We used the two-sided Wilcoxon test to compare differences in the composition of 22 immune cell subtypes between two groups (MI vs. CAD, SD vs. control) and visualized the results with violin plots using the "vioplot" package in R. Correlation analysis of 22 immune cell subtypes was visualized using the "corrplot" package.

Correlation Analysis Between Diagnostic Biomarkers and Immune Cell Subtypes

The correlation of the diagnostic biomarkers with the differentially distributed immune cell subtypes was analyzed among the GSE59867, GSE62646, and GSE37667 datasets. To further explore the correlation with specific immune cell markers, we downloaded gene sets related to specific human immune cell markers from the CellMarker database (http://biocc.hrbmu.edu.cn/CellMarker/) and performed Pearson correlation analysis between diagnostic biomarkers and each gene for immune cell markers.

Functional Enrichment Analysis of DEGs

To explore potential biological functions and significant signaling pathways of DEGs associated with the diagnostic biomarker, we performed Gene Ontology (GO) and KEGG pathway enrichment analyses (24) based on the DAVID tools (http://david.ncifcrf.gov/) and visualized the results using the "clusterProfiler" package in R. The strict cut-off of a false discovery rate (FDR) < 0.05 and adjusted P-value < 0.05 was used to identify statistically significant GO terms. In addition, GSEA was also conducted to explore the functional terms correlated to diagnostic biomarkers based on an NOM P-value < 0.05 and NES > 1.

Statistical Analysis

All statistical analyses were conducted using R software (Version 4.0.2; R Foundation for Statistical Computing, Vienna, Austria). Two groups of boxplots for continuous variables were analyzed using the Wilcoxon test. ROC curve analysis was conducted to evaluate the diagnostic efficacy of diagnostic biomarkers for MI. All statistical tests were two-sided, and a P-value < 0.05 was considered statistically significant.

RESULTS

Identification of DEGs

The overall data processing workflow is presented in **Figure 1**. For DEGs between the MI and CAD samples, 491 DEGs were screened from the GSE59867 dataset, including 282 downregulated and 209 upregulated genes (**Figure 2A** and **Supplementary Table 1**). A total of 1,108 DEGs were identified from the GSE62646 dataset, including 593 downregulated and 515 upregulated genes (**Figure 2B** and **Supplementary Table 1**). In addition, a total of 102 DEGs between the SD and control samples were obtained from the GSE37667 dataset, including 68 downregulated genes and 34 upregulated genes (**Figure 2C** and **Supplementary Table 1**). Volcano plots were used to visualize the distribution of the DEGs (**Figure 2**). Hierarchical clustering analysis demonstrated differences in the expression patterns of the top 20 MI-DEGs and SD-DEGs between the two groups (**Figure 2**).

Identification of Diagnostic Biomarkers

We integrated the two sets of MI-DEGs and one set of SD-DEGs using a Venn diagram, as shown in **Figure 3A**. A total of 10 genes overlapping among the three datasets were identified as co-DEGs, all of which were downregulated in both the MI-DEGs and SD-DEGs. Next, we performed LASSO regression analysis to identify the diagnostic biomarkers for MI in the GSE59867 dataset (**Figures 3B,C**). After running cross-validation likelihood 1,000 times, a subset of three biomarkers from the co-DEGs was determined: Synaptotagmin Like 2 (SYTL2), Killer Cell Lectin Like Receptor D1 (KLRD1), and Chromosome 12 Open Reading Frame 75 (C12orf75). To validate the different expression levels of the three diagnostic biomarkers between MI and CAD samples, we analyzed the different expression levels of the three diagnostic biomarkers between MI and CAD PBMC samples in the three datasets and found that the expression levels of all of these genes were notably lower in MI samples compared with CAD samples (all $P < 0.05$) (**Figure 3D**).

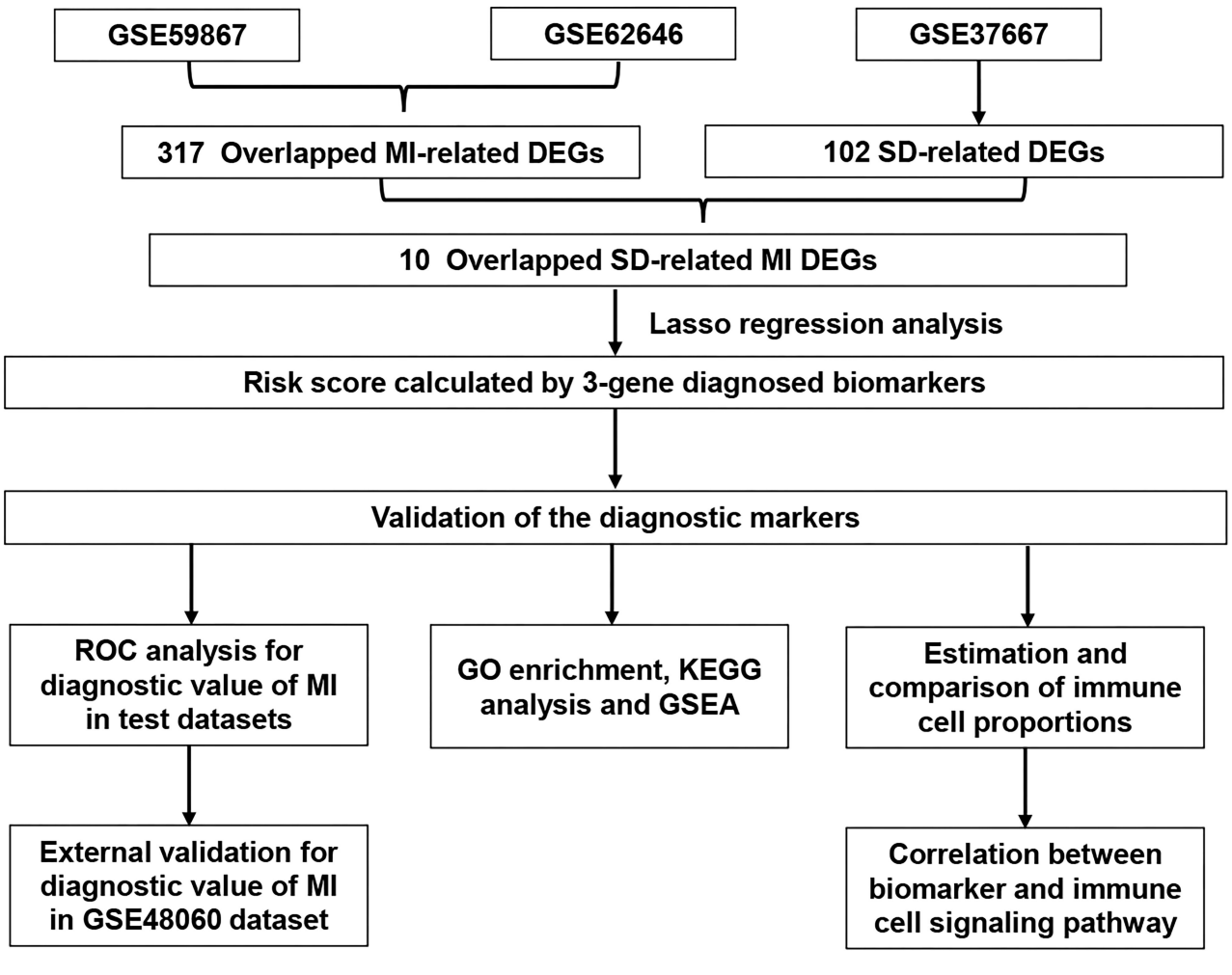

FIGURE 1 | Flowchart describing the process used to identify and validate the diagnostic biomarkers of myocardial infarction. DEGs, differentially expressed genes; MI, myocardial infarction; SD, sleep deprivation; ROC, receiver operating characteristic.

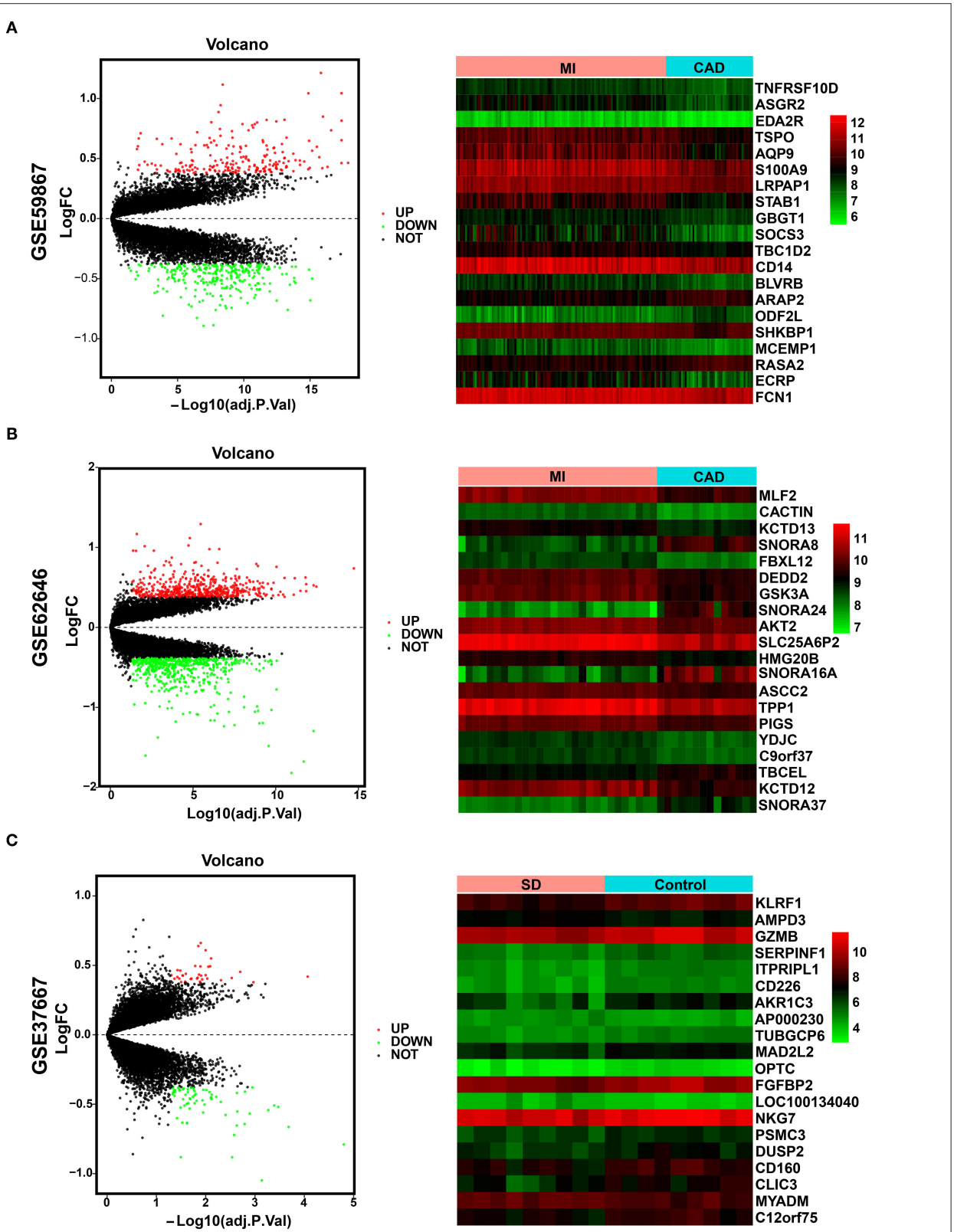

FIGURE 2 | Identification of MI-DEGs and SD-DEGs. **(A)** Volcano plot (left) and heatmap (right) of the GSE59867 dataset. In total, 491 MI-DEGs were identified from the GSE59867 dataset between the MI and CAD PBMC samples, including 282 downregulated and 209 upregulated genes. **(B)** Volcano plot (left) and heatmap (right)

(Continued)

FIGURE 2 | of the GSE62646 dataset. In total, 1,108 MI-DEGs were identified from the GSE62646 dataset between the MI and CAD PBMC samples, including 593 downregulated and 515 upregulated genes. **(C)** Volcano plot (left) and heatmap (right) of the GSE37667 dataset. In total, 102 SD-DEGs were identified from the GSE37667 dataset between the SD and control PBMC samples, including 68 downregulated and 34 upregulated genes. DEGs, differentially expressed genes; MI, myocardial infarction; SD, sleep deprivation; CAD, coronary artery disease; PBMCs, peripheral blood mononuclear cells.

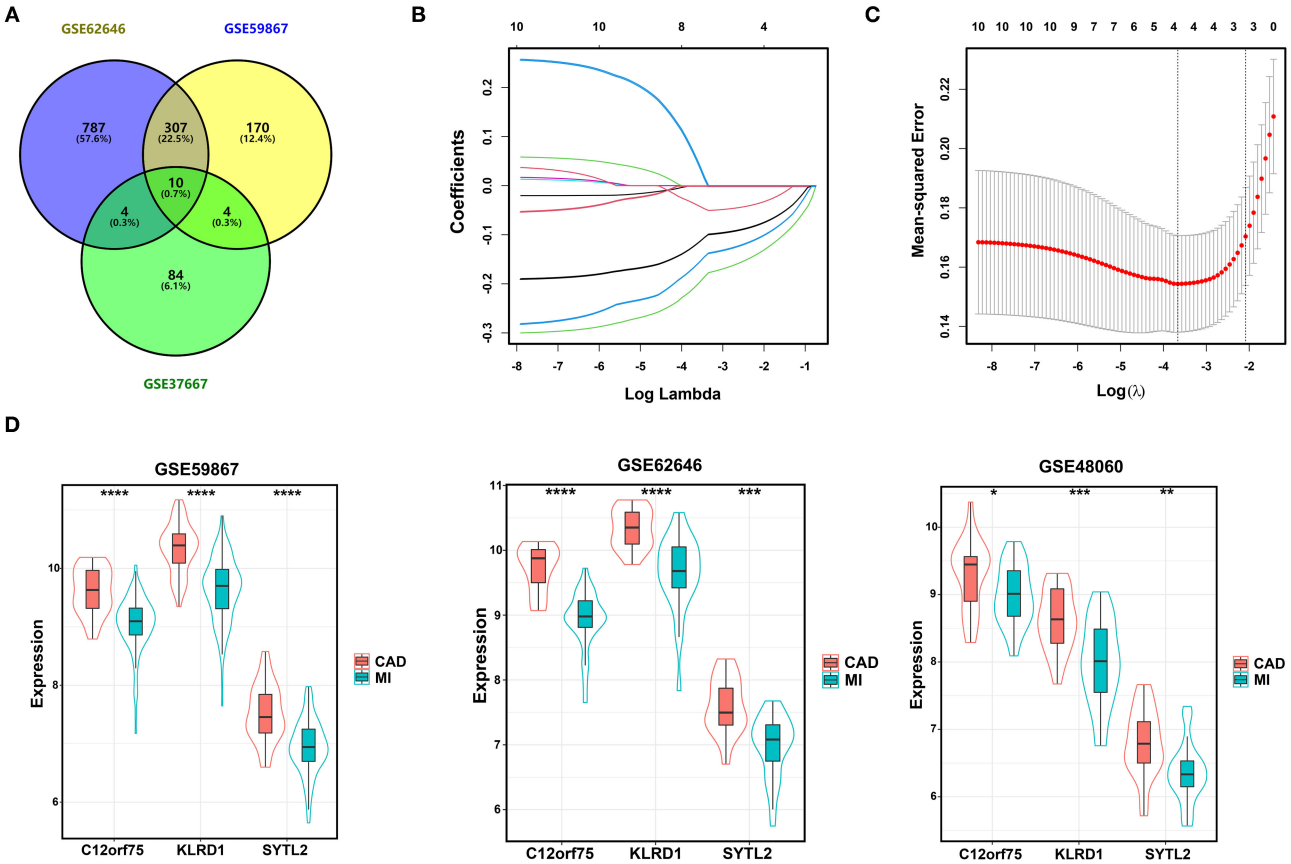

FIGURE 3 | Identification of diagnostic biomarkers for SD-related MI. **(A)** Venn diagram of two sets of MI-DEGs and a set of SD-DEGs. **(B,C)** LASSO coefficient profiles and LASSO deviance profiles. **(D)** The expression levels of three biomarkers identified by LASSO regression analysis between MI and CAD samples in the GSE59867, GSE62646, and GSE48060 datasets. *$P < 0.05$; **$P < 0.01$; ***$P < 0.001$; ****$P < 0.0001$. MI, myocardial infarction; SD, sleep deprivation; CAD, coronary artery disease.

Validation of Diagnostic Biomarkers

After constructing the model using LASSO regression analysis, the risk score was calculated for each sample based on the corresponding coefficients and expression value of genes as follows: Risk score = [(-0.02072662) × Expression value of SYTL2] + [(-0.13152628) × Expression value of KLRD1] + [(-0.06924624) × Expression value of C12orf75]. As shown in **Figure 4A** and **Supplementary Figure 1**, ROC analysis demonstrated favorable diagnostic efficacy of the above three biomarkers in discriminating MI from CAD samples with an AUC of 0.807 (95% CI 0.732–0.883) for SYTL2, 0.843 (95% CI 0.776–0.909) for KLRD1, and 0.829 (95% CI 0.758–0.901) for C12orf75. For the risk score, the diagnostic ability in terms of AUC was 0.862 (95% CI 0.800–0.924). The risk score also showed a high discrimination ability in the GSE62646 dataset with an AUC of 0.936 (95% CI 0.869–1.000). To externally validate the diagnostic value of the three identified biomarkers, the GSE48060 dataset was also used, and the results indicated a powerful diagnostic ability for the feature biomarkers (AUC 0.782, 95% CI 0.657–0.907). Unsupervised hierarchical clustering of three biomarkers showed different gene expression between MI and CAD samples with high sensitivity and specificity (**Figure 4B**).

Enrichment of Immune Cells in the MI and CAD Samples

To better understand the difference in the enrichment degree of immune cell subtypes between the MI and CAD groups, 22 available immune cell subtypes, including the major cell types related to adaptive immunity [i.e., naïve B cells, memory B cells, naïve CD4 T cells, resting memory CD4 T cells, activated memory CD4 T cells, CD8 T cells, gamma delta T (Tgd) cells, T follicular helper (Tfh) cells, and regulatory T (Treg) cells]

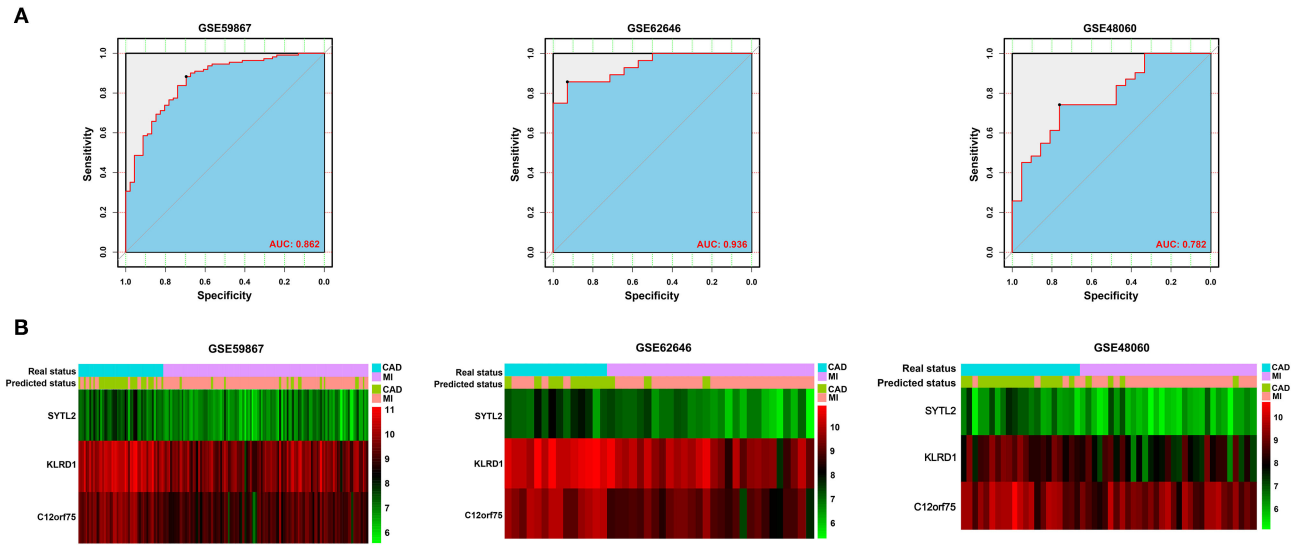

FIGURE 4 | Validation of diagnostic biomarkers for SD-related MI. **(A)** ROC analysis revealed good diagnostic performance of the risk score associated with MI among the three datasets. **(B)** Unsupervised hierarchical clustering of risk scores in the diagnostic prediction model among the three MI-related datasets.

and innate immunity [i.e., activated dendritic cells (DCs), resting DCs, eosinophils, activated mast cells, macrophages (M0–M2), resting mast cells, monocytes, resting NK cells, activated natural killer (NK) cells, neutrophils, and plasma cells], were assessed using CIBERSORT. GSE59867 dataset results showed that five types of immune cells were significantly enriched in a higher proportion in the CAD group, and four types of immune cells were significantly increased in the MI samples (all $P < 0.05$) (**Figure 5A**). After clustering the 22 immune cell types into four aggregated immune cell types, the total lymphocytes and total macrophages were significantly enriched in the CAD samples, whereas mast cells were enriched in the MI group (all $P < 0.05$) (**Figure 5B**). The GSE62646 dataset was used to validate the distribution of immune cells. The proportions of three immune cell subtypes, including resting memory CD4 T cells, resting NK cells, and M2 macrophages, were significantly lower in MI samples compared with CAD samples (all $P < 0.05$) (**Figure 5D**). These results are consistent with the GSE59867 dataset results. However, only total macrophages were significantly enriched in the CAD groups ($P < 0.05$) (**Figure 5E**). As shown in **Figures 5C,F**, the interrelation among the various immune cell subtypes in the GSE59867 and GSE62646 datasets varied from weak to moderate.

Immune Cell Infiltration in SD Samples and Control Samples

To verify whether the distribution of immune cells in the SD/control groups was consistent with that in the MI/CAD groups, we also employed the CIBERSORT algorithm on the GSE37667 dataset. The results indicated that the proportion of resting NK cells was significantly lower in the SD group than in the control group ($P < 0.05$) (**Figure 6A**). Although 4 aggregated immune cell types showed insignificant differences between the two groups, resting NK cells were negatively correlated with gamma delta T (Tgd) cells, which were significantly enriched in the SD samples ($P < 0.05$) (**Figures 6B,C**). These results suggested that immune cells, especially resting NK cells, were actively involved in SD-induced disease processes. To further analyse the functional enrichment during the SD process, GO enrichment analysis was performed with SD-DEGs using the online DAVID tool. As shown in **Figure 6D**, the SD-DEGs were significantly enriched in the following biological processes: regulation of immune response and negative regulation of apoptotic processes (all $P < 0.05$).

Correlation of Diagnostic Biomarkers and Immune Cell Types

Combined with the above results, the expression levels of three diagnostic biomarkers were downregulated in both the SD and MI samples, and resting NK cells were not enriched in either the SD or MI groups among the three datasets. Next, we conducted correlation analyses in two MI-related datasets and an SD-related dataset to explore the relationship between the diagnostic biomarkers and immune cell types. As shown in **Figures 7A–C**, SYTL2 showed a significantly strong positive correlation with resting NK cells in the MI-related datasets as well as the SD dataset, which is consistent with the changes induced by MI or SD mentioned above (all $P < 0.05$). However, these trends were not reflected in KLRD1 and C12orf75 (**Supplementary Figure 2**). Moreover, we downloaded gene sets related to NK cell markers from CellMarker and performed Pearson correlation analysis between SYTL2 and gene sets in three datasets (**Figure 7D**). The results indicated that SYTL2 was also strongly positively correlated

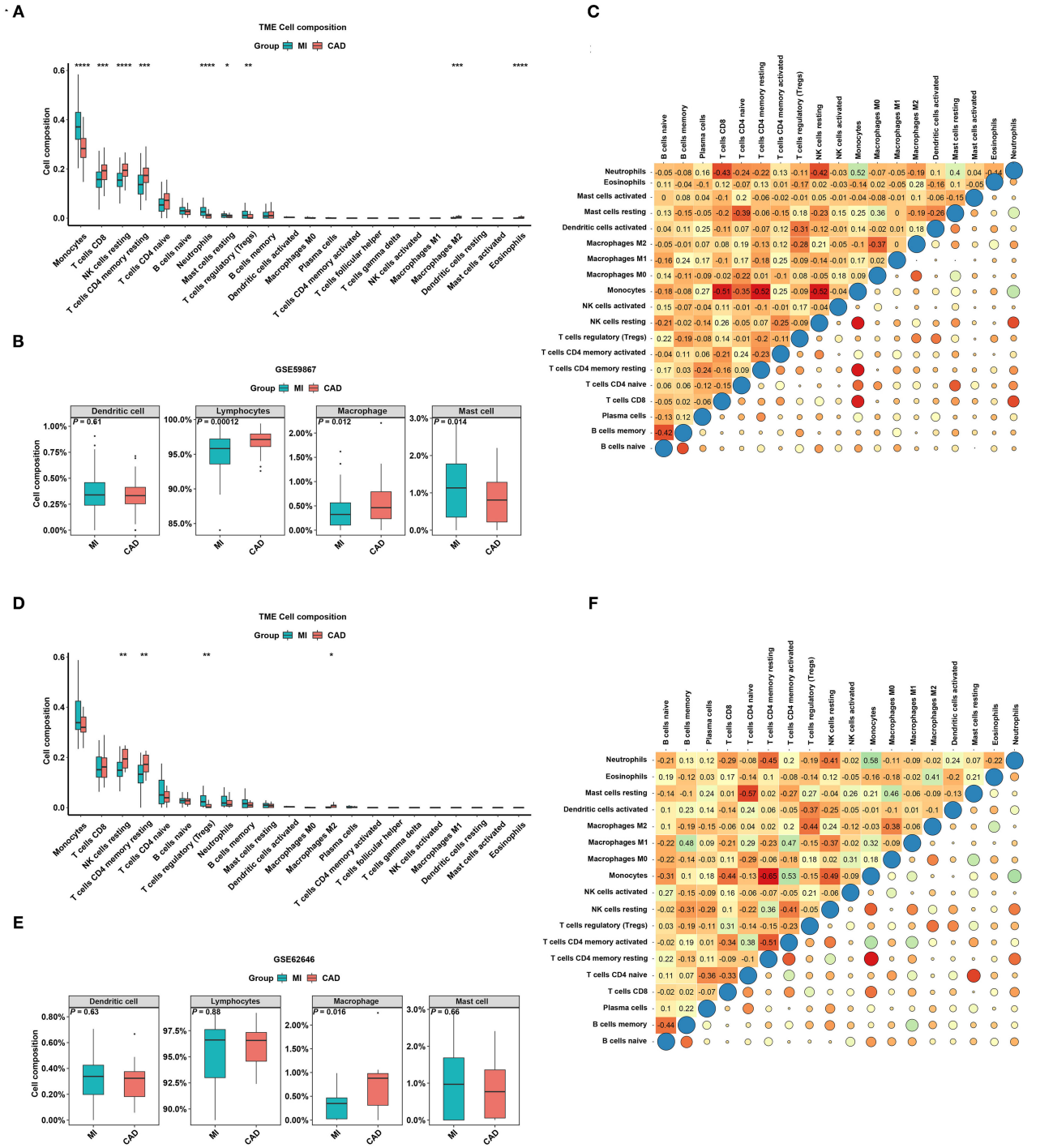

FIGURE 5 | The distribution of 22 types of immune cells between the MI and CAD samples. **(A,D)** Violin plots of 22 types of immune cells that are differentially enriched in the **(A)** GSE59867 dataset and **(D)** GSE62646 dataset. **(B,E)** Violin plot of four aggregated immune cell types that are differentially enriched in the **(B)** GSE59867 dataset and **(E)** GSE62646 dataset. **(C,F)** Heatmap of correlations for 22 types of immune cells in the **(C)** GSE59867 dataset and **(F)** GSE62646 dataset. The size of the colored squares represents the strength of the correlation. Darker color implies stronger association. $^{*}P < 0.05$; $^{**}P < 0.01$; $^{***}P < 0.001$; $^{****}P < 0.0001$.

with most genes related to NK cell markers (all $P < 0.05$). These results indicate that SYTL2 plays an important role in regulating NK cell activation during the process of SD-induced MI.

Involvement of SYTL2 in the NK Cell Signaling Pathway

NK cell signaling pathways are of great importance for NK cell activation and are currently the target of several

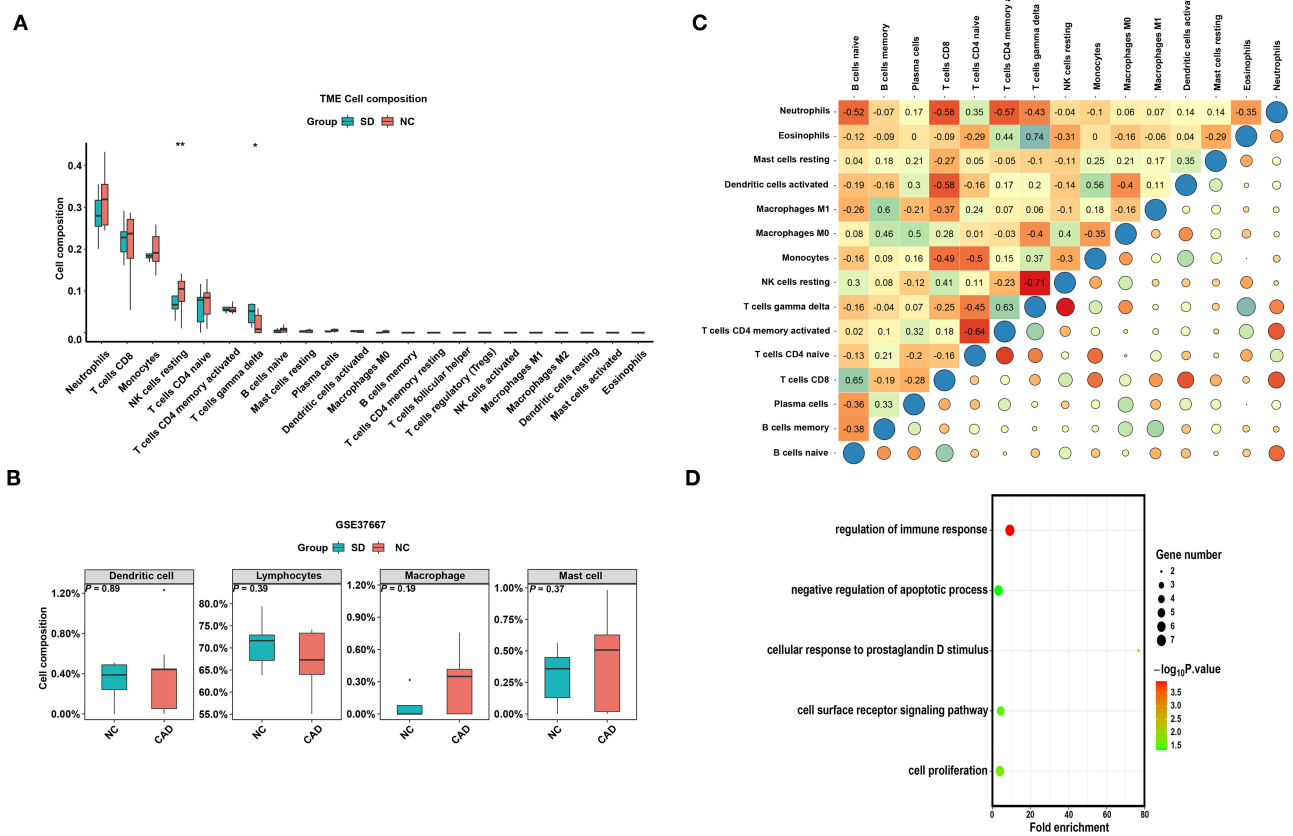

FIGURE 6 | The distribution of 22 types of immune cells between the SD and control samples. **(A)** Violin plot of 22 types of immune cells differentially enriched between the SD and negative control (NC) samples in the GSE37667 dataset. **(B)** Violin plot of four aggregated immune cell types differentially enriched in the GSE37667 dataset. **(C)** Heatmap of correlation of 22 types of immune cells in the GSE37667 dataset. The size of the colored squares represents the strength of the correlation. Darker color implies stronger association. **(D)** Biological process of SD-DEGs from the GSE37667 dataset. *$P < 0.05$; **$P < 0.01$.

therapeutic strategies (25, 26). NK cells express many receptors that activate their cytotoxic and secretory functions, which contribute to immune defense (27). Therefore, we investigated the correlation of SYTL2 with the genes in the NK cell signaling pathway that were obtained from the KEGG database (**Supplementary Table 2**). As shown in **Figure 8**, SYTL2 was highly associated with the genes in the MAPK signaling pathway (PIK3R3, PIK3CD, SHC1, PAK1, NRAS, and HRAS, all *P*-values < 0.05), cytotoxic granule movement and exocytosis (PRF1 and FASLG, all *P*-values < 0.05), and NK cell activation (SH2D1B and CD244, all *P*-values < 0.05) and might be partially related to the calcium signaling pathway (PPP3CB, *P*-value < 0.05).

Detection of Biological Function for SYTL2

To explore the biological function of SYTL2 in the MI process, we obtained the DEGs using 111 MI samples from the GSE59867 dataset that were divided into the high-SYTL2 ($n = 55$) and the low-SYTL2 groups ($n = 56$) with the median value as the cut-off. A total of 2 upregulated DEGs and 91 downregulated DEGs were identified with the high-SYTL2 expression sample as a reference (**Figures 9A,B**). Then, GO and KEGG analyses were performed to analyse the DEGs, indicating the potential function of SYTL2. The results also suggested a strong association with NK cell-mediated cytotoxicity and regulation of the immune response (**Figures 9C,D** and **Supplementary Table 3**). Moreover, GSEA was performed between low- and high-SYTL2 expression samples in the GSE59867 dataset. Several immune pathways that involve SYTL2 in relation to MI, such as "natural killer cell mediated immunity," "positive regulation of natural killer cell mediated cytotoxicity," and "regulation of natural killer cell mediated immunity," were identified (**Supplementary Table 4**).

DISCUSSION

MI is an extremely dangerous cardiovascular disease that causes rapid deterioration due to the sudden rupture of plaques associated with the chronic inflammatory disease called atherosclerosis. Sleep is a key factor in regulating immune homeostasis of the body. The imbalance of circulating immune cells caused by sleep deprivation may represent a risk factor leading to the rapid deterioration of plaques. Therefore, it is vital

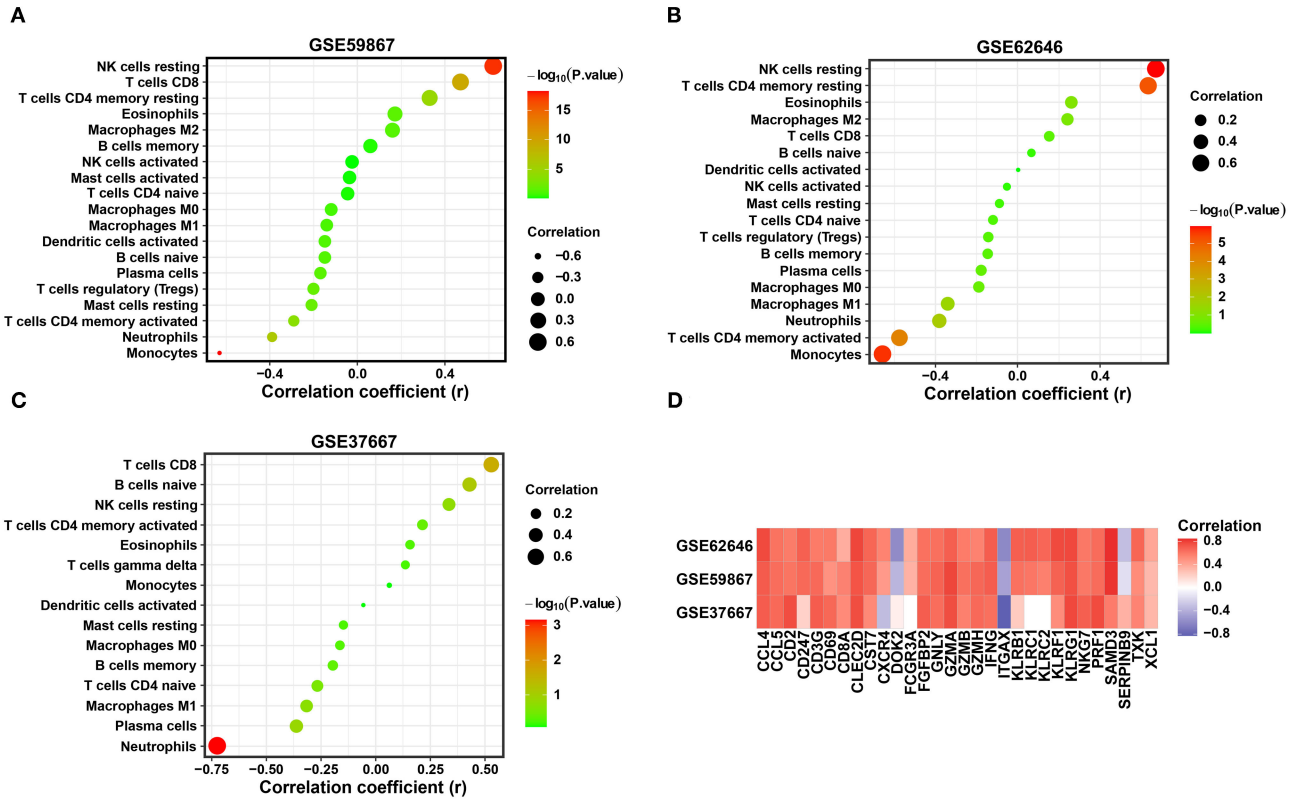

FIGURE 7 | Correlation between the expression level of SYTL2 and enriched immune cells. **(A)** Correlation between the expression level of SYTL2 and enriched immune cells in the GSE59867 dataset. **(B)** Correlation between the expression level of SYTL2 and enriched immune cells in the GSE62646 dataset. **(C)** Correlation between the expression level of SYTL2 and enriched immune cells in the GSE37667 dataset. The size of the dots represents the strength of the correlation between SYTL2 and immune cells; the color of the dots represents the *P*-value; the greener the color, the larger the *P*-value; and the red the color, the lower the *P*-value. $P < 0.05$ was considered statistically significant. **(D)** Heatmap showing the correlation between SYTL2 and the marker genes of NK cells.

to explore diagnostic biomarkers and analyse the association with immune cell enrichment to improve the prognosis of MI.

In the present study, we identified 1,599 DEGs between the MI and CAD PBMC samples based on the GSE59867 and GSE62646 datasets as well as 102 DEGs between SD and control PBMC samples from the GSE37667 dataset. Then, a total of 10 co-DEGs were obtained from the MI-DEGs and SD-DEGs. After applying LASSO regression analysis, SYTL2, KLRD1, and C12orf75 were selected and validated as diagnostic biomarkers using ROC analysis. Next, we found that resting NK cells were downregulated in both the MI samples and SD samples, which is similar to the change noted for SYTL2. Importantly, SYTL2 was strongly positively correlated not only with resting NK cells but also with most genes related to NK cell markers among the MI datasets and SD dataset. Moreover, we performed correlation analysis between SYTL2 and the genes in the NK cell signaling pathway that were obtained from the KEGG database. The results indicated that SYTL2 was highly associated with genes in the MAPK signaling pathway, cytotoxic granule movement and exocytosis, and NK cell activation. Furthermore, GSEA and KEGG analyses suggested a strong association with regulation of the immune response and NK cell-mediated cytotoxicity for the DEGs between low- and high-SYTL2 expression samples in GSE59867, which were classified based on a median cut-off value. All of the above evidence demonstrated that the biological function of SYTL2 might be strongly correlated with the immune response in SD-related MI processes, especially with NK cells.

Biomarkers in the circulation play a key role in risk stratification and therapeutic management of cardiovascular diseases due to the difficulty of obtaining anatomical tissue biopsies (28, 29). A previous study indicated that the expression levels of over 80% of peripheral blood transcriptomes were shared among 9 different human tissue types, suggesting that PBMCs are sensitive to ongoing cardiac dysfunction and respond by altering their transcriptome. However, the reason why tissue-specific upregulated or downregulated gene patterns are synchronized to circulating cells remains unclear (18, 30). In this context, our current study highlights the potential to use mRNA signatures in PBMCs as diagnostic biomarkers of SD-related MI. PBMCs are an innate circulating cell population with inflammatory properties that have significant associations with atherosclerotic plaque formation and MI risk and progression (31–33). A transcriptome study of PBMCs from early onset MI patients indicated that lncRNA-*NEAT1*

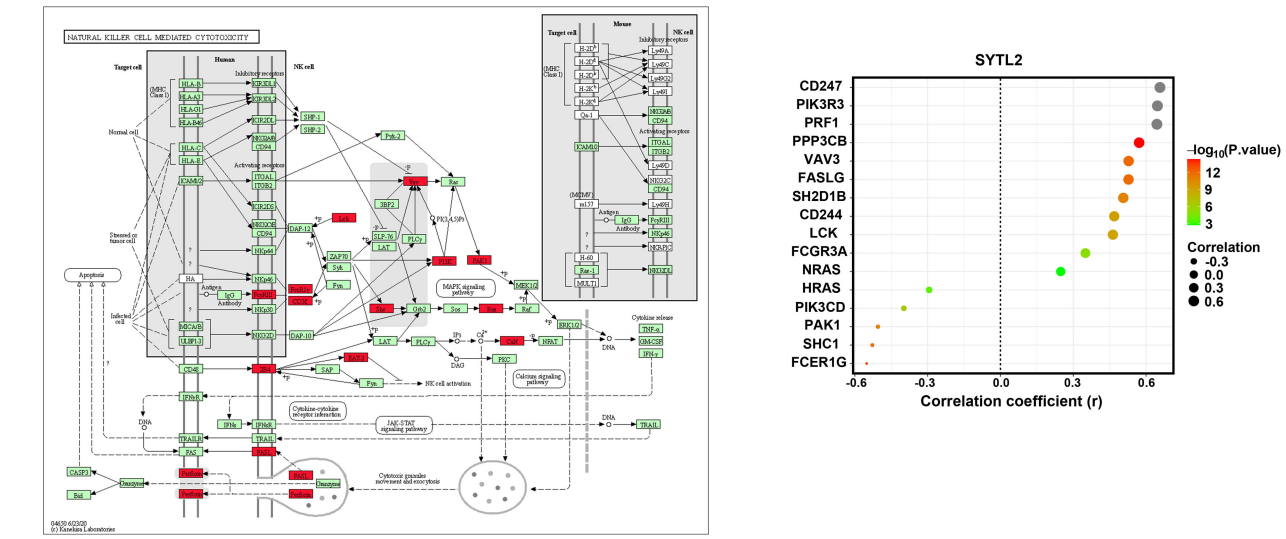

FIGURE 8 | Association between SYTL2 and the NK cell-mediated cytotoxicity signaling pathway. **(A)** Regulation network of the NK cell-mediated cytotoxicity signaling pathway as obtained from the KEGG database. The red square indicates that the gene was significantly correlated with SYTL2 ($P < 0.05$). **(B)** Correlation between the expression level of SYTL2 and the genes in the NK cell-mediated cytotoxicity signaling pathway.

expression levels were significantly downregulated in MI PBMC samples. LncRNA-*NEAT1* was identified as an immunoregulator affecting T cell and monocyte-macrophage lineage differentiation and functions *in vivo*, which may impact the course of diseases (34). ALK4 expression levels in PBMCs of MI patients were significantly higher than that in PBMCs of healthy volunteers, and ALK4 function was associated with cardiac inflammation and vulnerability to ventricular arrhythmia after acute myocardial injury. The establishment of an MI mouse model suggested the potential involvement of macrophage-mediated ALK4 expression in the inflammatory phase of MI (35). Moreover, a bioinformatics study based on the gene expression profiles of PBMCs between AMI samples and controls was performed. IL1R2, IRAK3, and THBD were collectively identified as a diagnostic marker of AMI and showed a close correlation with immune cells, such as M2 macrophages, monocytes, activated NK cells, and gamma delta T cells (14). The present study identified SYTL2, KLRD1, and C12orf75 as diagnostic markers of SD-related MI and demonstrated that immune cells, especially resting NK cells, played important roles in disease progression. Therefore, this gene set represents a promising measurement from a clinical perspective. Specifically, the PBMC expression profile of atherosclerosis patients who undergo SD might have prognostic value regarding the clinical course or response to anti-inflammatory treatment.

The amount of sleep time has drastically decreased in modern society due to changes in lifestyle behavior and the presence of sleep disorders. Several intermediate pathophysiological mechanisms have been reported to be induced by short sleep duration, such as inflammatory responses, atherosclerosis, oxidative stress, and insulin resistance, resulting in the development of cardiovascular and metabolic disorders (36–40). In a large prospective study from London with more than 10,000 participants and a mean follow-up time of 15 years, participants with a short sleep duration showed the highest risk of CAD (MI and angina, relative risk 1.55, 95% CI 1.33–1.81), especially in people with sleep disorders (41). Sleep loss exerts a strong regulatory influence on peripheral levels of inflammatory mediators of the immune response, which contributes to the development of atherosclerosis (42). Inflammatory cytokines, such as IL-1α, IL-1β, IL-6, and TNF-α, exhibit a positive linear association with habitual short sleep duration. C-reactive protein (CRP), which is considered a predictor of cardiovascular events, was also elevated in plasma after partial SD, and the levels remained high even after two nights of sleep recovery (42, 43). As the main source of these cytokines, the expression levels in monocytes are strongly regulated by circadian rhythms (44). Generally, the leukocyte population increases after acute SD. However, the number of circulating NK cells was decreased after SD, which subsequently led to an increase in B and T lymphocytes and total white blood cells (43). A previous study indicated that the number of apoptotic NK cells in peripheral blood was significantly increased in CAD patients compared to healthy patients, and this effect was induced by oxidative stress (45). Our study found that resting NK cells were enriched in neither MI samples nor SD samples. One reasonable hypothesis is that NK cells undergo apoptosis due to oxidative stress induced by SD, which subsequently stimulates the increase in other inflammatory cells and enhances the inflammatory response, finally increasing cardiovascular events.

Three diagnostic biomarkers, including SYTL2, KLRD1, and C12orf75, were identified to be associated with SD-related MI. The synaptotagmin-like protein homology domain (SHD) of SYTL2 specifically binds to the GTP-bound form of Ras-related

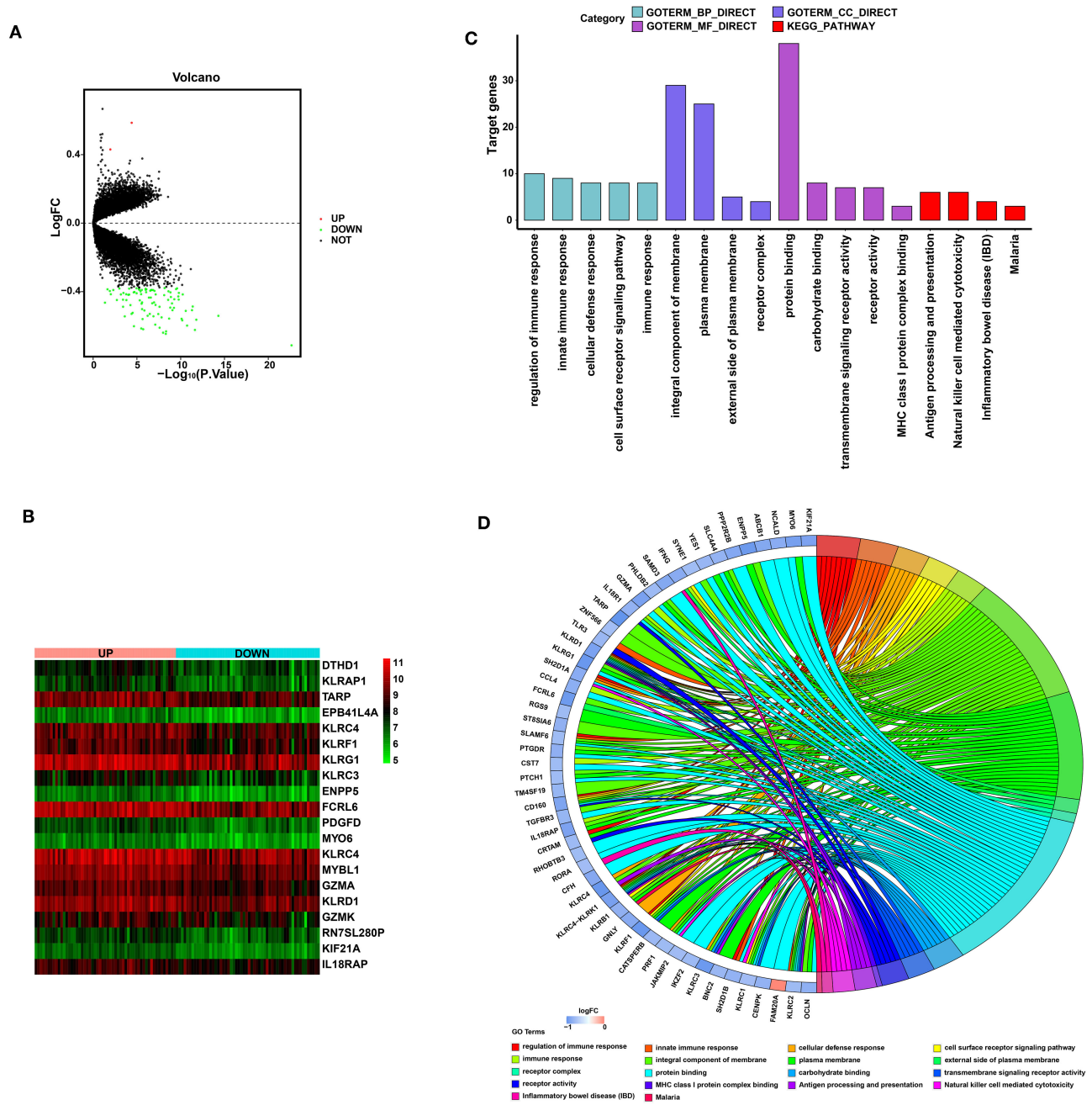

FIGURE 9 | Significant pathways influenced by SYTL2 in the GSE59867 dataset. **(A)** Volcano plot of the GSE59867 dataset. A total of two upregulated DEGs and 91 downregulated DEGs were identified between low- and high-SYTL2 expression samples. **(B)** Heatmap of DEGs between low- and high-SYTL2 expression samples in the GSE59867 dataset. **(C)** DEGs with the top 15 enriched GO terms and KEGG terms. **(D)** Distribution of DEGs for different GO-enriched functions.

protein Rab-27A (RAB27A), which suggests a role of vesicle trafficking and exocytosis in epithelial cells and haematopoietic cells, including neutrophils, cytotoxic T cells, NK cells, and mast cells (46–48). SYTL2 has been reported to control the podocalyxin-rich vesicles tethering and fusion in conjunction with Rab27/Rab3/Rab8 *via* synaptotagmin-like protein 4a (Slp4a) to promote vascular lumen formation (49). SYTL2 is recruited to the apical membrane where it regulates secretion of Weibel-Palade Body components into the luminal space (50). Knockout of SYTL2 blunts the vascular lumen formation during angiogenic development, suggested its potential role in the setting of MI (50). KLRD1, which is also named CD94, is an antigen preferentially expressed on NK cells (51). NK cells are important in the onset of AMI given their ability to secrete IFN-γ and other

inflammatory cytokines (52). However, NK cell activity and quantity were suppressed in MI patients with significant mRNA downregulation of inhibitory and activating NK cell receptors (53, 54). The specific mechanism of these clinical manifestations remains unclear. The present study might provide potential evidence that the downregulated expression levels of SYTL2 and KLRD1 in SD-related MI patients lead to dysfunction of exocytosis in NK cells and suppress NK cell activity, which subsequently contributes to neutrophil and T cell activity and the immune response. This hypothesis also needs to be further validated by *in vivo* and *in vitro* experiments.

It should be noted that cardiac troponin (cTn), including cardiac-specific troponin T (cTnT) and I (cTnI), are now widely used as a gold standard to identify patients with MI (55). Despite the cardiac specificity of troponin, there are other clinical conditions except for MI in which troponin may be elevated, including cardiac and non-cardiac causes (56). Previous studies indicated that high-sensitivity cTnI was elevated in patients with obstructive sleep apnea (OSA), which higher OSA severity was related to higher concentrations of high-sensitivity cTnI (57, 58). However, the presence of OSA may have a protective effect on myocardial ischemic injury in the setting of AMI, which was manifested as lower concentrations of cTnI than patients without OSA (59). These above evidences showed that the use of troponin to diagnose MI caused by sleep disorders is still controversial. Thus, the exploration for other interesting insights of areas like peripheral blood genomics biomarkers might assist troponin in the diagnosis of true MI in patients with sleep disorder.

Several unavoidable limitations in the present study should be acknowledged. First, the sample size of the included study was relatively small, and only 9 individuals were recruited in the GSE37667 dataset for SD. Second, due to the rapid progress of sequencing technology, heterogeneity exists between different batches and experimental platforms. Third, the study was performed based on microarray datasets with two different populations to explore the role of genes from PBMCs in SD-related MI. However, direct evidence, such as clinical studies or *in vivo* experiments, are not available to support the conclusion. It is better to design study as in the previous literature. They collected peripheral blood samples from 302 patients for a case-control study to further confirm the bioinformatics analysis results based on the GSE59867 and GSE62646 datasets that dysregulated circulating hub genes expression were associated with MI development (60). Therefore, experiments using *in vitro* and *in vivo* models as well as prospective clinical studies will be indispensable for validation of the diagnostic and theragnostic value of these biomarkers.

CONCLUSION

In summary, a set of genes from PBMCs, including SYTL2, KLRD1, and C12orf75, were identified as diagnostic biomarkers for SD-related MI. SYTL2 exhibited a strong positive correlation with resting NK cells, which were both downregulated in the MI samples and SD samples and involved in NK cell signaling pathways, including the MAPK signaling pathway, cytotoxic granule movement and exocytosis, and NK cell activation. These diagnostic biomarkers and hypothetical signaling axes may provide prognostic value and therapeutic targets for SD-related MI.

DATA AVAILABILITY STATEMENT

The datasets presented in this study can be found in online repositories. The names of the repository/repositories and accession number(s) can be found in the article/**Supplementary Material**.

AUTHOR CONTRIBUTIONS

EW supervised the project, designed the study, interpreted the data, and wrote and reviewed the manuscript. XC and QL performed data management and analyzed the data. ZZ and MY took part in analyzing the data. XC wrote the first draft of the manuscript. All authors approved the final version of the manuscript.

FUNDING

This study was funded by the National Key Research and Development Program of China (No: 2020YFC2005300).

SUPPLEMENTARY MATERIAL

The Supplementary Material for this article can be found online at: https://www.frontiersin.org/articles/10.3389/fcvm.2022.843426/full#supplementary-material

Supplementary Figure 1 | Validation of diagnostic biomarkers for SD-related MI.

Supplementary Figure 2 | Correlation between the expression level of two diagnostic biomarkers and immune cell enrichment.

REFERENCES

1. Thygesen K, Alpert JS, Jaffe AS, Simoons ML, Chaitman BR, White HD, et al. Third universal definition of myocardial infarction. *Eur Heart J.* (2012) 33:2551–67. doi: 10.1093/eurheartj/ehs184
2. Virani SS, Alonso A, Benjamin EJ, Bittencourt MS, Callaway CW, Carson AP, et al. Heart disease and stroke statistics-2020 update: a report from the american heart association. *Circulation.* (2020) 141:e139–596. doi: 10.1161/CIR.0000000000000757
3. Reed GW, Rossi JE, Cannon CP. Acute myocardial infarction. *Lancet.* (2017) 389:197–210. doi: 10.1016/S0140-6736(16)30677-8
4. Valensi P, Lorgis L, Cottin Y. Prevalence, incidence, predictive factors and prognosis of silent myocardial infarction: a review of the literature. *Arch Cardiovasc Dis.* (2011) 104:178–88. doi: 10.1016/j.acvd.2010.11.013
5. Baigent C, Blackwell L, Emberson J, Holland LE, Reith C, Bhala N, et al. Efficacy and safety of more intensive lowering of LDL cholesterol: a meta-analysis of data from 170,000 participants in 26 randomised trials. *Lancet.* (2010) 376:1670–81. doi: 10.1016/S0140-6736(10)61350-5

6. Brinton EA. Management of hypertriglyceridemia for prevention of atherosclerotic cardiovascular disease. *Cardiol Clin.* (2015) 33:309–23. doi: 10.1016/j.ccl.2015.02.007
7. Daghlas I, Dashti HS, Lane J, Aragam KG, Rutter MK, Saxena R, et al. Sleep duration and myocardial infarction. *J Am Coll Cardiol.* (2019) 74:1304–14. doi: 10.1016/j.jacc.2019.07.022
8. Cappuccio FP, Miller MA. Sleep and cardio-metabolic disease. *Curr Cardiol Rep.* (2017) 19:110. doi: 10.1007/s11886-017-0916-0
9. Altman NG, Izci-Balserak B, Schopfer E, Jackson N, Rattanaumpawan P, Gehrman PR, et al. Sleep duration vs. sleep insufficiency as predictors of cardiometabolic health outcomes. *Sleep Med.* (2012) 13:1261–70. doi: 10.1016/j.sleep.2012.08.005
10. Cappuccio FP, Cooper D, D'Elia L, Strazzullo P, Miller MA. Sleep duration predicts cardiovascular outcomes: a systematic review and meta-analysis of prospective studies. *Eur Heart J.* (2011) 32:1484–92. doi: 10.1093/eurheartj/ehr007
11. Cassidy S, Chau JY, Catt M, Bauman A, Trenell MI. Cross-sectional study of diet, physical activity, television viewing and sleep duration in 233,110 adults from the UK Biobank: the behavioural phenotype of cardiovascular disease and type 2 diabetes. *BMJ Open.* (2016) 6:e10038. doi: 10.1136/bmjopen-2015-010038
12. Itani O, Jike M, Watanabe N, Kaneita Y. Short sleep duration and health outcomes: a systematic review, meta-analysis, and meta-regression. *Sleep Med.* (2017) 32:246–56. doi: 10.1016/j.sleep.2016.08.006
13. Meier-Ewert HK, Ridker PM, Rifai N, Regan MM, Price NJ, Dinges DF, et al. Effect of sleep loss on C-reactive protein, an inflammatory marker of cardiovascular risk. *J Am Coll Cardiol.* (2004) 43:678–83. doi: 10.1016/j.jacc.2003.07.050
14. Zhao E, Xie H, Zhang Y. Predicting diagnostic gene biomarkers associated with immune infiltration in patients with acute myocardial infarction. *Front Cardiovasc Med.* (2020) 7:586871. doi: 10.3389/fcvm.2020.586871
15. Peet C, Ivetic A, Bromage DI, Shah AM. Cardiac monocytes and macrophages after myocardial infarction. *Cardiovasc Res.* (2020) 116:1101–12. doi: 10.1093/cvr/cvz336
16. Besedovsky L, Lange T, Born J. Sleep and immune function. *Pflugers Arch.* (2012) 463:121–37. doi: 10.1007/s00424-011-1044-0
17. Leek JT, Johnson WE, Parker HS, Jaffe AE, Storey JD. The sva package for removing batch effects and other unwanted variation in high-throughput experiments. *Bioinformatics.* (2012) 28:882–3. doi: 10.1093/bioinformatics/bts034
18. Mohr S, Liew CC. The peripheral-blood transcriptome: new insights into disease and risk assessment. *Trends Mol Med.* (2007) 13:422–32. doi: 10.1016/j.molmed.2007.08.003
19. Kiliszek M, Burzynska B, Michalak M, Gora M, Winkler A, Maciejak A, et al. Altered gene expression pattern in peripheral blood mononuclear cells in patients with acute myocardial infarction. *PLoS ONE.* (2012) 7:e50054. doi: 10.1371/journal.pone.0050054
20. Maciejak A, Kiliszek M, Michalak M, Tulacz D, Opolski G, Matlak K, et al. Gene expression profiling reveals potential prognostic biomarkers associated with the progression of heart failure. *Genome Med.* (2015) 7:26. doi: 10.1186/s13073-015-0149-z
21. Pellegrino R, Sunaga DY, Guindalini C, Martins RC, Mazzotti DR, Wei Z, et al. Whole blood genome-wide gene expression profile in males after prolonged wakefulness and sleep recovery. *Physiol Genomics.* (2012) 44:1003–12. doi: 10.1152/physiolgenomics.00058.2012
22. Newman AM, Liu CL, Green MR, Gentles AJ, Feng W, Xu Y, et al. Robust enumeration of cell subsets from tissue expression profiles. *Nat Methods.* (2015) 12:453–7. doi: 10.1038/nmeth.3337
23. Li B, Cui Y, Nambiar DK, Sunwoo JB, Li R. The immune subtypes and landscape of squamous cell carcinoma. *Clin Cancer Res.* (2019) 25:3528–37. doi: 10.1158/1078-0432.CCR-18-4085
24. Kanehisa M, Goto S. KEGG: kyoto encyclopedia of genes and genomes. *Nucleic Acids Res.* (2000) 28:27–30. doi: 10.1093/nar/28.1.27
25. Gotthardt D, Trifinopoulos J, Sexl V, Putz EM. JAK/STAT cytokine signaling at the crossroad of NK cell development and maturation. *Front Immunol.* (2019) 10. doi: 10.3389/fimmu.2019.02590
26. Khan M, Arooj S, Wang H. NK cell-based immune checkpoint inhibition. *Front Immunol.* (2020) 11:167. doi: 10.3389/fimmu.2020.00167
27. Kumar S. Natural killer cell cytotoxicity and its regulation by inhibitory receptors. *Immunology.* (2018) 154:383–93. doi: 10.1111/imm.12921
28. Gupta MK, Halley C, Duan ZH, Lappe J, Viterna J, Jana S, et al. MiRNA-548c: a specific signature in circulating PBMCs from dilated cardiomyopathy patients. *J Mol Cell Cardiol.* (2013) 62:131–41. doi: 10.1016/j.yjmcc.2013.05.011
29. Manzano-Fernandez S, Boronat-Garcia M, Albaladejo-Oton MD, Pastor P, Garrido IP, Pastor-Perez FJ, et al. Complementary prognostic value of cystatin C, N-terminal pro-B-type natriuretic Peptide and cardiac troponin T in patients with acute heart failure. *Am J Cardiol.* (2009) 103:1753–9. doi: 10.1016/j.amjcard.2009.02.029
30. Liew CC, Ma J, Tang HC, Zheng R, Dempsey AA. The peripheral blood transcriptome dynamically reflects system wide biology: a potential diagnostic tool. *J Lab Clin Med.* (2006) 147:126–32. doi: 10.1016/j.lab.2005.10.005
31. Lassale C, Curtis A, Abete I, van der Schouw YT, Verschuren W, Lu Y, et al. Elements of the complete blood count associated with cardiovascular disease incidence: findings from the EPIC-NL cohort study. *Sci Rep.* (2018) 8:3290. doi: 10.1038/s41598-018-21661-x
32. Rogacev KS, Cremers B, Zawada AM, Seiler S, Binder N, Ege P, et al. CD14++CD16+ monocytes independently predict cardiovascular events: a cohort study of 951 patients referred for elective coronary angiography. *J Am Coll Cardiol.* (2012) 60:1512–20. doi: 10.1016/j.jacc.2012.07.019
33. Yamamoto H, Yoshida N, Shinke T, Otake H, Kuroda M, Sakaguchi K, et al. Impact of CD14(++)CD16(+) monocytes on coronary plaque vulnerability assessed by optical coherence tomography in coronary artery disease patients. *Atherosclerosis.* (2018) 269:245–51. doi: 10.1016/j.atherosclerosis.2018.01.010
34. Gast M, Rauch BH, Haghikia A, Nakagawa S, Haas J, Stroux A, et al. Long noncoding RNA NEAT1 modulates immune cell functions and is suppressed in early onset myocardial infarction patients. *Cardiovasc Res.* (2019) 115:1886–906. doi: 10.1093/cvr/cvz085
35. Yang Y, Wang Q, Cai X, Wei Z, Hou J, Fei Y, et al. Activin receptor-like kinase 4 haplodeficiency alleviates the cardiac inflammation and pacing-induced ventricular arrhythmias after myocardial infarction. *Aging (Albany NY).* (2021) 13:17473–88. doi: 10.18632/aging.203236
36. Ferrie JE, Kivimaki M, Akbaraly TN, Singh-Manoux A, Miller MA, Gimeno D, et al. Associations between change in sleep duration and inflammation: findings on C-reactive protein and interleukin 6 in the Whitehall II Study. *Am J Epidemiol.* (2013) 178:956–61. doi: 10.1093/aje/kwt072
37. Nakazaki C, Noda A, Koike Y, Yamada S, Murohara T, Ozaki N. Association of insomnia and short sleep duration with atherosclerosis risk in the elderly. *Am J Hypertens.* (2012) 25:1149–55. doi: 10.1038/ajh.2012.107
38. Sauvet F, Drogou C, Bougard C, Arnal PJ, Dispersyn G, Bourrilhon C, et al. Vascular response to 1 week of sleep restriction in healthy subjects. A metabolic response? *Int. J Cardiol.* (2015) 190:246–55. doi: 10.1016/j.ijcard.2015.04.119
39. Tobaldini E, Cogliati C, Fiorelli EM, Nunziata V, Wu MA, Prado M, et al. One night on-call: sleep deprivation affects cardiac autonomic control and inflammation in physicians. *Eur J Intern Med.* (2013) 24:664–70. doi: 10.1016/j.ejim.2013.03.011
40. Tobaldini E, Fiorelli EM, Solbiati M, Costantino G, Nobili L, Montano N. Short sleep duration and cardiometabolic risk: from pathophysiology to clinical evidence. *Nat Rev Cardiol.* (2019) 16:213–24. doi: 10.1038/s41569-018-0109-6
41. Chandola T, Ferrie JE, Perski A, Akbaraly T, Marmot MG. The effect of short sleep duration on coronary heart disease risk is greatest among those with sleep disturbance: a prospective study from the Whitehall II cohort. *Sleep.* (2010) 33:739–44. doi: 10.1093/sleep/33.6.739
42. Hurtado-Alvarado G, Pavón L, Castillo-García SA, Hernández ME, Gómez-González B. Sleep loss as a factor to induce cellular and molecular inflammatory variations. *Clin Dev Immunol.* (2015) 2013:801341. doi: 10.1155/2013/801341
43. van Leeuwen WM, Lehto M, Karisola P, Lindholm H, Luukkonen R, Sallinen M, et al. Sleep restriction increases the risk of developing cardiovascular diseases by augmenting proinflammatory responses through IL-17 and CRP. *PLoS ONE.* (2009) 4:e4589. doi: 10.1371/journal.pone.0004589
44. Lange T, Dimitrov S, Born J. Effects of sleep and circadian rhythm on the human immune system. *Ann N Y Acad Sci.* (2010) 1193:48–59. doi: 10.1111/j.1749-6632.2009.05300.x

45. Li W, Lidebjer C, Yuan XM, Szymanowski A, Backteman K, Ernerudh J, et al. NK cell apoptosis in coronary artery disease: relation to oxidative stress. *Atherosclerosis.* (2008) 199:65–72. doi: 10.1016/j.atherosclerosis.2007.10.031
46. Bello OD, Jouannot O, Chaudhuri A, Stroeva E, Coleman J, Volynski KE, et al. Synaptotagmin oligomerization is essential for calcium control of regulated exocytosis. *Proc Natl Acad Sci USA.* (2018) 115:E7624–31. doi: 10.1073/pnas.1808792115
47. Catz SD. Regulation of vesicular trafficking and leukocyte function by Rab27 GTPases and their effectors. *J Leukoc Biol.* (2013) 94:613–22. doi: 10.1189/jlb.1112600
48. Holt O, Kanno E, Bossi G, Booth S, Daniele T, Santoro A, et al. Slp1 and Slp2-a localize to the plasma membrane of CTL and contribute to secretion from the immunological synapse. *Traffic.* (2008) 9:446–57. doi: 10.1111/j.1600-0854.2008.00714.x
49. Galvez-Santisteban M, Rodriguez-Fraticelli AE, Bryant DM, Vergarajauregui S, Yasuda T, Banon-Rodriguez I, et al. Synaptotagmin-like proteins control the formation of a single apical membrane domain in epithelial cells. *Nat Cell Biol.* (2012) 14:838–49. doi: 10.1038/ncb2541
50. Francis CR, Claflin S, Kushner EJ. Synaptotagmin-like protein 2a regulates angiogenic lumen formation *via* weibel-palade body apical secretion of angiopoietin-2. *Arterioscler Thromb Vasc Biol.* (2021) 41:1972–86. doi: 10.1161/ATVBAHA.121.316113
51. Bongen E, Vallania F, Utz PJ, Khatri P. KLRD1-expressing natural killer cells predict influenza susceptibility. *Genome Med.* (2018) 10:45. doi: 10.1186/s13073-018-0554-1
52. Ortega-Rodriguez AC, Marin-Jauregui LS, Martinez-Shio E, Hernandez CB, Gonzalez-Amaro R, Escobedo-Uribe CD, et al. Altered NK cell receptor repertoire and function of natural killer cells in patients with acute myocardial infarction: a 3-month follow-up study. *Immunobiology.* (2020) 225:151909. doi: 10.1016/j.imbio.2020.151909
53. Klarlund K, Pedersen BK, Theander TG, Andersen V. Depressed natural killer cell activity in acute myocardial infarction. *Clin Exp Immunol.* (1987) 70:209–16.
54. Yan W, Zhou L, Wen S, Duan Q, Huang F, Tang Y, et al. Differential loss of natural killer cell activity in patients with acute myocardial infarction and stable angina pectoris. *Int J Clin Exp Pathol.* (2015) 8:14667–75.
55. Boateng S, Sanborn T. Acute myocardial infarction. *Dis Mon.* (2013) 59:83–96. doi: 10.1016/j.disamonth.2012.12.004
56. Korff S, Katus HA, Giannitsis E. Differential diagnosis of elevated troponins. *Heart.* (2006) 92:987–93. doi: 10.1136/hrt.2005.071282
57. Gunnar E, Helge R, Anna R, Namtvedt SK, Harald HS, Jon B, et al. Severity of obstructive sleep apnea is associated with cardiac troponin I concentrations in a community-based sample: data from the Akershus Sleep Apnea Project. *Sleep.* (2014) 6:1111–6. doi: 10.5665/sleep.3772
58. Querejeta RG, Redline S, Punjabi N, Claggett B, Ballantyne CM, Solomon SD, et al. Sleep apnea is associated with subclinical myocardial injury in the community. The ARIC-SHHS study. *Am J Respir Crit Care Med.* (2013) 188:1460–5. doi: 10.1164/rccm.201309-1572OC
59. Sanchez-de-la-Torre A, Soler X, Barbe F, Flores M, Maisel A, Malhotra A, et al. Cardiac troponin values in patients with acute coronary syndrome and sleep apnea: a pilot study. *Chest.* (2018) 153:329–38. doi: 10.1016/j.chest.2017.06.046
60. Zhang X, Lv X, Li X, Wang Y, Lin HY, Zhang J, et al. Dysregulated circulating SOCS3 and haptoglobin expression associated with stable coronary artery disease and acute coronary syndrome: an integrated study based on bioinformatics analysis and case-control validation. *Anatol J Cardiol.* (2020) 24:160–74. doi: 10.14744/AnatolJCardiol.2020.56346

Conflict of Interest: The authors declare that the research was conducted in the absence of any commercial or financial relationships that could be construed as a potential conflict of interest.

frontiers | Frontiers in Cardiovascular Medicine

ORIGINAL RESEARCH
published: 15 June 2022
doi: 10.3389/fcvm.2022.834199

Altered Peroxisome Proliferator-Activated Receptor Alpha Signaling in Variably Diseased Peripheral Arterial Segments

*Connor Engel[1], Rodrigo Meade[1], Nikolai Harroun[1], Amanda Penrose[1], Mehreen Shafqat[1], Xiaohua Jin[1], Gayan DeSilva[1], Clay Semenkovich[5] and Mohamed Zayed[1,2,3,4]**

[1] Section of Vascular Surgery, Department of Surgery, Washington University in St. Louis School of Medicine, St. Louis, MO, United States, [2] Division of Molecular Cell Biology, Washington University in St. Louis School of Medicine, St. Louis, MO, United States, [3] Department of Biomedical Engineering, McKelvey School of Engineering, Washington University in St. Louis, St. Louis, MO, United States, [4] Veterans Affairs St. Louis Health Care System, St. Louis, MO, United States, [5] Division of Endocrinology, Metabolism and Lipid Research, Department of Medicine, Washington University in St. Louis School of Medicine, St. Louis, MO, United States

OPEN ACCESS

Edited by:
Ying Wang,
University of British Columbia, Canada

Reviewed by:
Valentin Blanchard,
University of British Columbia, Canada
Minerva Garcia-Barrio,
University of Michigan, United States

***Correspondence:**
Mohamed Zayed
zayedm@wustl.edu

Specialty section:
This article was submitted to Atherosclerosis and Vascular Medicine, a section of the journal Frontiers in Cardiovascular Medicine

Received: 13 December 2021
Accepted: 04 May 2022
Published: 15 June 2022

Citation:
Engel C, Meade R, Harroun N, Penrose A, Shafqat M, Jin X, DeSilva G, Semenkovich C and Zayed M (2022) Altered Peroxisome Proliferator-Activated Receptor Alpha Signaling in Variably Diseased Peripheral Arterial Segments. Front. Cardiovasc. Med. 9:834199. doi: 10.3389/fcvm.2022.834199

Objective: Peripheral atherosclerosis that accumulates in the extracranial carotid and lower extremity arteries can lead to significant morbidity and mortality. However, atherosclerotic disease progression is often not homogenous and is accelerated by diabetes. We previously observed increased phospholipid content in minimally (Min)-diseased arterial segments compared to maximally (Max)-diseased segments. Since Peroxisome Proliferator-Activated Receptor alpha (PPARα) is a key regulator of lipid metabolism, we hypothesized that it may have differential expression and signaling in Min vs. Max-diseased peripheral arterial segments.

Methods: Eighteen patients who underwent carotid endarterectomy (CEA), and 34 patients who underwent major lower extremity amputation were prospectively enrolled into a vascular tissue biobank. Min and Max-diseased segments were obtained in real-time from CEA plaque and amputated lower extremity arterial segments. mRNA and protein were isolated from specimens and the relative expression of *ppara*, and its downstream genes Acyl-CoA Oxidase 1 (*acox1*) and Carnitine Palmitoyltransferase 1A (*cpt1a*) were also evaluated. We evaluated gene expression and protein content relative to atherosclerotic disease severity and clinical diabetes status. Gene expression was also evaluated relative to Hemoglobin A1c and serum lipid profiles.

Results: In CEA segments of patients with diabetes, we observed significantly higher *ppara* and *acox1* gene expression ($p < 0.01$ and $p < 0.001$ respectively), and higher PPARα protein content ($p < 0.05$). Hemoglobin A1c significantly correlated with expression of *ppara* ($R^2 = 0.66$, $p < 0.001$), *acox1* ($R^2 = 0.31$, $p < 0.05$), and *cpt1a* ($R^2 = 0.4$, $p < 0.05$). There was no significant difference in gene expression between Min vs. Max-diseased CEA plaque segments. Conversely, in lower extremity arterial segments of patients with diabetes, we observed significantly lower *ppara*, *acox1*, and

cpt1a expression ($p < 0.05$, $p < 0.001$, and $p < 0.0001$ respectively). Interestingly, CPT1A content was lower in arterial segments of patients with diabetes ($p < 0.05$). Hemoglobin A1c and HDL-cholesterol had negative correlations with *ppara* ($R^2 = 0.44$, $p < 0.05$; $R^2 = 0.42$, $p < 0.05$; respectively).

Conclusion: This study demonstrates the significant differential expression of *ppara* and its immediate downstream genes in human carotid and lower extremity arteries relative to disease severity and diabetes. These findings highlight that mechanisms that influence atheroprogression in the carotid and lower extremities peripheral arteries are not homogenous and can be impacted by patient diabetes status and serum cholesterol profiles. Further elucidating these differential molecular mechanisms can help improve targeted therapy of atherosclerosis in different peripheral arterial beds.

Keywords: PPARα, *acox1*, *cpt1a*, peripheral arterial disease, atherosclerosis, diabetes

INTRODUCTION

Atheroprogression progresses at different rates in the peripheral arterial system—with areas that are more likely to develop a high burden of disease and others that are often rarely impacted (**Figure 1**; 1, 2). The extracranial carotid arteries and lower leg popliteal-tibial arterial segments are especially prone to atheroprogression and can lead to significant clinical morbidity (3–5). Approximately 20–30% of ischemic strokes that occur each year result from advanced atherosclerotic plaque formation in the carotid arteries (6–9). Similarly, in the lower extremities, nearly one million Americans will develop symptomatic lower extremity intermittent claudication each year, of which, 20% are estimated to progress to Chronic Limb-Threatening Ischemia (CLTI) (4, 9, 10). Patients with diabetes (11, 12) and hyperlipidemia (13, 14) are especially prone to carotid and popliteal-tibial arterial atheroprogression. Although significant strides have been made in the last two decades to decrease the morbidity associated atherosclerosis in these arterial beds, the continued high prevalence of disease necessitates continued investigation of the differential metabolic mechanisms that influence disease progression.

Peroxisome proliferator-activated receptor-alpha (PPARα) is an important transcription factor that in the liver regulates expression of enzymes required for β-fatty acid oxidation. These enzymes influence production of serum triglycerides and total serum cholesterol (15–17). In arterial tissue, PPARα is known to regulate arterial wall inflammation, lipid metabolism, and even atherosclerotic plaque formation (18–21). Our group recently demonstrated that choline-ethanolamine phosphotransferase 1 (*cept1*), an upstream regulator of PPARα, had increased gene expression in minimally (Min)-diseased peripheral tibial arterial segments in patients with diabetes (22, 23). Increased *cept1* gene expression in the peripheral arteries of individuals with diabetes led us to hypothesize that PPARα and its downstream effectors, Acyl-CoA Oxidase 1 (*acox1*) and Carnitine Palmitoyltransferase 1A (*cpt1a*), may also be increased in the setting of diabetes and vary relative to atherosclerotic disease severity. To evaluate this, we performed a novel assessment of Min vs. Max-diseased peripheral arterial segments that were harvested in real-time from patients who underwent carotid endarterectomy (CEA) or lower extremity amputation. The relative content of PPARα and its downstream genes were then correlated with arterial disease severity and patient diabetes status.

MATERIALS AND METHODS

Human Subjects and Vascular Tissue Biobank

Between August 2015 and February, 2020, 52 patients underwent elective CEA or major lower extremity amputation and were prospectively enrolled to participate in an institutional review board-approved human vascular tissue biobank. All recruited patients provided informed consent for harvesting of intra-operative CEA plaque or lower extremity popliteal-tibial arterial segments from the amputated limb. All harvested specimens were de-identified and cataloged in a vascular tissue biobank for further analysis.

Patient Demographics

Patient demographics were collected via chart review and maintained in a de-identified secure patient database. These demographics were collected by chart review, and included sex, age, body mass index (BMI), smoking status, and medical history of diabetes (defined as a previous diagnosis of diabetes), hemoglobin A1c, fasting glucose, hypertension (defined as a systolic pressure $\geq$ 140 mmHg and/or a diastolic pressure $\geq$ 90 mmHg), hyperlipidemia (cholesterol levels $\geq$240 mg/dl, triglyceride levels $\geq$ 200 mg/dl, or LDL levels $\geq$ 160 mg/dl) (24; **Table 1**). Fasting glucose and hemoglobin A1c levels were measured the day of surgery, and lipid panels within 6 months of the operative date were also reviewed for analysis. Diabetes severity was evaluated using a Diabetes Clinical Severity Index (DCSI) as previously described (25), which is scored by compiling a patient's history of diabetes-related complications and range from 0 to 13. Patients with a DCSI score above the mean in each surgical group were categorized as "High DCSI" while patients below the mean were categorized as "Low DCSI."

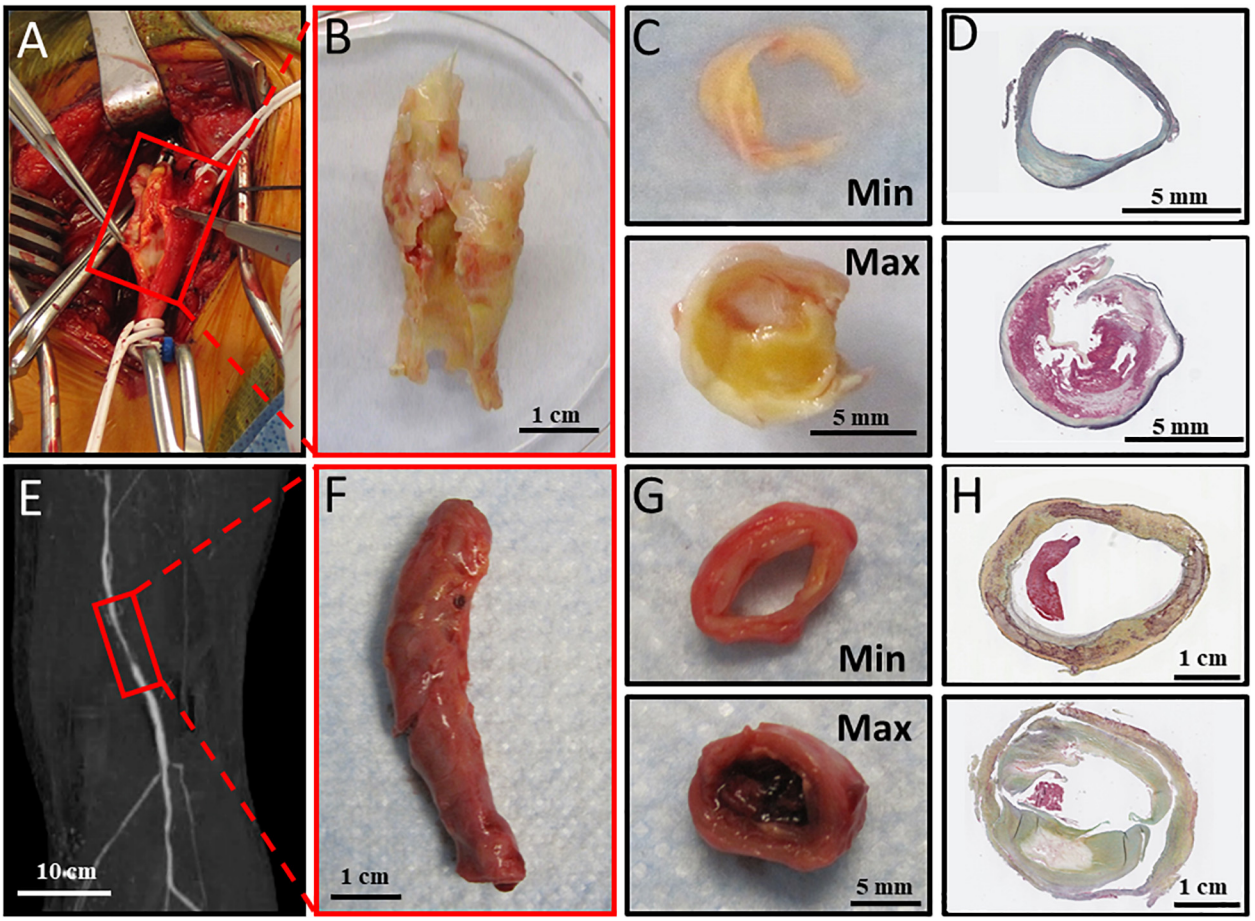

FIGURE 1 | Atheroprogression of carotid artery bifurcation and lower extremity. **(A)** Carotid bulb before endarterectomy, **(B)** Carotid endarterectomy harvested from operating room, **(C)** Carotid Endarterectomy sectioned into Min and Max diseased sections. **(D)** Carotid endarterectomy Min and maximally Max sections with Movat Pentachrome staining. **(E)** Preoperative imaging showing reduced perfusion in the popliteal artery. **(F)** Dissected popliteal artery collected immediately from operating room. **(G)** Anterior tibial artery sectioned into minimally (Min) and maximally (Max) diseased components. **(H)** Min and Max sections stained with Movat Pentachrome staining. Movat pentachrome stains elastic fibers black, Nuclei Blue, Collagen Yellow, reticular fibers yellow, mucin bright blue, and fibrin red.

Human Tissue Processing

For CEA specimens, plaque was immediately transferred to the research laboratory in cold saline on ice. Specimens were sectioned into Min and Max-diseased segments as previously described (26). Approximately 5 mm sections of tissue at the carotid bifurcation demonstrating American Heart Association (AHA) Type IV–VIII plaque were designated as Max-diseased tissue segment. Sections of tissue at the peripheral end of the plaque demonstrating AHA type I-III plaques was designated as Min-diseased segments (**Figures 1A–D**). Min and Max-diseased carotid plaque segments were isolated, partitioned into segments for paraffin embedding, and segments were used to isolate mRNA and protein purification (22). For each patient, Min-diseased segments served as internal controls for the Max-diseased segments. For mRNA isolation, specimens were placed in Trizol (1 mL for 50 mg of tissue) and grinded with mortar and pestle.

Similarly, lower extremity arterial segments were harvested immediately following major lower extremity amputation in the operating room. If available, preoperative imaging was evaluated to determine which lower leg arterial segments were indeed Min or Max-diseased. At least a 5 cm segment of the popliteal artery, anterior tibial, posterior tibial, and/or peroneal arteries were dissected from adjacent tissue in the amputated limb, and arterial segments were placed in cold saline solution and immediately transported to the laboratory on ice. Approximately a 1 cm section of tissue of the most diseased region was designated as Max-diseased while the least diseased segments from the same limb was used as an internal control and designated as Min-diseased (**Figures 1E–H**). The arterial adventitia was carefully removed from the intima and media layers. Min and Max-diseased arterial segments were embedded in paraffin, or placed in Trizol solution for subsequent mRNA isolation.

mRNA Isolation and RT-PCR

mRNA was purified from Min and Max-diseased CEA and lower leg arterial segments. All samples were treated with chloroform

TABLE 1 | Patient clinical demographics.

	All Patients	CEA Patients	Amputation Patients	CEA vs. Amputation	NDM	DM	NDM vs. DM
Demographics	*n* = 52	*n* = 18	*n* = 34	*p*	26	*n* = 26	*p*
Sex (male: female)	32:20:00	11:7	21:13	1	15:11	17:09	0.78
Mean age (years) ± SD	63.4 ± 10.0	66 ± 9.3	62.1 ± 10.2	0.23	63.2 ± 9.4	63 ± 10.7	0.59
Mean BMI (kg/m^2) ± SD	28.5 ± 8.3	29.1 ± 7.9	28.2 ± 8.7	0.23	26.7 ± 7.0	30 ± 9.3	0.23
Co-morbid conditions							
Diabetes mellitus (% of total)	26 (45.61%)	9 (50%)	17 (50%)	1	0	26 (100%)	n/a
Insulin Dependent (% of Diabetics)	7 (26.9%)	0 (0%)	7 (41%)	0.27	0	7 (27.0%)	n/a
Tobacco smoker (% of total)	44 (85%)	15 (84.6%)	29 (85.3%)	1	22 (84.5%)	22 (84.5%)	1
Hyperlipidemia (% of total)	39 (75%)	16 (88.9%)	23 (67.6%)	0.17	18 (69.2.0%)	21 (80.1%)	0.52
Mean DCSI ± SD	4.9 ± 2.1	4.1 ± 1.85	5.4 ± 2.2	0.21	N/A	4.9 ± 2.2	n/a
High DCSI (% of Diabetics)	N/A*	5 (55.6%)	7 (41%)	N/A*	N/A*	N/A*	n/a
Symptomatic Carotid Disease (% of CEA)	N/A	4 (44.4%)	N/A	N/A	2 (22.2%)	4 (44.4%)	0.67
Receiving Fenofribrate (% Total)	4 (7.7%)	3 (16.7%)	1 (2.9%)	28.3	1 (3.8%)	3 (11.5%)	0.61
Receiving Statin (% of total)	35 (67.7%)	13 (72.2%)	22 (64.7%)	0.76	14 (53.8%)	21 (80.7%)	0.07
Hypertension (% of total)	44 (84.6%)	16 (88.9%)	28 (82.3%)	1	22 (85.6%)	22 (84.6%)	1
Anthropometric characteristics							
HbA1c (mg/dL) ± SD	7.1 ± 1.8	6.8 ± 1.6	7.1 ± 2.0	0.55	5.7 ± 1.4	7.9 ± 1.7	**0.0002**
Fasting Glucose (mg/dL) ± SD	129.3 ± 41.1	135.2 ± 44.7	124.8 ± 38.7	0.69	103.5 ± 19.6	147 ± 43.8	**0.007**
Triglycerides (mg/dL) ± SD	149.5 ± 47.3	137.8 ± 76.8	144.1 ± 84.4	0.83	115.2 ± 66.8	159.8 ± 85.9	0.07
Total Cholesterol (mg/dL) ± SD	149.5 ± 46.8	172.1 ± 44.1	133.5 ± 44.0	**0.02**	149 ± 41.9	148 ± 51.8	0.66
LDL Cholesterol (mg/dL) ± SD	77.0 ± 37.0	95.5 ± 32.9	65.0 ± 35.3	**0.01**	84.1 ± 36.3	72.4 ± 36.4	0.47
HDL Cholesterol (mg/dL) ± SD	38.4 ± 13.0	40.2 ± 12.2	38.7 ± 13.8	0.64	39.7 ± 9.8	37 ± 15.054	0.58
Non-HDL Cholesterol (mg/dL) ± SD	119.8 ± 45.6	132 ± 47.75	96.3 ± 38.7	**0.04**	110.6 ± 43.2	110 ± 48.24	1

**Mean DCSI was calculated for each surgical group.*
DCSI, diabetes clinical severity index; HbA1c, hemoglobin A1c.

and centrifuged at 16,000 g at 4°C for 15 min. Supernatants were mixed with an equal volume of 70% ethanol, and centrifuged again at 10,000 g for 1 min. RNA was then isolated from the supernatant using a Qiagen RNA mini-column isolation kit (74104, Qiagen, Venlo, Netherlands). The extracted RNA mixture was amplified using SYBR Green PCR Master Mix (4309155, Thermo Fisher) and a 7500 Fast Real-Time PCR system (Applied Bio-systems, Carlsbad, CA, United States). mRNA primers (**Supplementary Table III**) were used to evaluate the relative expression of *rpl32, ppara, acox1* and *cpt1a*. Values were calculated using the $2^{-\Delta\Delta CT}$ method, and normalized relative to the abundance of *rpl32.* The normalized *rpl32* levels were based on abundance of gene expression in the Min-diseased samples from patients with no diabetes.

Western Blot Analysis

Carotid endarterectomy and lower extremity tissue were also homogenized in cold mammalian cell lysis kit (MCL1-KT; Millipore Sigma). Total protein for both Min and Max-diseased was determined using Bradford Protein Assay and loaded onto Bis-Tris gel (NW00082BOX; Thermo Fisher Scientific) and transferred to polyvinylidene fluoride membranes for Western blotting. Protein was detected with mouse anti-PPARα (SAB4502260; Millipore Sigma), mouse anti-ACOX1 (sc-517306, Santa Cruz), and mouse anti-CPT1a (66039–1-Ig; Proteintech). Rabbit anti-beta actin (ab8227, Abcam) or rabbit anti-GAPDH (G9545, Sigma) was used for Western blot loading controls. Band densitometry analysis was performed using ImageJ software as previously described (27). Band densities were expressed as ratios relative to the protein loading control.

Tissue Histology

Following collection from the operating room, arterial samples were then prepared as previously described (28). Briefly, Min or Max-diseased arterial samples were sectioned into 3 mm sections, fixed in 10% formalin and decalcified in EDTA for 2 weeks. Samples were washed with 70% ethanol and embedded into paraffin blocks. Paraffin samples were cut into 10 μm sections using a HM324 Rotary Microtome (902100A, ThermoFisher Scientific, Waltham, MA, United States). Slides were stained with pentachrome staining (KTRMP, StatLab, McKinney, TX, United States). Images of stained arterial segments were captured with a NanoZoomer 2.0-HT (Hamamatsu Photonics, K.K., Japan).

Statistical Analysis

Non-parametric two-tailed Man-Whitney tests were used to evaluate the differences of mRNA expression between diabetic and non-diabetic patients, and non-parametric two tailed Wilcoxon matched-pairs test were used to compare Min and Max samples. Additionally, Kruskal-Wallis Tests and Dunn's multiple comparisons tests were used to measure

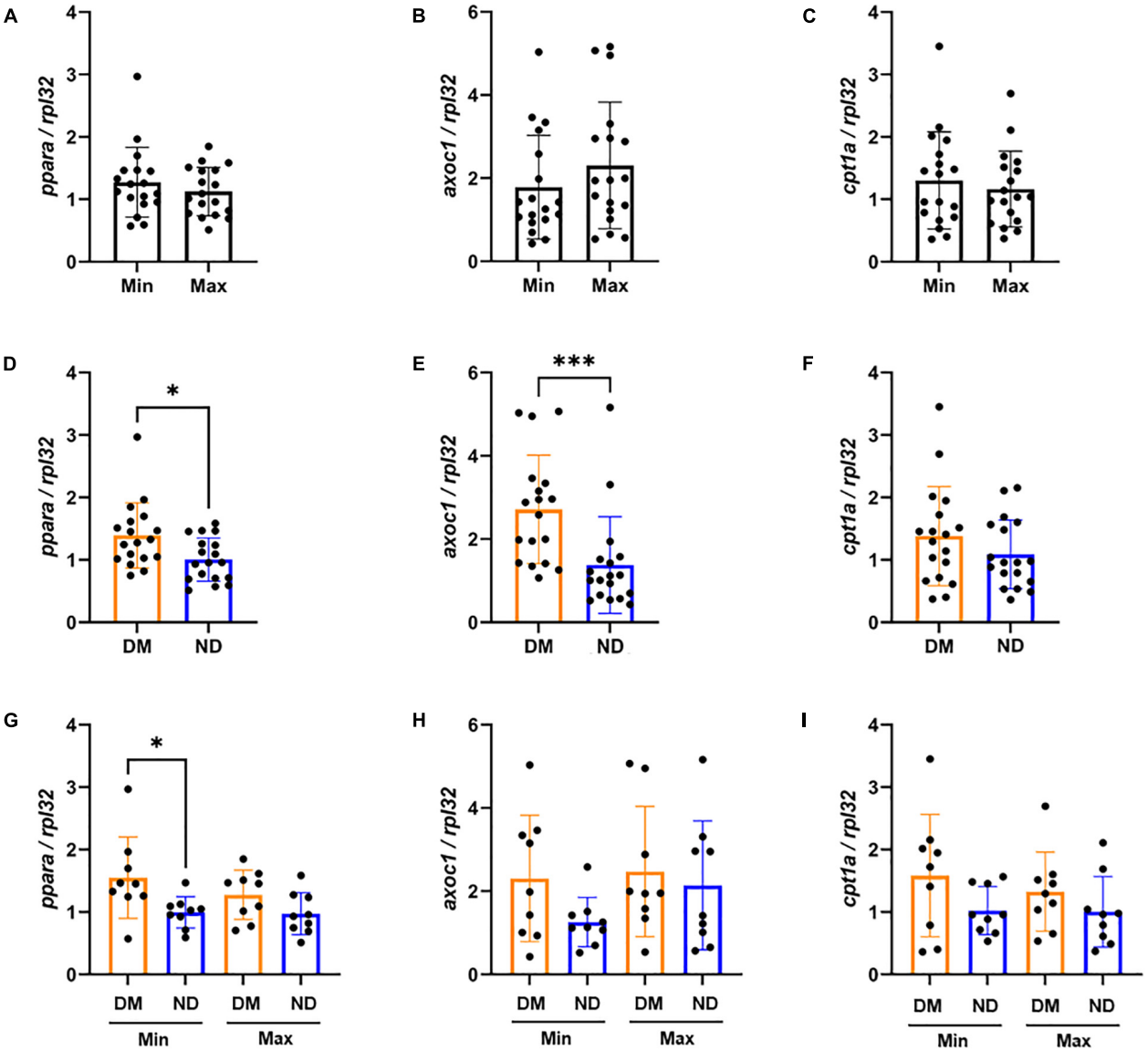

FIGURE 2 | mRNA expression variability of carotid endarterectomy plaques by lesion severity and diabetic status **(A–C)** No significant difference in carotid artery plaque expression between the Min (n = 18) and Max (n = 18) segments of *ppara*, *acox1*, and *cpt1a* mRNA expression. **(D–F)** Combined Min and Max analysis of patients with diabetes (n = 18) demonstrate significantly higher mRNA expression of *ppara* ($p < 0.05$), and *acox1* ($p < 0.001$) compared to patients without diabetes. We did not observe a difference between *cpt1a* mRNA expression between patients with or without diabetes. **(G–I)** When distinguishing both disease severity and diabetic status, we found significant increase in *ppara* mRNA expression in patients with diabetes (n = 9) compared to patients without diabetes (n = 9). We found no significant differences in *acox1* or *cpt1a* expression. DM, Diabetic. ND, Non-diabetic. Min, Minimally diseased. Max, Maximally diseased. Data are presented as mean ± SD, and each point represents one patient sample. *$p < 0.05$ and ***$p < 0.001$.

differences in mRNA and protein expression between Min and Max diseased segments of patients with and without diabetes. Non-parametric Spearman correlations were calculated comparing the mRNA $2^{-\Delta\Delta CT}$ values and relative mRNA levels to patient demographics. Outliers were determined by ROUT test and not included in analyses. All analyses were performed using GraphPad Prism (GraphPad Prism 9.1 software, GraphPad Software Inc., United States). We considered $p < 0.05$ to be significant. Data are presented as mean ± SD.

RESULTS

ppara-Related Gene Expression and Relative Protein Content in Carotid Endarterectomy Plaques

We evaluated *ppara*, and its downstream genes *acox1* and *cpt1a* in Min and Max-diseased CEA plaques from patients with or without diabetes. Although we observed no overall difference in gene expression between Min and Max CEA

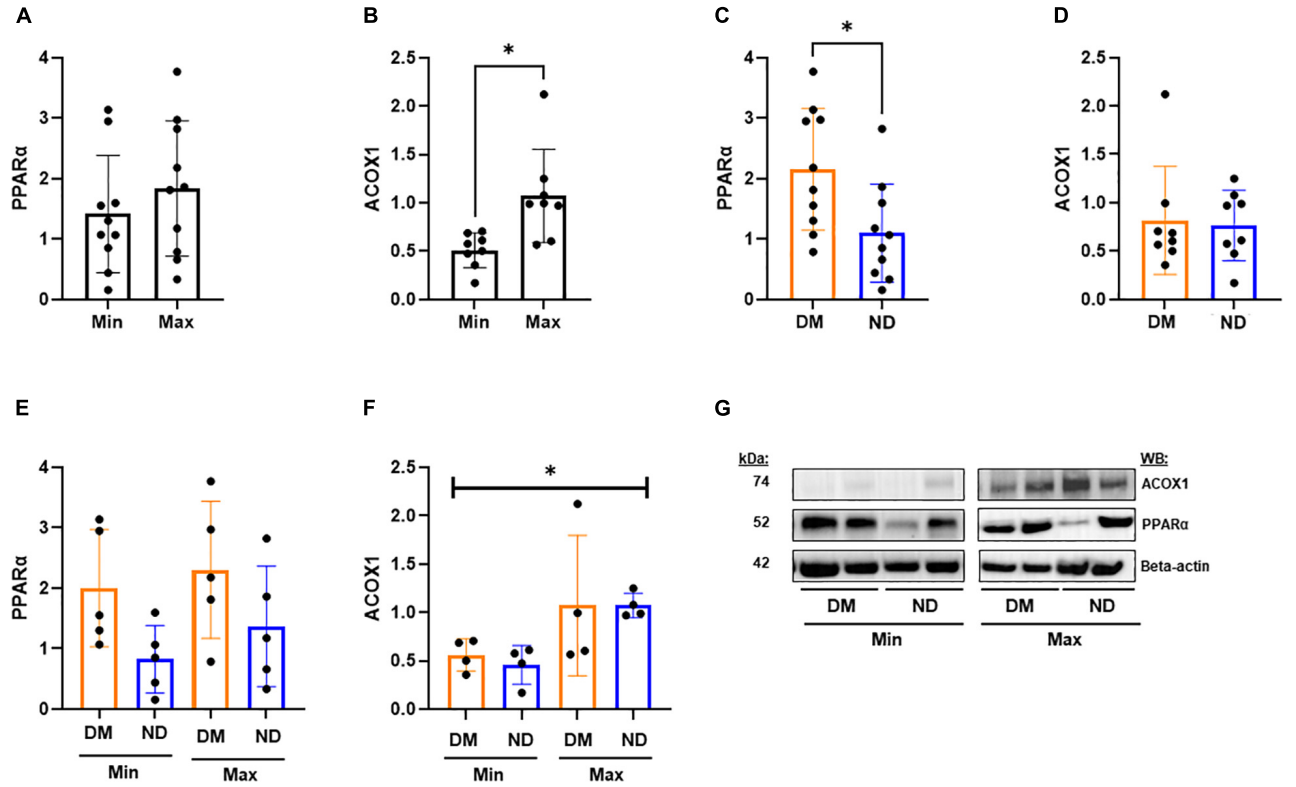

FIGURE 3 | Western blot analysis from CEA in varying disease and diabetic status. **(A,B)** We observed no significant difference in PPARα protein expression between Min (n = 10) and Max (n = 10) segments, but a significant decrease in relative ACOX1 abundance in Min tissues compared to Max ($p < 0.05$). **(C)** Patients with diabetes (n = 10) demonstrate significantly higher relative PPARα abundance compared to patients without diabetes ($p < 0.05$). **(D)** No significant difference in ACOX1 expression among patients with an without diabetes. **(E)** No significant variability in PPARα from combined analysis of diabetic status and lesion severity analysis. **(F)** Kruskal-Wallis test shows significant variability in relative ACOX1 abundance between Min and Max specimens from patients with (n = 4) or without (n = 5) diabetes. **(G)** Representative Western Blots from analysis. Samples were normalized to beta-actin content. DM, Diabetic. ND, Non-diabetic. Min, Minimally diseased. Max, Maximally diseased. Data are presented as Mean ± SD, and each point represents one patient sample. *$p < 0.05$.

plaque segments (**Figures 2A–C**), there was higher *ppara* and *acox1* in CEA plaques of patients with diabetes ($p < 0.01$, $p < 0.001$, respectively; **Figures 2D–H**). No difference in *cpt1a* expression was observed (**Figure 2F**). When samples were stratified by diabetes status and disease severity, Min were observed to have higher *ppara* ($p < 0.05$; **Figure 2G**) compared to Max in individuals with diabetes. There was no difference in *acox1* or *cpt1a* relative to diabetes status or disease severity (**Figures 2H,I**), and no differences between Min and Max relative to high or low DCSI scores (**Supplementary Figure 1**).

We evaluated relative protein abundance to determine whether differences in gene expression translated into differences in PPARα downstream signaling in CEA tissue (**Figure 3**). Although no difference was observed in PPARα between Min and Max, there was higher ACOX1 in Max segments ($p < 0.05$; **Figures 3A,B**). Consistent with gene expression, we observed higher PPARα among patients with diabetes ($p < 0.05$; **Figure 3C**). A combined analysis of diabetes status and disease severity showed no difference in PPARα (**Figure 3E**). However, a combined analysis demonstrated significant variability in relative ACOX1 abundance by ANOVA ($p < 0.05$, **Figure 3F**), and a non-significant increase in Max samples compared to Min samples in patients with diabetes (**Figure 3F**, $p = 0.07$) as demonstrated by western blot analysis (**Figure 3G**).

Correlation of *ppara*-Related Gene Expression in Carotid Endarterectomy Plaques With Hemoglobin A1c and Serum Glycemic Profiles

Gene expression in Min and Max-diseased CEA plaque segments were evaluated relative to hemoglobin A1c and serum fasting glucose (**Supplementary Table I**). In Min-diseased CEA plaque segments we observed a significant positive correlation between hemoglobin A1c and *ppara* ($R^2 = 0.66$, $p < 0.001$), *acox1* ($R^2 = 0.31$, $p < 0.05$), and *cpt1a* ($R^2 = 0.40$, $p < 0.05$). In Max-diseased plaque segments there was also a significant correlation between hemoglobin A1c and *ppara* ($R^2 = 0.32$, $p < 0.05$, **Supplementary Figure 2A**) and *acox1* ($R^2 = 0.45$, $p < 0.05$, **Supplementary Figure 2B**) expression, but no significant correlation in relative *cpt1a* mRNA expression (**Supplementary Figure 2C**). We also observed a significant correlation between fasting glucose and *ppara* gene expression in Min diseased

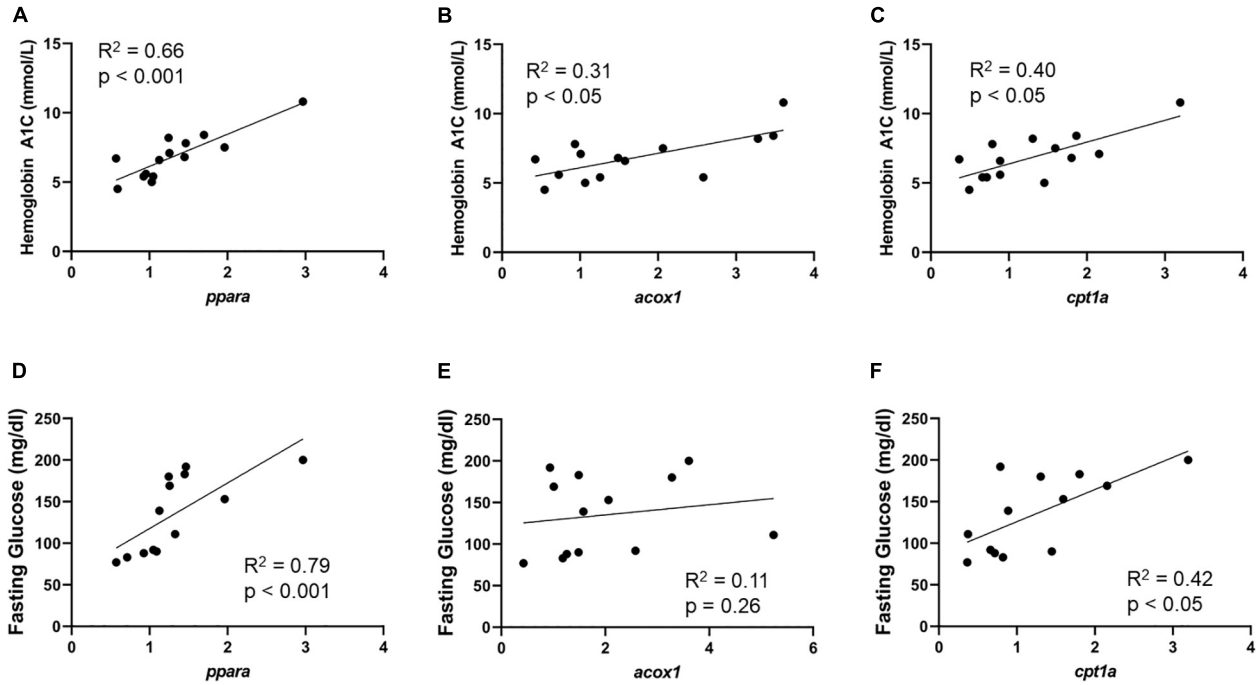

FIGURE 4 | Min carotid plaque mRNA correlates with HbA1c, and fasting glucose content. **(A–C)** Min-diseased carotid plaque mRNA content demonstrates significant positive correlation between *ppara* ($p < 0.0001$, $R^2 = 0.66$, $n = 14$), *acox1* ($p < 0.05$, $R^2 = 0.31$, $n = 14$) and *cpt1a* ($p < 0.05$, $R^2 = 0.40$, $n = 14$) in comparison to HbA1c content. **(D–F)** Min-diseased carotid plaque *ppara* ($p < 0.001$, $R^2 = 0.79$, $n = 13$), and *cpt1a* ($p < 0.05$, $R^2 = 0.42$, $n = 13$) Demonstrates significant positive correlation with fasting glucose levels. We did not observe a correlation between *acox1* ($p = 0.26$, $R^2 = 0.12$, $n = 13$) and fasting glucose.

plaques ($R^2 = 0.79$, $p < 0.001$; **Figure 4D**), and *cpt1a* ($R^2 = 0.42$, $p < 0.05$; **Figure 4F**), as well as a significant correlation between fasting glucose and *ppara* in Max diseased plaques ($R^2 = 0.38$, $p < 0.05$, **Supplementary Figure 2D**). No correlations were observed with hemoglobin A1C (**Figures 4A–C**), and we observed no correlation between fasting glucose and *acox1* in Min (**Figure 4E**) and *acox1* or *cpt1a* Max diseased plaques (**Supplementary Figures 2D–F**).

Correlation between gene expression in CEA plaque segments and triglyceride, total cholesterol, LDL, HDL, non-HDL cholesterol, and DCSI score were performed. With the exception to moderate positive correlation between *cpt1a* and triglyceride in Min segments ($R^2 = 0.37$, $p < 0.05$; **Supplementary Table I**), and a negative correlation of DCSI scores to *cpt1a* in Max segments ($R^2 = 0.54$, $p < 0.05$, **Supplementary Table I**), no other correlations were observed (**Supplementary Table I**).

ppara-Related Gene Expression and Relative Protein Abundance in Lower Extremity Arterial Segments

Expression of *ppara, acox1*, and *cpt1a* was evaluated in Min and Max-diseased lower extremity arterial segments in individuals with or without diabetes. Similar to findings in CEA plaques, we observed no differences in *ppara,* and *cpt1a* in Min-diseased lower extremity arterial segments, but 44% lower *acox1* expression ($p = 0.05$; **Figures 5A–C**). Unlike CEA plaque, there was lower *ppara* ($p < 0.05$), *acox1* ($p < 0.001$) and *cpt1a* ($p < 0.0001$) expression in lower extremity segments from patients with diabetes (**Figures 5D–F**). Combined analysis of arterial disease severity and diabetes status demonstrated no difference in *ppara* (**Figure 5G**), but significant variability among in *acox1* ($p < 0.01$; **Figure 5H**) and *cpt1a* expression ($p < 0.01$; **Figure 5I**) particularly in Min segments. Unlike individuals with low DCSI scores, we observed that individuals with high DCSI scores had higher relative *acox1* ($p < 0.05$) and *cpt1a* ($p < 0.05$) expression in Max segments (**Supplementary Figure 3**).

There was no difference in relative PPARα or CPT1A protein abundance between Min or Max-diseased lower extremity arterial segments, but there was significant lower ACOX1 in Min segments ($p < 0.05$, **Figures 6A–C**). While no difference in PPARα or ACOX1 was observed in individuals with and without diabetes, individuals with diabetes had higher CPT1A ($p < 0.05$) compared to those without diabetes (**Figures 6D–F**). A combined analysis of lesion severity and diabetes status found no difference in PPARα, or ACOX1, but a significant increase of CPT1A ($p < 0.05$) in Max segments in individuals without diabetes (**Figures 6G–I**) as demonstrated by western blot analysis (**Figure 6J**).

Lower Extremity *ppara* Signaling Correlates With Hyperlipidemic Markers

Similar to analysis in CEA segments, we evaluated the correlation of lower extremity arterial segment gene expression and serum glycemia and lipid profiles (**Supplementary Table II**).

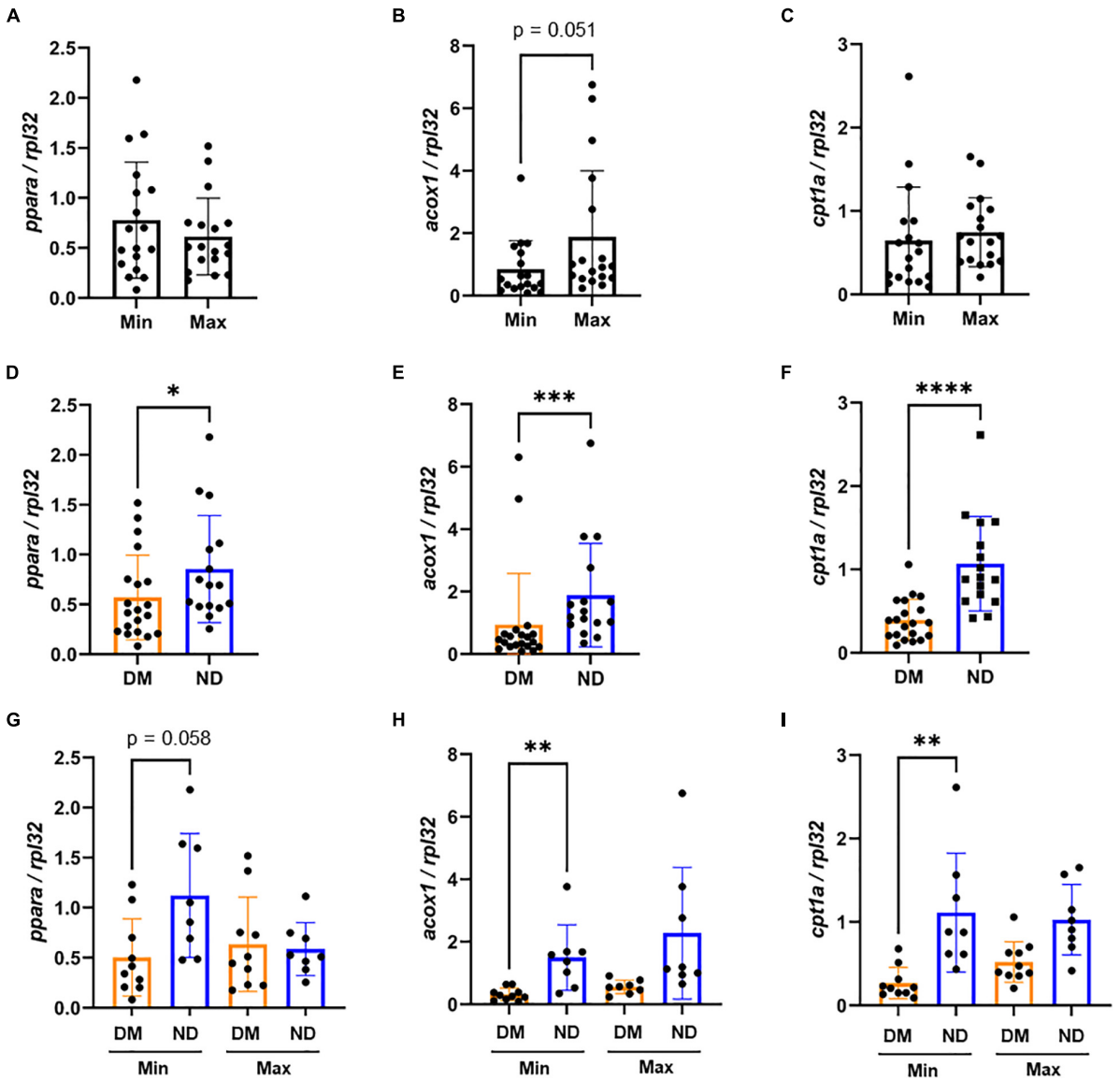

FIGURE 5 | mRNA expression variability of lower extremity segments by lesion severity and diabetic status: **(A–C)** In Lower extremity samples, we observed no significant difference in *ppara* and *cpt1a* mRNA expression between Min (n = 18) and Max (n = 18) diseased segments. However, we found Min-diseased samples had non-significantly lower expression of *acox1* (p = 0.051, n = 18) compared to Max-diseased. **(D–F)** We found that patients with diabetes (n = 20) demonstrated significantly lower *ppara* ($p < 0.05$), *acox1* ($p < 0.001$) and *cpt1a* ($p < 0.0001$) mRNA expression compared to patients without diabetes (n = 16). **(G–I)** When categorizing segments between diseased and diabetic status, we observed no significant variability of *ppara*. However, we found a significant decrease of *acox1* ($p < 0.01$) and *cpt1a* ($p < 0.01$) in patients with diabetes (n = 10) compared to patients without diabetes (n = 8) from Min-diseased tissues. DM, Diabetic. ND, Non-diabetic. Min, minimally diseased. Max, maximally diseased. Data are presented as Mean ± SD and, each point represents one patient sample. *$p < 0.05$, **$p < 0.01$, and ***$p < 0.001$.

Unlike findings in CEA, we observed a negative correlation between *ppara* and hemoglobin A1c (R^2 = 0.44, $p < 0.05$), fasting glucose (R^2 = 0.54, $p < 0.05$; **Figure 7**), and a positive correlation with HDL (R^2 = 0.42, $p < 0.05$; **Supplementary Table II**). *acox1* in lower extremity Min segments has a positive correlation with total cholesterol as well as HDL (R^2 = 0.42, $p < 0.05$; R^2 = 0.60, $p < 0.05$; respectively; **Supplementary Table II**). No significant correlation was observed between *cpt1a* from Min segments, or *ppara, acox1,* and *cpt1a* from Max segments (**Supplementary Table II**).

DISCUSSION

This study provides novel findings on *ppara*-related gene expression and relative protein content in peripheral carotid and lower leg arterial segments—two variant anatomical

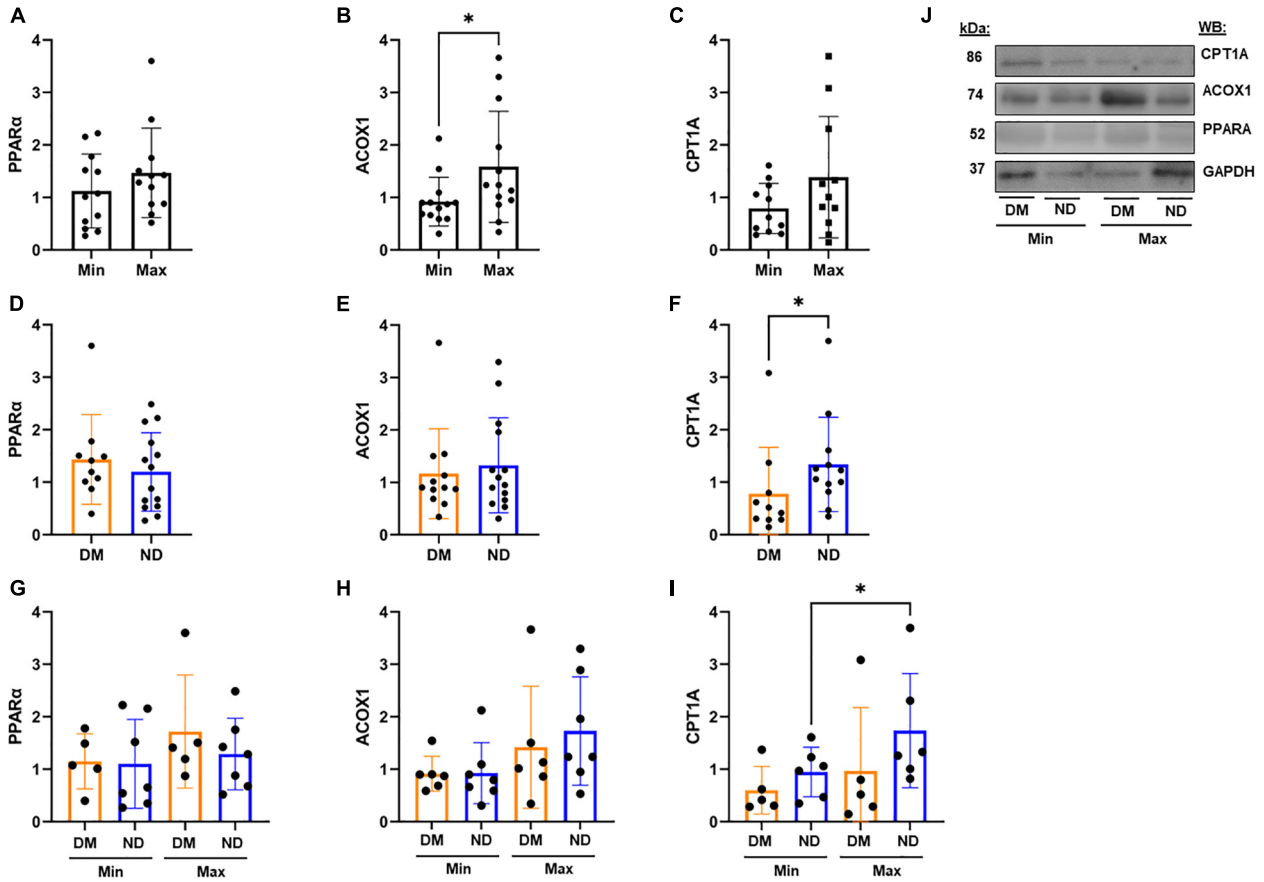

FIGURE 6 | Western Blot Analysis from Lower Extremity Segments in Varying Disease and Diabetic Status. **(A–C)** In lower extremity arterial segments, we found no difference in relative PPARα (n = 12) or CPT1A (n = 11) abundance between Min or Max segments. However, we found Min segments demonstrate a decrease in ACOX1 compared to Max samples ($p < 0.05$, n = 13). **(D–F)** We found no difference in relative PPARα abundance between patients with and without diabetes. ACOX1 demonstrated decreased expression in patients with diabetes (n = 13) compared to patients without diabetes (n = 13), and CPT1A similarly showed a decrease in expression in patients with diabetes (n = 10) compared to patients without (n = 12). **(G–I)** Subdividing tissue segments into both disease and diabetic status showed no significant variability in PPARα or ACOX1 expression. However, CPT1A expression was decreased in Min samples compared to Max samples in patients without diabetes (n = 6). **(J)** Representative Western Blots from analysis. Samples were normalized to GAPDH content. DM, Diabetic. ND, Non-diabetic. Min, Minimally diseased. Max, Maximally diseased. Data are presented as Mean ± SD, and each point represents one patient sample. *$p < 0.05$.

regions that are prone to high burden of atherosclerotic disease progression in patients with cardiovascular risk factors such as diabetes and hyperlipidemia (11–14). We observed that *ppara* and its downstream genes, *acox1* and *cpt1a,* indeed have significant variable expression between individuals with and without diabetes in both carotid and lower leg arterial tissue. In particular, Min tissue from CEA plaques and lower extremities both demonstrated lower ACOX1. Interestingly, in CEA tissue, we observed that PPARα was significantly higher in patients with diabetes, and had a significant positive correlation with hemoglobin A1c and fasting glucose. PPARα is a key transcription factor for downstream genes such as *acox1* and *cpt1a*, which both also significantly correlated with hemoglobin A1c levels. On the other hand, in lower extremity arterial segments, *ppara, acox1,* and *cpt1a* all had lower expression in individuals with diabetes. CPT1A was also lower in lower extremity arterial tissue from individuals with diabetes. Furthermore, Min segments demonstrated a negative correlation between *ppara* and hemoglobin A1c. Taken together these findings demonstrate that in the setting of diabetes, *ppara* expression and signaling is highly variable in different arterial beds—particularly in the carotid and lower leg arterial systems. These observations may have important implications in understanding risk factors for atheroprogression in these anatomical regions, as well as the impact of current PPARα-targeting pharmacological therapy.

PPARα is a major regulator of lipid metabolism, serum triglycerides, and peripheral atherosclerosis (18, 20, 21, 28). It is expressed as a nuclear membrane protein in metabolic tissue that utilizes β-fatty acid oxidation for cellular signaling and homeostasis (29–31). In organ tissue such as liver, kidney, heart, and muscle, PPARα is activated by lipid precursors such as phosphatidylcholines (PCs), and forms a heterodimer with retinoid X receptor (RXR) to activate downstream target genes such as *acox1* and *cpt1a*

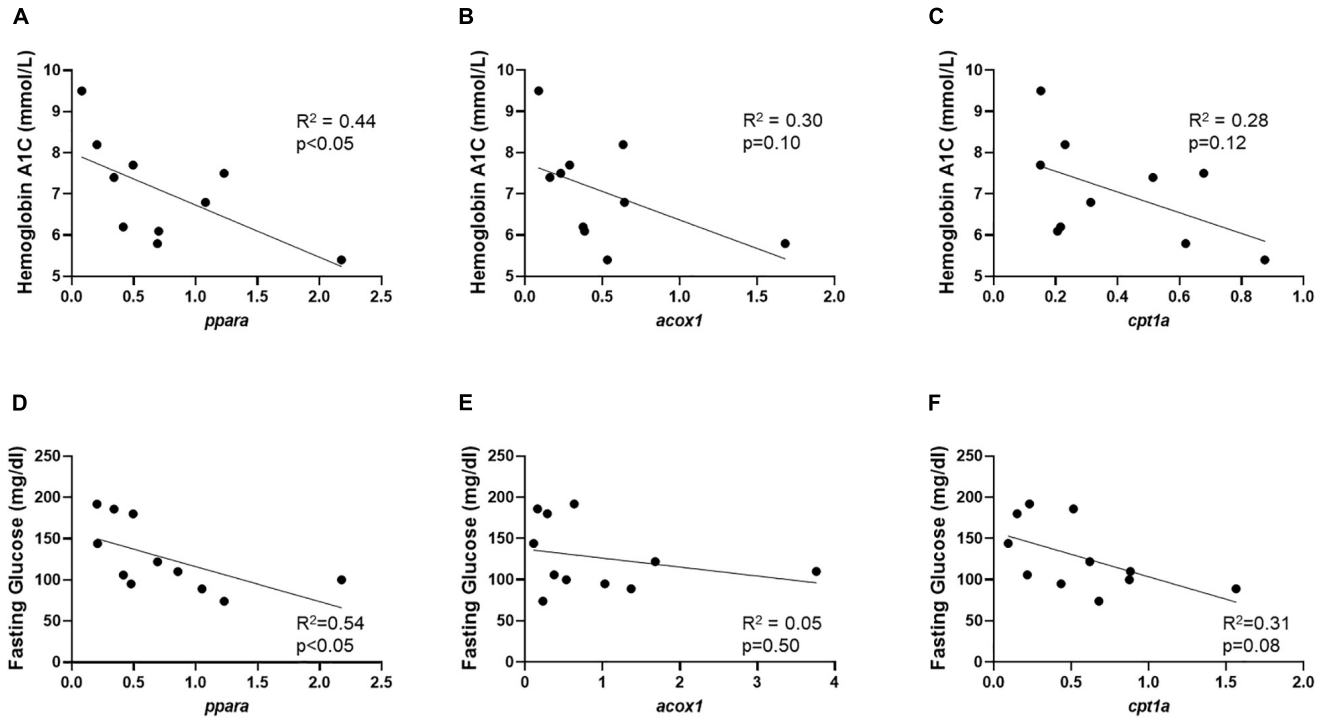

FIGURE 7 | Min lower extremity mRNA correlates with HbA1c and fasting glucose content. **(A)** Min-diseased lower extremity segment relative mRNA content demonstrates significant negative correlation between *ppara* ($p < 0.05$, $R^2 = 0.44$, $n = 10$) compared to HbA1c content. **(B,C)** No significant correlation was observed between *acox1* ($p = 0.10$, $R^2 = 0.30$, $n = 10$) and *cpt1a* ($p = 0.12$, $R^2 = 0.28$, $n = 10$) relative mRNA abundance compared to HbA1c content in Min-diseased lower extremity segments. **(D)** Min-diseased lower extremity segment *ppara* ($p < 0.05$, $R^2 = 0.54$, $n = 11$) relative mRNA abundance shows significant correlation with fasting glucose. **(E,F)** No significant correlation was observed between fasting glucose and *axoc1* ($p = 0.50$, $R^2 = 0.05$, $n = 11$) or *cpt1a* ($p = 0.08$, $R^2 = 0.31$, $n = 11$) relative mRNA abundance.

(17, 32–36). While PPARα has hundreds of downstream targets, upregulation of *acox1* is critically important for peroxisomal fatty acid beta-oxidation that breaks down very long-chain fatty acids (34, 37). Similarly, PPARα activates *cpt1a* which is responsible for attaching carnitine subgroups to long-chain fatty acids so that they can be metabolized in the mitochondria to produce ATP (38). While PPARα expression is thought to modulate inflammation and reduce atherosclerosis in the vessel wall, it is largely unknown what roles its downstream genes *acox1* and *cpt1a* play in accumulating saturated fatty acids and contribute to atheroprogression in carotid and lower extremity arterial distributions (18–21).

Previous studies have evaluated the impact of targeting PPARα on atheroprogression. For example, the FIELD study is a multi-center, prospective, randomized clinical trial that evaluated the impact of fenofibrate, a PPARα-agonist, on cardiovascular outcomes in individuals with diabetes (39). The study observed no difference in primary composite endpoints of coronary artery disease, death, and non-fatal myocardial infarction (MI). However, the study secondary composite endpoint of total cardiovascular disease events were reduced in patients who were randomized to fenofibrate. In fact, the study uniquely demonstrated that treatment with fenofibrate can decrease the risk of lower extremity amputations, particularly minor amputations without known large-vessel inflow arterial obstruction in the upper leg. These findings suggested that fenofibrate can potentially impact atheroprogression in lower extremity arterial beds. Several subsequent studies have argued that the impact of fenofibrate on the peripheral arterial tissue may be occurring though non-lipid mechanisms (40, 41), and determining the impact of fenofibrate on peripheral arterial tissue remains a topic of investigation.

Similar studies have also evaluated the impact of PPARα signaling in carotid atheroprogression. A within-gene haplotype analysis demonstrated that *ppara* was one of 10 genes that impacts inflammation and endothelial function in individuals with dense carotid plaque as demonstrated on ultrasound B-mode imaging (42). Genotyping of genetic variants in > 3,300 individuals from the Framingham Offspring Study also demonstrated that a *ppara* genetic variant (L162V) was associated with incidence of carotid artery stenosis (43). Pharmacological targeting of PPARα with fenofibrate in pre-clinical models has demonstrated atherosclerotic plaque regression in the setting of hyperlipidemia (44). In human subjects, fenofibrate has also been linked to reduced carotid intima-media thickness in a subpopulation of individuals with diabetes in the FIELD study, highlighting the systemic benefits of reduced hypertriglyceridemia, as well as the potential benefits of reducing carotid

atheroprogression (45). Our study builds on this, and examines whether *ppara* and its downstream genes are differentially expressed relative to disease severity and diabetes status.

Our study observed different gene expression patters of *ppara*, *acox1*, and *cpt1a* in carotid and lower extremity arterial tissue, suggesting that atherosclerotic disease progression is unlikely homogeneous. We similarly observed that other critical lipid mediators are differentially expressed and activated in carotid and lower extremity arterial tissue (23, 46, 47). For example, choline-ethanolamine phosphotransferase 1 (CEPT1), a key regulator of *de novo* phospholipogenesis, is highly expressed in Min-diseased carotid arterial segments particularly in individuals with diabetes (22). Here we observed similar patterns in Min-diseased CEA segments from individuals with diabetes, which demonstrated higher relative *ppara, acox1,* and *cpt1a* mRNA abundance. Taken in context with our previous observations demonstrating increased pro-inflammatory phospholipid content in Min diseased CEA segments, altered beta-fatty acid oxidation signaling via *ppara* may be contributing to endothelial dysfunction, inflammation, and foam cell development—leading to further atheroprogression in at risk populations (48–51). Ongoing studies are evaluating whether similar gene expression patterns are also evident in individuals with other risk factors such as age and smoking habits.

In the lower extremity, we observed totally different gene expression patterns and correlations. Specifically, we observed lower relative *ppara*, *acox1*, and *cpt1a* mRNA abundance from patients with diabetes, and a negative correlation between *ppara* mRNA abundance, hemoglobin A1c, and fasting glucose. These findings are striking given their clear divergence from observations on CEA tissues. These findings suggest that in the setting of diabetes arterial beds vary in β-fatty acid oxidation metabolism particularly in lower extremities compared to carotid arteries. We previously observed similar expression patterns in CEPT1 metabolism in Max-diseased lower extremity arterial segments, suggesting that arterial lipid metabolism is significantly impacted by disease progression and endothelial dysfunction in these segments (23). Interestingly, our current study did not observe that DCSI score was indicative of altered β-fatty acid oxidation. We suspect that this may be either due to the multi-factorial DCSI scoring algorithm that is not entirely based on severity of peripheral arterial disease, or may be due to lack of statistical power in the current analysis. Ongoing investigation in larger populations, and utilization of additional surrogate measurements for peripheral arterial disease severity, will help further clarify to what extent *ppara* gene expression is impacted by atherosclerotic disease severity in the setting of diabetes.

We acknowledge that our current study has some limitations. First, the limited number of patients could have led to some sampling errors, and may not have fully accounted for the range of co-morbidities that can impact carotid and lower extremity atheroprogression. Ongoing studies are prospectively enrolling larger patient populations to validate our reported study findings. Second, due to the number of recruited patients, we were not able to fully match gene expression analysis by age, co-morbidities, and sex demographics. It is possible that such demographics, in addition to smoking history and variation in lipid parameters (total cholesterol, LDL, and HDL), could have impacted our study results. Third, RNA analysis with RTPCR was limited to CEA or lower leg arterial segments, and did not differentiate cell types with in the tissue specimens. Due to the severity of occlusive disease in patients undergoing lower extremity amputation, harvesting a completely "healthy" sample as a control for analysis was not possible. Alternatively, Min-diseased segments were routinely harvested and served as an internal patient control for gene expression analysis. Finally, despite careful tissue sample dissection, we acknowledge that carotid and lower extremity arterial tissue represents a heterogenous cellular phenotype. Future analysis with single-cell techniques can help further delineate expression patterns across unique cell types of interest.

In conclusion, we report novel findings on the variable *ppara* gene expression in Min vs. Max CEA and lower extremity arterial segments. We also demonstrate that PPARα downstream genes *acox1* and *cpt1a* have different expression patterns relative to tissue type, arterial disease severity, and patient diabetes status. We postulate that differences in relative *ppara* expression and downstream activation may impact arterial atheroprogression and have important implications on future pharmacotherapy options.

DATA AVAILABILITY STATEMENT

The original contributions presented in the study are included in the article/**Supplementary Material**, further inquiries can be directed to the corresponding author.

ETHICS STATEMENT

The studies involving human participants were reviewed and approved by Washington University School of Medicine IRB. The patients/participants provided their written informed consent to participate in this study.

AUTHOR CONTRIBUTIONS

CE, NH, GD, CS, and MZ: conception and design. CE, NH, RM, AP, XJ, CS, and MZ: analysis and interpretation. CE, NH, RM, AP, and MS: data collection. CE and MZ: writing the manuscript. CE, NH, RM, AP, MS, XJ, GD, CS, and MZ: critical revision and final approval of the manuscript. CE, AP, and XJ: statistical analysis. MZ: obtained funding and overall responsibility. All authors contributed to the article and approved the submitted version.

FUNDING

This work was supported by the Washington University School of Medicine Vascular Surgery Biobank Core Facility, Hope Center Alafi Neuroimaging Lab, Vascular Cures Foundation Wylie Scholar Award (MZ), American Surgical Association Research Fellowship Award (MZ), Society for Vascular Surgery Foundation Research Investigator Award (MZ), and Neuroscience Blueprint Interdisciplinary Center Core award to Washington University (P30 NS057105). Grant support for this work was provided by the Washington University School of Medicine Diabetes Research Center NIH/NIDDK P30 DK020589 (MZ), NIH/NIDDK R01 DK101392 (CS), NIH/NHLBI K08 HL132060 (MZ), and NIH/NHLBI R01 HL153262 (MZ).

ACKNOWLEDGMENTS

We thank Batool Arif for generous technical assistance and general laboratory supervision, Theresa Belgeri for administrative support, and the Washington University Vascular Biobank Team and Ashley Cosentino for specimen procurement.

SUPPLEMENTARY MATERIAL

The Supplementary Material for this article can be found online at: https://www.frontiersin.org/articles/10.3389/fcvm.2022.834199/full#supplementary-material

REFERENCES

1. Hansen T, Wikström J, Johansson LO, Lind L, Ahlström H. The prevalence and quantification of atherosclerosis in an elderly population assessed by whole-body magnetic resonance angiography. *Arterioscler Thromb Vasc Biol.* (2007) 27:649–54. doi: 10.1161/01.ATV.0000255310.47940.3b
2. Mackinnon AD, Jerrard-Dunne P, Sitzer M, Buehler A, Von Kegler S, Markus HS. Rates and determinants of site-specific progression of carotid artery intima-media thickness: the carotid atherosclerosis progression study. *Stroke.* (2004) 35:2150–4. doi: 10.1161/01.STR.0000136720.21095.f3
3. Kranjec I. Atherosclerotic burden in coronary and peripheral arteries in patients with first clinical manifestation of coronary artery disease. *J Cardiovasc Med.* (2011) 12:297–9. doi: 10.2459/JCM.0b013e328343e962
4. Weitz JI, Byrne J, Patrick Clagett G, Farkouh ME, Porter JM, Sackett DL, et al. Diagnosis and treatment of chronic arterial insufficiency of the lower extremities: a critical review. *Circulation.* (1996) 94:3026–49. doi: 10.1161/01.CIR.94.11.3026
5. Agnelli G, Belch JJF, Baumgartner I, Giovas P, Hoffmann U. Morbidity and mortality associated with atherosclerotic peripheral artery disease: a systematic review. *Atherosclerosis.* (2020) 293:94–100. doi: 10.1016/j.atherosclerosis.2019.09.012
6. Virani SS, Alonso A, Benjamin EJ, Bittencourt MS, Callaway CW, Carson AP, et al. Heart disease and stroke statistics—2020 update: a report from the American Heart Association. *Circulation.* (2020) 141:e139–596. doi: 10.1161/CIR.0000000000000757
7. Timsit SG, Sacco RL, Mohr JP, Foulkes MA, Tatemichi TK, Wolf PA, et al. Early clinical differentiation of cerebral infarction from severe atherosclerotic stenosis and cardioembolism. *Stroke.* (1992) 23:486–91. doi: 10.1161/01.STR.23.4.486
8. Inzitari D, Eliasziw M, Gates P, Sharpe BL, Chan RKT, Meldrum HE, et al. The causes and risk of stroke in patients with asymptomatic internal-carotid-artery stenosis. *N Engl J Med.* (2000) 342:1693–700. doi: 10.1056/NEJM200006083422302
9. Famakin BM, Chimowitz MI, Lynn MJ, Stern BJ, George MG. Causes and severity of ischemic stroke in patients with symptomatic intracranial arterial stenosis. *Stroke.* (2009) 40:1999–2003. doi: 10.1161/STROKEAHA.108.546150
10. Ahmad N, Thomas GN, Chan C, Gill P. Ethnic differences in lower limb revascularisation and amputation rates. Implications for the aetiopathology of atherosclerosis?. *Atherosclerosis.* (2014) 233:503–7. doi: 10.1016/j.atherosclerosis.2013.12.039
11. Stavroulakis K, Borowski M, Torsello G, Bisdas T, Adili F, Balzer K, et al. Association between statin therapy and amputation-free survival in patients with critical limb ischemia in the CRITISCH registry. *J Vasc Surg.* (2017) 66:1534–42. doi: 10.1016/j.jvs.2017.05.115
12. Henry RMA, Kostense PJ, Dekker JM, Nijpels G, Heine RJ, Kamp O, et al. Carotid arterial remodeling. A maladaptive phenomenon in type 2 diabetes but not in impaired glucose metabolism: the hoorn study. *Stroke.* (2004) 35:671–6. doi: 10.1161/01.STR.0000115752.58601.0B
13. Nelson RH. Hyperlipidemia as a risk factor for cardiovascular disease. *Primary Care.* (2013) 40:195–211. doi: 10.1016/j.pop.2012.11.003
14. Lee JS, Chang PY, Zhang Y, Kizer JR, Best LG, Howard BV. Triglyceride and HDL-C dyslipidemia and risks of coronary heart disease and ischemic stroke by glycemic dysregulation status: the strong heart study. *Diabetes Care.* (2017) 40:529–37. doi: 10.2337/dc16-1958
15. Wang YX. PPARs: diverse regulators in energy metabolism and metabolic diseases. *Cell Res.* (2010) 20:124–37. doi: 10.1038/cr.2010.13
16. Minnich A, Tian N, Byan L, Bilder G. A potent PPARα agonist stimulates mitochondrial fatty acid β-oxidation in liver and skeletal muscle. *Am J Physiol Endocrinol Metab.* (2001) 280:270–9. doi: 10.1152/ajpendo.2001.280.2.e270
17. Schoonjans K, Peinado-Onsurbe J, Lefebvre AM, Heyman RA, Briggs M, Deeb S, et al. PPARalpha and PPARgamma activators direct a distinct tissue-specific transcriptional response via a PPRE in the lipoprotein lipase gene. *EMBO J.* (1996) 15:5336–48. doi: 10.1002/j.1460-2075.1996.tb00918.x
18. Zandbergen F, Plutzky J. PPARα in atherosclerosis and inflammation. *Biochim Biophys Acta.* (2007) 1771:972–82. doi: 10.1016/j.bbalip.2007.04.021
19. Marx N, Sukhova GK, Collins T, Libby P, Plutzky J. PPAR α activators inhibit cytokine-induced vascular cell adhesion molecule-1 expression in human endothelial cells. *Circulation.* (1999) 99:3125–31. doi: 10.1161/01.CIR.99.24.3125
20. Marx N, Kehrle B, Kohlhammer K, Grüb M, Koenig W, Hombach V, et al. PPAR activators as antiinflammatory mediators in human T lymphocytes: implications for atherosclerosis and transplantation-associated arteriosclerosis. *Circ Res.* (2002) 90:703–10. doi: 10.1161/01.RES.0000014225.20727.8F
21. Pawlak M, Lefebvre P, Staels B. Molecular mechanism of PPARα action and its impact on lipid metabolism, inflammation and fibrosis in non-alcoholic fatty liver disease. *J Hepatol.* (2015) 62:720–33. doi: 10.1016/j.jhep.2014.10.039
22. Zayed MA, Hsu FF, Patterson BW, Yan Y, Naim U, Darwesh M, et al. Diabetes adversely affects phospholipid profiles in human carotid artery endarterectomy plaques. *J Lipid Res.* (2018) 59:730–8. doi: 10.1194/jlr.M081026
23. Zayed MA, Jin X, Yang C, Belaygorod L, Engel C, Desai K, et al. CEPT1-mediated phospholipogenesis regulates endothelial cell function and ischemia-induced angiogenesis through PPARα. *Diabetes.* (2021) 70:549–61. doi: 10.2337/db20-0635
24. Grundy SM, Cleeman JI, Bairey Merz CN, Brewer HB, Clark LT, Hunninghake DB, et al. Implications of recent clinical trials for the National Cholesterol Education Program Adult Treatment Panel III guidelines. *Circulation.* (2004) 110:227–39. doi: 10.1161/01.CIR.0000133317.49796.0E
25. Young BA, Lin E, Von Korff M, Simon G, Ciechanowski P, Ludman EJ, et al. Diabetes complications severity index and risk of mortality, hospitalization, and healthcare utilization. *Am J Manag Care.* (2008) 14:15–24.
26. Hetterich H, Webber N, Willner M, Herzen J, Birnbacher L, Hipp A, et al. AHA classification of coronary and carotid atherosclerotic plaques by grating-based phase-contrast computed tomography. *Eur Radiol.* (2016) 26:3223–33. doi: 10.1007/s00330-015-4143-z

27. Zayed MA, Yuan W, Leisner TM, Chalothorn D, McFadden AW, Schaller MD, et al. CIB1 regulates endothelial cells and ischemia-induced pathological and adaptive angiogenesis. *Circ Res.* (2007) 101:1185–93. doi: 10.1161/CIRCRESAHA.107.157586
28. Auwerx J, Schoonjans K, Fruchart JC, Staels B. Regulation of triglyceride metabolism by PPARs: fibrates and thiazolidinediones have distinct effects. *J Atheroscler Thromb.* (1996) 3:81–9. doi: 10.5551/jat1994.3.81
29. Moreno M, Lombardi A, Silvestri E, Senese R, Cioffi F, Goglia F, et al. PPARs: nuclear receptors controlled by, and controlling, nutrient handling through nuclear and cytosolic signaling. *PPAR Res.* (2010) 2010:435689. doi: 10.1155/2010/435689
30. Chakravarthy MV, Pan Z, Zhu Y, Tordjman K, Schneider JG, Coleman T, et al. "New" hepatic fat activates PPARα to maintain glucose, lipid, and cholesterol homeostasis. *Cell Metab.* (2005) 1:309–22. doi: 10.1016/j.cmet.2005.04.002
31. Akiyama TE, Nicol CJ, Fievet C, Staels B, Ward JM, Auwerx J, et al. Peroxisome proliferator-activated receptor-α regulates lipid homeostasis, but is not associated with obesity. Studies with congenic mouse lines. *J Biol Chem.* (2001) 276:39088–93. doi: 10.1074/jbc.M107073200
32. Chandra V, Huang P, Hamuro Y, Raghuram S, Wang Y, Burris TP, et al. Structure of the intact PPAR-γ-RXR-α nuclear receptor complex on DNA. *Nature.* (2008) 456:350–6. doi: 10.1038/nature07413
33. Braissant O, Foufelle F, Scotto C, Dauca M, Wahli W. Differential expression of peroxisome proliferator-activated receptors (PPARs): tissue distribution of PPAR-α, -β, and -γ in the adult rat. *Endocrinology.* (1996) 137:354–66. doi: 10.1210/endo.137.1.8536636
34. Kersten S, Rakhshandehroo M, Knoch B, Müller M. Peroxisome proliferator-activated receptor alpha target genes. *PPAR Res.* (2010) 2010:612089. doi: 10.1155/2010/612089
35. Plutzky J. The PPAR-RXR transcriptional complex in the vasculature: energy in the balance. *Circ Res.* (2011) 108:1002–16. doi: 10.1161/CIRCRESAHA.110.226860
36. Chakravarthy MV, Lodhi IJ, Yin L, Malapaka RRV, Xu HE, Turk J, et al. Identification of a physiologically relevant endogenous ligand for PPARα in liver. *Cell.* (2009) 138:476–88. doi: 10.1016/j.cell.2009.05.036
37. Rakhshandehroo M, Hooiveld G, Müller M, Kersten S. Comparative analysis of gene regulation by the transcription factor PPARα between mouse and human. *PLoS One.* (2009) 4:e6796. doi: 10.1371/journal.pone.0006796
38. McGarry JD, Brown NF. The mitochondrial carnitine palmitoyltransferase system. From concept to molecular analysis. *Eur J Biochem.* (1997) 244:1–14. doi: 10.1111/j.1432-1033.1997.00001.x
39. Rajamani K, Colman PG, Li LP, Best JD, Voysey M, D'Emden MC, et al. Effect of fenofibrate on amputation events in people with type 2 diabetes mellitus (FIELD study): a prespecified analysis of a randomised controlled trial. *Lancet.* (2009) 373:1780–8. doi: 10.1016/S0140-6736(09)60698-X
40. Hamilton-Craig I, Kostner KM, Woodhouse S, Colquhoun D. Use of fibrates in clinical practice: queensland lipid group consensus recommendations. *Int J Evid Based Healthc.* (2012) 10:181–90. doi: 10.1111/j.1744-1609.2012.00275.x
41. Belfort R, Berria R, Cornell J, Cusi K. Fenofibrate reduces systemic inflammation markers independent of its effects on lipid and glucose metabolism in patients with the metabolic syndrome. *J Clin Endocrinol Metab.* (2010) 95:829–36. doi: 10.1210/jc.2009-1487
42. Gardener H, Beecham A, Cabral D, Yanuck D, Slifer S, Wang L, et al. Carotid plaque and candidate genes related to inflammation and endothelial function in hispanics from Northern Manhattan. *Stroke.* (2011) 42:889–96. doi: 10.1161/STROKEAHA.110.591065
43. Elosua R, Cupples LA, Fox CS, Polak JF, D'Agostino RA, Wolf PA, et al. Association between well-characterized lipoprotein-related genetic variants and carotid intimal medial thickness and stenosis: the Framingham Heart Study. *Atherosclerosis.* (2006) 189:222–8. doi: 10.1016/j.atherosclerosis.2005.12.005
44. Corti R, Osende J, Hutter R, Viles-Gonzalez JF, Zafar U, Valdivieso C, et al. Fenofibrate induces plaque regression in hypercholesterolemic atherosclerotic rabbits: *in vivo* demonstration by high-resolution MRI. *Atherosclerosis.* (2007) 190:106–13. doi: 10.1016/j.atherosclerosis.2006.02.036
45. Harmer JA, Keech AC, Veillard A-S, Skilton MR, Watts GF, Celermajer DS. Fenofibrate effects on carotid artery intima-media thickness in adults with type 2 diabetes mellitus: a FIELD substudy. *Diabetes Res Clin Prac.* (2018) 141:156–67. doi: 10.1016/j.diabres.2018.05.006
46. Tay S, Silva GSD, Engel CM, Harroun N, Penrose AS, Desai KA, et al. Prevalence of elevated serum fatty acid synthase in chronic limb - threatening ischemia. *Sci Rep.* (2021) 11:19272. doi: 10.1038/s41598-021-98479-7
47. De Silva GS, Desai K, Darwech M, Naim U, Jin X, Adak S, et al. Circulating serum fatty acid synthase is elevated in patients with diabetes and carotid artery stenosis and is LDL-associated. *Atherosclerosis.* (2019) 287:38–45. doi: 10.1016/j.atherosclerosis.2019.05.016
48. Daniel LW, King L, Waite M. Source of arachidonic acid for prostaglandin synthesis in Madin-Darby canine kidney cells. *J Biol Chem.* (1981) 256:12830–5. doi: 10.1016/s0021-9258(18)42970-5
49. Miyazawa T, Nakagawa K, Shimasaki S, Nagai R. Lipid glycation and protein glycation in diabetes and atherosclerosis. *Amino Acids.* (2012) 42:1163–70. doi: 10.1007/s00726-010-0772-3
50. Kume S, Takeya M, Mori T, Araki N, Suzuki H, Horiuchi S, et al. Immunohistochemical and ultrastructural detection of advanced glycation end products in atherosclerotic lesions of human aorta with a novel specific monoclonal antibody. *Am J Pathol.* (1995) 147:654–67.
51. Summerhill VI, Grechko AV, Yet SF, Sobenin IA, Orekhov AN. The atherogenic role of circulating modified lipids in atherosclerosis. *Int J Mol Sci.* (2019) 20:3561. doi: 10.3390/ijms20143561

Conflict of Interest: The authors declare that the research was conducted in the absence of any commercial or financial relationships that could be construed as a potential conflict of interest.

Publisher's Note: All claims expressed in this article are solely those of the authors and do not necessarily represent those of their affiliated organizations, or those of the publisher, the editors and the reviewers. Any product that may be evaluated in this article, or claim that may be made by its manufacturer, is not guaranteed or endorsed by the publisher.

frontiers | Frontiers in Cardiovascular Medicine

ORIGINAL RESEARCH
published: 20 June 2022
doi: 10.3389/fcvm.2022.875244

Urinary Fatty Acid Binding Protein 3 Has Prognostic Value in Peripheral Artery Disease

Ben Li[1], *Abdelrahman Zamzam*[1], *Muzammil H. Syed*[1], *Niousha Jahanpour*[1], *Shubha Jain*[1], *Rawand Abdin*[2] *and Mohammad Qadura*[1,3,4]*

[1] Division of Vascular Surgery, St. Michael's Hospital, Unity Health Toronto, University of Toronto, Toronto, ON, Canada, [2] Department of Medicine, McMaster University, Hamilton, ON, Canada, [3] Department of Surgery, University of Toronto, Toronto, ON, Canada, [4] Keenan Research Center for Biomedical Science, Li Ka Shing Knowledge Institute, St. Michael's Hospital, Unity Health Toronto, University of Toronto, Toronto, ON, Canada

Background: Despite its significant association with limb loss and death, peripheral artery disease (PAD) remains underdiagnosed and undertreated. The current accepted gold-standard for PAD screening, the ankle brachial index (ABI), is limited by operator dependence, erroneous interpretation, and unreliability in patients with diabetes. Fatty acid binding protein 3 (FABP3) is an intracellular protein that becomes released into circulation and excreted into urine following skeletal muscle injury. We examined the prognostic ability of urinary FABP3 (uFABP3) in predicting adverse PAD-related events.

Methods: In this prospective case-control study, urine samples were collected from patients with PAD (n = 142) and without PAD (n = 72). The cohort was followed for 2 years. uFABP3 was normalized to urinary creatinine (uCr) (uFABP3/uCr). The primary outcome was major adverse limb event (MALE; composite of vascular intervention [open or endovascular] or major limb amputation). The secondary outcome was worsening PAD status (drop in ABI≥0.15). Cox regression analyses with multivariable adjustment for baseline demographic and clinical variables were performed to assess the prognostic value of uFABP3/uCr with regards to predicting MALE and worsening PAD status.

Results: Patients with PAD had significantly higher median [IQR] uFABP3/uCr levels (3.46 [2.45–6.90] vs. 2.61 [1.98–4.62], p = 0.001). MALE and worsening PAD status were observed in 21 (10%) and 28 (14%) patients, respectively. uFABP3/uCr predicted MALE and worsening PAD status with adjusted hazard ratios (HR) of 1.28 (1.16–1.41, p = 0.001) and 1.16 (1.02–1.27, p = 0.021), respectively. Patients with high uFABP3/uCr had a lower 2-year freedom from MALE (86 vs. 96%, p = 0.047) and worsening PAD status (78 vs. 99%, p = 0.001). There was good discriminatory ability for uFABP3/uCr in predicting the primary outcome of MALE, with an area under the receiver operating characteristics curve (AUROC) of 0.78.

Conclusions: Measuring uFABP3/uCr levels in patients with PAD can help identify those at high risk of adverse PAD-related events. This study highlights the prognostic value of uFABP3 in risk-stratifying individuals for further diagnostic vascular evaluation or aggressive medical management.

Keywords: fatty acid binding protein 3, urine, prognosis, peripheral artery disease, biomarker

OPEN ACCESS

Edited by:
Michal Mokry,
University Medical Center Utrecht, Netherlands

Reviewed by:
Rie Matsumori,
Juntendo University, Japan
Yi-Bang Cheng,
Shanghai Institute of Hypertension, China

***Correspondence:**
Mohammad Qadura
mohammad.qadura@utoronto.ca

Specialty section:
This article was submitted to Atherosclerosis and Vascular Medicine, a section of the journal Frontiers in Cardiovascular Medicine

Received: *14 February 2022*
Accepted: *05 May 2022*
Published: *20 June 2022*

Citation:
Li B, Zamzam A, Syed MH, Jahanpour N, Jain S, Abdin R and Qadura M (2022) Urinary Fatty Acid Binding Protein 3 Has Prognostic Value in Peripheral Artery Disease. Front. Cardiovasc. Med. 9:875244. doi: 10.3389/fcvm.2022.875244

INTRODUCTION

Peripheral artery disease (PAD) involves atherosclerosis of the lower extremity arteries and affects over 200 million people worldwide (1). Despite its significant association with limb loss and death, PAD remains undertreated (2). As a result, patients with PAD usually have worse long-term prognosis compared to patients with coronary artery disease (3). One reason for this is the lack of a validated prognostic biomarker for PAD (4). The ankle brachial index (ABI) is currently the only validated screening tool for PAD; however, it is limited by operator dependence, erroneous interpretation, and unreliability in patients with diabetes due to calcified vessels (5, 6). Furthermore, ABI's are rarely performed in the primary care setting due to generalists' lack of comfort with performing and interpretating this test (7). A recent survey found that 79% of primary care providers did not perform ABI's routinely in their clinical practice, citing time constraints, unavailability of skilled personnel, and complexity of result interpretation as major barriers (8). Most clinicians viewed alternative forms of diagnosis, such as a blood or urine test, as preferable to ABI's and would enhance diagnostic simplicity and efficiency (8). Therefore, the identification and validation of a biomarker for PAD may improve cardiovascular risk stratification through early initiation of aggressive medical management, close ambulatory follow up, and arterial interventions.

In addition, ABI's are poor predictors of PAD-related complications (9). Pasqualini et al. (2012) showed that both low and high ABI were associated with cardiovascular mortality (10). Furthermore, Hatmi et al. (2014) demonstrated that a low ABI only had a sensitivity of 64% for predicting adverse cardiovascular events (11). Identification of better prognostic markers for PAD-related complications would improve risk-stratification and allow clinicians to identify patients who require further diagnostic evaluation, close follow-up, and aggressive medical/surgical therapy. For example, the Cardiovascular Outcomes for People Using Anticoagulation Strategies (COMPASS) trial demonstrated a significant reduction in major adverse cardiovascular events for patients with atherosclerotic vascular disease taking low-dose rivaroxaban (2.5 mg oral twice daily) in addition in ASA (12). Therefore, identifying high-risk PAD patients using a novel prognostic biomarker can allow clinicians to better select patients for intensive medical therapy including COMPASS trial low-dose rivaroxaban.

Fatty acid binding protein 3 (FABP3) is an intracellular protein that is normally absent from plasma but becomes released into circulation and excreted into urine following skeletal muscle injury, which may occur due to ischemia from PAD (13). Previous groups have demonstrated that FABP3 is associated with mitochondrial dysfunction, metabolic syndrome, and cardiovascular disease (14, 15). We previously demonstrated that FABP3 is associated with both the presence of PAD and severity of disease (16, 17). Given that urine samples can be obtained non-invasively and require less health care resources/personnel to collect and test compared to blood specimens, we assessed the diagnostic and prognostic value of urinary FABP3 (uFABP3) in PAD.

METHODS

Ethics Approval

This study received approval from the research ethics board at Unity Health Toronto, University of Toronto, Canada. Informed consent was obtained from all participants, and all method were carried out in accordance with the World Medical Association Declaration of Helsinki (18).

Patient Recruitment

A single-center prospective case-control study was conducted. Consecutive patients with and without PAD presenting to vascular surgery ambulatory clinics at St. Michael's Hospital, University of Toronto between April-December 2019 were recruited. PAD was defined as ABI < 0.9 or toe brachial index (TBI) < 0.67 and absent/diminished pedal pulses (19). Patients with chronic kidney disease (estimated glomerular filtration rate < 60 mL/min/1.73 m^2), acute ischemia or acute on chronic limb threatening ischemia, or acute coronary syndrome, congestive heart failure, uncontrolled arrhythmia, or elevated troponin within the past 12 months were excluded. Patients with recent cardiac disease were excluded to reduce the risk of confounding because FABP3 can be released secondary to myocardial ischemia and troponin elevation.

Demographic and Clinical Characteristics

A complete medical history, physical exam, ABI values and symptomatic status relating to PAD were collected for each patient prior to recruitment. Baseline demographic and clinical characteristics recorded included age, sex, and history of hypertension (systolic blood pressure $\geq$ 130 mmHg, diastolic blood pressure $\geq$80 mmHg, or taking blood pressure lowering therapy), dyslipidemia (total cholesterol $>$5.2 mmol/L, triglyceride $>$1.7 mmol/L, or taking lipid lowering therapy), diabetes (hemoglobin A1c $\geq$ 6.5% or taking an antidiabetic medication), smoking (current or past), coronary artery disease, congestive heart failure, and ABI (16). Definitions for cardiovascular risk factors were based on American College of Cardiology guidelines (20, 21). Risk-reduction medications recorded included statins, angiotensin converting enzyme inhibitors (ACE-I) or angiotensin II receptor blockers (ARB), beta blockers, diuretics, acetylsalicylic acid (ASA), antiplatelets other than ASA, and low-dose rivaroxaban (2.5 mg oral twice daily).

Urinary Sample Collection and FABP3 Multiplex Assay

Mid-stream urine samples were collected, aliquoted, and stored at -80°C prior to analysis. Urine samples were thawed on ice prior to analysis. To determine the concentration of FABP3 levels in the urine, samples were examined in duplicate using the MILLIPLEX MAP Human Cardiovascular Disease Magnetic Bead Panel 1 (EMD-Millipore; Billerica, MA) (22). To minimize any inter-assay variability, all analyses were carried out on the same day. Sample intra-assay and inter-assay coefficients of variability were $<$10%, which meets the threshold for statistical acceptability (23). Prior to any sample analysis, Fluidics

Verification and Calibration bead kits (Luminex Corp) (24) were used to calibrate the MagPix analyzer (Luminex Corp; Austin, Texas) (25). At least 50 beads for uFABP3 were acquired using Luminex xPonent software and analyzed using Milliplex Analyst software (v5.1; EMD-Millipore) (26).

Normalization of UFABP3 to Urinary Creatinine

Urine creatinine (uCr) levels were measured at the core laboratory at St. Michael's Hospital, University of Toronto using the Beckman Coulter AU680 laboratory analyzer (Beckman Coulter; Pasadena, California) (27). The uFABP3 concentration was normalized to uCr using single-spot urine samples (uFABP3/uCr: μg/g). This allowed for adjustment in urinary concentration errors and differences in hydration status.

Follow-Up and Outcomes

Outpatient clinic visits were performed at 12-months as well as at the end of the study. During these follow-up visits, ABI was recorded in addition to PAD symptomatic status, PAD related interventions "revascularization or amputation," and any changes made to concomitant treatment. Information regarding PAD-related hospitalizations and emergency room admissions was also collected. The primary outcome was 2-year major adverse limb events (MALE), defined as need for vascular intervention (open or endovascular lower extremity revascularization) or major amputation (any lower extremity amputation above the ankle). The individual components of MALE were also investigated. The secondary outcome was 2-year worsening PAD, defined as ABI drop $\geq$0.15, which has previously been demonstrated to be clinically relevant (28–30).

Statistical Analysis

Baseline demographic and clinical characteristics were summarized as means and standard deviations (SDs) or numbers and proportions. Baseline differences between groups were calculated using independent *t*-test for continuous variables and chi-square test for categorical variables. uFABP3/uCr levels were not normally distributed, as determined by the Kolmogorov–Smirnov test, and were summarized as medians and interquartile ranges (IQRs). Event rates for MALE, vascular intervention, major amputation, and worsening PAD status (drop in ABI $\geq$ 0.15) at 2 years were reported for the overall cohort and compared between PAD and non-PAD patients using chi-square test. Hazard ratios (HRs) and 95% confidence intervals (95% CIs) for events per one unit increase in uFABP3/uCr were calculated using univariable and multivariable models, which were adjusted for age, sex, hypertension, dyslipidemia, diabetes, smoking, coronary artery disease, congestive heart failure, medications (statins, ACE-I/ARB, beta blockers, diuretics, ASA, antiplatelets other than ASA, and low-dose rivaroxaban), and serum creatinine. To find the relationship between uFAB*P3*/uCr and PAD severity based on ABI, we measured uFAB*P3*/uCr levels in subgroups of patients with no PAD (ABI $\geq$ 0.90), mild PAD (ABI 0.89–0.75), moderate PAD (ABI 0.74–0.50), and severe PAD (ABI $<$ 0.50) as defined by the European Society for Vascular Medicine (ESVM) guidelines and compared the groups using independent *t-test* using the no PAD group as a reference *standard* (31). We also performed subgroup analysis assessing the impact of baseline ABI on outcomes. Using the whole cohort, receiver operator curve (ROC) analysis was conducted to identify a cut-off value for normalized uFABP3/uCr which could stratify our cohort into low and high uFABP3/uCr groups. The cut-off value was chosen based on the highest yielded Youden index. The overall event free survival rates of both groups were displayed using Kaplan-Meier curves, and differences between curves were compared with log-rank test. Significance was set at a two-tailed $p < 0.05$. All analyses were carried out using SPSS software version 23 (SPSS Inc., Chicago, Illinois, USA) (32).

RESULTS

Characteristics of Patients With and Without PAD

Two-hundred and fourteen patients were included (142 with PAD and 72 without PAD). Mean age was 68 (SD 11) Years and 33% were female, 67% had hypertension, and 83% were current or past smokers, with no differences between groups. Patients with PAD were more likely to have dyslipidemia (85 vs. 58%, $p = 0.001$), diabetes (39 vs. 10%, $p = 0.001$), and coronary artery disease (CAD) (35 vs. 19%, $p = 0.02$). A greater proportion of patients with PAD were taking statins (87 vs. 62%, p = 0.001) and ACE-I/ARB (59 vs. 39%). Our results demonstrate that 62% of patients with pad received ASA; however, only 3% received low-dose rivaroxaban (2.5 mg oral twice daily) (**Table 1**). At baseline, our data demonstrates that patients with PAD had significantly higher median [IQR] UFABP3/uCr levels (3.46 [2.45–6.90] vs. 2.61 [1.98–4.62], $p = 0.001$).

Two-Year Follow-Up and Clinical Event Rates

Complete 2-year follow-up was available for 201/214 (94%) patients, with a mean duration of 21.4 (SD 5.4) months. Overall, 21/214 (10%) patients had MALE (21/142 [15%, PAD] vs. 0 [non-PAD], $p = 0.001$) and 28/214 (14%) developed worsening PAD status (28/142 [22%, PAD] vs. 0 [non-PAD], $p = 0.001$). Furthermore, 18/214 (8%) required vascular intervention (18/142 [13%, PAD] vs. 0 [non-PAD], $p = 0.002$) and 3/214 (1%) underwent major amputation (3/142 [2%, PAD] vs. 0 [non-PAD], $p = 0.21$) (**Table 2**).

Cox Regression Analysis of Association Between uFABP3/uCr and PAD-Related Outcomes

There was a significant association between one unit increase of uFABP3/uCr and MALE (unadjusted HR 1.24 [95% CI 1.10–1.40], $p = 0.001$; adjusted HR 1.28 [95% CI 1.16–1.41], $p = 0.001$), need for vascular intervention (unadjusted HR 1.15 [95% CI 1.02–1.28], $p = 0.031$; adjusted HR 1.13 [95% CI 1.02–1.26], $p = 0.034$), and worsening PAD status (unadjusted HR 1.15 [95% CI 1.04–1.27], $p = 0.009$; adjusted HR 1.16 [95% CI 1.02–1.27], $p = 0.021$). There was no significant association between uFABP3/uCr and major amputation (unadjusted HR 1.19 [95%

TABLE 1 | Demographic and clinical characteristics of patients with and without peripheral artery disease (PAD).

	Overall ($n = 214$)	Non-PAD ($n = 72$)	PAD ($n = 142$)	*P*
Mean (SD) ‡				
Age, years	68 (11)	68 (12)	69 (10)	0.36
Ankle brachial index	0.78 (0.26)	1.08 (0.09)	0.62 (0.16)	**0.001**
Demographics/ comorbidities: *N* (%) ¶				
Sex, male	144 (67)	49 (68)	95 (67)	0.87
Hypertension	143 (67)	42 (58)	101 (72)	0.05
Dyslipidemia	162 (76)	42 (58)	120 (85)	**0.001**
Diabetes	62 (29)	7 (10)	55 (39)	**0.001**
Smoking (current and past)	178 (83)	55 (76)	123 (87)	0.06
Coronary artery disease	63 (30)	14 (19)	49 (35)	**0.018**
Congestive heart failure	5 (2)	1 (1)	4 (3)	0.46
Medications: *N* (%) ¶				
Statins	164 (79)	44 (62)	120 (87)	**0.001**
ACE-I/ARB	109 (52)	28 (39)	81 (59)	**0.007**
Beta blockers	61 (29)	19 (27)	42 (31)	0.56
Diuretics	16 (8)	3 (4)	13 (10)	0.17
ASA	123 (58)	35 (49)	88 (62)	0.06
Antiplatelets (Other than ASA)	41 (19)	11 (15)	30 (21)	0.30
Rivaroxaban (low dose 2.5 mg oral twice daily)	4 (2)	0 (0)	4 (3)	0.15

‡Compared using independent t-test; ¶Compared using chi-square test; ACE-I, angiotensin converting enzyme inhibitor; ARB, angiotensin II receptor blocker; ASA, acetylsalicylic acid. Bold values represent statistically significant values ($p < 0.05$).

TABLE 2 | Event rates for primary and secondary outcomes.

	Overall ($n = 214$)	Non-PAD ($n = 72$)	PAD ($n = 142$)	*P**
	N (%)	*N* (%)	*N* (%)	
MALE	21 (10)	0 (0)	21 (15)	**0.001**
Vascular intervention	18 (8)	0 (0)	18 (13)	**0.002**
Major amputation	3 (1)	0 (0)	3 (2)	0.21
Worsening PAD (drop in ABI ≥ 0.15)	28 (14)	0 (0)	28 (22)	**0.001**

*MALE, major adverse limb event: composite of vascular intervention and major amputation; PAD, peripheral artery disease; ABI, ankle brachial index; *Compared using chi-square test. Bold values represent statistically significant values ($p < 0.05$).*

CI 0.92–1.55], $p = 0.19$; adjusted HR 1.19 [95% CI 0.81–1.76], $p = 0.32$) (**Table 3**).

Risk Stratification of Patients Based on uFABP3/uCr Levels

Based on receiver operating characteristic (ROC) curve analysis, our data demonstrates an ideal uFABP3/uCr cut-off value for PAD of 2.70 using a Youden index of 54%. We observed a good discriminatory ability of uFABP3/uCr for predicting the primary outcome of MALE with an area under the curve (AUC) of 0.783, sensitivity of 86%, and specificity of 68%. To investigate the potential of uFABP3/uCr in risk stratifying patients, the uFABP3/uCr cut-off value based on ROC curve analysis was used to stratify patients into two groups: low uFABP3/uCr ($\leq 2.70\,\mu g/g$; $n = 79$) and high uFABP3/uCr ($>2.70\,\mu g/g$; $n = 135$). Patients with high uFABP3/uCr were older (70 [SD 9] vs. 65 [SD 12] years, $p = 0.003$), had a lower mean ABI (0.73 [SD 0.24] vs. 0.84 [SD 0.26], $p = 0.006$), and were more likely to be diagnosed with dyslipidemia (81 vs. 68%, $p = 0.035$) and PAD (83 vs. 38%, $p = 0.001$). There were no differences in risk reduction medications between groups, with only 2% of patients with high uFABP3/uCr taking low-dose rivaroxaban.

TABLE 3 | Hazard ratios for events per one unit increase in uFABP3/uCr.

	Unadjusted HR (95% CI)	*P*	Adjusted HR (95% CI)‡	*P*
MALE	1.24 (1.10–1.40)	**0.001**	1.28 (1.16–1.41)	**0.001**
Vascular intervention	1.15 (1.02–1.28)	**0.031**	1.13 (1.02–1.26)	**0.034**
Major amputation	1.19 (0.92–1.55)	0.19	1.19 (0.81–1.76)	0.32
Worsening PAD (drop in ABI ≥ 0.15)	1.15 (1.04–1.27)	**0.009**	1.16 (1.02–1.27)	**0.021**

MALE, major adverse limb event: composite of vascular intervention and major amputation; PAD, peripheral artery disease; ABI, ankle brachial index.
‡Adjusted for age, sex, hypertension, dyslipidemia, diabetes, smoking, coronary artery disease, congestive heart failure, medications (statins, ACE-I/ARB, beta blocker, diuretic, ASA, antiplatelets other than ASA, and low-dose rivaroxaban), and serum creatinine. Bold values represent statistically significant values ($p < 0.05$).

Over the study 2-year period, patients with high uFABP3/uCr were more likely to develop MALE (14 vs. 4%, $p = 0.034$), require a vascular intervention (12 vs. 4%, $p = 0.046$), and have worsening PAD (22 vs. 1%, $p = 0.001$). There was no difference in major amputation rates between groups (2 vs. 0%, $p = 0.18$) (**Table 4**).

Two-Year Event-Free Analysis in Patients With Low and High uFABP3/uCr

MALE-free survival rates at 1 year and 2 years were 97, and 96% in the low uFABP3/uCr group and 94, and 86% in the high uFABP3/uCr group ($p = 0.047$; log rank = 3.64). Freedom from vascular intervention at 1 year and 2 years were 98, and 96% in the low uFABP3/uCr group and 94, and 88% in the high uFABP3/uCr group ($p = 0.045$; log rank = 4.03). On the other hand, there was no significant difference in the event-free survival rate for major amputations between low and high uFABP3/uCr groups ($p = 0.18$; log rank = 1.76). Event-free survival rates for worsening PAD status at 1 year and 2 years were 100% and 99% in the low uFABP3/uCr group and 89, and 78% in the high uFABP3/uCr group ($p = 0.001$; log rank = 16.07) (**Figure 1**).

Subgroup Analysis of uFABP3/uCr Levels and Outcomes Based on PAD Severity

There was a significant correlation between median uFABP3/uCr levels and PAD severity: (ABI ≥ 0.90 [2.61 (IQR 1.98–4.62)],

TABLE 4 | Demographic and clinical characteristics of patients with low and high uFABP3/uCr.

	Low uFABP3/uCr ($n = 79$)	High uFABP3/uCr ($n = 135$)	*P*
Mean (SD) ‡			
Age, years	65 (12)	70 (9)	**0.003**
Ankle brachial index	0.84 (0.26)	0.73 (0.24)	**0.006**
Demographics/ comorbidities: *N* (%) ¶			
Peripheral artery disease	35 (38)	112 (83)	**0.001**
Sex, male	58 (73)	86 (64)	0.18
Hypertension	46 (59)	97 (72)	0.06
Dyslipidemia	53 (68)	109 (81)	**0.035**
Diabetes	17 (22)	45 (33)	0.07
Smoking (current and past)	66 (84)	112 (83)	0.91
Coronary artery disease	22 (28)	41 (31)	0.67
Medications: *N* (%) ¶			
Statins	56 (74)	108 (81)	0.20
ACE-I/ARB	34 (45)	75 (57)	0.09
Beta blockers	21 (28)	40 (30)	0.68
Diuretics	5 (7)	11 (8)	0.64
ASA	44 (56)	79 (59)	0.69
Antiplatelets (Other than ASA)	17 (22)	24 (18)	0.50
Rivaroxaban (low dose 2.5 mg oral twice daily)	1 (1)	3 (2)	0.62
Events: *N* (%) ¶			
MALE	3 (4)	19 (14)	**0.034**
Vascular intervention	3 (4)	16 (12)	**0.046**
Major amputation	0 (0)	3 (2)	0.18
Worsening PAD (drop in ABI ≥ 0.15)	1 (1)	27 (22)	**0.001**

ACE-I, angiotensin converting enzyme inhibitor; ARB, angiotensin II receptor blocker; ASA, acetylsalicylic acid; MALE, major adverse limb event: composite of vascular intervention and major amputation; PAD, peripheral artery disease; ABI, ankle brachial index.; uFABP3/uCr [urinary fatty acid binding protein 3 (uFABP3) normalized to urinary creatinine (uCr)]; Low uFABP3/uCr defined as ≤ 2.70 μg/g; High uFABP3/uCr defined as >2.70 μg/g; ‡Compared using independent t-test; ¶Compared using chi-square test. Bold values represent statistically significant values ($p < 0.05$).

ABI 0.89 – 0.75 [3.13 (IQR 2.61 – 5.49), p = 0.047], ABI 0.74–0.50 [3.55 (IQR 2.42–6.94), $p = 0.002$], ABI < 0.50 [3.99 (IQR 2.32–7.12), p = 0.002]). Patients with no PAD did not develop any primary or secondary outcomes. Compared to patients with mild PAD, those with moderate PAD were more likely to develop MALE (62 vs. 29%), require vascular intervention (50 vs. 39%), and have worsening PAD status (54 vs. 46%). Since most patients with acute on chronic ischemia who typically have an ABI < 0.5 were excluded from the study, we recruited few patients with severe PAD. In this subset of patients, we noted a small proportion of individuals with severe PAD (ABI < 0.5) who suffered adverse events [MALE (10%), vascular intervention (11%), major amputation (33%), and worsening PAD status (0%)] (**Supplementary Table 1**).

DISCUSSION

Our single-center prospective case-control study demonstrates that uFABP3/uCr has diagnostic and prognostic value in PAD. We identified a cohort of 214 patients with and without PAD and demonstrated that uFABP3/uCr was elevated in the PAD group. Furthermore, higher levels of uFABP3/uCr predicted future PAD-related complications. Interestingly, most of the observed adverse events occurred in patients with moderate PAD based on ABI rather than patients with severe PAD, therefore our data suggests that ABI at baseline is not a good predictor of future adverse events, as corroborated by previous work by other groups (10, 11). This prompted us to risk stratified our cohort into low and high uFABP3/uCr based on ROC analysis. Our data demonstrated that patients with high uFABP3/uCr had a lower mean ABI and were more likely to be diagnosed with PAD. Finally, we showed that patients with high uFABP3/uCr were more likely to progress in their PAD disease state and require vascular intervention over a 2-year period. Overall, uFABP3/uCr had good discriminatory ability to predict our primary outcome of MALE, with an AUROC of 0.78. This is the first study validating a urinary biomarker for the prognosis of PAD in humans.

FABP3 belongs to a family of multi-gene fatty acid binding proteins (FABP's) and is primarily expressed in skeletal muscle and myocardial tissue (33). FABP3 is found predominantly intracellularly within the cytosol, where it mediates the uptake and transport of fatty acids (34). Previous studies have demonstrated the release of FABP3 from skeletal muscle in patients following exercise or muscle injury (13, 35, 36). In a similar context, patients with PAD experience muscle ischemia either transiently (claudication) or constantly (chronic limb threatening ischemia) (37, 38). This leads to FABP3 release into circulation and eventual excretion into the urine (39, 40). Others have demonstrated that FABP3 is associated with endothelial dysfunction, which may result from PAD (41). These are potential biochemical pathways by which FABP3 acts as a biomarker for PAD.

Previous studies have examined FABP's as biomarkers for other disease states. Ozawa et al. showed that FABP3 may be a potential mediator for diabetic nephropathy in murine models (42). Hayashida et al. demonstrated that serum and urine FABP3 may be early markers of myocardial injury in patients undergoing cardiac surgery (43). Others have investigated urinary FABP's as biomarkers for patients with acute kidney injury requiring renal replacement therapy (44). Given accumulating evidence demonstrating the value of FABP's in acting as biomarkers for life-threatening diseases, ongoing study in this area is warranted, particularly with a view to translate research findings into clinical practice to improve patient outcomes through early diagnosis and treatment. This is the first study to demonstrate the prognostic value of uFABP3/uCr in PAD patients.

There are several potential explanations for our findings. First, we demonstrated that PAD patients are more likely to have coronary artery disease (CAD) due to a greater burden of related cardiovascular risk factors including dyslipidemia and diabetes. This corroborates previous evidence demonstrating that

A

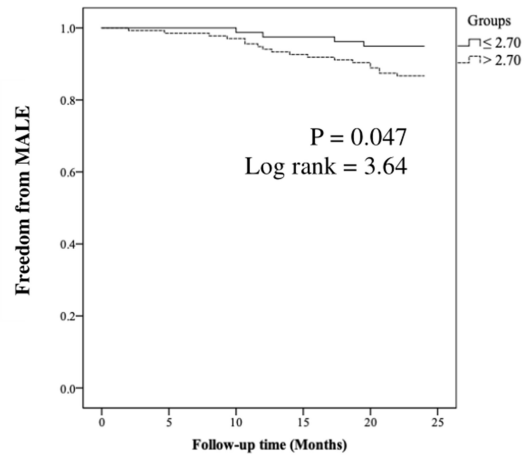

	Year	Freedom from MALE (%)	SE
Low uFABP3/uCr ≤ 2.70	1	97	0.01
	2	96	0.02
High uFABP3/uCr > 2.70	1	94	0.02
	2	86	0.03

B

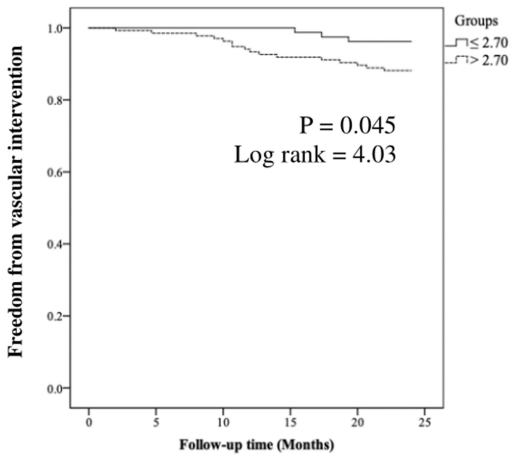

	Year	Freedom from vascular intervention (%)	SE
Low uFABP3/uCr ≤ 2.70	1	98	0.01
	2	96	0.02
High uFABP3/uCr > 2.70	1	94	0.03
	2	88	0.03

C

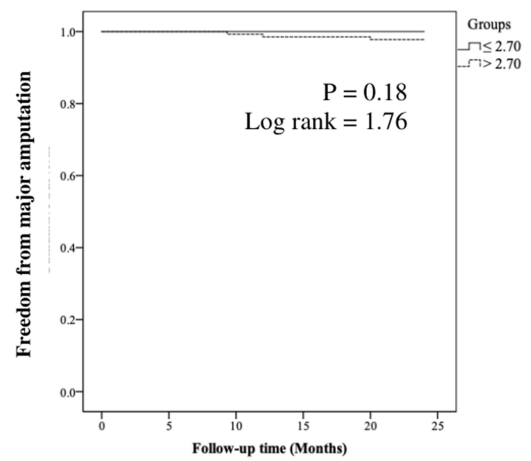

	Year	Freedom from major amputation (%)	SE
Low uFABP3/uCr ≤ 2.70	1	100	-
	2	100	-
High uFABP3/uCr > 2.70	1	99	<0.01
	2	97	0.01

D

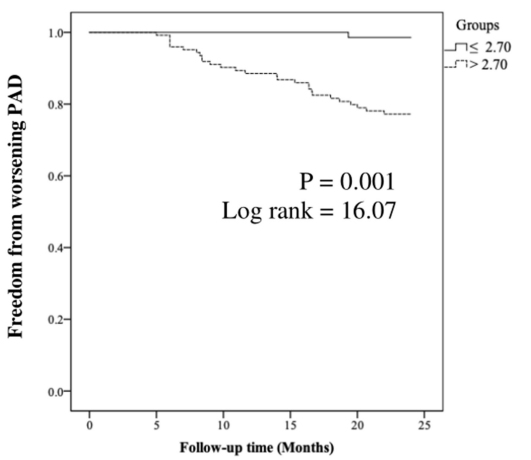

	Year	Freedom from worsening PAD (%)	SE
Low uFABP3/uCr ≤ 2.70	1	100	-
	2	99	0.01
High uFABP3/uCr > 2.70	1	89	0.03
	2	78	0.04

FIGURE 1 | Kaplan-Meier analysis of event free survival rates in patients with low vs. high urinary fatty acid binding protein 3 normalized to urinary creatinine (uFABP3/uCr) for **(A)** MALE (major adverse limb event), **(B)** vascular intervention, **(C)** major amputation, and **(D)** worsening PAD (ankle brachial index drop ≥ 0.15). SE (standard error).

individuals with PAD often have widespread arterial disease, with 61% of PAD patients being diagnosed with co-morbid CAD (45). As a result, they are at a 6-fold increased risk of cardiovascular death compared to patients without PAD (46). This highlights the importance of developing a widely applicable screening and prognostic tool for PAD. Second, we found that uFABP3/uCr levels were higher in PAD patients. This is likely because muscle ischemia secondary to PAD leads to release of uFABP3 into circulation, which then becomes excreted into urine. This provides a valuable biomarker that can be measured non-invasively in patients to screen for PAD. Third, patients with high uFABP3/uCr were more likely to develop MALE, require vascular intervention, and have worsening PAD over a 2-year period. There was also an association between every one unit increase in uFABP3/uCr and PAD-related complications. This suggests that uFABP3/uCr not only has diagnostic value, but also provides prognostic information regarding disease trajectory. Importantly, we demonstrated that high uFABP3/uCr was associated with worse PAD prognosis independent of CAD. Specifically, patients with active CAD were excluded from our analysis (acute coronary syndrome, congestive heart failure, uncontrolled arrhythmia, or elevated troponin within the past 12 months), which significantly reduced the risk of confounding. Even after adjusting for comorbidities including CAD and diabetes, there remained an independent association between uFABP3/uCr and MALE / worsening PAD status, which corroborates previous findings from our group (17). Therefore, this biomarker has the potential to risk stratify patients and guide healthcare providers with regards to aggressiveness of medical and surgical therapy, intensity of follow-up, and allocation of health care resources. Less than 5% of patients with PAD in our study were taking low-dose rivaroxaban, which has been demonstrated to provide significant cardiovascular benefit in patients with atherosclerotic vascular disease based on the COMPASS trial (12). Furthermore, only 62% and 87% of patients with PAD were taking ASA and statins respectively, despite these risk-reduction medications being Grade 1A recommendations for cardiovascular mortality and limb salvage benefit based on American Heart Association guidelines (47). Therefore, there are significant gaps in medical management of PAD, which may be addressed through a prognostic biomarker that can improve identification of high-risk patients that require more intensive therapy. Fourth, there was likely no difference in 2-year major amputation between groups due to the low incidence of this event ($n = 3/214$) as well as the fact that patients were followed closely in this prospective study and underwent early revascularization to prevent limb loss. Fifth, our subgroup analysis demonstrated a significant association between uFABP3/uCr and PAD severity based on ABI, which corroborates previous evidence from our group (17). Our analysis of outcomes based on PAD severity showed that patients with moderate PAD were more likely to develop adverse events compared to those with mild PAD or no PAD. Only a small number of patients with severe PAD (ABI $<$ 0.5) were included in this study. This might be due to the fact that patients with acute on chronic limb ischemia who typically have an ABI $<$ 0.5 were excluded from this study. These patients were excluded since they already possess some of the recorded events for the study, such as need for vascular intervention or limb amputation. Within this small subset of patients and relative to patients with moderate PAD, we noted that a small number of patients with severe PAD based on ABI developed MALE or worsening PAD. This information reflects the poor prognostic ability of baseline ABI in predicting future adverse events, as demonstrated by other groups (10, 11). However, larger clinical trials are needed to investigate the prognostic ability of ABI. Our study suggests that uFAB *P3*/uCr may be a better prognostic marker for adverse PAD-related events.

This study has several limitations. First, this was not a randomized study and there were differences in baseline characteristics between groups. However, our analysis adjusted for important baseline characteristics including age, sex, hypertension, dyslipidemia, diabetes, smoking, coronary artery disease, congestive heart failure, medications (statins, ACE-I/ARB, beta blocker, diuretic, ASA, antiplatelets other than ASA, and low-dose rivaroxaban), and serum creatinine. Second, 2-year outcomes are reported, and longer follow-up is needed to better understand the prognostic value of uFABP3/uCr given that PAD is generally a long-standing disease. Third, we excluded patients with eGFR $<$60, acute limb ischemia, or acute coronary syndrome, congestive heart failure, uncontrolled arrhythmia, or elevated troponin within the past 12 months. Therefore, the results may not apply to all patients with suspected PAD and further investigation of uFABP3 is needed to better understand how the biomarker can be effectively implemented as a screening and prognostic tool in clinical practice. Fourth, additional variables including body weight, lean body mass, percent body fat, lipid profiles, and echocardiogram data were not collected and may provide additional information regarding our patient population. The demographic and clinical variables reported in our study reflect clinically relevant indicators of the health of vascular surgery patients. Future study could collect more granular data to better understand the impact of baseline factors on PAD progression. Fifth, the major amputation rate was low in our study ($n = 3/214$) and likely contributed to statistically insignificant findings for this *second* ary outcome. We hypothesize that with longer follow-up and more events, our study would have detected a significant difference in major amputation rates based on uFAB *P3*/uCr levels.

CONCLUSIONS

Our study demonstrates three important findings. First, elevated uFABP3/uCr is associated with PAD. Second, patients with high uFABP3/uCr are more likely to develop MALE, require vascular intervention, and have worsening PAD even after adjusting for CAD history. Finally, uFABP3/uCr predicts MALE with an AUROC of 0.78. These results suggest that uFABP3/uCr has good diagnostic and prognostic value in PAD independent of CAD. The severity of PAD both at baseline and over the study period were captured in our study. Measurement of uFABP3/uCr can improve risk-stratification and identify patients at high risk for developing PAD-related complications who require additional diagnostic evaluation, close follow-up, and aggressive medical

management, including prescription of low-dose rivaroxaban. Given that urine samples are easily collected and analyzed in the primary care setting, this biomarker has potential for widespread clinical implementation as a PAD screening and prognostic tool. Larger studies, particularly clinical trials, should be performed to confirm our findings.

DATA AVAILABILITY STATEMENT

The original contributions presented in the study are included in the article/**Supplementary Material**, further inquiries can be directed to the corresponding author/s.

ETHICS STATEMENT

The studies involving human participants were reviewed and approved by Unity Health Toronto Research Ethics Board, University of Toronto. The patients/participants provided their written informed consent to participate in this study.

AUTHOR CONTRIBUTIONS

SJ, NJ, and MS: acquisition, analysis, and interpretation of data, revising the manuscript for important intellectual content, and approval of the final manuscript draft submitted for publication. BL and AZ: methodology, statistical analysis, data analysis and interpretation, writing—original draft, revising the manuscript for important intellectual content, and approval of the final manuscript draft submitted for publication. RA and MQ: study concept and design, methodology, data analysis and interpretation, writing—original draft, revising the manuscript for important intellectual content, and approval of the final manuscript draft submitted for publication. All authors contributed to the article and approved the submitted version.

SUPPLEMENTARY MATERIAL

The Supplementary Material for this article can be found online at: https://www.frontiersin.org/articles/10.3389/fcvm.2022.875244/full#supplementary-material

REFERENCES

1. Zemaitis MR, Boll JM, Dreyer MA. *Peripheral Arterial Disease*, *StatPearls*. Treasure Island (FL): StatPearls Publishing (2021). Available online at: http://www.Ncbi.nlm.nih.gov/books/NBK430745/ (accessed June 14, 2021).
2. Olin JW, Sealove BA. Peripheral artery disease: current insight into the disease and its diagnosis and management. *Mayo Clin Proc.* (2010) 85:678–92. doi: 10.4065/mcp.2010.0133
3. Welten GMJM, Schouten O, Hoeks SE, Chonchol M, Vidakovic R, van Domburg RT, et al. Long-term prognosis of patients with peripheral arterial disease: a comparison in patients with coronary artery disease. *J Am Coll Cardiol.* (2008) 51:1588–96. doi: 10.1016/j.jacc.2007.11.077
4. Cooke JP, Wilson AM. Biomarkers of peripheral arterial disease. *J Am Coll Cardiol.* (2010) 55:2017–23. doi: 10.1016/j.jacc.2009.08.090
5. AbuRahma AF, Adams E, AbuRahma J, Mata LA, Dean LS, Caron C, et al. Critical analysis and limitations of resting ankle-brachial index in the diagnosis of symptomatic peripheral arterial disease patients and the role of diabetes mellitus and chronic kidney disease. *J Vasc Surg.* (2020) 71:937–45. doi: 10.1016/j.jvs.2019.05.050
6. Stein R, Hriljac I, Halperin JL, Gustavson SM, Teodorescu V, Olin JW. Limitation of the resting ankle-brachial index in symptomatic patients with peripheral arterial disease. *Vasc Med Lond Engl.* (2006) 11:29–33. doi: 10.1191/1358863x06vm663oa
7. Mohler ER, Treat-Jacobson D, Reilly MP, Cunningham KE, Miani M, Criqui MH, et al. Utility and barriers to performance of the ankle-brachial index in primary care practice. *Vasc Med Lond Engl.* (2004) 9:253–60. doi: 10.1191/1358863x04vm559oa
8. Chiu LYC, Syed MH, Zamzam A, Rotstein OD, Abdin R, Laraya N, et al. Perceived challenges to routine uptake of the ankle brachial index within primary care practice. *J Clin Med.* (2021) 10:4371. doi: 10.3390/jcm10194371
9. Wolosker N, Rosoky RA, Nakano L, Basyches M, Puech-Leão P. Predictive value of the ankle-brachial index in the evaluation of intermittent claudication. *Rev Hosp Clin.* (2000) 55:61–4. doi: 10.1590/S0041-87812000000200005
10. Pasqualini L, Schillaci G, Pirro M, Vaudo G, Leli C, Colella R, et al. Prognostic value of low and high ankle-brachial index in hospitalized medical patients. *Eur J Intern Med.* (2012) 23:240–4. doi: 10.1016/j.ejim.2011.09.004
11. Hatmi ZN, Dabiran S, Kashani AS, Heidarzadeh Z, Darvishi Z, Raznahan M. Ankle-brachial index as a prognostic factor and screening tool in coronary artery disease: does it work? *J Tehran Heart Cent.* (2014) 9:174–8.
12. Eikelboom JW, Connolly SJ, Bosch J, Dagenais GR, Hart RG, Shestakovska O, et al. Rivaroxaban with or without aspirin in stable cardiovascular disease. *N Engl J Med.* (2017) 377:1319–30. doi: 10.1056/NEJMoa1709118
13. Pritt ML, Hall DG, Recknor J, Credille KM, Brown DD, Yumibe NP, et al. Fabp3 as a biomarker of skeletal muscle toxicity in the rat: comparison with conventional biomarkers. *Toxicol Sci.* (2008) 103:382–96. doi: 10.1093/toxsci/kfn042
14. Zhang Y, Kent JW, Lee A, Cerjak D, Ali O, Diasio R, et al. Fatty acid binding protein 3 (fabp3) is associated with insulin, lipids and cardiovascular phenotypes of the metabolic syndrome through epigenetic modifications in a Northern European family population. *BMC Med Genomics.* (2013) 6:9. doi: 10.1186/1755-8794-6-9
15. Kawahata I, Bousset L, Melki R, Fukunaga K. Fatty acid-binding protein 3 is critical for α-synuclein uptake and MPP+/-induced mitochondrial dysfunction in cultured dopaminergic neurons. *Int J Mol Sci.* (2019) 20:E5358. doi: 10.3390/ijms20215358
16. Syed MH, Zamzam A, Khan H, Singh K, Forbes TL, Rotstein O, et al. Fatty acid binding protein 3 is associated with peripheral arterial disease. *JVS-Vasc Sci.* (2020) 1:168–75. doi: 10.1016/j.jvssci.2020.08.003
17. Zamzam A, Syed MH, Harlock J, Eikelboom J, Singh KK, Abdin R, et al. Urinary fatty acid binding protein 3 (uFABP3) is a potential biomarker for peripheral arterial disease. *Sci Rep.* (2021) 11:11061. doi: 10.1038/s41598-021-90395-0
18. World Medical Association. World medical association declaration of Helsinki: ethical principles for medical research involving human subjects. *JAMA.* (2013) 310:2191–4. doi: 10.1001/jama.2013.281053
19. Gul F, Janzer SF. "*Peripheral Vascular Disease*," *StatPearls*. Treasure Island (FL): StatPearls Publishing (2021). Available online at: http://www.ncbi.nlm.nih.gov/books/NBK557482/ (accessed June 30, 2021).
20. Grundy SM, Stone NJ, Bailey AL, Beam C, Birtcher KK, Blumenthal RS, et al. AHA/ACC/AACVPR/AAPA/ABC/ACPM/ADA/AGS/APhA/ASPC/NLA/PCNA guideline on the management of blood cholesterol. J Am Coll Cardiol. (2018) 73:e285–e350. doi: 10.1016/j.jacc.2018.11.003
21. Whelton PK, Carey RM, Aronow WS, Casey DE, Collins KJ, Dennison HC, et al. 2017 ACC/AHA/AAPA/ABC/ACPM/AGS/APhA/ASH/ASPC/NMA/PCNA guideline for the prevention, detection, evaluation, and management of high blood pressure in adults. *J Am Coll Cardiol.* (2018) 71:e127–248. doi: 10.1016/j.jacc.2017.11.006

22. MILLIPLEX MAP Human Cardiovascular Disease (CVD) magnetic bead panel 1 - cardiovascular disease multiplex assay | HCVD1MAG-67K. Available online at: https://www.emdmillipore.com/CA/en/product/MILLIPLEX-MAP-Human-Cardiovascular-Disease-CVD-Magnetic-Bead-Panel-1-Cardiovascular-Disease-Multiplex-Assay,MM_NF-HCVD1MAG-67K (accessed December 18, 2021).
23. Reed GF, Lynn F, Meade BD. Use of coefficient of variation in assessing variability of quantitative assays. *Clin Diagn Lab Immunol.* (2002) 9:1235–9. doi: 10.1128/CDLI.9.6.1235-1239.2002
24. Luminex Assays - CA. Available online at: https://www.thermofisher.com/ca/en/home/life-science/antibodies/immunoassays/procartaplex-assays-luminex.html (accessed December 18, 2021).
25. MAGPIX® System | xMAP Instrument | Luminex Corporation. Available online at: https://www.luminexcorp.com/magpix-system/ (accessed December 18, 2021).
26. MILLIPLEX® Analyst 5.1 Software from Merck | SelectScience. Available online at: https://www.selectscience.net/products/milliplex-analyst-51-software/?prodID=171598 (accessed December 18, 2021).
27. AU 680. Available online at: https://www.beckmancoulter.com/products/chemistry/au680 (accessed December 18, 2021).
28. Wassel CL, Allison MA, Ix JH, Rifkin DE, Forbang NI, Denenberg JO, Criqui MH. Ankle-brachial index predicts change over time in functional status in the San Diego Population Study. *J Vasc Surg.* (2016) 64:656–62.e1. doi: 10.1016/j.jvs.2016.02.066
29. McClary KN, Massey P. "Ankle Brachial Index," *StatPearls*. Treasure Island (FL): StatPearls Publishing (2021). Available online at: http://www.ncbi.nlm.nih.gov/books/NBK544226/ (accessed December 19, 2021).
30. Khan TH, Farooqui FA, Niazi K. Critical review of the ankle brachial index. *Curr Cardiol Rev.* (2008) 4:101–6. doi: 10.2174/157340308784245810
31. Frank U, Nikol S, Belch J, Boc V, Brodmann M, Carpentier PH, et al. ESVM guideline on peripheral arterial disease. *VASA Z Gefasskrankheiten.* (2019) 48:1–79. doi: 10.1024/0301-1526/a000834
32. SPSS Software. (2021). Available online at: https://www.ibm.com/analytics/spss-statistics-software (accessed December 18, 2021).
33. Vogel Hertzel A, Bernlohr DA. The mammalian fatty acid-binding protein multigene family: molecular and genetic insights into function. *Trends Endocrinol Metab.* (2000) 11:175–80. doi: 10.1016/S1043-2760(00)00257-5
34. Stremmel W, Strohmeyer G, Borchard F, Kochwa S, Berk PD. Isolation and partial characterization of a fatty acid binding protein in rat liver plasma membranes. *Proc Natl Acad Sci.* (1985) 82:4–8. doi: 10.1073/pnas.82.1.4
35. Sorichter S, Mair J, Koller A, Pelsers MM, Puschendorf B, Glatz JF. Early assessment of exercise induced skeletal muscle injury using plasma fatty acid binding protein. *Br J Sports Med.* (1998) 32:121–4. doi: 10.1136/bjsm.32.2.121
36. Burch PM, Greg Hall D, Walker EG, Bracken W, Giovanelli R, Goldstein R, et al. Evaluation of the relative performance of drug-induced skeletal muscle injury biomarkers in rats. *Toxicol Sci.* (2016) 150:247–56. doi: 10.1093/toxsci/kfv328
37. Patel SK, Surowiec SM. "Intermittent Claudication," *StatPearls*. Treasure Island (FL): StatPearls Publishing (2021). Available online at: http://www.ncbi.nlm.nih.gov/books/NBK430778/ (accessed June 30, 2021).
38. Farber A. Chronic limb-threatening ischemia. *N Engl J Med.* (2018) 379:171–80. doi: 10.1056/NEJMcp1709326
39. Pipinos II, Sharov VG, Shepard AD, Anagnostopoulos PV, Katsamouris A, Todor A, et al. Abnormal mitochondrial respiration in skeletal muscle in patients with peripheral arterial disease. *J Vasc Surg.* (2003) 38:827–32. doi: 10.1016/S0741-5214(03)00602-5
40. Pipinos II, Judge AR, Zhu Z, Selsby JT, Swanson SA, Johanning JM, et al. Mitochondrial defects and oxidative damage in patients with peripheral arterial disease. *Free Radic Biol Med.* (2006) 41:262–9. doi: 10.1016/j.freeradbiomed.2006.04.003
41. Wu Y-W, Chen J-W, The potential link between fatty acid-binding protein 3 and endothelial dysfunction. *J Am Coll Cardiol.* (2020) 75:185. doi: 10.1016/S0735-1097(20)30812-3
42. Ozawa S, Ueda S, Li Y, Mori K, Asanuma K, Yanagita M, et al. Fatty acid binding protein 3 as a potential mediator for diabetic nephropathy in eNOS deficient mouse. *Biochem Biophys Res Commun.* (2014) 454:531–6. doi: 10.1016/j.bbrc.2014.10.121
43. Hayashida N, Chihara S, Akasu K, Oda T, Tayama E, Kai E, et al. Plasma and urinary levels of heart fatty acid-binding protein in patients undergoing cardiac surgery. *Jpn Circ J.* (2000) 64:18–22. doi: 10.1253/jcj.64.18
44. Dihazi H, Koziolek MJ, Datta RR, Wallbach M, Jung K, Heise D, et al. FABP1 and FABP3 have high predictive values for renal replacement therapy in patients with acute kidney injury. *Blood Purif.* (2016) 42:202–13. doi: 10.1159/000447115
45. Bhatt DL, Steg PG, Ohman EM, Hirsch AT, Ikeda Y, Mas J-L, et al. International prevalence, recognition, and treatment of cardiovascular risk factors in outpatients with atherothrombosis. *JAMA.* (2006) 295:180. doi: 10.1001/jama.295.2.180
46. Criqui MH, Langer RD, Fronek A, Feigelson HS, Klauber MR, McCann TJ, et al. Mortality over a period of 10 years in patients with peripheral arterial disease. *N Engl J Med.* (1992) 326:381–6. doi: 10.1056/NEJM199202063260605
47. Gerhard-Herman MD, Gornik HL, Barrett C, Barshes NR, Corriere MA, Drachman DE, et al. 2016 AHA/ACC guideline on the management of patients with lower extremity peripheral artery disease: a report of the American College of Cardiology/American Heart Association Task Force on Clinical Practice Guidelines. *J Am Coll Cardiol.* (2017) 69:e71–e126. doi: 10.1016/j.jacc.2016.11.007

Conflict of Interest: The authors declare that the research was conducted in the absence of any commercial or financial relationships that could be construed as a potential conflict of interest.

frontiers | Frontiers in Cardiovascular Medicine

MINI REVIEW
published: 07 July 2022
doi: 10.3389/fcvm.2022.948492

Opportunities and Challenges in Understanding Atherosclerosis by Human Biospecimen Studies

*Maria Elishaev[1], Chani J. Hodonsky[2], Saikat Kumar B. Ghosh[3], Aloke V. Finn[3], Moritz von Scheidt[4,5] and Ying Wang[1]**

[1] Department of Pathology and Laboratory Medicine, Center for Heart Lung Innovation, University of British Columbia, Vancouver, BC, Canada, [2] Center for Public Health Genomics, Department of Public Health Sciences, University of Virginia, Charlottesville, VA, United States, [3] Cardiovascular Pathology Institute, Gaithersburg, MD, United States, [4] Department of Cardiology, Deutsches Herzzentrum München, Technische Universität München, Munich, Germany, [5] Deutsches Zentrum für Herz-Kreislauf-Forschung, Partner Site Munich Heart Alliance, Munich, Germany*

Over the last few years, new high-throughput biotechnologies and bioinformatic methods are revolutionizing our way of deep profiling tissue specimens at the molecular levels. These recent innovations provide opportunities to advance our understanding of atherosclerosis using human lesions aborted during autopsies and cardiac surgeries. Studies on human lesions have been focusing on understanding the relationship between molecules in the lesions with tissue morphology, genetic risk of atherosclerosis, and future adverse cardiovascular events. This review will highlight ways to utilize human atherosclerotic lesions in translational research by work from large cardiovascular biobanks to tissue registries. We will also discuss the opportunities and challenges of working with human atherosclerotic lesions in the era of next-generation sequencing.

Keywords: atherosclerosis, biobanked human biospecimens, next-generation sequencing, bioinformatic analyses, spatial biology

OPEN ACCESS

Edited by:
Vicente Andres, Spanish National Centre for Cardiovascular Research, Spain

Reviewed by:
Jose Luis Martin-Ventura, Universidade Autónoma de Lisboa, Portugal

****Correspondence:***
Ying Wang
Wang85@mail.ubc.ca
orcid.org/0000-0002-1444-5778

Specialty section:
This article was submitted to Atherosclerosis and Vascular Medicine, a section of the journal Frontiers in Cardiovascular Medicine

Received: *19 May 2022*
Accepted: *07 June 2022*
Published: *07 July 2022*

Citation:
Elishaev M, Hodonsky CJ, Ghosh SKB, Finn AV, von Scheidt M and Wang Y (2022) Opportunities and Challenges in Understanding Atherosclerosis by Human Biospecimen Studies. Front. Cardiovasc. Med. 9:948492. doi: 10.3389/fcvm.2022.948492

INTRODUCTION

Ischemic cardiovascular events, including heart attack and strokes, is the leading cause of mortality and morbidity worldwide (1). Atherosclerosis, the build-up of lesion cells on the wall of the blood vessels, is a chronic process underlying most ischemic cardiovascular events. Studies of human biospecimens have played an indispensable part in understanding the pathophysiology of atherosclerosis because neither cell culture nor animal models can recapitulate the complex components and structure of advanced human atherosclerotic lesions (2, 3). Before next-generation sequencing was invented, human biospecimen studies focused on the morphology and a few lesion components such as collagen, foam cells, and smooth muscle cells. Even with limited dimension, the classic histology methods have set the widely-accepted lesion classification standards and found the association between lesion morphology and ischemic events (4). The era of next-generation sequencing brought opportunities to explore the molecular features of atherosclerotic lesions in depth and *in situ*. Hence, researchers have multiple options to apply the classic and new technologies to human biospecimens. The question is how to match the research scope and approach with the human biospecimens available in large biobanks or small-scale tissue registries. This review will provide a few examples to showcase current advances in utilizing human atherosclerotic lesions, share our views of challenges in knowledge translation and vision of future needs to advance research on human biospecimens in the area of atherosclerosis.

CURRENT ADVANCES IN HUMAN BIOSPECIMEN STUDIES

Morphological Insights

Histology assessment is a routine in most tissue biobanks. Traditional hematoxylin-eosin and Movat's Pentachrome stainings visualize the structure and basic components of the lesions. These widely adopted methods revealed not only the association between morphology and cardiovascular events, but also risk factors that contribute to disease progression. Biopsy studies found that the morphological features of lesions underneath cardiac thrombosis fall into three categories: rupture, erosion, and calcified nodule (5), indicating the connection between morphology and risk of ischemic cardiovascular events. Following this notion, Virmani et al. developed a comprehensive assessment criteria using morphology to define the trajectory of lesion progression (5). Correlation studies can further infer the pathogenic drive of lesion progression by connecting the traditional risk factors of atherosclerosis with morphology. Burke et al. found that patients having plaque rupture also had higher cholesterol levels as recorded in their postmortem toxicological tests (6). It suggests that the traditional risk factor, cholesterol levels, drives lesion progression toward a rupture-prone structure and lipid-lowering drugs will benefit patients having this type of lesions. In addition to studying lesions at late stages, Nakashima et al. observed that vascular beds that develop diffuse intimal thickening in early childhood are also the "hot spots" for atherogenesis in later life (7). Large biobanks have a statistically powerful amount of samples to explore how lesion morphology is affected by genetic risk factors in patients of different ethnicities. CVPath Institute has the world's largest and most comprehensive collection of heart samples from more than 8,500 sudden coronary death cases. Their studies have shown a higher risk of sudden coronary death in the African American population compared to the Caucasian population (8). Guo et al. explored the genetic reasons behind this phenomenon and found that more African Americans carry a single nucleotide polymorphism rs7136716 than the Caucasian population and this genetic variant is correlated with increased expression of CD163 macrophages in ruptured lesions (9). Then they determined that $CD163^{+}$ macrophages contribute to intraplaque microvessels and inflammation, remodeling lesion structure to be rupture-prone. This data suggests that rs7136716 is a genetic risk variant particularly enriched in patients of an African ancestry. Hence, the integration of pathology and genetics from large biobank studies can provide new insights into the discovery of biomarkers and personalized medicine.

Molecular Phenotyping

There has been an explosive increase in atherosclerosis research using single-cell RNA sequencing (scRNA-seq). These studies have revealed the vast heterogeneity in the cell components of atherosclerotic lesions, including more than six phenotypes of SMCs (10–12) and at least three macrophage subsets (13, 14) among eleven distinct leukocyte populations (15). Most previous studies applied next-generation sequencing to animal models, in which disease stages can be controlled, and cell lineage tracing is available. These advantages made them better tools for understanding the trajectory of phenotypic changes and trans-differentiation of lesion cells in the early disease stage (10, 16). Applying next-generation sequencing to human lesions has its own technical challenges and limitations, discussed in several recent reviews (17–19). Nevertheless, single-cell sequencing of human lesions will distinguish cell phenotypes and signaling pathways in categorized patient cohorts, the differences in which can be used to predict therapeutic targets and treatment outcomes. Slenders et al. projected GWAS loci into scRNA-seq data of human carotid lesions and defined cell-specific risk genes that can be translated to therapeutic targets (20). Fernandez et al. applied several single-cell sequencing technologies to human carotid lesions. They found that differences in the interleukin-1β (IL-1β) signaling pathway between symptomatic and asymptomatic patients may lead to diverse treatment outcomes in the CANTOS trial, which aims to block IL-1β to reduce the risks of cardiovascular events (21). One limitation of using scRNA-seq to predict cellular function is that it ignores all the post-transcriptional regulation of gene expression. Quantitative proteomics uses technologies such as mass spectrometry to characterize proteins, molecules that eventually execute gene function. Since traditional mass spectrometry usually requires a few milligrams of input material, most previous studies focus on cultured cells instead of digested lesions to obtain the protein atlas of a single cell type. Okui et al. applied mass spectrometry to cultured human coronary artery SMCs and found that carnitine O-octanoyltransferase increases during osteogenic transition of SMCs, which will lead to calcification during atherogenesis (22). The Athero-Express study used proteomics to analyze the protein features of human carotid lesions and found that osteopontin was strongly associated with cardiovascular events during the follow-up post endarterectomy surgery. suggesting that pathologists can use osteopontin as a biomarker to predict patients' future risk of cardiovascular events (23). The Athero-Express study collects carotid lesions from endarterectomy surgeries and follows up with the clinical records of donors to determine the relationship between lesion composition and future adverse cardiovascular events (23). It embraces the idea that atherosclerosis is a systemic disease and biopsy tests of surgically aborted lesions will inform the progression of lesions in other vascular beds (24). The Athero-Express study has recently applied state-of-the-art scRNA-seq technology to their biobank to advance our understanding of the transcriptome landscape of human lesions (25), and more specific biomarkers are expected with accumulated data of clinical follow-up. Hence, when the molecular features of human lesions are linked to clinical follow-up of the specimen donors, it will support the discovery of biomarkers.

Proof of Concept

Compared to large biobanks, sample availability in small-scale tissue registries is often too low to support genetic studies such as investigating the polygenic risk factors. Without follow-up of clinical outcomes, the archived tissue samples are not ideal for biomarker studies. However, these tissues can be readily

used to prove the concepts of basic sciences: "reality check" that observations in animal studies or cultured cells will apply to human atherogenesis. It is now well-known that vascular smooth muscle cells (SMCs) undergo phenotypic changes during atherogenesis and most of them do not express lineage markers such as myosin heavy chain 11 and smooth muscle alpha-actin, but it was not till the invention of SMC-lineage tracing mice when researchers realized about this (26). To prove the presence of de-differentiated SMCs in human atherogenesis, Gomez et al. developed a staining method to visualize cells of SMC origin using SMC-lineage tracing mice and then applied the technique to human carotid lesions ($n = 5$) (27). Clinical information can be completely detached from the biospecimen studies in such proof of concept research and small sample size is acceptable. Working with archived samples shortens the time of ethical approval for researchers. Proof of concept studies allow archived specimens to be repurposed and maximized in the tissue registries. For example, the Cardiovascular Tissue Registry at the Centre for Heart Lung Innovation at the University of British Columbia collects hearts donated by heart transplant patients, and the myocardium has been utilized to support studies of cardiac allograft vasculopathy (28). In parallel, Allahverdian et al. characterized the atherosclerotic coronary arteries from these hearts and discovered that an underestimated amount of foam cells are derived from SMCs instead of macrophages (29). This study, along with growing evidence from GWAS of coronary artery disease (30–32), has changed the traditional dogma that atherosclerosis is mainly a macrophage-driven disease.

CURRENT GAPS IN KNOWLEDGE TRANSLATION

Despite the current advances in new technologies, guidelines of research design (19) and customized protocols (33) to maximize the utilization of human biospecimen, translation of biobank research to biomarkers and therapeutic targets is still limited. Current gaps in knowledge translation include the lack of tailored bioinformatics tools to interpret "Omics" data, "Omics" in the tissue context, and connections of traits in the lesions with blood-borne biomarkers, which is more applicable for clinical testing.

Bioinformatic Tools

As more human biospecimen studies have embraced scRNA-seq technology, bioinformatics tools that are primarily R- and python-based have been developed, including Seurat (34), Signac (35), archR (36), singleR (37), scCATH (38), and Garnett (39). Additionally, the less robust single-cell sequencing data can intersect with large bulk sequencing datasets, such as the Human Cell Atlas (40) through Cibersort (41) and MuSiC (42), to estimate the portion of specific cell types in the bulk-seq data. However, only a few tools incorporate established pipelines into webapps or standalone applications to allow scientists without programming experience to analyse their data. Most bioinformatics tools are also incompatible with integrating datasets published in various formats. This problem is accompanied by bioethical considerations of what clinical information affiliated with the human biospecimen can be shared and how to oversee the appropriate use of shared datasets (43–46). Furthermore, myriad analysis options are available: over 1,000 tools are developed for scRNA-seq alone (47), with limited benchmarking for atherosclerotic lesions. The nature of cells in the atherosclerotic lesion: cell plasticity and dynamic phenotypic changes during atherogenesis (10, 48), is especially challenging for bioinformatics tools that rely on: (1) reference datasets to define a cell type, and (2) the persistent presence of a phenotype in transition to trace the trajectory of atherogenic changes (49–52).

Lack of Spatial "Omics" Data

Gene ontology analyses of scRNA-seq data predict the function of each cell subset based on signaling pathways and biological processes involving genes specific to that subset. However, cells are unevenly distributed among the atherosclerotic lesions. In the traditional diagram of a fibroatheroma, endothelial cells are located at the luminal side with SMCs underneath and macrophages form foam cells in the intima and shoulder region. After the discovery of cell subsets and phenotypic transition of lesion cells, now we know that the fibrous cap is derived from SMCs and endothelial cells that have undergone endothelial-to-mesenchymal transition (16). $CD68^+$ "macrophages" in the deep intima are made of leukocytes and SMCs (29). The stability of lesion structure is affected by the distribution of these cell subsets and their interactions with the others. Within the several types of SMCs in atherosclerotic lesions, some are fibroblast-like, potentially forming a protective fibrous cap (53), whereas pro-inflammatory macrophages and SMCs may enlarge the necrotic core by altering the function of each other (54). These assumptions can be validated only when we see fibroblast-like SMCs on the fibrous cap of stable lesions and more impaired macrophages are close to the pro-inflammatory SMCs near the necrotic core. In the absence of lesion context, it can be misleading to predict lesion progression purely based on signaling pathways and biological processes represented by gene expression. The same mitogenic signaling pathway turned on by IL-1β in SMCs may cause pathogenic expansion of the atherosclerotic lesions (55) when these SMCs are located in the intima, but it may be athero-protective when these cells are in the fibrous cap. Blocking IL-1β in animals with established fibroatheroma resulted in lesion destabilization, suggesting that at least a subset of SMCs executed IL-1β's mitogenic effects in an athero-protective manner by investing into the fibrous cap (56). Hence, it is critical to consider spatial "Omics" data when translating single-cell "Omics" data to therapeutic targets and biomarkers.

Connection to Traits in the Blood

Tissue biopsy examinations are well-accepted for phenotyping tumors but are not practical in the clinical practice of atherosclerotic disease where not all patients require surgical treatment. Connecting the traits of atherosclerotic lesions to those in the blood will help the discovery of blood-borne biomarkers that can be easily implemented in clinical laboratories. Phenotyping blood cells has the potential to

TABLE 1 | Spatial gene expression technologies.

Technology	Resolution	Applications	Time	Common features/differences
Visium Tissue sections are mounted on top of capture spots. Each spot has a unique spatial barcode to retrieve its location. For frozen tissues, mRNA is directly released to bind to spatially barcoded oligonucleotides on the capture spots. For FFPE tissues, mRNA is first hybridized with pairs of specific probes for each targeted gene. Probe pairs are then ligated and released to bind to the spatial barcode on the capture spot (73)	Capture spot of 55 μm diameter; 100 μm distance between the centers of two capture spots (73) Maximum capture area: 6.5 × 6.5 mm² and 4,992 spots per capture area (73)	Frozen: Heart (74–76), Liver (77), Spinal cord (78), Skin (79), and Breast cancer (80) FFPE: Brain, ovarian cancer, lung, and kidney (81)	Hours to days (82)	- Fixed positions of capture spots include 0 to 10 cells. - RNA capture utilizes pre-existing lab equipment. - Gene expression data is layered over a morphological image of the same tissue section. - 4–5 protein markers can be combined by immunofluorescence staining with gene expression.
GeoMx DSP Tissue sections are stained with a mix of RNA or antibody probes, each contains a unique UV-cleavable oligonucleotide barcode. These barcodes are released by UV light illuminated at defined regions of interest (ROIs) and then counted. Reads are mapped back to each ROI, generating a map of genes or/and proteins expression within the tissue architecture (83)	As low as 10 μm (73) Minimum ROI: 5 × 5μm² Maximum ROI: 660 × 785 μm² (84)	FFPE: *Transcriptome*: Lymphoid and colorectal (83), Kidney (85), Brain tumor (86), Heart, lung, and liver (87) *Proteins:* Breast cancer 70-plex (88)	10–20 tissue sections in 1.5–2.5 days (depends on the number of ROI) (83)	- Flexible choice of regions respects boundaries of cells and tissue components. - RNA/protein capture require a specific instrument. - Use fluorescent morphology markers to guide selection of ROIs. - Up to 96 protein markers can be counted by nCounter, or more than 100 proteins using next-generation sequencing

reveal cellular biomarkers in the circulation (57). Hamers et al. explored protein expression of circulating monocytes using a 39-plex CyTOF panel and found a positive correlation between $Slan^{+}CXCR6^{+}$ monocyte population in the blood and the severity of atherosclerotic disease estimated by medical imaging, suggesting that this monocyte population could be a biomarker for disease progression (57). More importantly, studying biopsy and blood samples from the same donor will determine whether molecules in the blood mirror biological activities in the lesion. The interleukin-6 (IL-6) signaling pathway is a crucial mediator of inflammation in the lesions (58), and elevated plasma IL-6 in patients with acute coronary syndrome is currently the most powerful predictor of increased mortality in both short and long terms (59, 60). To explore its utilization as a biomarker for risk of cardiovascular events, the Biobank of Karolinska Endarterectomies study found that plasma IL-6 is positively correlated with those in the carotid lesions (61), but no significant differences were observed between symptomatic and asymptomatic patients (62). Hence, plasma IL-6 does not precisely reflect lesion progression and risk of adverse cardiovascular events. Until now, we have not found clinically applicable biomarkers to mirror biological activities in atherosclerotic lesions. Clonal hematopoiesis of indeterminate potential (CHIP), a phenomenon by which blood precursor cells in bone marrow obtain mutations during aging, is associated with a higher risk of atherosclerosis (63). In this original study, the authors found more than one hundred CHIP mutations in peripheral blood cells but did not have access to any molecular information about the atherosclerotic lesions. This study left the knowledge gap on how specific CHIP mutations will reflect lesion progression and can be promising biomarkers for risk prediction.

OPPORTUNITIES AND CHALLENGES IN FUTURE STUDIES

Collaborations are the key to advancing knowledge translation of human biospecimen studies. Publicly available "Omics" data from multiple studies can be pooled together to enhance the diversity of the studied population given that most data are based on European descendants. For researchers who already have the datasets, meta-analysis will combine different studies, as applied in the Coronary Artery Disease Genome-wide Replication and Meta-analysis plus The Coronary Artery Disease Genetics consortium. It is critical for researchers working on human atherosclerotic lesions to assess the potential pitfalls of applying a bioinformatic pipeline tested on other tissues to work on atherosclerotic lesions, which requires communication between the dry and wet labs to reflect on the principles of the pipelines and biological features of the tissues. For example, a spectrum of early to late staged atherosclerotic lesions need to be incorporated into the research design to answer questions about cell trajectories. For bioinformaticians, a consortium that integrates RNA-seq datasets has not been established yet, but initiatives have been made for sharing datasets in a user-friendly way. PlaqView is the first platform that empowers researchers who do not have access to human atherosclerotic lesions or who do not have bioinformatics expertise to re-analyze published scRNA-seq data (64). More biobanks have started to investigate blood and lesion samples from the same donor side-by-side to develop blood-borne biomarkers. The recently established Munich Cardiovascular Studies Biobank at the German Heart Center Munich has collected more than 800 pairs of blood and lesion samples to connect molecular traits in atherosclerotic

TABLE 2 | Spatial protein expression technologies.

Technology	Resolution	Applications	Time	Common features/differences
PhenoCycler (CODEX) Tissue sections are stained with a cocktail of antibodies conjugated with unique oligonucleotide barcodes. For each imaging cycle, reporters that carry fluorescence dyes and oligonucleotides complementary to the barcodes will bind to the antibodies to visualize the locations of 3 targeted proteins. These reporters are then removed and the cycle will repeat until all proteins are imaged.	200 nm (89, 90) Single cell level Maximum addressable sample size depends on the microscope and objective lens	FFPE: Colorectal cancer 56-plex (91) and Bladder cancer 35-plex (92) Frozen: Muscle 9-plex (93)and Spleen 30-plex (94)	Depends on the number of probes. 30-plex in 3.5 h (93)	- Autofluorescence from tissue exists. - Signals from three antibodies are captured per cycle. - Number of antibodies is theoretically unlimited. - Capable of imaging large tissue section. - Tissue section reusable
Hyperion (IMC) Tissue sections are stained with a cocktail of antibodies conjugated with metal tags. Stained tissue sections are ablated by a laser beam focused at 1 μm and then nebulized. The ionized metal tags are distinguished by the differences in the time of flight in the mass spectrometry.	1 μm^2 (73, 89) Single cell level Maximum size: 15 × 55 mm^2; Maximum ROI: 2.25 mm^2 (95)	FFPE: Oropharyngeal cancer 33-plex (96), Lung cancer 14-plex (97), Bladder cancer 34-plex (98), and Brain 11-plex (99)	2 h to scan 1.5 mm^2 using 200 spots/sec speed (90)	- Not affected by tissue autofluorescence. - Signals from all the antibodies are captured simultaneously. - Number of antibodies limited by available metal isotopes (∼40). - Tissue section not reusable
MIBIscope Tissue sections are stained with a cocktail of antibodies coupled to metal tags. The primary ion beam strikes the samples to liberate the lanthanide adducts of the bound antibodies. This generates the second ions that are analyzed by the mass spectrometer. MIBI utilizes adjustable ion beams to accommodate sample acquisition at varying depth and spot size.	200 nm to 1 μm (89, 100) 5–30 nm (101) Single cell and subcellular levels Range of ROI: 400 × 400–800 × 800 μm^2 (100)	FFPE: Breast cancer 37-plex (102), Tuberculosis lung 37-plex (103), Lymphoid, bladder, and placenta 16-plex (104)	25 min for two fields of 80 μm diameter (105) 90 ROIs (800 × 800 μm^2 each) per day (100) 1 mm/5 h with 500 nm resolution (90)	- Similar to Hyperion but resolution can reach subcellular level

lesions to those in blood. Small-scale tissue registries have the opportunity to collaborate with biobanks that have access to blood samples and patients' clinical follow-up records to validate molecular targets or biomarkers found in tissue studies. Spatial gene expression (**Table 1**) and multiplex imaging technologies (**Table 2**) have been commercialized to optimize the use of archived tissue blocks by measuring gene and protein expression in a high-throughput fashion. Roadblocks to applying them to human atherosclerotic lesions are mainly technical. Regarding histology integrity, lesion sections can easily fold and tear during sample preparation due to the natural curvature of the lumen and the presence of calcification and large necrotic cores. Regarding quality control of the RNA, atherosclerotic lesions, especially the highly necrotic ones, have low cellularity compared to the more frequently reported tumor, brain, and myocardium tissues. Based on our experience and previous research (65), a large part of one lesion (at least 100 μm long) is required to extract an adequate amount of RNA for quality assessment: 5 ng for the 2100 Agilent bioanalyzer (RNA 6000 Nano kit) or RT-PCR to amplify housekeeping genes. Moreover, Formalin-Fixed Paraffin-Embedded is the standard archiving format in biobanks to preserve lesion morphology. RNA stability remains unchanged for up to 10 years in this format (65). Previous research found that RNA is unevenly degraded within the same lesion section (66). Hence, we think that *in situ* assessment of RNA quality (67) is more suitable than extracting RNA from the whole section to select samples for spatial gene expression. Such a method can advise which lesion region has high quality input material to generate sequencing reads of high fidelity. Regarding the interpretation of data, cell segmentation has been the most problematic step for all the spatial biology tools. So far, most software and analysis pipelines assign the signals to a cell nucleus nearby based on algorithms trained in cancer tissues (68–70), assuming that cells in other tissues have similar size and shape. This may lead to inaccurate cell segmentation in lesion sections when the spindle-shaped 200 μm long SMCs, spherical lymphocytes of 7–10 μm in diameter, and foam cells with various sizes are all in close proximity. For spatial gene expression, transcriptomes from multiple cells can be mixed in one captured region and devolution of cell types requires reference scRNA-seq data (71, 72). Unlike working with dissociated cells, multiple sections are required to assess the entire lesion using spatial biology technologies, significantly increasing the cost. Removing these roadblocks requires efforts from both the academic and the technology industries.

CONCLUSION

Human atherosclerotic lesions carry valuable morphological and molecular information to decipher the mechanism of atherogenesis and reveal therapeutic targets and biomarkers for patients. While large biobanks with adequate sample numbers

and clinical data can perform genetic and biomarker studies, a smaller sample pool in the tissue registry also plays a vital role in translating basic sciences to a human disease scenario. New biotechnologies, along with bioinformatic tools to process the data, are modernizing biobank-based research in atherosclerosis, providing opportunities to maximize the utilization of human biospecimen. However, these new tools validated in other tissues are not one-size-fits-all, given the complex cell components in human atherosclerotic lesions. Collaborations from researchers in cardiovascular disease, bioinformaticians, and technology developers are essential for benchmarking and customization of available tools to address the unique challenges in future studies of human atherosclerotic lesions.

AUTHOR CONTRIBUTIONS

YW designed the topic of this review article and wrote 70% of the manuscript with ME. ME performed literature review and designed the tables. SG, CH, AF, and MS wrote the rest of the manuscript and contributed to the design of review topic. All authors contributed to the article and approved the submitted version.

FUNDING

This study was supported by the Canadian Institutes of Health Research (GR022678 to YW) and the Fondation Leducq (PlaqOmics 18CVD02 to AF and its Junior Investigator Award to CH, SG, MS, and YW).

ACKNOWLEDGMENTS

The authors wish to acknowledge Gurpreet Singhera and the Cardiovascular Tissue Registry at Centre for Heart Lung Innovation for critical input on the manuscript.

REFERENCES

1. World Health Organization. *The Top 10 Causes of Death.* (2020). Available online at: https://www.who.int/news-room/fact-sheets/detail/the-top-10-causes-of-death (accessed April 28, 2022].
2. Silvestre-Roig C, de Winther MP. Weber, C., Daemen MJ, Lutgens E, Soehnlein O. Atherosclerotic plaque destabilization: mechanisms, models, therapeutic strategies. *Circ Res.* (2014) 114:214–26. doi: 10.1161/CIRCRESAHA.114.302355
3. Hartwig H, Silvestre-Roig C, Hendrikse J, Beckers L, Paulin N, Van der Heiden K, et al. Atherosclerotic plaque destabilization in mice: a comparative study. *PLoS ONE.* (2015) 10:e0141019. doi: 10.1371/journal.pone.0141019
4. Sakakura K, Nakano M, Otsuka F, Ladich E, Kolodgie FD, Virmani R. Pathophysiology of atherosclerosis plaque progression. *Heart Lung Circ.* (2013) 22:399–411. doi: 10.1016/j.hlc.2013.03.001
5. Virmani R, Kolodgie FD, Burke AP, Farb A, Schwartz SM. Lessons from sudden coronary death: a comprehensive morphological classification scheme for atherosclerotic lesions. *Arterioscler Thromb Vasc Biol.* (2000) 20:1262–75. doi: 10.1161/01.ATV.20.5.1262
6. Burke AP, Farb A, Malcom GT, Liang YH, Smialek J, Virmani R. Coronary risk factors and plaque morphology in men with coronary disease who died suddenly. *N Engl J Med.* (1997) 336:1276–82. doi: 10.1056/NEJM199705013361802
7. Nakashima Y, Chen YX, Kinukawa N, Sueishi K. Distributions of diffuse intimal thickening in human arteries: preferential expression in atherosclerosis-prone arteries from an early age. *Virchows Arch.* (2002) 441:279–88. doi: 10.1007/s00428-002-0605-1
8. Burke AP, Farb A, Pestaner J, Malcom GT, Zieske A. Kutys R, et al. Traditional risk factors and the incidence of sudden coronary death with and without coronary thrombosis in blacks. *Circulation.* (2002) 105:419–24. doi: 10.1161/hc0402.102952
9. Guo L, Akahori H, Harari E, Smith SL, Polavarapu R. Karmali V, et al. CD163+ macrophages promote angiogenesis and vascular permeability accompanied by inflammation in atherosclerosis. *J Clin Invest.* (2018) 128:1106–24. doi: 10.1172/JCI93025
10. Pan H, Xue C, Auerbach BJ, Fan J, Bashore AC, Cui J, et al. Single-cell genomics reveals a novel cell state during smooth muscle cell phenotypic switching and potential therapeutic targets for atherosclerosis in mouse and human. *Circulation.* (2020) 142:2060–75. doi: 10.1161/CIRCULATIONAHA.120.048378
11. Yap C, Mieremet A, de Vries CJM, Micha D, de Waard V. Six shades of vascular smooth muscle cells illuminated by KLF4 (Kruppel-Like Factor 4). *Arterioscler Thromb Vasc Biol.* (2021) 41:2693–707. doi: 10.1161/ATVBAHA.121.316600
12. Alencar GF, Owsiany KM, Karnewar S, Sukhavasi K, Mocci G, Nguyen AT, et al. Stem cell pluripotency genes Klf4 and Oct4 regulate complex SMC phenotypic changes critical in late-stage atherosclerotic lesion pathogenesis. *Circulation.* (2020) 142:2045–59. doi: 10.1161/CIRCULATIONAHA.120.046672
13. Cochain C, Vafadarnejad E, Arampatzi P, Pelisek J, Winkels H, Ley K, et al. Single-cell RNA-Seq reveals the transcriptional landscape and heterogeneity of aortic macrophages in murine. *Atheroscler Circ Res.* (2018) 122:1661–74. doi: 10.1161/CIRCRESAHA.117.312509
14. Zernecke A, Winkels H, Cochain C, Williams JW, Wolf D, Soehnlein O, et al. Meta-analysis of leukocyte diversity in atherosclerotic mouse. *Aortas Circ Res.* (2020) 127:402–26. doi: 10.1161/CIRCRESAHA.120.316903
15. Winkels H, Ehinger E, Vassallo M, Buscher K, Dinh HQ, Kobiyama K, et al. Atlas of the immune cell repertoire in mouse atherosclerosis defined by single-cell RNA-sequencing and mass cytometry. *Circ Res.* (2018) 122:1675–88. doi: 10.1161/CIRCRESAHA.117.312513
16. Newman AAC. Serbulea V, Baylis RA, Shankman LS, Bradley X, Alencar GF, et al. Multiple cell types contribute to the atherosclerotic lesion fibrous cap by PDGFRbeta and bioenergetic mechanisms. *Nat Metab.* (2021) 3:166–81. doi: 10.1038/s42255-020-00338-8
17. Iqbal F, Lupieri A, Aikawa M, Aikawa E. Harnessing single-cell RNA sequencing to better understand how diseased cells behave the way they do in cardiovascular disease. *Arterioscler Thromb Vasc Biol.* (2021) 41:585–600. doi: 10.1161/ATVBAHA.120.314776
18. Slenders L, Tessels DE, van der Laan SW, Pasterkamp G, Mokry M. The applications of single-cell RNA sequencing in atherosclerotic disease. *Front Cardiovasc Med.* (2022) 9:826103. doi: 10.3389/fcvm.2022.826103
19. Williams JW, Winkels H, Durant CP, Zaitsev K, Ghosheh Y, Ley K. Single cell RNA sequencing in atherosclerosis research. *Circ Res.* (2020) 126:1112–26. doi: 10.1161/CIRCRESAHA.119.315940
20. Slenders L, Landsmeer LPL, Cui K, Depuydt MAC, Verwer M, Mekke J, et al. Intersecting single-cell transcriptomics and genome-wide association studies identifies crucial cell populations and candidate genes for atherosclerosis. *Eur Heart J Open*. (2022) 2:oeab043. doi: 10.1093/ehjopen/oeab043
21. Fernandez DM, Rahman AH, Fernandez NF, Chudnovskiy A, Amir ED. Amadori, L, et al. Single-cell immune landscape of human atherosclerotic plaques. *Nat Med.* (2019) 25:1576–88. doi: 10.1038/s41591-019-0590-4
22. Okui T, Iwashita M, Rogers MA, Halu A, Atkins SK, Kuraoka S, et al. CROT (Carnitine O-Octanoyltransferase) is a novel contributing factor in vascular calcification via promoting fatty acid metabolism and

mitochondrial dysfunction. *Arterioscler Thromb Vasc Biol.* (2021) 41:755–68. doi: 10.1161/ATVBAHA.120.315007
23. de Kleijn DP, Moll FL, Hellings WE, Ozsarlak-Sozer G, de Bruin P, Doevendans PA, et al. Local atherosclerotic plaques are a source of prognostic biomarkers for adverse cardiovascular events. *Arterioscler Thromb Vasc Biol.* (2010) 30:612–9. doi: 10.1161/ATVBAHA.109.194944
24. Hellings WE, Moll FL, de Kleijn DP, Pasterkamp G. 10-years experience with the Athero-Express study. *Cardiovasc Diagn Ther.* (2012) 2:63–73. doi: 10.3978/j.issn.2223-3652.2012.02.01
25. Depuydt MAC, Prange KHM, Slenders L, Ord T, Elbersen D, Boltjes A, et al. Microanatomy of the human atherosclerotic plaque by single-cell transcriptomics. *Circ Res.* (2020) 127:1437–55. doi: 10.1161/CIRCRESAHA.120.316770
26. Feil S, Fehrenbacher B, Lukowski R, Essmann F, Schulze-Osthoff K, Schaller M, et al. Transdifferentiation of vascular smooth muscle cells to macrophage-like cells during atherogenesis. *Circ Res.* (2014) 115:662–7. doi: 10.1161/CIRCRESAHA.115.304634
27. Gomez D, Shankman LS, Nguyen AT, Owens GK. Detection of histone modifications at specific gene loci in single cells in histological sections. *Nat Methods.* (2013) 10:171–7. doi: 10.1038/nmeth.2332
28. Wong BW, Rahmani M, Luo Z, Yanagawa B, Wong D, Luo H, et al. Vascular endothelial growth factor increases human cardiac microvascular endothelial cell permeability to low-density lipoproteins. *J Heart Lung Transplant.* (2009) 28:950–7. doi: 10.1016/j.healun.2009.05.005
29. Allahverdian S, Chehroudi AC, McManus BM, Abraham T, Francis GA. Contribution of intimal smooth muscle cells to cholesterol accumulation and macrophage-like cells in human atherosclerosis. *Circulation.* (2014) 129:1551–9. doi: 10.1161/CIRCULATIONAHA.113.005015
30. Wong D, Turner AW, Miller CL. Genetic insights into smooth muscle cell contributions to coronary artery disease. *Arterioscler Thromb Vasc Biol.* (2019) 39:1006–17. doi: 10.1161/ATVBAHA.119.312141
31. Erdmann J, Kessler T, Munoz Venegas L, Schunkert H. A decade of genome-wide association studies for coronary artery disease: the challenges ahead. *Cardiovasc Res.* (2018) 114:1241–57. doi: 10.1093/cvr/cvy084
32. Hao K, Ermel R, Sukhavasi K, Cheng H, Ma L, Li L, et al. Integrative prioritization of causal genes for coronary artery disease. *Circ Genom Precis Med.* (2022) 15:e003365. doi: 10.1161/CIRCGEN.121.003365
33. Corces MR, Trevino AE, Hamilton EG, Greenside PG, Sinnott-Armstrong NA, Vesuna S, et al. An improved ATAC-seq protocol reduces background and enables interrogation of frozen tissues. *Nat Methods.* (2017) 14:959–62. doi: 10.1038/nmeth.4396
34. Satija R, Farrell JA, Gennert D, Schier AF, Regev A. Spatial reconstruction of single-cell gene expression data. *Nat Biotechnol.* (2015) 33:495–502. doi: 10.1038/nbt.3192
35. Stuart T, Srivastava A, Madad S, Lareau CA, Satija R. Single-cell chromatin state analysis with Signac. *Nat Methods.* (2021) 18:1333–41. doi: 10.1038/s41592-021-01282-5
36. Granja JM, Corces MR, Pierce SE, Bagdatli ST, Choudhry H, Chang HY, et al. ArchR is a scalable software package for integrative single-cell chromatin accessibility analysis. *Nat Genet.* (2021) 53:403–11. doi: 10.1038/s41588-021-00790-6
37. Aran D, Looney AP, Liu L, Wu E, Fong V, Hsu A, et al. Reference-based analysis of lung single-cell sequencing reveals a transitional profibrotic macrophage. *Nat Immunol.* (2019) 20:163–72. doi: 10.1038/s41590-018-0276-y
38. Shao X, Liao J, Lu X, Xue R, Ai N, Fan X. scCATCH: automatic annotation on cell types of clusters from single-cell RNA sequencing data. *iScience.* (2020) 23:100882. doi: 10.1016/j.isci.2020.100882
39. Pliner HA, Shendure J, Trapnell C. Supervised classification enables rapid annotation of cell atlases. *Nat Methods.* (2019) 16:983–6. doi: 10.1038/s41592-019-0535-3
40. Regev A, Teichmann SA, Lander ES, Amit I, Benoist C, Birney E, et al. The human cell atlas. *Elife.* (2017) 6. doi: 10.7554/eLife.27041
41. Newman AM, Liu CL, Green MR, Gentles AJ, Feng W. Xu, Y, et al. Robust enumeration of cell subsets from tissue expression profiles. *Nat Methods.* (2015) 12:453–7. doi: 10.1038/nmeth.3337
42. Wang X, Park J, Susztak K, Zhang NR Li M. Bulk tissue cell type deconvolution with multi-subject single-cell expression reference. *Nat Commun.* (2019) 10:380. doi: 10.1038/s41467-018-08023-x
43. Powell K. The broken promise that undermines human genome research. *Nature.* (2021) 590:198–201. doi: 10.1038/d41586-021-00331-5
44. Tsosie KS, Fox K, Yracheta JM. Genomics data: the broken promise is to Indigenous people. *Nature.* (2021) 591:529. doi: 10.1038/d41586-021-00758-w
45. Fox K. The illusion of inclusion - the "All of Us" Research Program and Indigenous Peoples' DNA. *N Engl J Med.* (2020) 383:411–3. doi: 10.1056/NEJMp1915987
46. Phillips M. International data-sharing norms: from the OECD to the General Data Protection Regulation (GDPR). *Hum Genet.* (2018) 137:575–82. doi: 10.1007/s00439-018-1919-7
47. Zappia L, Theis FJ. Over 1000 tools reveal trends in the single-cell RNA-seq analysis landscape. *Genome Biol.* (2021) 22:301. doi: 10.1186/s13059-021-02519-4
48. Wang Y, Gao H, Wang F, Ye Z, Mokry M, Turner AW, et al. Dynamic changes in chromatin accessibility are associated with the atherogenic transitioning of vascular smooth muscle cells. *Cardiovasc Res.* (2021). cvab347. doi: 10.1093/cvr/cvab347
49. Wagner DE, Klein AM. Lineage tracing meets single-cell omics: opportunities and challenges. *Nat Rev Genet.* (2020) 21:410–27. doi: 10.1038/s41576-020-0223-2
50. Zaccaria S, Raphael BJ. Characterizing allele- and haplotype-specific copy numbers in single cells with CHISEL. *Nat Biotechnol.* (2021) 39:207–14. doi: 10.1038/s41587-020-0661-6
51. Cao J, Spielmann M, Qiu X, Huang X, Ibrahim DM, Hill AJ, et al. The single-cell transcriptional landscape of mammalian organogenesis. *Nature.* (2019) 566:496–502. doi: 10.1038/s41586-019-0969-x
52. Bergen V, Lange M, Peidli S, Wolf FA, Theis FJ. Generalizing RNA velocity to transient cell states through dynamical modeling. *Nat Biotechnol.* (2020) 38:1408–14. doi: 10.1038/s41587-020-0591-3
53. Wirka RC, Wagh D, Paik DT, Pjanic M, Nguyen T, Miller CL, et al. Atheroprotective roles of smooth muscle cell phenotypic modulation and the TCF21 disease gene as revealed by single-cell analysis. *Nat Med.* (2019) 25:1280–9. doi: 10.1038/s41591-019-0512-5
54. Wang Y, Nanda V, Direnzo D, Ye J, Xiao S, Kojima Y, et al. Clonally expanding smooth muscle cells promote atherosclerosis by escaping efferocytosis and activating the complement cascade. *Proc Natl Acad Sci USA.* (2020) 117:15818–26. doi: 10.1073/pnas.2006348117
55. Libby P, Warner SJ, Friedman GB. Interleukin 1: a mitogen for human vascular smooth muscle cells that induces the release of growth-inhibitory prostanoids. *J Clin Invest.* (1988) 81:487–98. doi: 10.1172/JCI113346
56. Gomez D, Baylis RA, Durgin BG, Newman AAC, Alencar GF, Mahan S, et al. Interleukin-1beta has atheroprotective effects in advanced atherosclerotic lesions of mice. *Nat Med.* (2018) 24:1418–29. doi: 10.1038/s41591-018-0124-5
57. Hamers AAJ, Dinh HQ, Thomas GD, Marcovecchio P, Blatchley A, Nakao CS, et al. Human monocyte heterogeneity as revealed by high-dimensional mass cytometry. *Arterioscler Thromb Vasc Biol.* (2019) 39:25–36. doi: 10.1161/ATVBAHA.118.311022
58. Tousoulis D, Oikonomou E, Economou EK, Crea F, Kaski JC. Inflammatory cytokines in atherosclerosis: current therapeutic approaches. *Eur Heart J.* (2016) 37:1723–32. doi: 10.1093/eurheartj/ehv759
59. Andrie RP, Becher UM, Frommold R, Tiyerili V, Schrickel JW, Nickenig G, et al. Interleukin-6 is the strongest predictor of 30-day mortality in patients with cardiogenic shock due to myocardial infarction. *Crit Care.* (2012) 16:R152. doi: 10.1186/cc11467
60. Gager GM, Biesinger B, Hofer F, Winter MP, Hengstenberg C, Jilma B, et al. Interleukin-6 level is a powerful predictor of long-term cardiovascular mortality in patients with acute coronary syndrome. *Vascul Pharmacol.* (2020) 135:106806. doi: 10.1016/j.vph.2020.106806
61. Ziegler L, Lundqvist J, Dreij K, Wallen H, de Faire U, Paulsson-Berne G, et al. Expression of Interleukin 6 signaling receptors in carotid atherosclerosis. *Vasc Med.* (2021) 26:3–10. doi: 10.1177/1358863X20977662
62. Debing E, Peeters E, Demanet C, De Waele M, Van den Brande P. Markers of inflammation in patients with symptomatic and asymptomatic carotid

artery stenosis: a case-control study. *Vasc Endovascular Surg.* (2008) 42:122–7. doi: 10.1177/1538574407307406
63. Jaiswal S, Natarajan P, Silver AJ, Gibson CJ, Bick AG, Shvartz E, et al. Clonal hematopoiesis and risk of atherosclerotic cardiovascular disease. *N Engl J Med.* (2017) 377:111–21. doi: 10.1056/NEJMoa1701719
64. Ma WF, Hodonsky CJ, Turner AW, Wong D, Song Y, Mosquera JV, et al. Enhanced single-cell RNA-seq workflow reveals coronary artery disease cellular cross-talk and candidate drug targets. *Atherosclerosis.* (2022) 340:12–22. doi: 10.1016/j.atherosclerosis.2021.11.025
65. Pelisek J, Hegenloh R, Bauer S, Metschl S, Pauli J, Glukha N, et al. Biobanking: objectives, requirements, future challenges-experiences from the munich vascular biobank. *J Clin Med.* (2019) 8:251. doi: 10.3390/jcm8020251
66. Martinet W, De Meyer GR, Herman AG, Kockx MM. RNA damage in human atherosclerosis: pathophysiological significance and implications for gene expression studies. *RNA Biol.* (2005) 2:4–7. doi: 10.4161/rna.2.1.1430
67. Kvastad L, Carlberg K, Larsson L, Villacampa EG, Stuckey A, Stenbeck L, et al. The spatial RNA integrity number assay for in situ evaluation of transcriptome quality. *Commun Biol.* (2021) 4:57. doi: 10.1038/s42003-020-01573-1
68. Lee MY, Bedia JS, Bhate SS, Barlow GL, Phillips D, Fantl WJ, et al. CellSeg: a robust, pre-trained nucleus segmentation and pixel quantification software for highly multiplexed fluorescence images. *BMC Bioinformatics.* (2022) 23:46. doi: 10.1186/s12859-022-04570-9
69. Baars MJD. Sinha N, Amini M, Pieterman-Bos A, van Dam S, Ganpat MMP, et al. MATISSE: a method for improved single cell segmentation in imaging mass cytometry. *BMC Biol.* (2021) 19:99. doi: 10.1186/s12915-021-01043-y
70. Keren L, Bosse M, Marquez D, Angoshtari R, Jain S, Varma S, et al. A structured tumor-immune microenvironment in triple negative breast cancer revealed by multiplexed ion beam imaging. *Cell.* (2018) 174:1373–87 e1319. doi: 10.1016/j.cell.2018.08.039
71. Cable DM, Murray E, Zou LS, Goeva A, Macosko EZ, Chen F, et al. Robust decomposition of cell type mixtures in spatial transcriptomics. *Nat Biotechnol.* (2022) 40:517–26. doi: 10.1038/s41587-021-00830-w
72. Moncada R, Barkley D, Wagner F, Chiodin M, Devlin JC, Baron M, et al. Integrating microarray-based spatial transcriptomics and single-cell RNA-seq reveals tissue architecture in pancreatic ductal adenocarcinomas. *Nat Biotechnol.* (2020) 38:333–42. doi: 10.1038/s41587-019-0392-8
73. Sadeghi Rad H, Bazaz SR, Monkman J, Ebrahimi Warkiani M, Rezaei N, O'Byrne K, et al. The evolving landscape of predictive biomarkers in immuno-oncology with a focus on spatial technologies. *Clin Transl Immunol.* (2020) 9:e1215. doi: 10.1002/cti2.1215
74. Wu T, Liang Z, Zhang Z, Liu C, Zhang L, Gu Y, et al. PRDM16 is a compact myocardium-enriched transcription factor required to maintain compact myocardial cardiomyocyte identity in left ventricle. *Circulation.* (2022) 145:586–602. doi: 10.1161/CIRCULATIONAHA.121.056666
75. Porritt RA, Zemmour D, Abe M, Lee Y, Narayanan M, Carvalho TT, et al. NLRP3 inflammasome mediates immune-stromal interactions in vasculitis. *Circ Res.* (2021) 129:e183–200. doi: 10.1161/CIRCRESAHA.121.319153
76. Asp M, Salmén F, Ståhl PL, Vickovic S, Felldin U, Löfling M, et al. Spatial detection of fetal marker genes expressed at low level in adult human heart tissue. *Sci Rep.* (2017) 7:12941. doi: 10.1038/s41598-017-13462-5
77. Guilliams M, Bonnardel J, Haest B, Vanderborght B, Wagner C, Remmerie A, et al. Spatial proteogenomics reveals distinct and evolutionarily conserved hepatic macrophage niches. *Cell.* (2022) 185:379–96.e38. doi: 10.1016/j.cell.2021.12.018
78. Tavares-Ferreira D, Shiers S, Ray PR, Wangzhou A, Jeevakumar V, Sankaranarayanan I, et al. Spatial transcriptomics of dorsal root ganglia identifies molecular signatures of human nociceptors. *Sci Transl Med.* (2022) 14:eabj8186. doi: 10.1126/scitranslmed.abj8186
79. Zhu Y, Wu Z, Yan W, Shao F, Ke B, Jiang X, et al. Allosteric inhibition of SHP2 uncovers aberrant TLR7 trafficking in aggravating psoriasis. *EMBO Mol Med.* (2022) 14:e14455. doi: 10.15252/emmm.202114455
80. Andersson A, Larsson L, Stenbeck L, Salmén F, Ehinger A, Wu SZ, et al. Spatial deconvolution of HER2-positive breast cancer delineates tumor-associated cell type interactions. *Nat Commun.* (2021) 12:6012. doi: 10.1038/s41467-021-26271-2
81. Gracia Villacampa E, Larsson L, Mirzazadeh R, Kvastad L, Andersson A, Mollbrink A, et al. Genome-wide spatial expression profiling in formalin-fixed tissues. *Cell Genomics.* (2021) 1:100065. doi: 10.1016/j.xgen.2021.100065
82. Salmén F, Ståhl PL, Mollbrink A, Navarro JF, Vickovic S, Frisén J, et al. Barcoded solid-phase RNA capture for spatial transcriptomics profiling in mammalian tissue sections. *Nat Protoc.* (2018) 13:2501–34. doi: 10.1038/s41596-018-0045-2
83. Merritt CR, Ong GT, Church SE, Barker K, Danaher P, Geiss G, et al. Multiplex digital spatial profiling of proteins and RNA in fixed tissue. *Nat Biotechnol.* (2020) 38:586–99. doi: 10.1038/s41587-020-0472-9
84. Bergholtz H, Carter JM, Cesano A, Cheang MCU, Church SE, Divakar P, et al. Best practices for spatial profiling for breast cancer research with the GeoMx® digital spatial profiler. *Cancers.* (2021) 13:4456. doi: 10.3390/cancers13174456
85. Smith KD, Prince DK, Henriksen KJ, Nicosia RF, Alpers CE, Akilesh S. Digital spatial profiling of collapsing glomerulopathy. *Kidney Int.* (2022) 101:1017–26. doi: 10.1016/j.kint.2022.01.033
86. Dottermusch M, Schumann Y, Kordes U, Hasselblatt M, Neumann JE. Spatial molecular profiling of a central nervous system low-grade diffusely infiltrative tumour with INI1 deficiency featuring a high-grade atypical teratoid/rhabdoid tumour component. *Neuropathol Appl Neurobiol.* (2022) 48:e12777. doi: 10.1111/nan.12777
87. Delorey TM, Ziegler CGK, Heimberg G, Normand R, Yang Y, Segerstolpe Å, et al. COVID-19 tissue atlases reveal SARS-CoV-2 pathology and cellular targets. *Nature.* (2021) 595:107–13. doi: 10.1038/s41586-021-03570-8
88. Schlam I, Church SE, Hether TD, Chaldekas K, Hudson BM, White AM, et al. The tumor immune microenvironment of primary and metastatic HER2-positive breast cancers utilizing gene expression and spatial proteomic profiling. *J Transl Med.* (2021) 19:480. doi: 10.1186/s12967-021-03113-9
89. Bodenmiller B. Multiplexed epitope-based tissue imaging for discovery and healthcare applications. *Cell Syst.* (2016) 2:225–38. doi: 10.1016/j.cels.2016.03.008
90. Baharlou H, Canete NP, Cunningham AL, Harman AN, Patrick E. Mass cytometry imaging for the study of human diseases-applications and data analysis strategies. *Front Immunol.* (2019) 10:2657. doi: 10.3389/fimmu.2019.02657
91. Schürch CM, Bhate SS, Barlow GL, Phillips DJ, Noti L, Zlobec I, et al. Coordinated cellular neighborhoods orchestrate antitumoral immunity at the colorectal cancer invasive. *Front Cell.* (2020) 182:1341–59.e19. doi: 10.1016/j.cell.2020.07.005
92. Gouin KH, Ing N, Plummer JT, Rosser CJ. ben Cheikh B, Oh C, et al. An N-Cadherin 2 expressing epithelial cell subpopulation predicts response to surgery, chemotherapy and immunotherapy in bladder cancer. *Nat Commun.* (2021) 12:4906. doi: 10.1038/s41467-021-25103-7
93. Palla AR, Ravichandran M, Wang YX, Alexandrova L, Yang A v, Kraft P, et al. Inhibition of prostaglandin-degrading enzyme 15-PGDH rejuvenates aged muscle mass and strength. *Science.* (2021) 371. doi: 10.1126/science.abc8059
94. Goltsev Y, Samusik N, Kennedy-Darling J, Bhate S, Hale M, Vazquez G, et al. Deep profiling of mouse splenic architecture with CODEX multiplexed imaging. *Cell.* (2018) 174:968–81.e15. doi: 10.1016/j.cell.2018.07.010
95. Fluidigm Web Page (2022). Available online at: https://www.fluidigm.com (accessed April 28, 2022).
96. Abdulrahman Z, Santegoets SJ, Sturm G, Charoentong P, Ijsselsteijn ME, Somarakis A, et al. Tumor-specific T cells support chemokine-driven spatial organization of intratumoral immune microaggregates needed for long survival. *J Immunother Cancer.* (2022) 10:e004346. doi: 10.1136/jitc-2021-004346
97. Zheng Y, Han L, Chen Z, Li Y, Zhou B, Hu R, et al. PD-L1+CD8+ T cells enrichment in lung cancer exerted regulatory function and tumor-promoting tolerance. *IScience.* (2022) 25:103785. doi: 10.1016/j.isci.2022.103785
98. Feng C, Wang X, Tao Y, Xie Y, Lai Z, Li Z, et al. Single-cell proteomic analysis dissects the complexity of tumor microenvironment in muscle invasive bladder cancer. *Cancers.* (2021) 13:5440. doi: 10.3390/cancers13215440
99. Chen C, McDonald D, Blain A, Sachdeva A, Bone L, Smith ALM, et al. Imaging mass cytometry reveals generalised deficiency in OXPHOS complexes in Parkinson's disease. *NPJ Parkinsons Dis.* (2021) 7:39. doi: 10.1038/s41531-021-00182-x
100. Ionpath Web Page (2022). Available online at: https://www.ionpath.com (accessed April 28, 2022).

101. Rovira-Clavé X, Jiang S, Bai Y, Zhu B, Barlow G, Bhate S, et al. Subcellular localization of biomolecules and drug distribution by high-definition ion beam imaging. *Nat Commun.* (2021) 12:4628. doi: 10.1038/s41467-021-24822-1
102. Risom T, Glass DR, Averbukh I, Liu CC, Baranski A, Kagel A, et al. Transition to invasive breast cancer is associated with progressive changes in the structure and composition of tumor stroma. *Cell.* (2022) 185:299–310.e18. doi: 10.1016/j.cell.2021.12.023
103. McCaffrey EF, Donato M, Keren L, Chen Z, Delmastro A, Fitzpatrick MB, et al. The immunoregulatory landscape of human tuberculosis granulomas. *Nat Immunol.* (2022) 23:318–29. doi: 10.1038/s41590-021-01121-x
104. Liu CC, Bosse M, Kong A, Kagel A, Kinders R, Hewitt SM, et al. Reproducible, high-dimensional imaging in archival human tissue by multiplexed ion beam imaging by time-of-flight (MIBI-TOF). *Lab Invest.* (2022). doi: 10.1038/s41374-022-00778-8
105. Angelo M, Bendall SC, Finck R, Hale MB, Hitzman C, Borowsky AD, et al. Multiplexed ion beam imaging of human breast tumors. *Nat Med.* (2014) 20:436–42. doi: 10.1038/nm.3488

Conflict of Interest: The authors declare that the research was conducted in the absence of any commercial or financial relationships that could be construed as a potential conflict of interest.

frontiers | Frontiers in Cardiovascular Medicine

TYPE Original Research
PUBLISHED 08 August 2022
DOI 10.3389/fcvm.2022.969421

OPEN ACCESS

EDITED BY
Kathryn L. Howe,
University of Toronto, Canada

REVIEWED BY
Ayman Al Haj Zen,
Hamad Bin Khalifa University, Qatar
Laura Zelarayán,
University of Göttingen, Germany

*CORRESPONDENCE
Clint L. Miller
clintm@virginia.edu

SPECIALTY SECTION
This article was submitted to Atherosclerosis and Vascular Medicine, a section of the journal Frontiers in Cardiovascular Medicine

RECEIVED 15 June 2022
ACCEPTED 21 July 2022
PUBLISHED 08 August 2022

CITATION
Ma WF, Turner AW, Gancayco C, Wong D, Song Y, Mosquera JV, Auguste G, Hodonsky CJ, Prabhakar A, Ekiz HA, van der Laan SW and Miller CL (2022) PlaqView 2.0: A comprehensive web portal for cardiovascular single-cell genomics. *Front. Cardiovasc. Med.* 9:969421. doi: 10.3389/fcvm.2022.969421

PlaqView 2.0: A comprehensive web portal for cardiovascular single-cell genomics

Wei Feng Ma[1,2], Adam W. Turner[2], Christina Gancayco[3], Doris Wong[2,4], Yipei Song[2,5], Jose Verdezoto Mosquera[2,3], Gaëlle Auguste[2], Chani J. Hodonsky[2], Ajay Prabhakar[2], H. Atakan Ekiz[6], Sander W. van der Laan[7] and Clint L. Miller[2,4,8]*

[1]Medical Scientist Training Program, University of Virginia, Charlottesville, VA, United States, [2]Center for Public Health Genomics, University of Virginia, Charlottesville, VA, United States, [3]Research Computing, University of Virginia, Charlottesville, VA, United States, [4]Department of Biochemistry and Molecular Genetics, University of Virginia, Charlottesville, VA, United States, [5]Department of Computer Engineering, University of Virginia, Charlottesville, VA, United States, [6]Department of Molecular Biology and Genetics, Izmir Institute of Technology, Gülbahçe, Turkey, [7]Central Diagnostics Laboratory, Division Laboratories, Pharmacy, and Biomedical Genetics, University Medical Center Utrecht, Utrecht University, Utrecht, Netherlands, [8]Department of Public Health Sciences, University of Virginia, Charlottesville, VA, United States

Single-cell RNA-seq (scRNA-seq) is a powerful genomics technology to interrogate the cellular composition and behaviors of complex systems. While the number of scRNA-seq datasets and available computational analysis tools have grown exponentially, there are limited systematic data sharing strategies to allow rapid exploration and re-analysis of single-cell datasets, particularly in the cardiovascular field. We previously introduced PlaqView, an open-source web portal for the exploration and analysis of published atherosclerosis single-cell datasets. Now, we introduce PlaqView 2.0 (www.plaqview.com), which provides expanded features and functionalities as well as additional cardiovascular single-cell datasets. We showcase improved PlaqView functionality, backend data processing, user-interface, and capacity. PlaqView brings new or improved tools to explore scRNA-seq data, including gene query, metadata browser, cell identity prediction, *ad hoc* RNA-trajectory analysis, and drug-gene interaction prediction. PlaqView serves as one of the largest central repositories for cardiovascular single-cell datasets, which now includes data from human aortic aneurysm, gene-specific mouse knockouts, and healthy references. PlaqView 2.0 brings advanced tools and high-performance computing directly to users without the need for any programming knowledge. Lastly, we outline steps to generalize and repurpose PlaqView's framework for single-cell datasets from other fields.

KEYWORDS

scRNA-seq, single-cell, cardiovascular, genomics, web portal, database

Introduction

Named "Method of the Year" in 2013, single-cell RNA sequencing (scRNA-seq) technology has now been used in virtually every field of biology and medicine, including cancer biology and cardiovascular medicine (1, 2). While scRNA-seq technologies continue to evolve and multi-modal measurements become increasingly more common, there has been a rapid increase in both the number of analysis tools and the complexity of single-cell data. At the time of writing, scrna-tools.org reports over 1,000 tools dedicated to single-cell data analysis (3). Despite the abundance of single-cell analysis tools available, there are two major challenges that affect the single-cell community as a whole: (1) there are no standardized methods of single-cell data sharing, and (2) increasingly complex and large single-cell data require advanced bioinformatic skills and resources for comprehensive analysis and interpretation.

The lack of standardized data sharing leads to the omission of critical metadata needed for reproducible analysis, such as author-defined cluster and cell-type annotations, and variables such as sex and age group (4). Despite the existence of public archives such as the Gene Expression Omnibus (GEO) and Sequence Read Archive (SRA), there is no uniform requirement for the deposition of metadata. Even within SRA, some datasets require specialized cloud computing tools (e.g., Google Cloud Computing) to access, such as the data from Li et al. (5). A recent study has found that $<$ 50% of the published figures from public single-cell data can be reproduced as published (6). Furthermore, raw sequence files are very large (often $>$15 GB per file) and thus have very high computational resource requirements.

The fact that most tools require users to have significant programming skills remains a significant barrier to reanalyzing and exploring single-cell data, particularly across multiple datasets (7, 8). A few tools, such as the cBioPortal for Cancer Genomics (www.cbioportal.org), have distilled large bulk RNA-seq datasets, made them accessible to everyone, and provided multiple query functions, but none are designed for single-cell datasets (Supplemental Table 1) (9). Other portals, such as DISCO, provide real-time data integration and queries of multiple datasets across different tissues; however, DISCO currently lacks cardiovascular-specific datasets and comparison of analysis tools (Supplemental Table 1) (10). As more datasets emerge, the need for a centralized and domain-specific repository tailored for single-cell cardiovascular datasets becomes more pressing. A centralized repository packaged with tools specific for cardiovascular diseases will facilitate the advancement of the field as a whole and support the democratization and utility of single-cell data.

Previously, we introduced PlaqView, an open-source web portal focused on the exploration of the data generated by Wirka et al. (11) and a few other atherosclerosis-related datasets (12). Here, we introduce PlaqView 2.0, a significantly improved release with a broader scope to include, among others, datasets from other areas of the cardiovascular field, including human aortic aneurysm (13), healthy human heart atlas (14), human aortic valves (15), mouse models of atherogenesis (16), and others. We describe improvements to the user interface, new *ad hoc* functions to calculate trajectories on cells of interest, metadata exploration, and the ability to export publication-ready figures in addition to existing functions such as basic gene expression query and drug-gene interaction analysis. We also highlight several backend improvements that allow us to bring high-performance, reproducible computing environments to lay scientists *via* the web browser. Lastly, we outline basic steps to repurpose the PlaqView programming scaffold for other areas of single-cell investigation.

Results

PlaqView 2.0 includes significant expansion in data availability

Since our initial publication introducing PlaqView, which featured 7 datasets from 4 studies (12), PlaqView 2.0 now features 32 datasets: 23 from human tissues and 9 from mouse tissues (Figure 1, Supplemental Table 2). New single-cell datasets made available in this release include those from: mouse carotid ligation experiments (17), mouse adventitial cell layer (18), human adult heart compartments (14), human COVID-19 autopsy hearts (19), and human aortic leaflets (15). At the time of writing, PlaqView now contains over 1.7 million total cells. PlaqView will be actively maintained and we will continue to add new datasets upon their publication and release to the public.

PlaqView allows rapid query of gene expression of single cell datasets

Gene expression-based query is the mainstay for single-cell data exploration. However, this is also one of the most time-consuming steps because public data are often shared in various formats that require customized codes to be read and analyzed. In PlaqView 2.0, each dataset has been systematically preprocessed from various stages of upstream analysis to allow efficient querying on-demand. Upon launching the PlaqView homepage (www.plaqview.com), users can open the scRNA-seq portal (Figure 2), choose the scRNA-seq dataset of their interest, and load it into the memory of their dedicated

Abbreviations: CIPR, cell identity predictor; GSEA, gene-set enrichment analysis; scRNA-seq, single-cell RNA-sequencing; UMAP, uniform manifold approximation and projection.

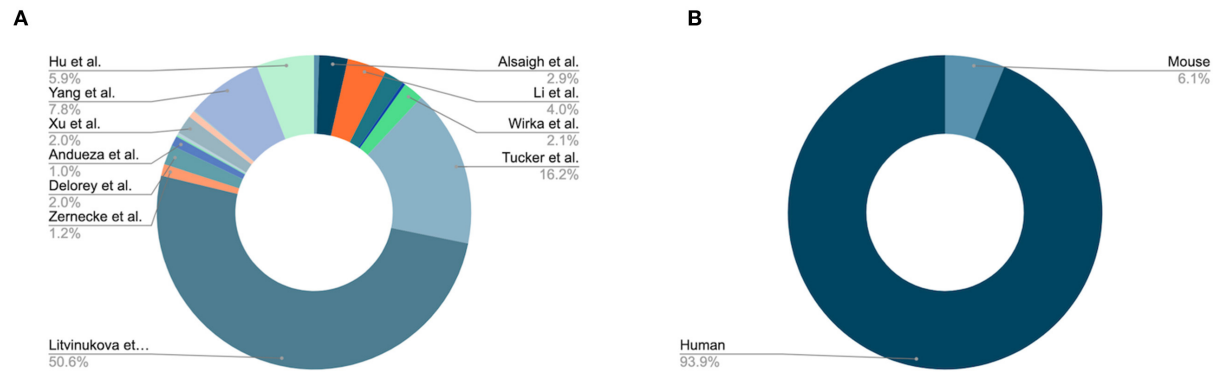

FIGURE 1
PlaqView 2.0 incorporates 32 cardiovascular-related datasets. **(A)** Major datasets available on PlaqView. PlaqView brings high-performance computing directly to the browser in order to handle large datasets such as ones from Litvinukova et al., which are atlas-type survey data that contain tissues from the entire human heart. **(B)** Species composition of PlaqView's database.

session. Manually curated information about each dataset is also available on the portal and on the main homepage. Once the dataset is loaded, users are directed to the "Gene Lookup" tab (Figure 3) where they can enter a single gene or multiple genes, select the plot type they prefer (e.g., Dot Plot, Feature Plot, or Ridge Plot), and choose from one of the available cell-labeling methods (see next section) for query. The Gene Query function is powered by Seurat (7). Gene symbol capitalizations are automatically corrected based on species of the dataset selected to conform to Human Gene Nomenclature Committee (HGNC) or Mouse Genome Informatics (MGI) gene nomenclature conventions (e.g., *APOE* for humans and *Apoe* for mice) (20, 21). The queried gene(s) plots then will appear alongside the conventional UMAP displaying the cell type, and users can download high-quality, publication-ready figures in .pdf format.

To facilitate functional interpretation within a given single-cell dataset, PlaqView conducts automated Pathway Enrichment Analysis with the queried genes, powered by EnrichR (22–24). Although not commonly a part of a standard single-cell RNA-seq pipeline, pathway enrichments provide additional insights into the biological importance and functional consequences. Users can choose their preferred databases from a list of well-annotated sources such as ENCODE (Encyclopedia of DNA Elements) and GO (Gene Ontology). For example, querying the two NADPH oxidase genes implicated in redox metabolism and atherosclerosis "CYBB" and "NOX4" (25, 26), in the Li et al. (13) dataset using the "GO_Biological_Process_2018" database shows the top function category as "superoxide anion generation," and that (FB), macrophages (Mø), and smooth muscle cells (SMCs) highly express these genes (Figure 3). This information allows users to quickly assess and generate hypotheses and aid in the design of future experiments.

Cell labeling and differential gene expression

Cell identity prediction remains one of the most time-intensive and critical steps in the single-cell analysis pipeline (27). Previously, we found that the upstream cell-state prediction step greatly affects downstream analysis such as cell-cell communication analysis (12), and multiple labeling methods should be compared for consistency. Automated labeling tools are great starting points and help eliminate the inherent bias introduced in cluster-based manual annotation (27). However, current references may not accurately predict novel cell types or transitional states, such as the "myofibroblasts" as shown in Wirka et al. (11). Furthermore, discovery of novel niche cell-types are difficult and require careful examination of the differential gene expression patterns.

PlaqView enables users to run and compare several methods of cell annotation and compare them against other databases, as well as exporting the entire differential gene expression matrix for manual exploration of rare cell types. In many areas of the application and specifically under the "Cell Labeling" tab, users have the ability to explore the cell identities as provided by the original authors (when available), by SingleR (28), and by Seurat V4 "label transfer" using the Tabula Sapiens atlas (7, 29). To demonstrate this, we explored the Livinukova et al., annotation (Figure 4A) against the annotation provided by Seurat's label transfer using the Tabula Sapiens reference (Figure 4B) (7, 29). These identity predictions are pre-run during the data processing stage and stored within each data object. By running the cell identity prediction during the preprocessing stage (see Methods) and not on-demand, PlaqView can rapidly display results with little downtime. To allow additional flexibility, transparency and further exploration of the differentially expressed genes in each cell type, we

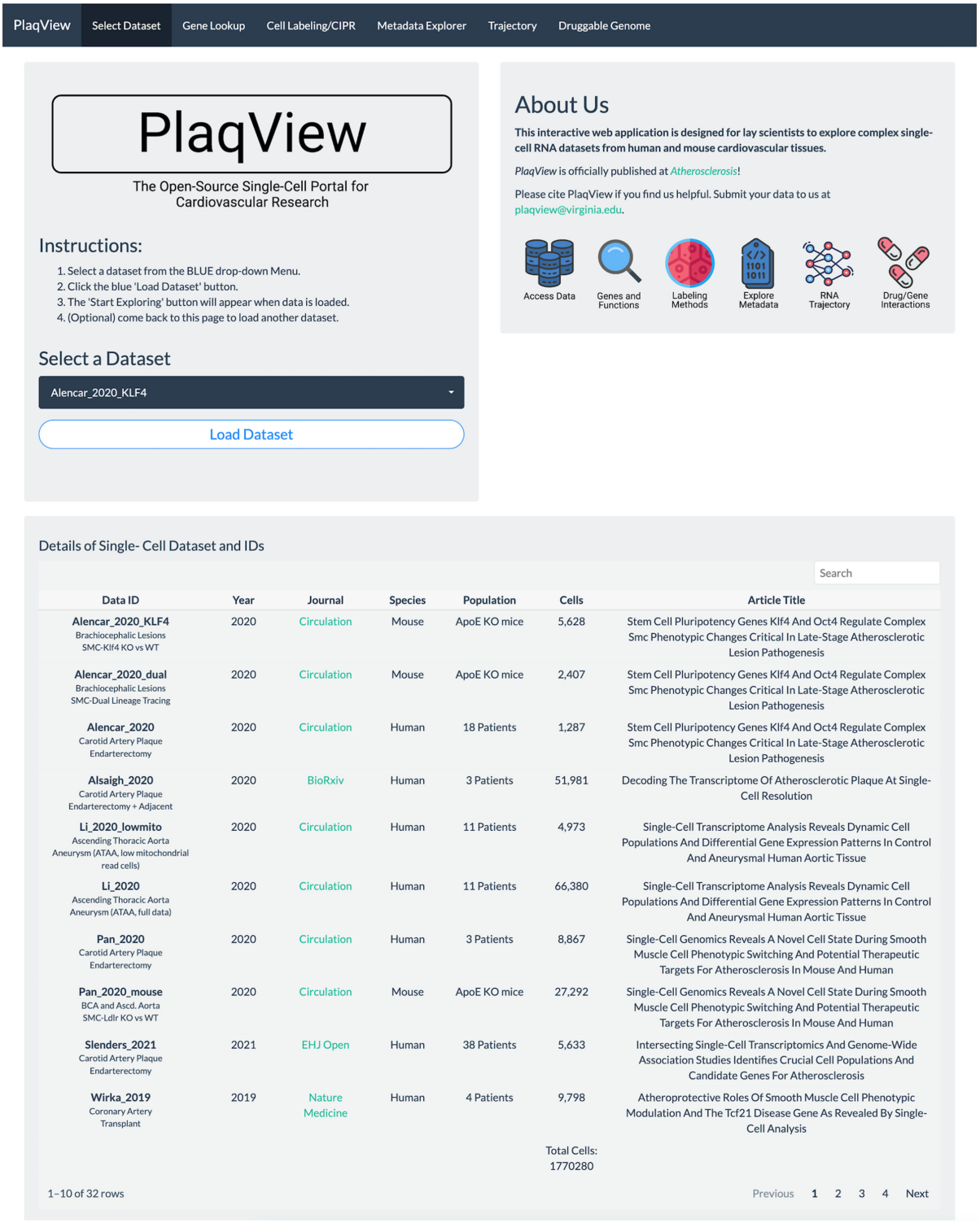

FIGURE 2
PlaqView 2.0 homepage facilitates selection and loading of relevant datasets. The homepage allows users to browse dataset details and load selected datasets into their dedicated session for further exploration.

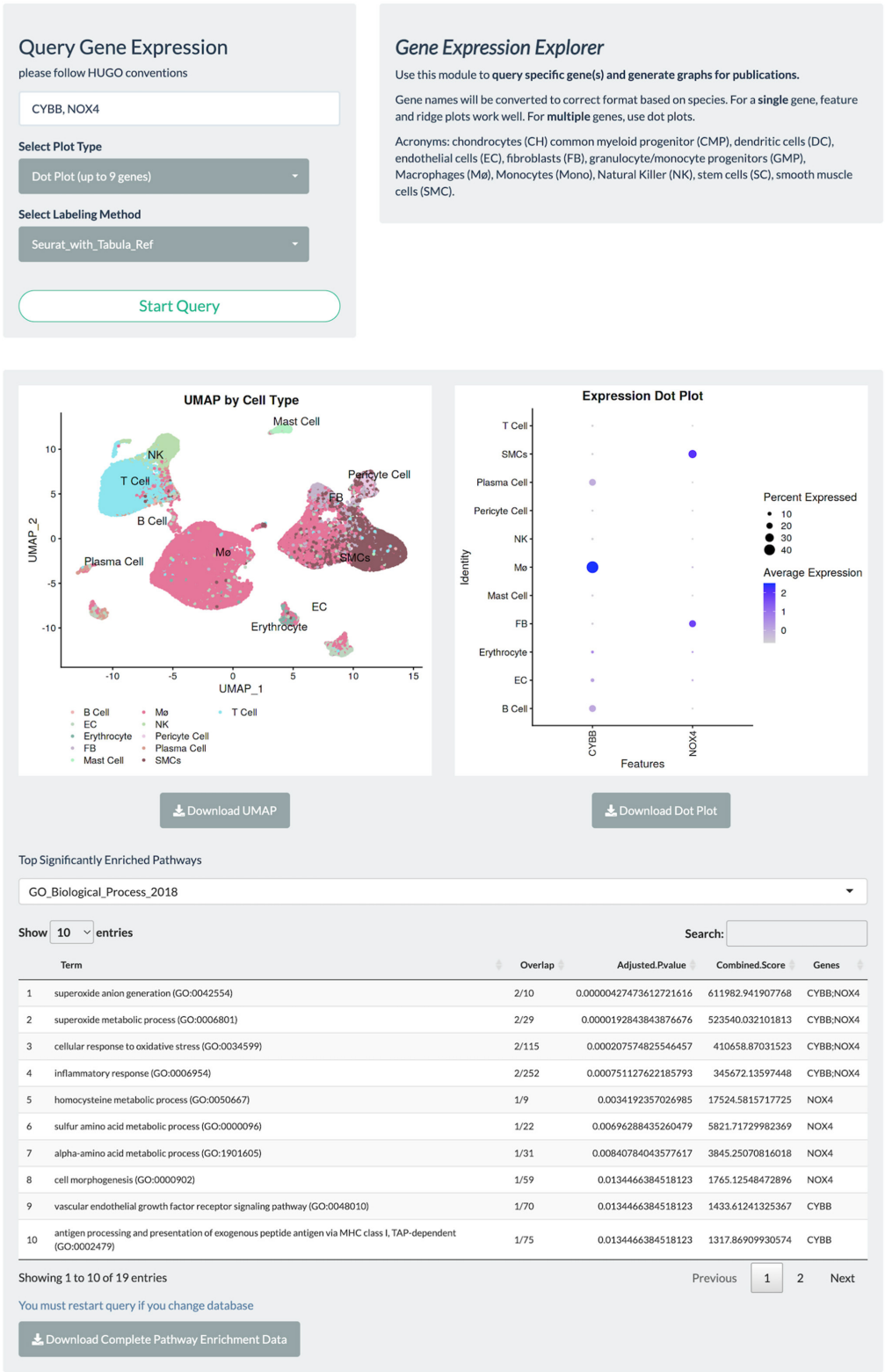

FIGURE 3
Gene query page allows rapid visualization of gene expression, UMAP embeddings, and facilitates automated GSEA. PlaqView 2.0 supports visualization of a single gene or multiple genes via feature, dot, and ridge plots, as powered by Seurat. Users can also choose their preferred annotation methods and download high-quality pdfs for publication. This instance is a demonstration using the Li et al. dataset.

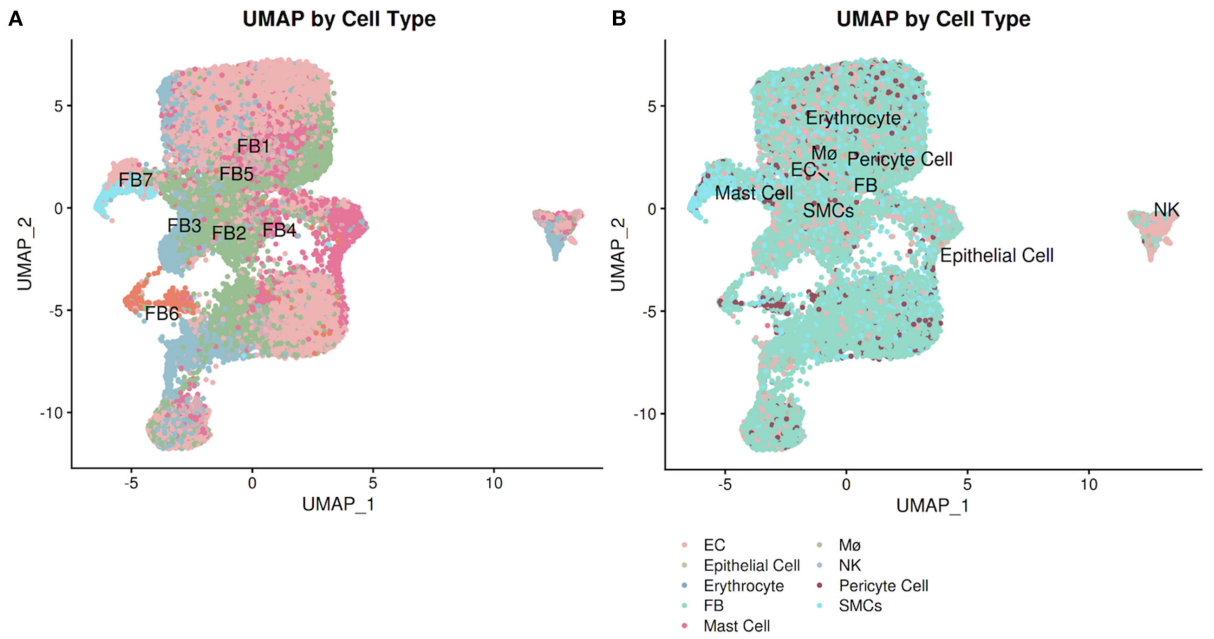

FIGURE 4
Annotation explorer page facilitates cell-level annotation comparison. Users can compare pre-computed cell identity annotations as well as author-provided labels (when available). Using the Litvinukova et al. dataset, we demonstrate the difference between the annotation from the **(A)** original authors and **(B)** Seurat label transfer using the Tabula Sapiens reference.

provide precomputed tables of the differentially expressed genes based on labeling methods in downloadable .csv format. By precomputing these tables during the preprocessing stage, we cut down hours of computing time for the end-user. These tables provide users the opportunities to review genes or cell groups of interests, and serve as starting points for downstream analysis such as drug-gene interaction analysis.

In PlaqView 2.0, we have incorporated a new interactive feature named Cell Identity PRedictor, or CIPR (Figure 5) (30). CIPR provides an additional opportunity for users to interact with the data and further explore and compare the cell annotations. CIPR calculates, in real-time, cluster-based gene expression similarity index scores against known references, such as the Database of Immune Cell Expression (DICE), Immunological GenomeProject (ImmGen), and the Human Primary Cell Atlas (30). To run CIPR on the loaded dataset, users need to select the starting labeling method (default is the unlabeled Seurat clusters) and the reference to benchmark against (default is ImmGen Mouse). CIPR was designed to be able to run against human and mouse references interchangeably. PlaqView will output an interactive CIPR plot where users can select the cluster(s) of interest and explore the top similar cell types, their descriptions, identity scores (calculated as a function of fold-change dot-product) and percent of genes that are similarly co-expressed. For example, when running the COVID-19 heart autopsy data from Delorey et al. (19) using the pre-sorted human RNAseq reference provided by CIPR, we noted a high concordance between the author-labeled "CD8 + *T*-cells" with the reference cluster "Effector memory CD8 *T* cells", with a 75.5% precent positive correlation in gene signature (Figure 5). Lastly, users can download a full table of the CIPR results in .csv format as well as the CIPR plot in .pdf format for publication.

PlaqView enables users to explore unstructured metadata

Currently, no systematic convention exists in sharing single-cell metadata that are essential for reproducible analysis and future meta-analysis. These important metadata, such as sex, age, sample location, and author-provided cell-type annotations, are often omitted when submitting data to public repositories. It is estimated that fewer than 25% of current single-cell studies have provided cell-level metadata (4). PlaqView 2.0 aims to provide a platform for easier standardization and sharing of cell-level metadata in three ways: (1) we curate and reformat existing metadata and append them into the Seurat object, (2) we require new submissions to have pre-embedded metadata, and (3) we developed features to explore all existing available metadata in their unabridged format.

When available, PlaqView separates the metadata into "Factor-Type" (Figure 6A) and "Continuous-Type"

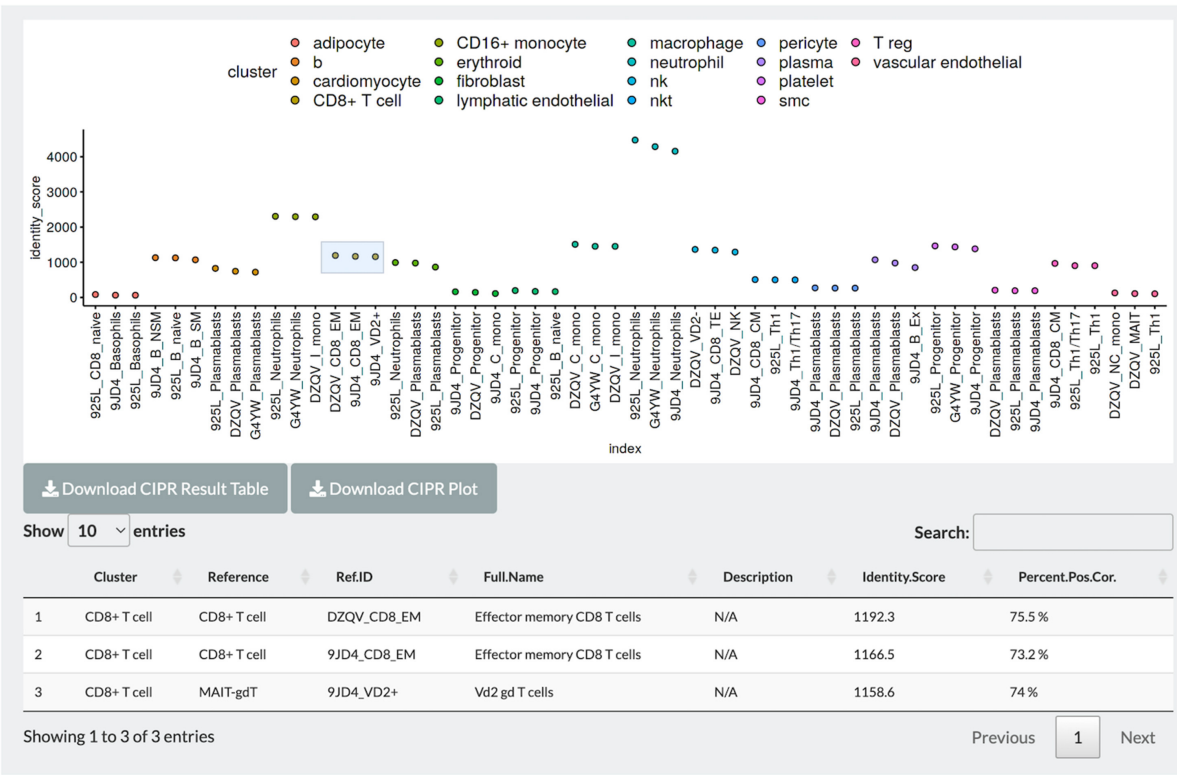

FIGURE 5
CIPR integration allows further exploration and interaction with cell-level annotation. Users can benchmark pre-computed annotations with existing single-cell references, and interactively compare and visualize identity scores and percent correlations with the top candidate reference identities. Light blue box indicates selected groups for detailed tables.

variables (Figures 6B,D). Examples of factor-type metadata include sex, age-group, biological individuals, and disease type, whereas continuous-type metadata include percent mitochondrial reads, age, and *p*-values of singleR annotations. PlaqView will output appropriate feature maps when these data are available. Furthermore, we introduce the ability to query gene expression based on factor-type variables. We demonstrate its use by querying the genes *APOE*, *COL1A1*, *FBLN1*, and *FBLN2* in the Tucker et al. (31) dataset using the "chamber" variable (Figure 6C). Interestingly, fibulins (*FBLN1* and *FBLN2*) are more highly expressed in the right atrium (RA) and left atrium (LA), compared to ventricular samples, most likely due to the differential behavior of atrial and ventricular fibroblasts (32). However, further interrogation using the "experiment" and "biological.individual" variables show significant variation of fibulin expression among the atrial samples as well as among individuals sampled (Supplemental Figures 1A,B). This particular example demonstrates the critical need for better metadata sharing as well as the utility of the metadata explorer feature.

Cell trajectories and re-clustering

RNA trajectory analysis, in conjunction with pseudotemporal ordering, has been widely used as a method to reconstruct cell fate, differentiation, and transition events (12, 33–35). In terms of cardiovascular data, RNA trajectories have been useful in studying the fate and transitions of fibroblasts, immune cells, smooth muscle cells and other intermediate cell types (12, 35–37). In PlaqView 2.0, we provide additional functionality in RNA trajectory estimation with Monocle3 (33) by integrating high-performance calculation steps directly within the browser. Upon opening the "Trajectory" page, the full pre-calculated RNA trajectory using the entire dataset is displayed. Now, users can select cells of interest and subset these cells for re-clustering and re-calculation of their RNA-trajectory (Figures 7A-C). This interactive feature allows supervised input and selection of relevant cells that can help reduce trajectory "noise." Furthermore, this feature is helpful because RNA trajectories may not always be applicable to every cell type in the study, such as those that are post-mitotic or slow-dividing. Depending

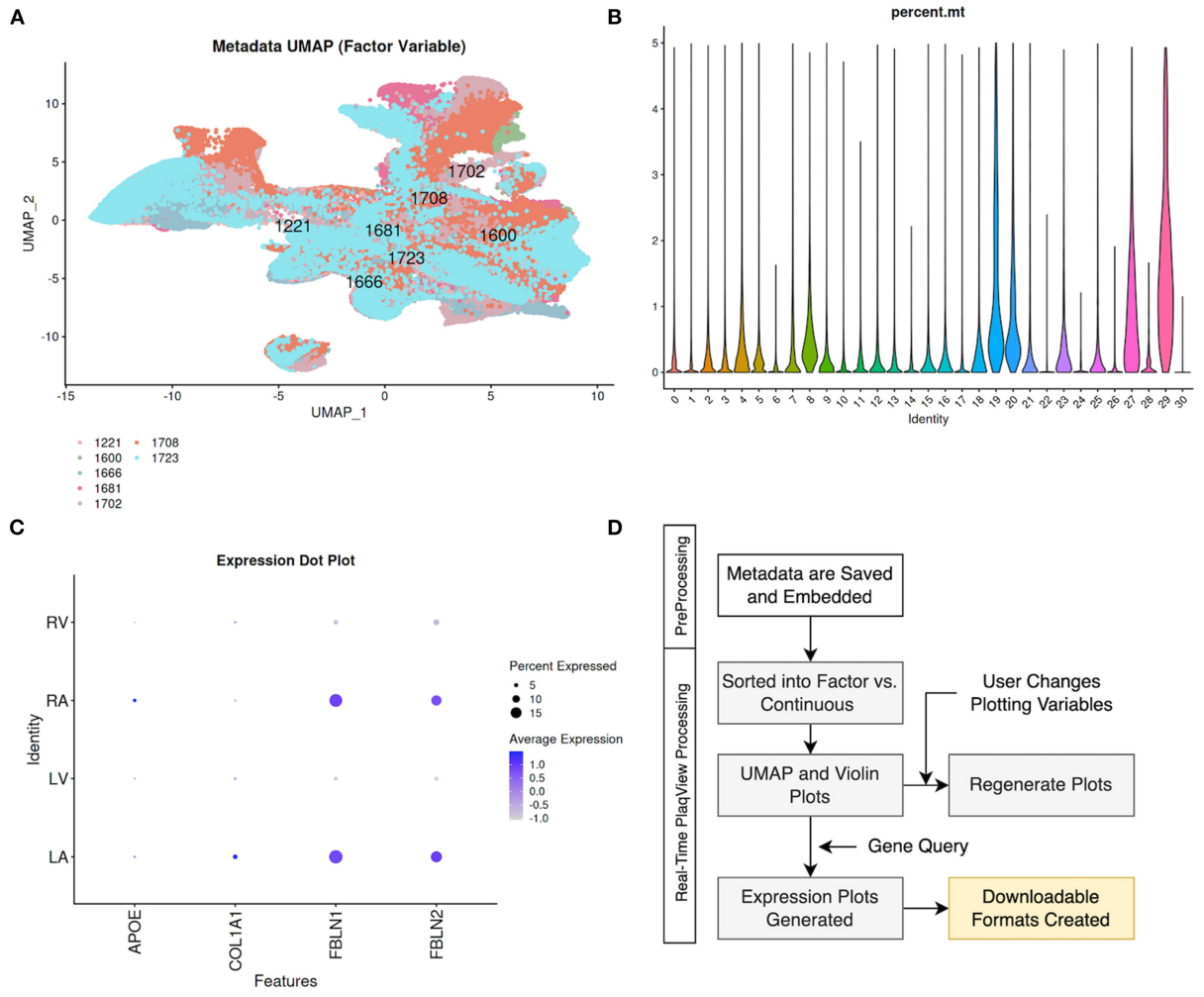

FIGURE 6
Metadata Explorer enables visualization and query of unabridged cell-level metadata. When available, cell-level metadata are divided into **(A)** factor-type such as cells separated by "biological_individuals," and **(B)** continuous-type such as percent mitochondria by seurat cluster for visualization. **(C)** Users can also query gene expression based on factor-type metadata such as the heart "chamber" in the case of Tucker et al. (31). **(D)** We embed the metadata during the preprocessing stage and PlaqView sorts the metadata and runs calculations in response to the user selection to generate corresponding UMAPs and Violin plots.

on the number of selected cells, *ad hoc* calculation of RNA-trajectory can take up to 10–15 min, which is longer than a typical shiny application timeout rule (Figure 7D). We made custom services rules in the backend container to ensure that RNA-trajectories are calculated in the most time-efficient manner possible and modified any timeout rules typically applied to reliably deliver RNA-trajectory results. To handle larger datasets in the future, we will implement a notification and ticketing system to allow users to return to the same session when calculations are complete. This new interactive feature allows users to focus on their cell types of interest to better develop future hypotheses and experiments.

Druggable genome and cell targeting

Lastly, to enable researchers to rapidly explore current drug databases in the context of relevant single-cell datasets, we integrated the Drug Gene Interaction Database (DGIdb v4) with PlaqView (38, 39). In the "Druggable Genome" tab, users can input a gene of interest to simultaneously query the gene expression within the loaded single-cell dataset as well as display potential drug interactions (Supplemental Figure 2). Now, users can select multiple databases including Catalog of Somatic Mutation in Cancer (COSMIC), Food and Drug Administration (FDA), and DrugBank as described in DGIdb v4 (40). Additionally, users can download the corresponding

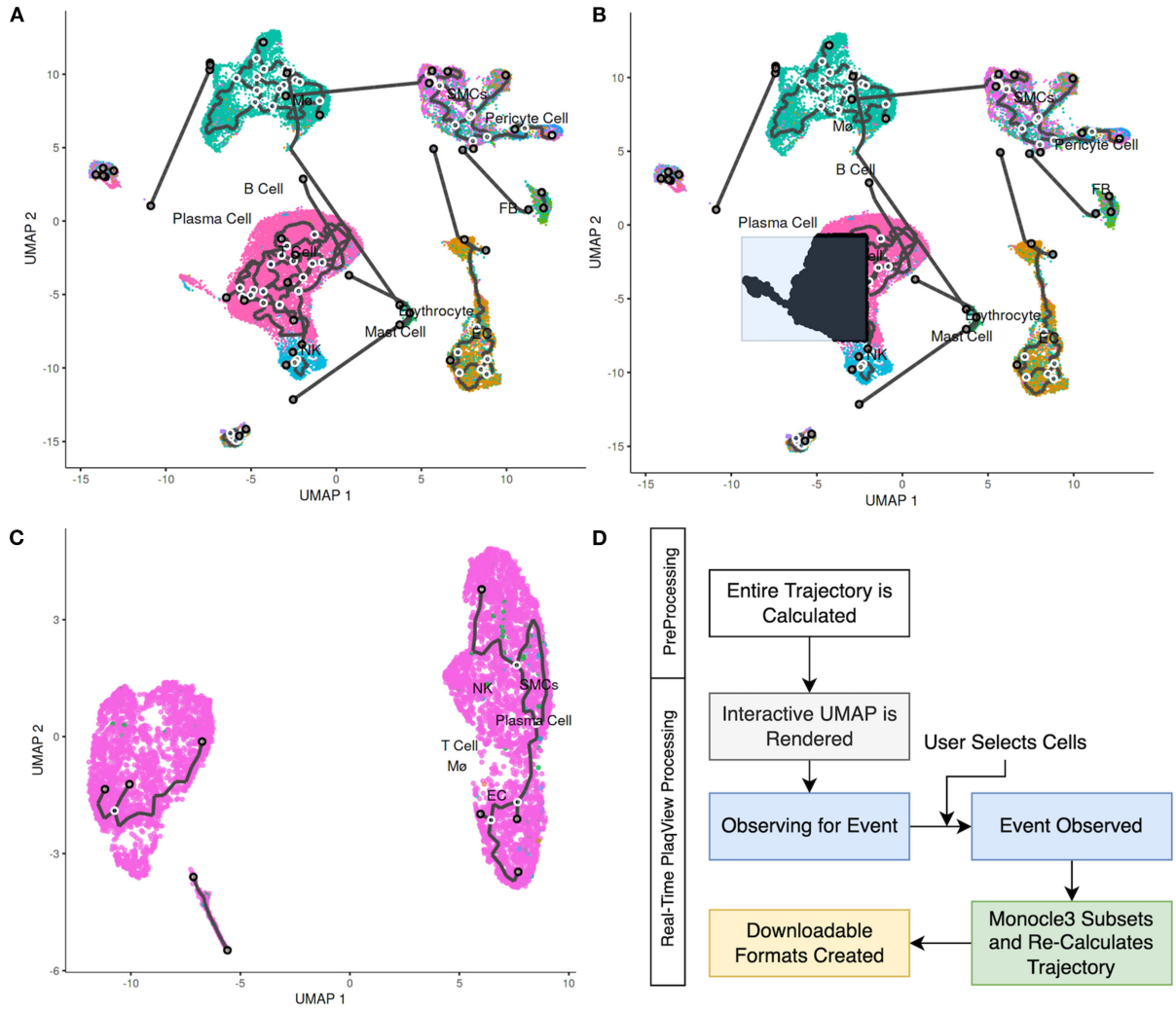

FIGURE 7
PlaqView 2.0 enables interactive RNA trajectory inference. **(A)** Full cell trajectory inferences are presented to the user, as demonstrated using the Alsaigh et al. dataset. **(B)** Selected cells are highlighted in black. These cells can be subsetted and their **(C)** trajectories can be re-calculated in PlaqView as powered by Monocle 3. **(D)** We pre-compute the overall trajectory during the pre-processing stage, and recalculations of subset trajectories are done *ad hoc* as needed by PlaqView as an on-demand function.

UMAP as .pdf as well as the full drug-interaction table as .csv formats. This feature is invaluable in rapidly formulating hypotheses and future drug-repurposing experiments.

Goals and future updates

We are committed to bringing the most updated and relevant cardiovascular datasets to PlaqView. Currently, we plan to update the PlaqView database at least once monthly as more datasets and studies are published. Furthermore, we are currently developing other multi-modal portals suited for data such as single-cell Assay for Transposase-Accessible Chromatin (scATAC-seq), spatial RNA-seq, and a separate portal to compare healthy and diseased tissues in a systematic manner.

Materials and methods

Data formatting

One of the major challenges of reproducible single-cell analysis is the lack of standardization in data-sharing format. We have found that the most commonly used methods are: (1) sharing processed data as matrices (e.g., one file for counts, one file for metadata, etc.), (2) sharing raw FASTQ files, (3) sharing processed Seurat objects as .rds files or equivalent, such

as .h5ad files. We have found that sharing single-cell data as .rds or equivalent is the most convenient and reproducible method as the metadata are matched at the cell-level. However, as noted above, fewer than 25% of published single-cell RNA-seq studies provide this cell-level metadata.

For PlaqView, each dataset curated or submitted is standardized and is ready to be read by the application. Although some efforts have been made to allow interconversions between file formats, such as sceasy (https://github.com/cellgeni/sceasy), manual effort is still required to standardize analysis input for PlaqView. Depending on the incoming file type, they are converted or updated into the latest Seurat object class in R, and are saved as .rds files. These processed files, along with their raw formats, are made publicly available on the PlaqView homepage at https://plaqview.com/data. Systematic processing script is available in in the PlaqView DataProcessing Github page (https://github.com/MillerLab-CPHG/PlaqView_DataProcessing) and can be used as a reference for other single-cell applications to readily convert datasets into R-readable formats.

Data processing steps

Once the datasets are converted into the raw Seurat objects, we process them in the same manner to generate several output files to be read by PlaqView (Figure 8). First, we filter out low quality cells that have <200 or >2,500 features, and those with >5% mitochondrial reads. Exceptions are made for particular datasets that evaluate mitochondrial read data, such as data from Li et al. (13). Then, standard Seurat preprocessing using the following functions are conducted: FindVariableFeatures(), NormalizeData(), ScaleData(), RunPCA(), RunUMAP(), FindNeighbors(), and FindClusters().

To infer cell identity using automatic methods, the scaled RNA matrix is extracted using the GetAssayData() function and fed into SingleR as a new singleR object using the SingleR() function. The identities called by singleR are added into the metadata slot within the Seurat object.

Similarly, we use Seurat's label transfer function FindTransferAnchors() and TransferData() to predict cell identity using the Tabula Sapiens and Tabula Muris (41) references, depending on the original species. Identity calls are added to the metadata column using the AddMetadata() function. Some longer cell labels, such as "Smooth_muscle_cells" are shortened to "SMC." The final Seurat object that contains the SingleR calls, Seurat calls, Seurat clusters (numbered clusters) are exported as an .rds file (Figure 8).

To enable trajectory analysis, we used custom scripts to extract Seurat data and place them into a Monocle3 CDS object using the new_cell_data_set() function. The new CDS object is preprocessed using the following functions: preprocess_cds(), reduce_dimension(), cluster_cells() (33, 34). A custom script is used to overlay the Seurat UMAP embedding into the Monocle3 object for consistent visualization. Then, starting nodes are selected automatically based on the closest vertex followed by learn_graph() and order_cells(). The resulting Monocle3 object is exported as an _cds.rds file (Figure 8).

Finally, we compute the entire differential expression for all cell types labeled by different methods (i.e., Seurat clusters, author-provided, singleR, and Seurat/Tabula Sapiens annotations) using the FindAllMarkers() function. This is the most time-consuming and memory intensive part of the preprocessing pipeline and we use the Future package to parallelize this step. The full R script for the preprocessing pipeline is located in our Data Processing Github page (https://github.com/MillerLab-CPHG/PlaqView_DataProcessing).

Data storage, submission and requests

Raw human sequencing data often require specialized secured storage both due to their size and institutional review board (IRB) compliance regulations. Currently, PlaqView 2.0 only requires the downstream count matrices and does not use any raw sequencing. When data are submitted to PlaqView as raw sequences (such as FASTQ or BAM files), they are processed offline in a dedicated high-performance computing platform and only the count matrices are transferred to PlaqView storage, which is protected under an institutional firewall (Figure 8).

Nonetheless, most datasets currently on PlaqView are already open-access and are deposited in different public storage spaces in various raw formats. All datasets available on PlaqView have undergone systematic preprocessing and are saved in .rds formats that can be requested directly on PlaqView.com under "Data." Furthermore, researchers can directly and securely submit their dataset to PlaqView on the PlaqView homepage.

Reproducible computing environment

Various approaches in computer science and within the R community have been used to create reproducible and stable computing environments to facilitate faster new user setup, scalability for larger datasets, and increased stability of web applications. To our knowledge, popular built-in tools such as *renv* does not completely enable a reproducible environment and only records the versions of tools in an R computing environment (https://rstudio.github.io/renv/articles/renv.html). Recently, the combination of Docker and R gave rise to the Rocker Project (https://www.rocker-project.org/), which utilizes the image building capability of Docker in conjunction with R. Essentially, a predetermined set of R tools are installed on top of a basic operating system, such as Ubuntu. This enables programmers to capture the entire computing environment-including the base operating system, R, and all dependent

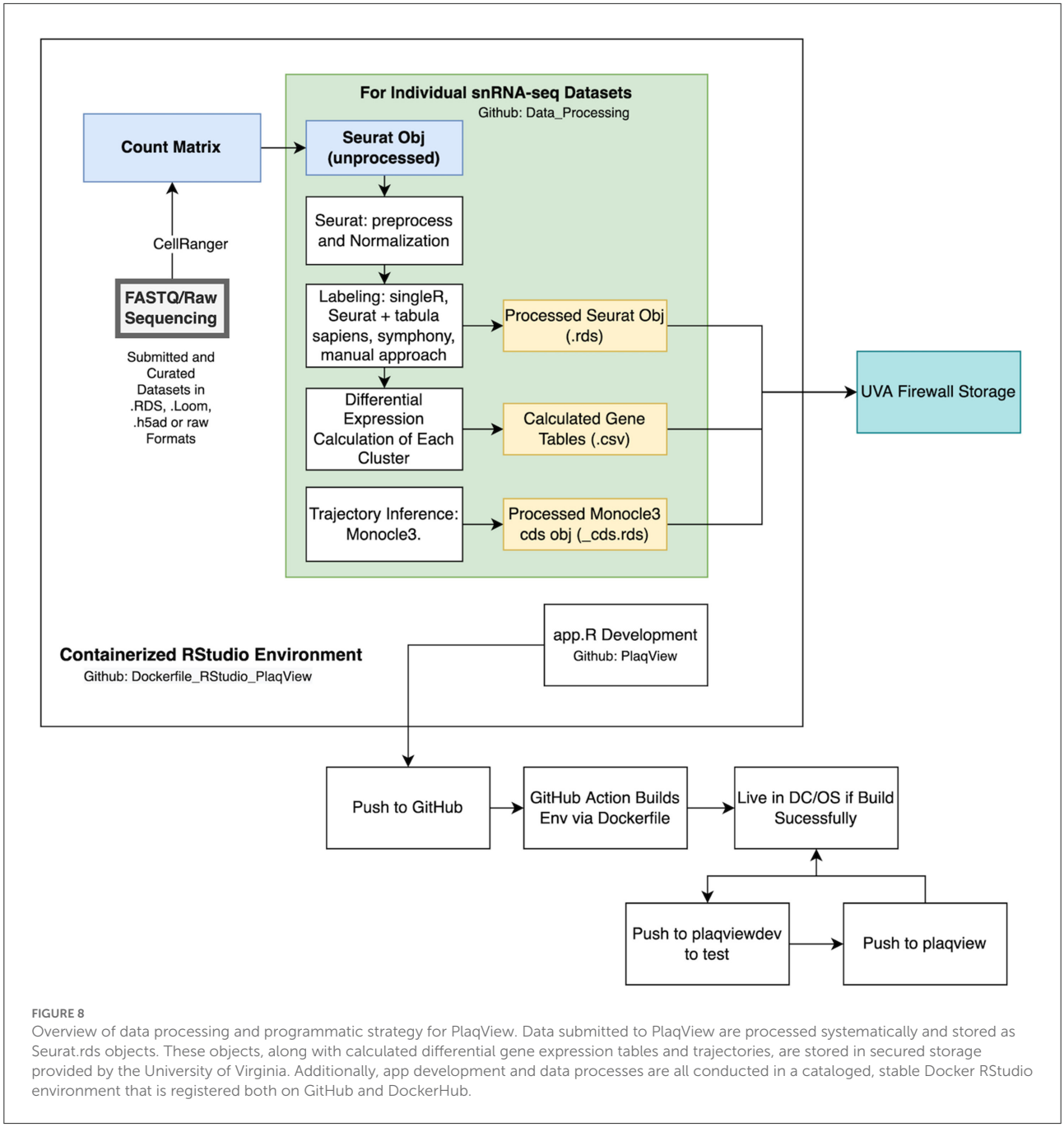

FIGURE 8
Overview of data processing and programmatic strategy for PlaqView. Data submitted to PlaqView are processed systematically and stored as Seurat.rds objects. These objects, along with calculated differential gene expression tables and trajectories, are stored in secured storage provided by the University of Virginia. Additionally, app development and data processes are all conducted in a cataloged, stable Docker RStudio environment that is registered both on GitHub and DockerHub.

packages- and can be downloaded to any computing platform reliably and in isolation. This has an advantage over other tools such as *renv* in that Docker images contain the actual packages and operating system, therefore in the event of version changes or deleted repositories, it will not break with the computing environment. Based on Rocker, we have built a custom Docker image that enables users to run the exact analysis pipelines with all dependencies already installed, and is available *via* DockerHub at millerlab/plaqviewmaster. This Docker image has two major utilizations: as a stable environment for feature development and as a base for the PlaqView application deployment, as it contains all the necessary packages and serves as a backbone for the web application (Figure 8).

Service structure overview

PlaqView is designed to enable researchers to interact with high-performance computing *via* the web browser. The superstructure of PlaqView is to translate user input and

selection from the browser *via* Shiny and run calculations in R, which runs in a clustered container orchestration environment alongside the University of Virginia High Performance Computing system (Supplemental Figure 3A). To enable user interactions with the data without coding knowledge, each interactive element in PlaqView is coded as Shiny Reactive elements, which change the underlying R code snippets in preparation for the analysis. For example, when a user selects a dataset, the corresponding values of the working directory is changed to the selected value, and when the user clicks "Load Dataset", Shiny monitors and triggers the event to execute the R code to load the .rds files within the working directories.

Currently, we are using DC/OS (Distributed Cloud Operating System) to regulate the amount of memory and processor each user can access. DC/OS also automatically handles the workload demand to scale up more service instances in response to increased user access. Furthermore, this infrastructure allows for isolated, or "sticky," instances so each user is given a dedicated R instance and cannot access other users' instances. This is commonly referred to as "stateless programming." Currently, PlaqView supports up to 32GB of memory per user (the memory required to access the largest dataset, and can be scaled up as needed). In the near future, we plan to further scale up using Kubernetes on large commercial-grade infrastructures such as Google Cloud Computing.

Development workflow

Typically, PlaqView development occurs in several stages: edit source code (app.r file), test locally and update Docker images, deployment, and bug fixes (Supplemental Figure 3B). The standard development workflow starts with editing the app.R script, which encompasses the UI (user interface) and the Server codes (codes that calculate and compute results). New features and codes are tested locally in the Dockerized RStudio container for bugs. Final edits are pushed to GitHub as "commits" and new changes initiate GitHub Actions to recompile the application from the base Docker image. Normally, this step involves reinstallation of the base operating Linux system and its dependencies, R, Shiny, and all dependent R packages from scratch, and typically takes about 60 min. However, at this stage, we have simplified the building process by pulling the aforementioned pre-built Docker base image. In our experience, the typical rebuild takes about 60 min whereas pulling the stable base Docker image from DockerHub takes only 3–4 min.

Once the app is live, we begin to capture user feedback and fix any additional bugs. We implement bug fixes and feature requests *via* GitHub as well as through internal runtime log reviews.

Alternative service structure and adaptation to other fields of research

PlaqView was originally developed for atherosclerosis-related cardiovascular datasets, but the underlying structure was designed to be easily adapted to other fields of research. The entirety of the source-code has been made available on GitHub. Furthermore, each iteration of PlaqView comes with a containerized base image hosted on DockerHub (wfma888/plaqviewmaster), which allows for immediate and reproducible deployment in virtually any computing structure. Essentially, there are two major steps to adapt PlaqView to other fields: minimal processing of the user interface script and deploying to a suitable service structure.

Due to the size of the single-cell datasets, PlaqView and adapted versions are best hosted on dedicated, large high-performance clusters. Commercial solutions that would work well are Google Cloud Services as Google Run instances or Amazon Web Services. Shinyapps.io also provides a native and easy way to deploy Shiny apps for beta testing, however limitations in memory per instance and slow performance limits its usefulness in analyzing large datasets.

Discussion

To date, very few single-cell portals like PlaqView exist for cardiovascular genomics research. ExpressHeart, a single-cell portal dedicated to non-cardiomyocyte cells, has several single-cell datasets but has limited scope and features for data re-analysis (Supplemental Table 1) (42). Other, larger data portals such as the Broad Single Cell Portal (SCP) have many large studies but failed to include many critical cardiovascular datasets such as Wirka et al. (11) and Xu et al. (15), and lack the focus on cardiovascular diseases in general. PlaqView aims to bridge the gap between large, multi-organ portals like SCP and niche portals such as ExpressHeart and serve as a critical resource for the cardiovascular field.

PlaqView helps to overcome many modern challenges in the single-cell field, such as the complex coding and computational knowledge needed to explore single-cell data and standardization for data sharing. Since its initial release, we have registered users from 35 countries, with the top being U.S., China, Germany, and the Netherlands. To our knowledge, PlaqView is the most comprehensive single-cell portal dedicated to cardiovascular research. We are committed to the longevity of PlaqView and are working on furthering PlaqView's capability as multimodal datasets are released, such as spatial and scATAC-seq data. Our immediate goals are (1) including additional relevant single-cell datasets, (2) creating a subportal for live single-cell dataset integration and comparison, and (3) creating a subportal for multimodal single-cell data visualization.

Contribution to the cardiovascular field

Single-cell data has always been challenging to share, analyze, and visualize. Typically, these datasets require specialized computing knowledge and high-performance computing tools not readily available. Previously, we presented PlaqView, a web-portal to allow lay scientists and benchtop researchers to rapidly view single-cell RNA-seq data for atherosclerosis. Here, we introduce PlaqView 2.0, a significant improvement to the PlaqView application. In this second major release, we introduce many new features, such as a metadata explorer, cell identity prediction, and *ad hoc* RNA-trajectory calculations. We further improved the usability, speed, stability, and scale of the application. PlaqView serves both as a repository of single-cell data for cardiovascular diseases as well as a tool to rapidly visualize, renalayze, and share scRNA-seq data without the need to code or have specialized computing knowledge. PlaqView is an invaluable resource that bridges the gap between computational and experimental research to advance cardiovascular medicine.

Data availability statement

Publicly available datasets were analyzed in this study. This data can be found here: www.plaqview.com.

Ethics statement

The studies involving human participants were reviewed and approved by Institutional Review Board (IRB) at the University of Virginia. The patients/participants provided their written informed consent to participate in this study.

Author contributions

WFM designed, tested, and wrote the PlaqView application. AWT provided feedback, programming help, and application testing. CG provided back-end infrastructure and deployment aid. DW, YS, JVM, GA, CJH, and AP provided feedback and application testing. SWvL and CLM guided and helped in the development of PlaqView. HAE developed the CIPR module. All authors provided feedback and editing for this manuscript.

Funding

Funding for this research was provided by National Institutes of Health (NIH) grants R00HL125912 and R01HL14823, a Leducq Foundation Transatlantic Network of Excellence (PlaqOmics) Young Investigator Grant, Netherlands CardioVascular Research Initiative of the Netherlands Heart Foundation (CVON 2011/B019 and CVON 2017-20: Generating the best evidence-based pharmaceutical targets for atherosclerosis [GENIUS I&II]), and the ERA-CVD program druggable-MI-targets (grant number: 01KL1802). SWvL was funded through EU H2020 TO_AITION (grant number: 848146).

Acknowledgments

We acknowledge the Research Computing group at the University of Virginia for their helpful suggestions and assistance in deploying PlaqView.

Conflict of interest

Author SWvL has received Roche funding for unrelated work.

The remining authors declare that the research was conducted in the absence of any commercial or financial relationships that could be construed as a potential conflict of interest.

Publisher's note

Supplementary material

The Supplementary Material for this article can be found online at: https://www.frontiersin.org/articles/10.3389/fcvm.2022.969421/full#supplementary-material

References

1. Method of the Year 2013. *Nat Methods*. (2014) 11:1–1. doi: 10.1038/nmeth.2801

2. Method of the Year 2019: single-cell multimodal omics. *Nat Methods*. (2020) 17:1–1. doi: 10.1038/s41592–019–0703–5

3. Zappia L, Theis FJ. Over 1000 tools reveal trends in the single-cell RNA-seq analysis landscape. *Genome Biol.* (2021) 22:301. doi: 10.1186/s13059-021-02519-4

4. Puntambekar S, Hesselberth JR, Riemondy KA, Fu R. Cell-level metadata are indispensable for documenting single-cell sequencing datasets. *PLoS Biol.* (2021) 19:e3001077. doi: 10.1371/journal.pbio.3001077

5. Li F, Yan K, Wu L, Zheng Z, Du Y, Liu Z, et al. Single-cell RNA-seq reveals cellular heterogeneity of mouse carotid artery under disturbed flow. *Cell Death Discov.* (2021) 7:180. doi: 10.1038/s41420-021-00567-0

6. Skinnider MA, Squair JW, Courtine G. Enabling reproducible re-analysis of single-cell data. *Genome Biol.* (2021) 22:215. doi: 10.1186/s13059-021-02422-y

7. Butler A, Hoffman P, Smibert P, Papalexi E, Satija R. Integrating single-cell transcriptomic data across different conditions, technologies, and species. *Nat Biotechnol*. (2018) 36:411–20. doi: 10.1038/nbt.4096

8. Bergen V, Lange M, Peidli S, Wolf FA, Theis FJ. Generalizing RNA velocity to transient cell states through dynamical modeling. *Nat Biotechnol*. (2020) 38:1408–14. doi: 10.1038/s41587-020-0591-3

9. Gao J, Aksoy BA, Dogrusoz U, Dresdner G, Gross B, Sumer SO, et al. Integrative analysis of complex cancer genomics and clinical profiles using the cBioPortal. *Sci Signal.* (2013) 6:pl1. doi: 10.1126/scisignal.2004088

10. Li M, Zhang X, Ang KS, Ling J, Sethi R, Lee NYS, et al. DISCO: a database of deeply integrated human single-cell omics data. *Nucleic Acids Res*. (2021) 50:gkab1020. doi: 10.1093/nar/gkab1020

11. Wirka RC, Wagh D, Paik DT, Pjanic M, Nguyen T, Miller CL, et al. Atheroprotective roles of smooth muscle cell phenotypic modulation and the TCF21 disease gene as revealed by single-cell analysis. *Nat Med*. (2019) 25:1280–9. doi: 10.1038/s41591-019-0512-5

12. Ma WF, Hodonsky CJ, Turner AW, Wong D, Song Y, Mosquera JV, et al. Enhanced single-cell RNA-seq workflow reveals coronary artery disease cellular cross-talk and candidate drug targets. *Atherosclerosis*. (2021) 340:12–22. doi: 10.1016/j.atherosclerosis.2021.11.025

13. Li Y, Ren P, Dawson A, Vasquez HG, Ageedi W, Zhang C, et al. Single-cell transcriptome analysis reveals dynamic cell populations and differential gene expression patterns in control and aneurysmal human aortic tissue. *Circulation.* (2020) 142:1374–88. doi: 10.1161/CIRCULATIONAHA.120.046528

14. Litvinuková M, Talavera-López C, Maatz H, Reichart D, Worth CL, Lindberg EL, et al. Cells of the adult human heart. *Nature.* (2020) 588:466–72. doi: 10.1038/s41586–020–2797–4

15. Xu K, Xie S, Huang Y, Zhou T, Liu M, Zhu P, et al. Cell-type transcriptome atlas of human aortic valves reveal cell heterogeneity and endothelial to mesenchymal transition involved in calcific aortic valve disease. *Arterioscler Thromb Vasc Biol.* (2020) 40:2910–21. doi: 10.1161/ATVBAHA.120.314789

16. Zhao G, Lu H, Liu Y, Zhao Y, Zhu T, Garcia-Barrio MT, et al. Single-cell transcriptomics reveals endothelial plasticity during diabetic atherogenesis. *Front Cell Dev Biol.* (2021) 9:689469. doi: 10.3389/fcell.2021.689469

17. Andueza A, Kumar S, Kim J, Kang D-W, Mumme HL, Perez JI, et al. Endothelial reprogramming by disturbed flow revealed by single-cell RNA and chromatin accessibility study. *Cell Rep.* (2020) 33:108491. doi: 10.1016/j.celrep.2020.108491

18. Gu W, Ni Z, Tan Y-Q, Deng J, Zhang S-J, Lv Z-C, et al. Adventitial cell atlas of wt (Wild Type) and ApoE (Apolipoprotein E)-deficient mice defined by single-cell RNA sequencing. *Arterioscler Thromb Vasc Biol.* (2019) 39:1055–71. doi: 10.1161/ATVBAHA.119.312399

19. Delorey TM, Ziegler CGK, Heimberg G, Normand R, Yang Y, Segerstolpe A, et al. A single-cell and spatial atlas of autopsy tissues reveals pathology and cellular targets of SARS-CoV-2. *Biorxiv*. (2021) 2021.02.25.430130. doi: 10.1101/2021.02.25.430130

20. Bult CJ, Blake JA, Smith CL, Kadin JA, Richardson JE, Anagnostopoulos A, et al. Mouse Genome Database (MGD) 2019. *Nucleic Acids Res.* (2019) 47:D801–6. doi: 10.1093/nar/gky1056

21. DiStefano MT, Goehringer S, Babb L, Alkuraya FS, Amberger J, Amin M, et al. The gene curation coalition: a global effort to harmonize gene–disease evidence resources. *Genet Med.* (2022). doi: 10.1101/2022.01.03.21268593

22. Kuleshov MV, Jones MR, Rouillard AD, Fernandez NF, Duan Q, Wang Z, et al. Enrichr: a comprehensive gene set enrichment analysis web server 2016 update. *Nucleic Acids Res.* (2016) 44:W90–7. doi: 10.1093/nar/gkw377

23. Chen EY, Tan CM, Kou Y, Duan Q, Wang Z, Meirelles GV, et al. Enrichr: interactive and collaborative HTML5 gene list enrichment analysis tool. *BMC Bioinform.* (2013) 14:128. doi: 10.1186/1471-2105-14-128

24. Xie Z, Bailey A, Kuleshov MV, Clarke DJB, Evangelista JE, Jenkins SL, et al. Gene set knowledge discovery with enrichr. *Curr Protoc.* (2021) 1:e90. doi: 10.1002/cpz1.90

25. Ma WF, Boudreau HE, Leto TL. Pan-cancer analysis shows TP53 mutations modulate the association of NOX4 with genetic programs of cancer progression and clinical outcome. *Antioxidants.* (2021) 10:235. doi: 10.3390/antiox10020235

26. Schürmann C, Rezende F, Kruse C, Yasar Y, Löwe O, Fork C, et al. The NADPH oxidase Nox4 has anti-atherosclerotic functions. *Eur Heart J.* (2015) 36:3447–56. doi: 10.1093/eurheartj/ehv460

27. Abdelaal T, Michielsen L, Cats D, Hoogduin D, Mei H, Reinders MJT, et al. A comparison of automatic cell identification methods for single-cell RNA sequencing data. *Genome Biol.* (2019) 20:194. doi: 10.1186/s13059-019-1795-z

28. Aran D, Looney AP, Liu L, Wu E, Fong V, Hsu A, et al. Reference-based analysis of lung single-cell sequencing reveals a transitional profibrotic macrophage. *Nat Immunol.* (2019) 20:163–72.

29. The Tabula Sapiens Consortium, Jones RC, Karkanias J, Krasnow MA, Pisco AO, Quake SR, et al. The tabula sapiens: a multiple-organ, single-cell transcriptomic atlas of humans. *Science.* (2022) 376:eabl4896.doi: 10.1126/science.abl4896

30. Ekiz HA, Conley CJ, Stephens WZ, O'Connell RM, CIPR. a web-based R/shiny app and R package to annotate cell clusters in single cell RNA sequencing experiments. *BMC Bioinform.* (2020) 21:191.

31. Tucker NR, Chaffin M, Fleming SJ, Hall AW, Parsons VA, Bedi KC, et al. Transcriptional and cellular diversity of the human heart. *Circulation.* (2020) 142:466–82.doi: 10.1161/CIRCULATIONAHA.119.045401

32. Burstein B, Libby E, Calderone A, Nattel S. Differential behaviors of atrial versus ventricular fibroblasts. *Circulation.* (2008) 117:1630–41. doi: 10.1161/CIRCULATIONAHA.107.748053

33. Cao J, Spielmann M, Qiu X, Huang X, Ibrahim DM, Hill AJ, et al. The single-cell transcriptional landscape of mammalian organogenesis. *Nature.* (2019) 566:496–502. doi: 10.1038/s41586-019-0969-x

34. Trapnell C, Cacchiarelli D, Grimsby J, Pokharel P, Li S, Morse M, et al. The dynamics and regulators of cell fate decisions are revealed by pseudotemporal ordering of single cells. *Nat Biotechnol.* (2014) 32:381–6. doi: 10.1038/nbt.2859

35. Turner AW, Hu SS, Mosquera JV, Ma WF, Hodonsky CJ, Wong D, et al. Single-nucleus chromatin accessibility profiling highlights regulatory mechanisms of coronary artery disease risk. *Nat Genet.* (2022)1–13. doi: 10.1038/s41588-022-01142-8

36. Alsaigh T, Evans D, Frankel D, Torkamani A. Decoding the transcriptome of atherosclerotic plaque at single-cell resolution. *Biorxiv*. (2020)2020.03.03.968123. doi: 10.1101/2020.03.03.968123

37. Jia G, Preussner J, Chen X, Guenther S, Yuan X, Yekelchyk M, et al. Single cell RNA-seq and ATAC-seq analysis of cardiac progenitor cell transition states and lineage settlement. *Nat Commun.* (2018) 9:4877. doi: 10.1038/s41467-018-07307-6

38. Cotto KC, Wagner AH, Feng Y-Y, Kiwala S, Coffman AC, Spies G. et al. DGIdb 30: a redesign and expansion of the drug–gene interaction database. *Nucleic Acids Res.* (2017) 46:D1068–73. doi: 10.1093/nar/gkx1143

39. Griffith M, Griffith OL, Coffman AC, Weible JV, McMichael JF, Spies NC, et al. DGIdb: mining the druggable genome. *Nat Methods.* (2013) 10:1209–10. doi: 10.1038/nmeth.2689

40. Freshour SL, Kiwala S, Cotto KC, Coffman AC, McMichael JF, Song JJ, et al. Integration of the drug–gene interaction database (DGIdb 4.0) with open crowdsource efforts. *Nucleic Acids Res.* (2020) 49:gkaa1084. doi: 10.1093/nar/gkaa1084

41. Schaum N, Karkanias J, Neff NF, May AP, Quake SR, Wyss-Coray T, et al. Single-cell transcriptomics of 20 mouse organs creates a Tabula Muris. *Nature.* (2018) 562:367–72. doi: 10.1038/s41586-018-0590-4

42. Li G, Luan C, Dong Y, Xie Y, Zentz SC, Zelt R, et al. ExpressHeart: web portal to visualize transcriptome profiles of non-cardiomyocyte cells. *Int J Mol Sci.* (2021) 22:8943. doi: 10.3390/ijms22168943

frontiers | Frontiers in Cardiovascular Medicine

TYPE Original Research
PUBLISHED 03 November 2022
DOI 10.3389/fcvm.2022.993592

OPEN ACCESS

EDITED BY
Michal Mokry,
University Medical Center Utrecht,
Netherlands

REVIEWED BY
Nazareno Paolocci,
Johns Hopkins University,
United States
Tingbo Jiang,
The First Affiliated Hospital
of Soochow University, China

*CORRESPONDENCE
Jianlei Cao
cjlzn14@whu.edu.cn
Xiaorong Hu
huxrzn@whu.edu.cn

†These authors have contributed equally to this work and share first authorship

SPECIALTY SECTION
This article was submitted to Atherosclerosis and Vascular Medicine, a section of the journal Frontiers in Cardiovascular Medicine

RECEIVED 13 July 2022
ACCEPTED 19 October 2022
PUBLISHED 03 November 2022

CITATION
Wu J, Cai H, Lei Z, Li C, Hu Y, Zhang T, Zhu H, Lu Y, Cao J and Hu X (2022) Expression pattern and diagnostic value of ferroptosis-related genes in acute myocardial infarction. *Front. Cardiovasc. Med.* 9:993592. doi: 10.3389/fcvm.2022.993592

Expression pattern and diagnostic value of ferroptosis-related genes in acute myocardial infarction

Jiahe Wu[1,2†], Huanhuan Cai[1,2†], Zhe Lei[1,2†], Chenze Li[1,2], Yushuang Hu[1,2], Tong Zhang[1,2], Haoyan Zhu[1,2], Yi Lu[1,2], Jianlei Cao[1,2*] and Xiaorong Hu[1,2*]

[1]Department of Cardiology, Zhongnan Hospital of Wuhan University, Wuhan, China, [2]Institute of Myocardial Injury and Repair, Wuhan University, Wuhan, China

Background: Ferroptosis is a form of regulatory cell death (RCD) caused by iron-dependent lipid peroxidation. The role of ferroptosis in the process of acute myocardial infarction (AMI) is still unclear and requires further study. Therefore, it is helpful to identify ferroptosis related genes (FRGs) involved in AMI and explore their expression patterns and molecular mechanisms.

Methods: The AMI-related microarray datasets GSE66360 and GSE61144 were obtained using the Gene Expression Omnibus (GEO) online database. GO annotation, KEGG pathway enrichment analysis and Protein-protein interaction (PPI) analysis were performed for the common significant differential expression genes (CoDEGs) in these two datasets. The FRGs were obtained from the FerrDb V2 and the differentially expressed FRGs were used to identify potential biomarkers by receiver operating characteristic (ROC) analysis. The expression of these FRGs was verified using external dataset GSE60993 and GSE775. Finally, the expression of these FRGs was further verified in myocardial hypoxia model.

Results: A total of 131 CoDEGs were identified and these genes were mainly enriched in the pathways of "inflammatory response," "immune response," "plasma membrane," "receptor activity," "protein homodimerization activity," "calcium ion binding," "Phagosome," "Cytokine-cytokine receptor interaction," and "Toll-like receptor signaling pathway." The top 7 hub genes ITGAM, S100A12, S100A9, TLR2, TLR4, TLR8, and TREM1 were identified from the PPI network. 45 and 14 FRGs were identified in GSE66360 and GSE61144, respectively. FRGs ACSL1, ATG7, CAMKK2, GABARAPL1, KDM6B, LAMP2, PANX2, PGD, PTEN, SAT1, STAT3, TLR4, and ZFP36 were significantly differentially expressed in external dataset GSE60993 with AUC $\geq$ 0.7. Finally, ALOX5, CAMKK2, KDM6B, LAMP2, PTEN, PTGS2, and ULK1 were identified as biomarkers of AMI based on the time-gradient transcriptome dataset of AMI mice and the cellular hypoxia model.

Conclusion: In this study, based on the existing datasets, we identified differentially expressed FRGs in blood samples from patients with AMI and further validated these FRGs in the mouse time-gradient transcriptome dataset of AMI and the cellular hypoxia model. This study explored the expression pattern and molecular mechanism of FRGs in AMI, providing a basis for the accurate diagnosis of AMI and the selection of new therapeutic targets.

KEYWORDS

acute myocardial infarction, ferroptosis, bioinformatics analysis, biomarker, ROC analysis

Introduction

Acute myocardial infarction (AMI), with its high morbidity and mortality, is one of the leading causes of death and disability among the middle-aged and elderly worldwide (1).

AMI is often characterized by destructive atherosclerotic plaques superimposed on acute thrombosis, and is the result of ischemic myocardial necrosis caused by acute interruption of myocardial blood flow (2). AMI is the result of interaction between genetic and environmental factors, and risk factors include obesity, hypertension, diabetes, and hypercholesterolemia (3). Myocardial cell death plays an important role in the development of AMI. Dead cardiomyocytes cannot be replaced by living cardiomyocytes because of their very limited potential for regeneration and repair (4). The intervention of myocardial cell death is important to improve the prognosis of AMI. Immediate restoration of coronary blood flow, that is, early successful reperfusion therapy, including thrombolysis or percutaneous coronary intervention (PCI), is the key measure to reduce myocardial injury and improve the prognosis of AMI patients (5). At present, ECG results and high-sensitive Cardiac troponin I are often used as the diagnosis basis of AMI, but they still have certain defects in the identification of early myocardial infarction, mild myocardial injury or stable coronary artery disease (6). Therefore, finding new biomarkers of AMI and studying the molecular mechanisms of myocardial cell death are of great clinical significance for the early diagnosis and treatment of AMI.

Abbreviations: AMI, Acute myocardial infarction; AUC, Area under the curve; BP, Biological process; CAD, Coronary artery disease; CC, Cellular component; CoDEGs, Common significant differential expression genes; DAMPs, Damage associated molecular patterns; DEG, Differentially expressed gene; FRGs, Ferroptosis-related genes; GEO, Gene Expression Omnibus; GO, Gene Ontology; I/R, Ischemia-reperfusion; KEGG, Kyoto Encyclopedia of Genes and Genomes; MF, Molecular function; NSTEMI, non-ST segment elevation myocardial infarction; PCI, Percutaneous coronary intervention; PPI, Protein-Protein Interaction; RCD, Regulatory cell death; ROC, Receiver operating characteristic; STEMI ST, segment elevation myocardial infarction; UA, Unstable angina.

The term "ferroptosis" was first reported in 2012 and was considered to be an iron-dependent non-apoptotic cell death (7). Ferroptosis is a form of regulatory cell death (RCD) caused by iron-dependent lipid peroxidation and is different from other RCD patterns such as apoptosis, autophagy, pyroptosis and necroptosis (8). Ferroptosis is mainly manifested by decreased GPX4 and inhibition of "System Xc-" activity, which is influenced by various metabolic related pathways, including redox homeostasis, iron metabolism, sugar, lipid, and amino acid metabolism and mitochondrial activity, etc. (9–12).

Ferroptosis participates in the occurrence and development of a variety of human diseases, and its research in the field of cardiovascular disease is gradually deepening. Studies have shown that the formation and progression of atherosclerosis is associated with ferroptosis, and ferroptosis inhibitors can reduce the formation of atherosclerosis and reduce endothelial dysfunction (13, 14). One study showed that that ferroptosis was involved in doxorubicin induced cardiotoxicity and ischemia-reperfusion (I/R) mediated heart failure via the Nrf2/Hmox1 pathway (15), another study showed that ubiquitin-specific protease 7 (USP7) was involved in the regulation of ferroptosis by activating the p53/TfR1 pathway during myocardial I/R injury (16). These results suggest that the biological process of ferroptosis is deeply related to cardiovascular disease and ferroptosis-related genes may be new biomarkers or therapeutic targets for cardiovascular disease.

The mechanism of ferroptosis involved in the regulation of AMI is still not very clear. This study was performed to identify novel AMI related FRGs. AMI related datasets GSE66360, GSE61144, GSE60993, and GSE775 were downloaded and then analyzed using Bioinformatics analysis. The expression patterns of FRGs in AMI were further identified based on the original gene expression data in these datasets. ROC analysis was performed to identify the diagnostic value of these FRGs in AMI. These identified FRGs were further verified in the cell hypoxia model. Our study will explore the molecular mechanism of ferroptosis in AMI, so as to guide the individualized diagnosis and treatment of AMI. The workflow of the specific analysis is shown in **Figure 1**.

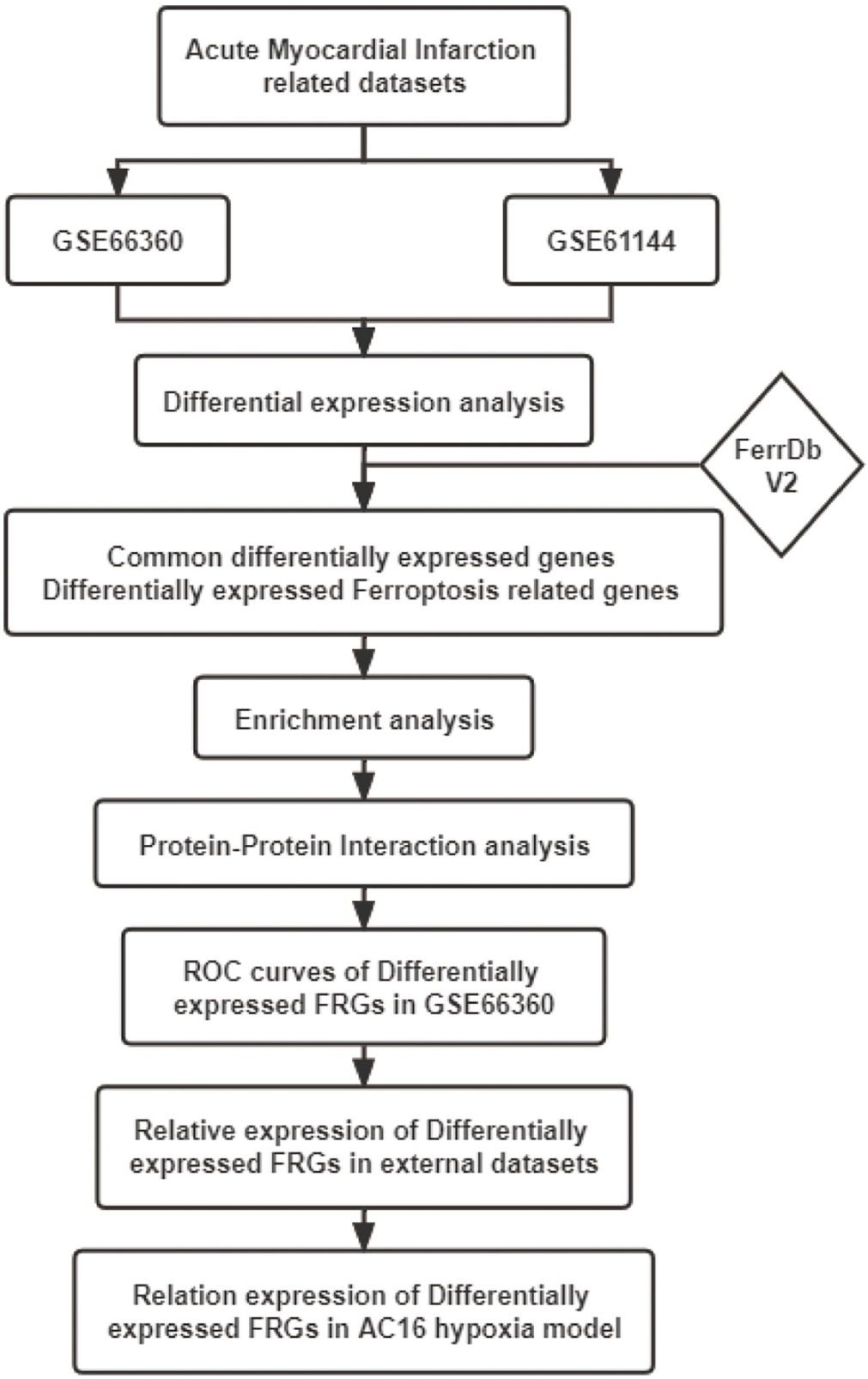

FIGURE 1
Flowchart of the steps performed in this study.

Materials and methods

Data resource

The Gene Expression Omnibus (GEO) database[1] was used to download the AMI related microarray datasets GSE66360 (mRNA), GSE61144 (mRNA), GSE60993 (mRNA), and GSE775 (mRNA). GSE66360 comes from the GPL570 platform ([HG-U133_Plus_2] Affymetrix Human Genome U133 Plus 2.0 Array). GSE61144 comes from the GPL6106 platform (Sentrix Human-6 v2 Expression BeadChip). GSE60993 comes from the GPL6884 platform (Illumina HumanWG-6 v3.0 expression beadchip). GSE775 comes from the GPL81 platform ([MG_U74Av2] Affymetrix Murine Genome U74A Version 2 Array). The samples in GSE66360, GSE61144 and GSE60993 were all derived from human blood and grouped into healthy control and AMI groups. The samples in GSE775 were derived from myocardial tissue of myocardial infarction mice. Groups in GSE775 were divided according to different time of infarction (1, 4, 24, 48 h, 1, and 8 week), and each group contained three sham operation mice and three infarction mice. **Table 1** shows the information of these 4 datasets obtained from the GEO database.

Differential expression analysis

Raw sequencing data of GSE66360 and GSE61144 were downloaded from GEO database. GEO2R[2] was used to perform the preliminary differential expression analysis. Benjamini-Hochberg method was used to correct adj. P for potential false positive results and adj. P-value < 0.05 and $|\log FC| > 0.8$ was set as the cut-off criteria of DEGs. Venn diagram web tool[3] was used to identify the CoDEGs in GSE66360 and GSE61144.

Identification of differential expression genes associated with ferroptosis

FerrDb V2[4] is the world's first database that dedicates to ferroptosis regulators and ferroptosis-disease associations. A total of 431 regulatory factors including drivers, suppressors and markers were downloaded from FerrDB V2 database (**Supplementary File 1**). The DEGs in GSE66360 and GSE61144 were intersected with the genes obtained from FerrDB V2 to obtain DEGs associated with Ferroptosis. Based on the raw sequencing data in GSE66360 and GSE61144, the heatmap of these differentially expressed FRGs were produced using the gg plots package of R software (version: x64 3.2.1) (17).

Functional and pathway enrichment analysis

The online biological tool, Database for Annotation, Visualization, and Integrated Discovery (DAVID; version6.8)[5] was used to perform Gene Ontology (GO) analysis and Kyoto Encyclopedia of Genes and Genomes (KEGG) pathway enrichment analysis of CoDEGs in GSE66360 and GSE61144. Pathways with $P < 0.05$ were considered statistically significant.

Construction of the protein-protein interaction network and identification of hub genes

In order to understand the mechanism of interaction between CoDEGs in AMI, a protein-protein interaction (PPI) network was constructed by string database (version10.0)[6]. This obtained PPI network was further visualized using Cytoscape software (version 3.7.1). The Cytohubba plug-in of Cytoscape software was used to screen out the top 10 key genes with high connectivity in this PPI network using the Maximal Clique Centrality (MCC) algorithm (18, 19). Multiple algorithms (Degree, EPC, Betweenness) continued to be used for prediction, and genes predicted by more than three methods at the same time are considered to be Hub Genes for AMI.

Validation of the expression of ferroptosis marker GPX4 in multiple acute myocardial infarction related datasets

GPX4 is significantly downregulated during ferroptosis occurrence and is a well-recognized marker of the ferroptosis pathway. The expression of GPX4 was validated in multiple datasets (GSE60993, GSE61144, and GSE775) to confirm whether ferroptosis was associated with AMI or not.

Further validation of differentially expressed ferroptosis related genes in external dataset GSE60993

GSE60993 was an AMI-related sequencing dataset comprising 7 healthy subjects, 9 patients with unstable

1 https://www.ncbi.nlm.nih.gov/
2 https://www.ncbi.nlm.nih.gov/geo/geo2r/
3 http://bioinformatics.psb.ugent.be/webtools/Venn/
4 http://www.zhounan.org/ferrdb/current/
5 https://david.ncifcrf.gov
6 http://string-db.org

TABLE 1 The information of the 4 microarray datasets obtained from the GEO database.

Data source	Organism	Platform	Year	Sample source	Sample size (AMI/CON)	Detected RNA type
GSE66360	Homo Sapiens	GPL570	2015	Blood	49/50	mRNA
GSE61144	Homo Sapiens	GPL6106	2015	Blood	7/10	mRNA
GSE60993	Homo Sapiens	GPL6884	2015	Blood	7/7	mRNA
GSE775	Mus musculus	GPL81	2003	Tissue	18/18	mRNA

angina (UA), 10 patients with non-ST segment elevation myocardial infarction (NSTEMI), and 7 patients with ST segment elevation myocardial infarction (STEMI). Based on the relative gene expression data in GSE60993, the abovementioned differentially expressed FRGs in GSE66360 and GSE61144 were further verified to study their expression differences in coronary artery disease (CAD).

Receiver operating characteristic curve analysis

Differentially expressed FRGs in validation dataset GSE60993 were considered as potential biomarkers for AMI. Based on the expression data of these FRGs in GSE66360, Graphpad Prism (version:8.0) software was used to compare the control and AMI groups. Independent sample *T*-test was used to compare the two groups and $P < 0.05$ was considered statistically significant. ROC analysis was used to evaluate the diagnostic value of these FRGs for AMI. FRGs with the area under the curve (AUC) ≥ 7.0 and $P < 0.05$ were screened as potential biomarkers.

Further validation of differentially expressed ferroptosis related genes in external dataset GSE775

The GSE775 dataset included myocardial tissue transcriptome data at 1, 4, 24, 48 h, 1 and 8 week after myocardial infarction in mice. Based on their raw expression data in GSE775, the expression of FRGs were further verified to study the change of expression of FRGs in myocardial infarction tissues over time. The comparison between Sham operation group and AMI group was performed by independent sample *T* test. $P < 0.05$ was considered statistically significant.

Cardiomyocyte cell line culture and treatment

The human cardiomyocyte AC16 cell line purchased from BeNa Culture Collection (Beijing, China) was cultured in Dulbecco's modified Eagle's medium (DMEM, Gibco) with 10% fetal bovine serum (FBS, Gibco) and 1% penicillin-streptomycin (Sigma, St. Louis, MO, USA) at 37°C with 5% CO_2. The three-gas incubator was used to establish an anoxic environment with 1% O_2, 5% CO_2, and 94% N_2. The AC16 cardiomyocytes were exposed to 24 h of this condition to generate a hypoxia model. AC16 cells in the control group were under normoxia condition (21% O_2, 5% CO_2, and 74% N_2) all the time.

Real-time quantitative polymerase chain reaction

The expression of these FRGs in AC16 hypoxia cell model was further verified by qPCR. According to the manufacturer's protocol, total RNA was isolated using FastPure® Cell/Tissue Total RNA Isolation Kit V2 (Vazyme, Nanjing, China), and then synthesized with Hifair® III 1st Strand cDNA Synthesis SuperMix for qPCR (Ye Sen, Shanghai, China). The Bio-Rad CFX96 Real-time PCR Detection System was performed to carry out the qRT-PCR, using Hieff UNICON® Universal Blue qPCR SYBR Green Master Mix (Ye Sen, Shanghai, China). β-actin was used as the reference gene and the relative fold change was calculated by the method of $2^{-\Delta\Delta Ct}$. Details of all primers were presented in **Supplementary File 2**. Data were presented as mean values ± standard error of mean (SEM) from at least three independent experiments. Independent sample *T* test was used to compare the normoxia group and hypoxia group. FRGs with $P < 0.05$ was considered statistically significant.

Results

Identification of differential expression genes and differentially expressed FRGs in acute myocardial infarction

The AMI related datasets GSE66360 and GSE61144 were downloaded from the Gene Expression Omnibus (GEO) database. Based on the screening criteria mentioned above (P value < 0.05 and $|\ logFC|\ > 0.8$), DEGs in each dataset were screened out. There were 1232 DEGs, including 688 high-expressed, and 544 low-expressed, in GSE66360. There were 468 DEGs, including 325 high-expressed, and

143 low-expressed, in GSE61144. **Supplementary File 3** presents detailed results of differential expression analysis. The top 5 upregulated DEGs and the top 5 downregulated DEGs in each dataset are shown in **Table 2**. The volcano plots of these DEGs in GSE66360 and GSE61144 are shown in **Figures 2A,B**. Based on the obtained DEGs and the ferroptosis related genes in FerrDB V2, the online venn tool was used to identify CoDEGs and differentially expressed FRGs (**Figure 2C**). A total of 131 CoDEGs were identified in GSE66360 and GSE61144. There are 45 and 14 differentially expressed FRGs in these two datasets respectively (**Supplementary File 4**). Seven ferroptosis related genes ACSL1, CREB5, GABARAPL1, LAMP2, PANX2, PGD, and TLR4 were significantly differentially expressed in both datasets. **Figure 2D** shows the heatmap of differentially expressed FRGs in GSE66360. **Figure 2E** shows the heatmap of differentially expressed FRGs in GSE61144.

TABLE 2 The top 5 upregulated DEGs and the top 5 downregulated DEGs in GSE66360 and GSE61144.

Dataset	Type	DEG	Expression	logFC	FDR
GSE66360	mRNA	NR4A2	up	3.37704444	7.83E-16
GSE66360	mRNA	MAFB	up	3.12991224	4.55E-11
GSE66360	mRNA	S100A12	up	2.98220317	1.26E-10
GSE66360	mRNA	CLEC7A	up	2.97162731	9.83E-08
GSE66360	mRNA	CXCL2	up	2.96654848	2.01E-09
GSE66360	mRNA	XIST	down	−4.0320135	2.33E-05
GSE66360	mRNA	TSIX	down	−2.9910711	3.35E-05
GSE66360	mRNA	CCR2	down	−2.1941029	4.15E-07
GSE66360	mRNA	LPAR5	down	−1.8493421	4.90E-05
GSE66360	mRNA	GIMAP8	down	−1.7295168	1.10E-04
GSE61144	mRNA	MMP9	up	2.70017256	1.55E-05
GSE61144	mRNA	ARG1	up	2.23048111	1.46E-04
GSE61144	mRNA	IL18R1	up	2.20219955	6.45E-07
GSE61144	mRNA	IL1R2	up	2.17550168	4.25E-07
GSE61144	mRNA	ORM1	up	2.05889349	1.30E-03
GSE61144	mRNA	GZMK	down	−2.0392509	3.56E-06
GSE61144	mRNA	GZMA	down	−1.8841985	5.76E-06
GSE61144	mRNA	GZMH	down	−1.7906003	2.93E-04
GSE61144	mRNA	NKG7	down	−1.7637924	1.32E-04
GSE61144	mRNA	EOMES	down	−1.6243454	1.14E-05

Analysis of enrichment of common significant differential expression genes in GSE66360 and GSE61144

Common DEGs in GSE66360 and GSE61144 were input into DAVID database for GO annotation and KEGG pathway enrichment analysis. **Figures 3A–D** shows the top 10 enriched GO annotation terms and KEGG pathways. For GO biological process (BP) analysis, the results showed that these CoDEGs are mainly enriched in the term of "innate immune response," "inflammatory response," "immune response," "response to lipopolysaccharide," and "defense response to bacterium" (**Figure 3A**). For GO cellular component (CC) analysis, the top 5 significantly enriched terms are "plasma membrane," "integral component of membrane," "extracellular exosome," "integral component of plasma membrane," and "extracellular region" (**Figure 3B**). For GO molecular function (MF) analysis, the top 5 significantly enriched terms are "receptor activity," "protein homodimerization activity," "calcium ion binding," "carbohydrate binding," "RAGE receptor binding" (**Figure 3C**). Furthermore, "Hematopoietic cell lineage," "Phagosome," "Cytokine-cytokine receptor interaction," "Toll-like receptor signaling pathway," and "TNF signaling pathway" are significant enrichment pathways in KEGG analysis (**Figure 3D**).

Construction of the protein-protein interaction network and identification of hub genes in acute myocardial infarction

The CoDEGs were introduced into the String database. Based on the String database's default execution criteria, a PPI network with 101 nodes and 370 edges was constructed and then visualized using Cytoscape software (**Figure 3E**). The 91 orange red nodes in this network represent high-expressed genes and the 10 blue nodes in this network represent low-expressed genes. The depth of the color represents the degree of upward or downward movement in the corresponding direction. Next, based on MCC algorithm, the top 10 genes (TLR2, TREM1, TLR8, TLR4, ITGAM, S100A9, S100A12, S100A8, NCF2, and MMP9) were screened out using the plug-in Cytohubba in Cytoscape (**Figure 3F**). KOBAS (version 3.0)[7] online tool was used for further path enrichment analysis of these genes. The result shows that TLR2, TLR4, NCF2, and ITGAM are involved in "Phagosome" pathway, S100A8, S100A9, and MMP9 are involved in "IL-17 signaling pathway" pathway, TLR2, TLR4, and TLR8 are involved in "Toll-like receptor signaling pathway" pathway, NCF2, ITGAM, and MMP9 are involved in "Leukocyte transendothelial migration" pathway. In addition, the other three algorithms (Degree, EPC, Betweenness) were continued to be used for prediction, and eventually the genes predicted by at least three algorithms simultaneously were considered as Hub genes (**Supplementary File 5** and **Supplementary Figure 1**). Finally, the top 7 hub genes ITGAM, S100A12, S100A9, TLR2, TLR4, TLR8, and TREM1 were considered as Hub Genes of AMI.

7 http://kobas.cbi.pku.edu.cn/genelist/

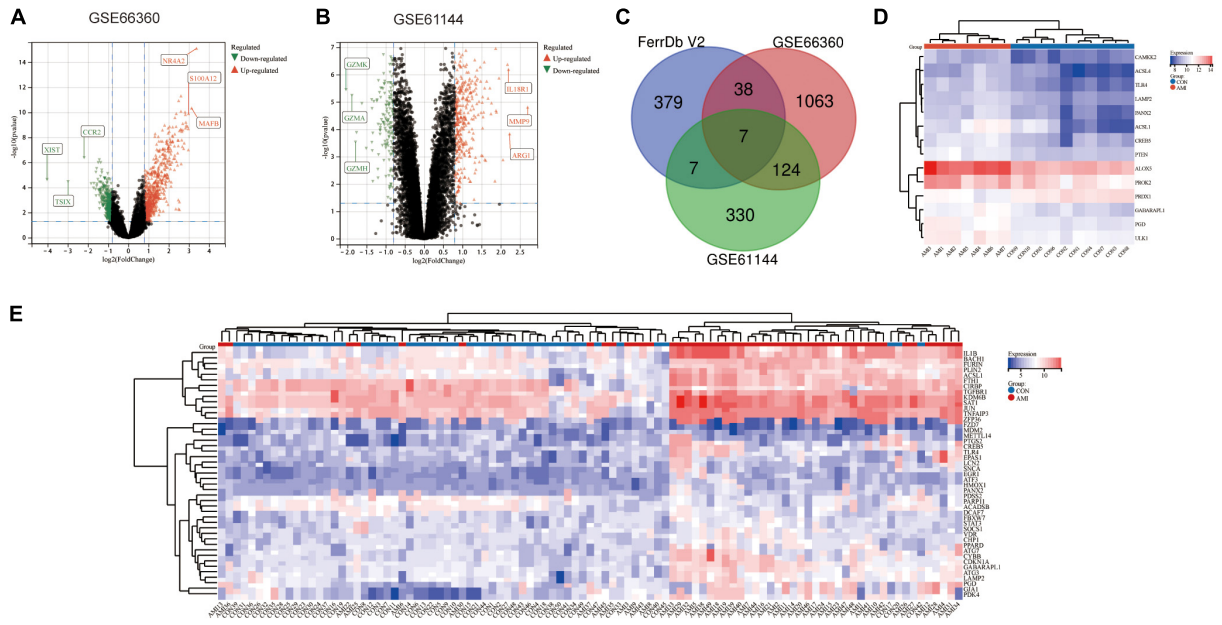

FIGURE 2
Identification of differentially expressed FRGs in GSE66360 and GSE61144. **(A)** The volcano plot of GSE66360. **(B)** The volcano plot of GSE61144. **(C)** Venn diagram of DEGs in GSE66360, GSE61144, and FRGs in FerrDb. **(D)** Heatmap of FRGs in GSE66360. **(E)** Heatmap of FRGs in GSE61144.

Expression patterns of ferroptosis related genes in GSE66360 and GSE61144

Based on their raw expression data in GSE66360 and GSE61144, FRGs in healthy and AMI patients were compared and analyzed. The results show that there are 45 and 14 FRGS in the dataset GSE66360 and GSE61144, respectively. The 45 FRGs in GSE66360 were all significantly differentially expressed, with high expression of all genes except for the low expression of nine genes, ACADSB, CIRBP, DCAF7, FZD7, MDM2, METTL14, PARP11, PDSS2, and TGFBR1 (**Figure 4A**). All 14 FRGs in GSE61144 were significantly increased except for the low expression of PRDX1 (**Figure 4B**). **Figure 4C** shows the Venn results of FRGs in these two datasets. Further PPI analysis and enrichment analysis were performed on FRGs mentionedabove. **Figure 4D**, consisting of 37 nodes and 121 edges, is the PPI network constructed by 45 FRGS identified in GSE66360. Similarly, **Figure 4E**, with 13 points and 33 edges, is the PPI network constructed by 14 FRGS identified in GSE61144. KEGG pathway enrichment analysis shows that FRGs in GSE66360 are significantly enriched in the term of "Ferroptosis," "Necroptosis," "NOD-like receptor signaling pathway," "AGE-RAGE signaling pathway in diabetic complications," and "Autophagy" (**Figure 4F**). FRGs in GSE61144 are significantly enriched in the term of "Autophagy," "Adipocytokine signaling pathway," "Peroxisome," "AMPK signaling pathway," "Fatty acid biosynthesis," "Ferroptosis," "Fatty acid metabolism," "PI3K-Akt signaling pathway," and "PPAR signaling pathway" (**Figure 4G**).

Validation of the expression of ferroptosis marker GPX4 in multiple acute myocardial infarction related datasets

The expression of GPX4 was verified in datasets GSE61144, GSE60993, and GSE775. As predicted, the expression of GPX4 was significantly down-regulated in all three datasets (**Figures 5A–C**), suggesting that the biological process of ferroptosis may be involved in AMI.

Further validation of differentially expressed ferroptosis related genes in external dataset GSE60993

The expression of 52 FRGs in GSE66360 and GSE61144 were further verified in external dataset GSE60993 (**Figures 6A–T**). Compared with healthy controls, a total of 19 FRGs, ACSL1, ACSL4, ALOX5, ATG7, CAMKK2, CREB5, GABARAPL1, KDM6B, LAMP2, PANX2, PGD, PROK2, PTEN, PTGS2, SAT1, STAT3, TLR4, ULK1, and ZFP36 were significantly up-regulated in STEMI patients, but only PRDX1 was down-regulated

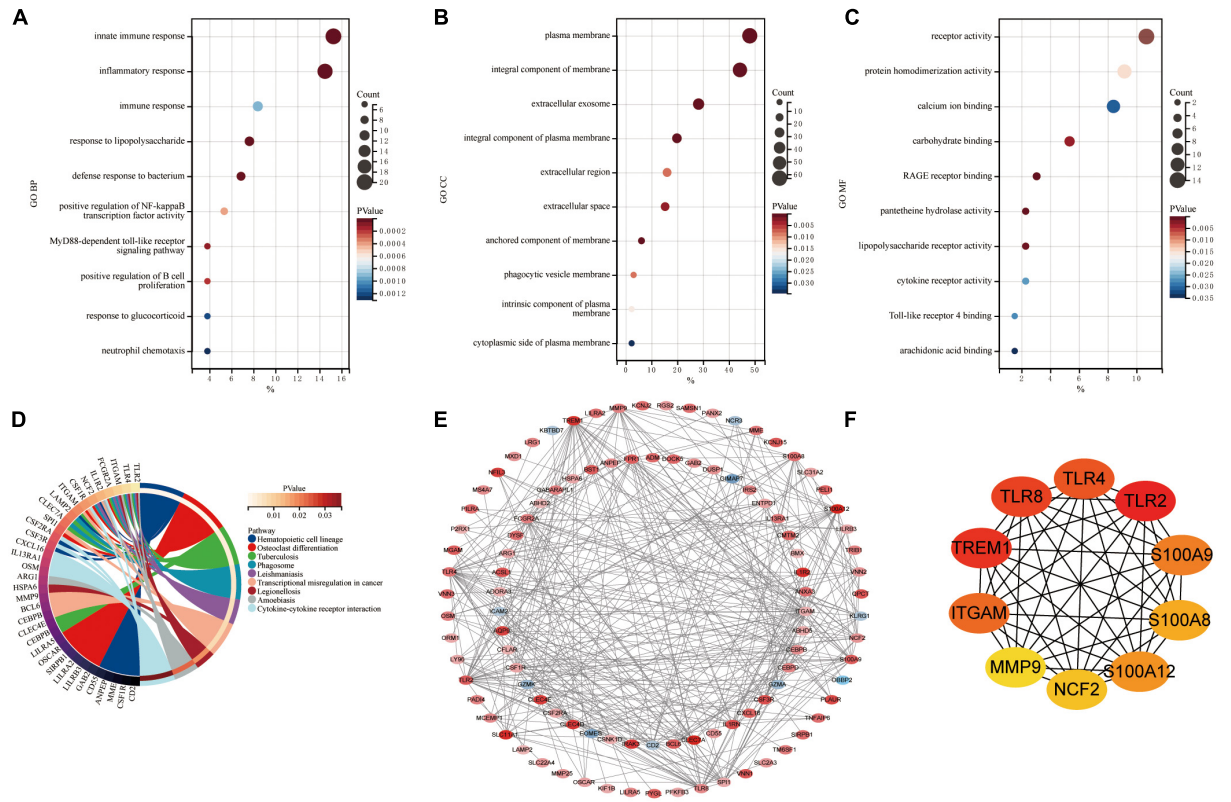

FIGURE 3
Enrichment analysis and PPI analysis of CoDEGs. **(A)** Bubble plot of biological process (BP; TOP10). **(B)** Bubble plot of cellular component (CC; TOP10). **(C)** Bubble plot of molecular function (MF; TOP10). **(D)** Circle plot of KEGG pathway enrichment analysis (TOP10). **(E)** The whole PPI Network. The 91 orange red nodes in the network represent up-regulated genes and the 10 blue nodes in the network represent down-regulated genes. **(F)** The top 10 genes predicted by the MCC algorithm.

in STEMI patients. In addition, the expression of PANX2 was significantly different between CON and UA groups, the expression of GABARAPL1, LAMP2, PANX2, PTEN, and ULK1 was significantly different between NSTEMI and STEMI groups.

Receiver operating characteristic curve analysis

Based on the raw expression data in GSE66360, ROC analysis was performed on these 20 differentially expressed FRGs (ACSL1, ACSL4, ALOX5, ATG7, CAMKK2, CREB5, GABARAPL1, KDM6B, LAMP2, PANX2, PGD, PRDX1, PROK2, PTEN, PTGS2, SAT1, STAT3, TLR4, ULK1 and ZFP36) and AUC values were calculated. Finally, the AUC of these 20 FRGs were all greater than 0.6, and 13 of them, ACSL1 (AUC = 0.8727), ATG7 (AUC = 0.7310), CAMKK2 (AUC = 0.7124), GABARAPL1 (AUC = 0.9016), KDM6B (AUC = 0.7286), LAMP2 (AUC = 0.7045), PANX2 (AUC = 0.8365), PGD (AUC = 0.7882), PTEN (AUC = 0.7257), SAT1 (AUC = 0.7980), STAT3 (AUC = 0.7792), TLR4 (AUC = 0.8290), and ZFP36 (AUC = 0.8796), with AUC $\geq$ 0.7 were identified as potential markers of AMI. Figures 7A–L shows the ROC analysis results of the top 12 AUC values. The ROC analysis results for the remaining eight FRGs are shown in Supplementary File 5 and Supplementary Figure 2.

Further validation of differentially expressed ferroptosis related genes in external dataset GSE775

The expression of 20 differentially expressed FRGs (ACSL1, ACSL4, ALOX5, ATG7, CAMKK2, CREB5, GABARAPL1, KDM6B, LAMP2, PANX2, PGD, PRDX1, PROK2, PTEN, PTGS2, SAT1, STAT3, TLR4, ULK1, and ZFP36) were further verified to study the expression changes of these FRGs in myocardial infarction tissues with time. As shown in Figures 8A–I, 9 FRGs (ACSL4, ATG7, LAMP2, PGD, PTEN, PTGS2, SAT1, STAT3, and ZFP36) were significantly differentially expressed at least twice at the six test time points

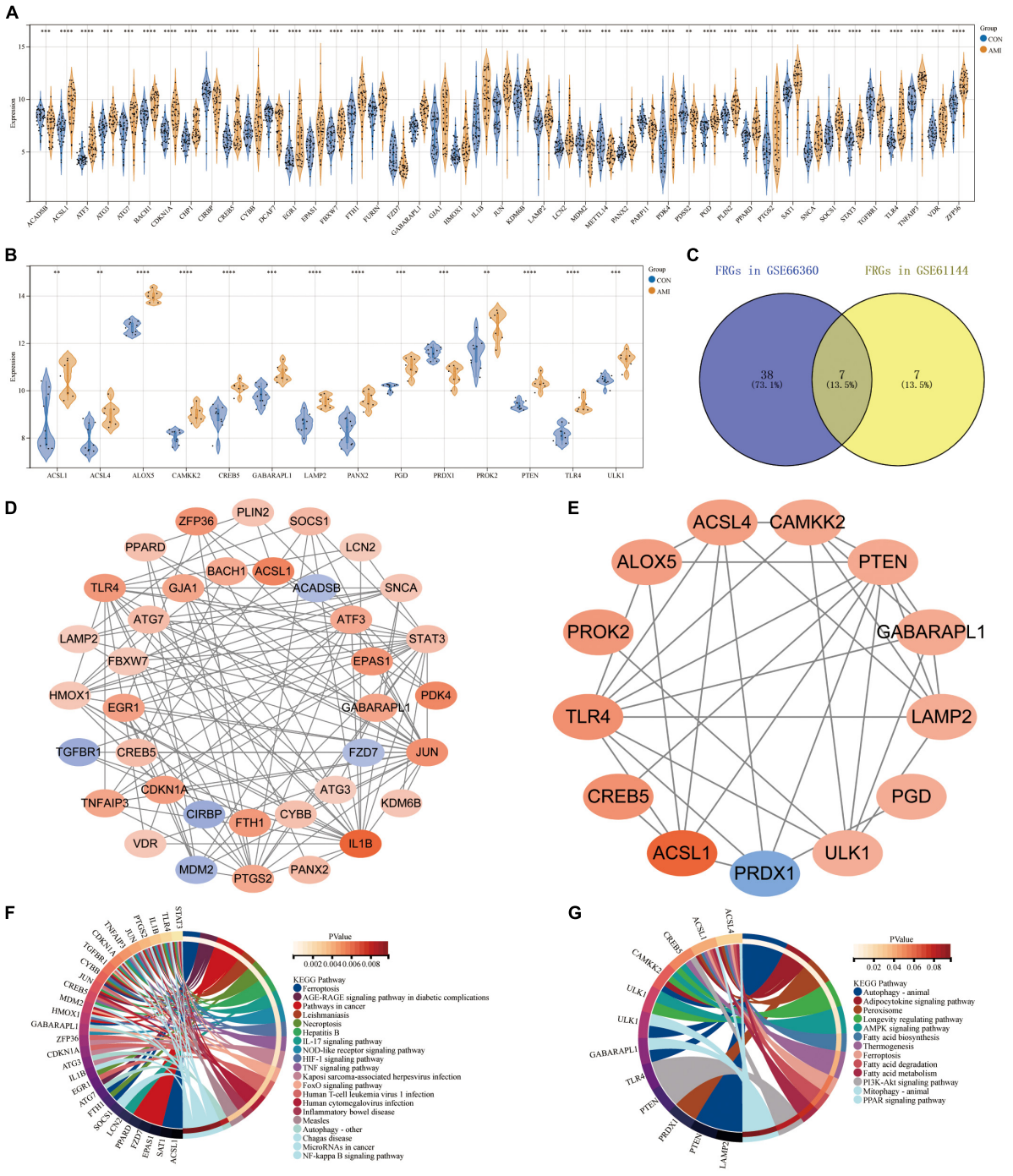

FIGURE 4
Expression patterns of FRGs in GSE66360 and GSE61144. **(A)** Expression patterns of FRGs in GSE66360. **(B)** Expression patterns of FRGs in GSE61144. **(C)** Venn diagram of FRGs in GSE66360 and GSE61144. **(D)** PPI network of FRGs in GSE66360. **(E)** PPI network of FRGs in GSE61144. **(F)** Circle plot of KEGG pathway enrichment analysis for FRGs on GSE66360. **(G)** Circle plot of KEGG pathway enrichment analysis for FRGs on GSE61144. **(A,B)** $^{**}P < 0.01$; $^{***}P < 0.001$; $^{****}P < 0.0001$.

(1, 4, 24, 48 h, 1, and 8 week after myocardial infarction). All these FRGs showed an upward trend in expression. The expression of STAT3 and ZFP36 was different only within 24 h after myocardial infarction. The differences in ATG7 expression and PGD expression did not occur until more than 48 h after myocardial infarction. The expression of ACSL4, LAMP2, PTEN, PTGS2, and SAT1 were different in the early and late stages of myocardial infarction.

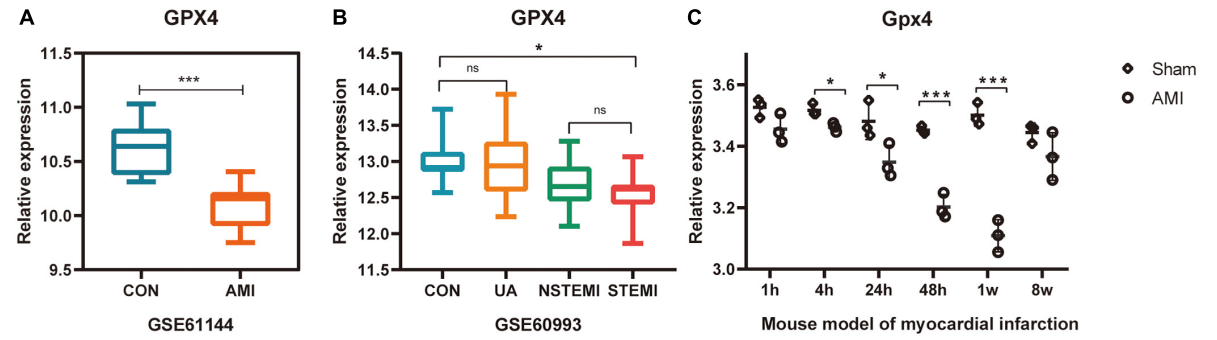

FIGURE 5
Validation of the expression of ferroptosis marker GPX4 in multiple AMI related datasets. **(A–C)** *$P < 0.05$; ***$P < 0.001$.

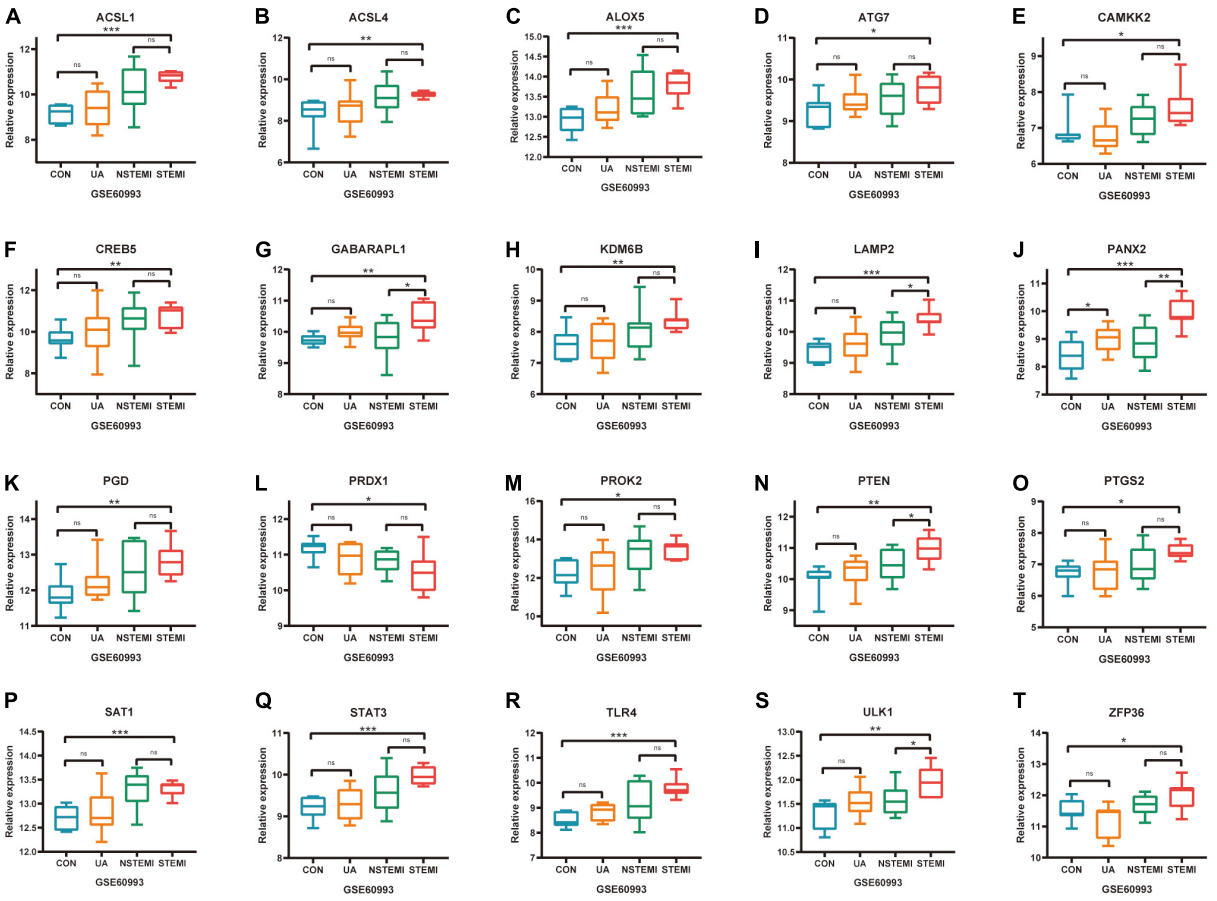

FIGURE 6
Further validation of differentially expressed FRGs in external dataset GSE60993. **(A–T)** *$P < 0.05$; **$P < 0.01$; ***$P < 0.001$.

qRT-PCR verification of ferroptosis related genes in AC16 hypoxia model

The expression of 20 differentially expressed FRGs (ACSL1, ACSL4, ALOX5, ATG7, CAMKK2, CREB5, GABARAPL1, KDM6B, LAMP2, PANX2, PGD, PRDX1, PROK2, PTEN, PTGS2, SAT1, STAT3, TLR4, ULK1, and ZFP36) were further verified to study the effect of hypoxia on FRGs. The results showed 12 of them were differentially expressed (**Figures 9A–L**). They were ALOX5 (up), CAMKK2 (up), CREB5 (down), GABARAPL1 (down), KDM6B (up), LAMP2 (up), PGD (down), PTEN (up), PTGS2 (up), STAT3 (down), ULK1 (up),

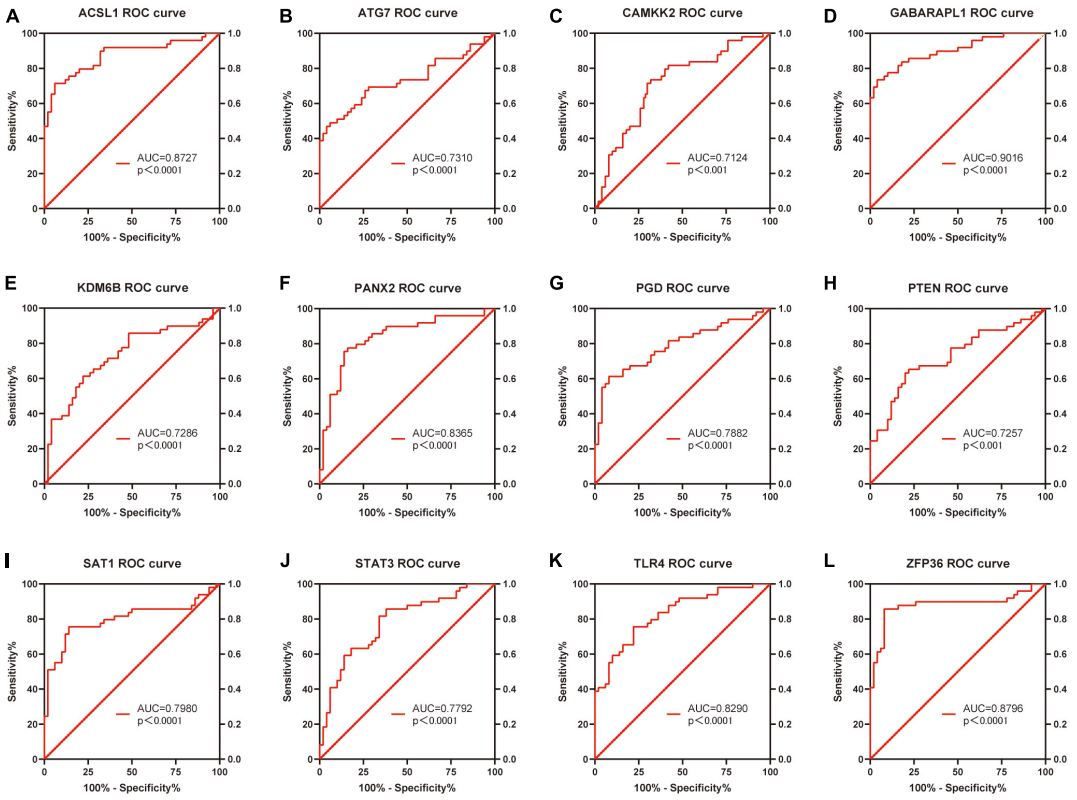

FIGURE 7
Receiver operating characteristic curve analysis of the top 12 ranked AUC values.

and ZFP36 (down). The expression of ALOX5, CAMKK2, KDM6B, LAMP2, PTEN, PTGS2, and ULK1 were consistent with the predicted result.

Discussion

Acute myocardial infarction (AMI) is one of the main causes of sudden cardiac death in middle-aged and elderly people (20). Early reperfusion therapy is still a key measure for the treatment of AMI. Studies have shown that early restoration of blood perfusion can help reduce the size of myocardial infarction and reduce the incidence of arrhythmia and heart failure (21, 22). Therefore, it is of great importance to further study the pathogenesis of AMI and to find new biomarkers for early mild myocardial injury. Ferroptosis as a modality of regulatory cell death has received extensive attention in recent years. The understanding of the mechanism of ferroptosis in AMI is still limited. We used bioinformatics method to mine information from existing AMI related sequencing datasets, aiming to explore the expression patterns and molecular mechanisms of FRGs in AMI.

In the present study, 131 CoDEGs were screened in AMI-related datasets GSE66360 and GSE61144. These genes were mainly enriched in the pathways of "inflammatory response," "immune response," "plasma membrane," "receptor activity," "protein homodimerization activity," "calcium ion binding," "Phagosome," "Cytokine-cytokine receptor interaction," and "Toll-like receptor signaling pathway." This suggests that inflammatory response is deeply involved in the pathogenesis of AMI. In the early stages of AMI, the injury is caused by a reduced blood supply to the tissue, and as cell death increases, the inflammatory response intensifies, which in turn further promotes cell death (23). In addition, it has also been shown that these pathways are associated with ferroptosis. The ferroptosis inhibitor ferrostatin-1 can inhibit TLR4 and inhibit LPS-induced cardiac dysfunction through TLR4/NF-κB signaling pathway (24). A PPI network of these CoDEGs was analyzed by String database. Based on this PPI network, 7 hub genes, ITGAM, S100A12, S100A9, TLR2, TLR4, TLR8, and TREM1 were identified. These genes are also enriched in inflammation-related pathways. It is reported that ITGAM is a key immune-related gene, which is significantly increased in blood samples of patients with AMI (25). S100A9 and S100A12 are up-regulated in the process of AMI and can induce macrophage/microglia inflammation (26, 27). Shuangxinfang (psycho-cardiology formula, PCF) could inhibit this process and improve the heart function of mice with myocardial infarction

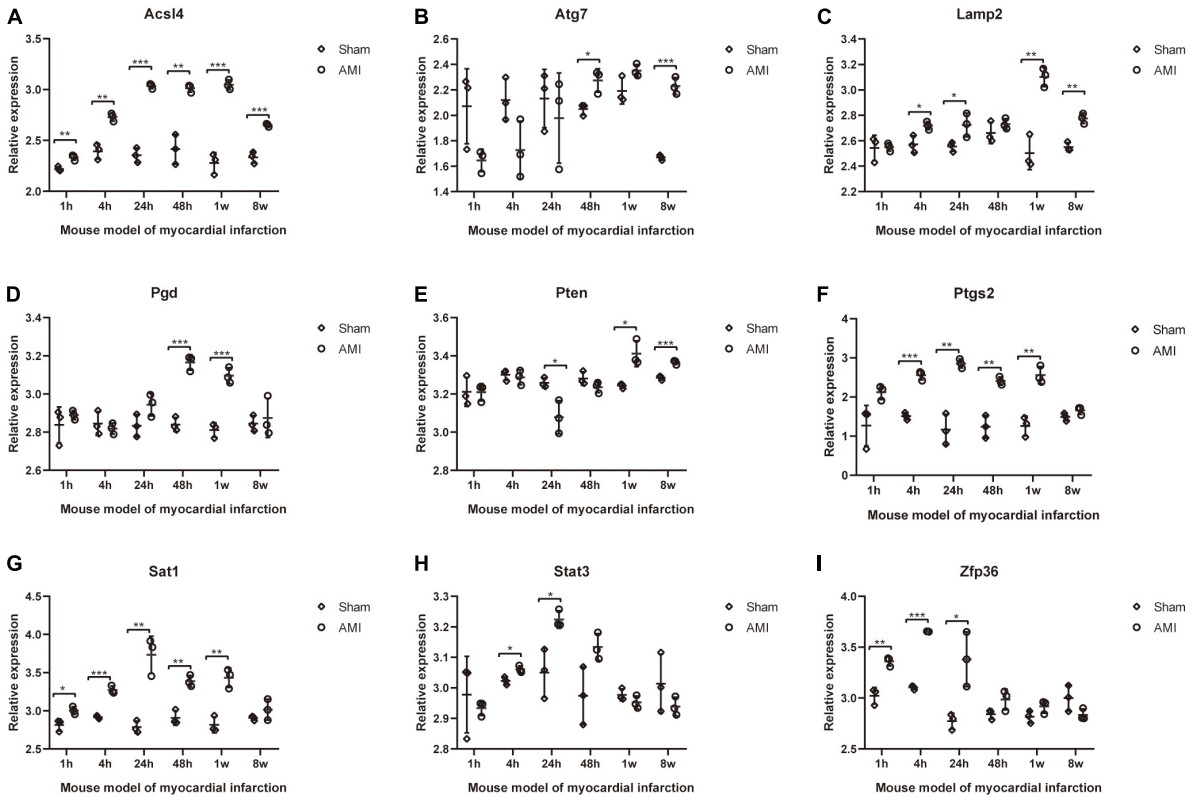

FIGURE 8
Further validation of differentially expressed FRGs in Mouse model of myocardial infarction dataset GSE775. **(A–I)** *$P < 0.05$; **$P < 0.01$; ***$P < 0.001$.

(26). TREM-1 is a receptor of immunoglobulin superfamily, which has been proved to induce and amplify inflammation in the progress of acute and chronic diseases (28). A study shows that the risk of death, recurrent myocardial infarction and stroke is increased in AMI patients with high expression of TREM-1 (29). A large number of studies have confirmed that the inflammatory response in AMI plays a key role in determining the size of myocardial infarction, and sustained proinflammatory response can lead to poor left ventricular remodeling after myocardial infarction (30, 31). The TLRs, include TLR1, TLR2, TLR4, TLR5, TLR6, and TLR11, act as sensors to damage associated molecular patterns (DAMPs) [such as heat shock proteins (HSPs), HMGB1, fibronectin-end domain A (FN-EDA)] (32). Inhibition of TLR2 or TLR4 can reduce myocardial infarction area and inhibit myocardial remodeling (33, 34).

Studies have shown that ferroptosis and inflammatory responses can interact. Cells undergoing ferroptosis are inherently more immunogenic because they release inflammatory cytokines and DAMPs, skewing the milieu to a proinflammatory state (35). Ferroptosis can also potently induce inflammation through the release of IL-33 and HMGB1 (36, 37). Some inflammatory cytokines (such as TNF, PGE2, IL-1β, IL-6, and IL-1) have been demonstrated to directly affect GPX4 levels. For example, TNF treatment of cells resulted in continuous downregulation of GPX4 and may further trigger ferroptosis (36). Therefore, Ferroptosis and inflammation may complement each other and participate in the regulation of AMI.

In addition, 45 and 14 FRGs were identified in GSE66360 and GSE61144, respectively. Enrichment analysis showed that these genes were involved in ferroptosis-related pathways. FRGs ACSL1, ATG7, CAMKK2, GABARAPL1, KDM6B, LAMP2, PANX2, PGD, PTEN, SAT1, STAT3, TLR4, and ZFP36 were significantly differentially expressed in external dataset GSE66360 with AUC $\geq$ 0.7, and may be potential biomarkers of AMI. These FRGs were further verified by external dataset GSE60993 (human, blood), GSE775 (mouse, tissue) and AC16 hypoxia model. The results showed that ACSL4, ATG7, LAMP2, PGD, PTEN, PTGS2, SAT1, STAT3, and ZFP36 were highly expressed in blood of patients with AMI and myocardial tissue of mice after AMI, among which LAMP2, PTEN, and PTGS2 were highly expressed in blood of patients with AMI, myocardial tissue of mice after AMI and myocardial cell hypoxia model. ALOX5, CAMKK2, KDM6B, and ULK1 were only significantly highly expressed in blood of patients with AMI and myocardial cell hypoxia model.

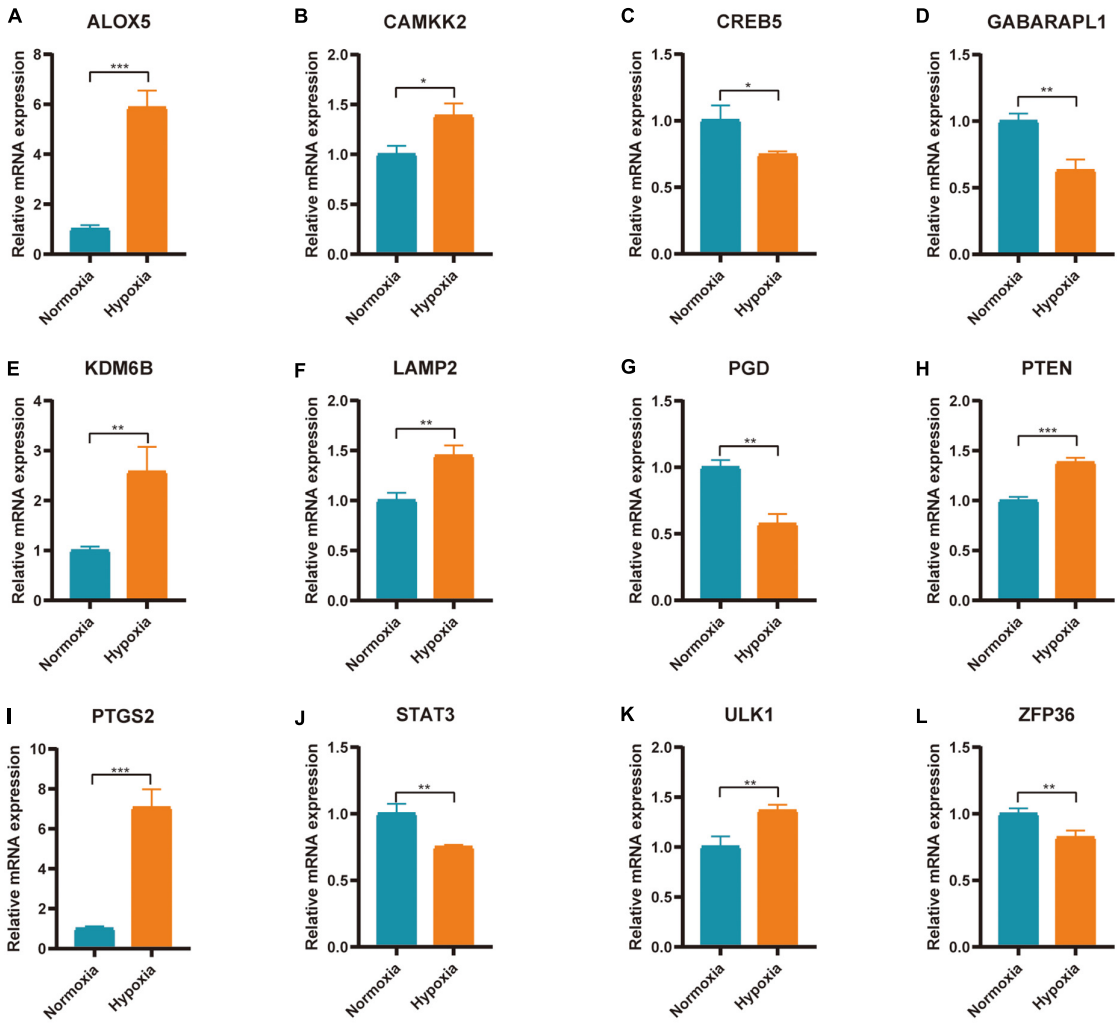

FIGURE 9
Expression of FRGs in AC16 cell hypoxia model. **(A–L)** *$P < 0.05$; **$P < 0.01$; ***$P < 0.001$.

The regulation of these genes on ferroptosis has been studied. LAMP2 (Lysosome-associated membrane glycoprotein 2) plays an important role in chaperone-mediated autophagy. Deficiency of LAMP2 increases the risk of reactive oxygen species-induced ferroptosis in retinal pigment epithelial cells (38). One study has shown that the loss of phosphatase and tensin homolog deleted on chromosome 10 (PTEN) function confers ferroptosis resistance in cancer cells, and the inhibition of the PI3K-AKT-mTOR signaling axis sensitizes cancer cells to ferroptosis induction (39). This indicated that PTEN has the function of promoting ferroptosis. ALOX5 (5-Lipoxygenase) is an iron-containing and non-heme dioxygenase that catalyzes the peroxidation of polyunsaturated fatty acids such as arachidonic acid (40). Another study has shown that N-acetylcysteine (NAC) targets ALOX5 derived toxic lipids and can synergize with prostaglandin E_2 to inhibit ferroptosis and improve outcomes following hemorrhagic stroke in mice (41). ULK1 (unc-51 like autophagy activating kinase 1) plays an important role in autophagy regulation. It is reported that ferritinophagy is involved in Bisphenol A-induced ferroptosis of renal tubular epithelial cells through the activation of the AMPK-mTOR-ULK1 pathway (42). In addition, CAMKK2, KDM6B, and PTGS2 have all been studied to be related to ferroptosis. These genes are activated in the biological process of ferroptosis and participate in the regulation of ferroptosis biological process (43, 44). Therefore, these identified FRGs (ALOX5, CAMKK2, KDM6B, LAMP2, PTEN, PTGS2, and ULK1) may be potential ferroptosis related biomarkers of AMI. It is important to note that the association of these genes with ferroptosis and AMI requires further clarification.

This study is based on the analysis of transcriptome data available in public databases and therefore has certain limitations. We need to collect blood samples in the population for testing to verify the diagnostic value of these biomarkers. It

is also necessary to establish cell models and animal models to further study the mechanism of ferroptosis in AMI.

Conclusion

We identified 131 differentially expressed genes in blood samples from patients with AMI. These genes are mainly associated with inflammatory reactions. Analysis of human blood sample sequencing datasets and mouse myocardial infarction sequencing datasets as well as cardiomyocyte hypoxia experiments indicated that FRGs ALOX5, CAMKK2, KDM6B, LAMP2, PTEN, PTGS2, and ULK1 may be potential biomarkers of AMI.

Data availability statement

The datasets presented in this study can be found in online repositories. The names of the repository/repositories and accession number(s) can be found in the article/**Supplementary material**.

Author contributions

JW, HC, and ZL performed the data analysis and drafted the manuscript. CL, YH, and TZ prepared the figures and contributed toward the study design. HZ and YL optimized the analysis protocol and completed the experimental part. XH and JC revised the figures, designed and supervised the study. All authors have read and approved the final manuscript.

Funding

This study was supported by the National Natural Science Foundation of China (grant no. 81370308, XH) and the research fund from medical Sci-Tech innovation platform of Zhongnan Hospital, Wuhan University (grant nos. PTXM2021009, JC and PTXM2022002, XH).

Acknowledgments

We sincerely appreciate the researchers for providing their GEO database information online, we are truly honored to acknowledge their contributions. We are also very grateful to sanger box online biomedical data analysis tool (http://sangerbox.com). It simplifies the analysis process.

Conflict of interest

The authors declare that the research was conducted in the absence of any commercial or financial relationships that could be construed as a potential conflict of interest.

Publisher's note

Supplementary material

The Supplementary Material for this article can be found online at: https://www.frontiersin.org/articles/10.3389/fcvm.2022.993592/full#supplementary-material

SUPPLEMENTARY TABLE 1
Ferroptosis-related genes in FerrDB V2.

SUPPLEMENTARY TABLE 2
The primer sequence information of qPCR experiment.

SUPPLEMENTARY TABLE 3
The detailed results of differential expression analysis.

SUPPLEMENTARY TABLE 4
Ferroptosis-related genes in GSE66360 and GSE61144.

References

1. Ramachandra, C, Hernandez-Resendiz S, Crespo-Avilan GE, Lin YH, Hausenloy DJ. Mitochondria in acute myocardial infarction and cardioprotection. *Ebiomedicine.* (2020) 57:102884. doi: 10.1016/j.ebiom.2020.102884

2. Gossage JR. Acute myocardial infarction. Reperfusion strategies. *Chest.* (1994) 106:1851–66. doi: 10.1378/chest.106.6.1851

3. Guo S, Wu J, Zhou W, Liu X, Liu Y, Zhang J, et al. Identification and analysis of key genes associated with acute myocardial infarction by integrated bioinformatics methods. *Medicine.* (2021) 100:e25553. doi: 10.1097/MD.0000000000025553

4. Xin M, Olson EN, Bassel-Duby R. Mending broken hearts: cardiac development as a basis for adult heart regeneration and repair. *Nat Rev Mol Cell Biol.* (2013) 14:529–41. doi: 10.1038/nrm3619

5. Yellon DM, Hausenloy DJ. Myocardial reperfusion injury. *N Engl J Med.* (2007) 357:1121–35. doi: 10.1056/NEJMra071667

6. Braunwald E. Unstable angina and non-ST elevation myocardial infarction. *Am J Respir Crit Care Med.* (2012) 185:924–32. doi: 10.1164/rccm.201109-1745CI

7. Dixon SJ, Lemberg KM, Lamprecht MR, Skouta R, Zaitsev EM, Gleason CE, et al. Ferroptosis: an iron-dependent form of nonapoptotic cell death. *Cell.* (2012) 149:1060–72. doi: 10.1016/j.cell.2012.03.042

8. Qiu Y, Cao Y, Cao W, Jia Y, Lu N. The application of ferroptosis in diseases. *Pharmacol Res.* (2020) 159:104919. doi: 10.1016/j.phrs.2020.104919

9. Jarvholm B, Sanden A. Estimating asbestos exposure: a comparison of methods. *J Occup Med.* (1987) 29:361–3.

10. Sharma A, Flora S. Positive and negative regulation of ferroptosis and its role in maintaining metabolic and redox homeostasis. *Oxid Med Cell Longev.* (2021) 2021:9074206. doi: 10.1155/2021/9074206

11. Li D, Li Y. The interaction between ferroptosis and lipid metabolism in cancer. *Signal Transduct Target Ther.* (2020) 5:108. doi: 10.1038/s41392-020-00216-5

12. Gan B. Mitochondrial regulation of ferroptosis. *J Cell Biol.* (2021) 220:e202105043. doi: 10.1083/jcb.202105043

13. Ajoolabady A, Aslkhodapasandhokmabad H, Libby P, Tuomilehto J, Lip GYH, Penninger JM, et al. Ferritinophagy and ferroptosis in the management of metabolic diseases. *Trends Endocrinol Metab.* (2021) 32:444–62. doi: 10.1016/j.tem.2021.04.010

14. Bai T, Li M, Liu Y, Qiao Z, Wang Z. Inhibition of ferroptosis alleviates atherosclerosis through attenuating lipid peroxidation and endothelial dysfunction in mouse aortic endothelial cell. *Free Radic Biol Med.* (2020) 160:92–102. doi: 10.1016/j.freeradbiomed.2020.07.026

15. Fang X, Wang H, Han D, Xie E, Yang X, Wei J, et al. Ferroptosis as a target for protection against cardiomyopathy. *Proc Natl Acad Sci USA.* (2019) 116:2672–80. doi: 10.1073/pnas.1821022116

16. Tang LJ, Zhou YJ, Xiong XM, Li NS, Zhang JJ, Luo XJ, et al. Ubiquitin-specific protease 7 promotes ferroptosis via activation of the p53/TfR1 pathway in the rat hearts after ischemia/reperfusion. *Free Radic Biol Med.* (2021) 162:339–52. doi: 10.1016/j.freeradbiomed.2020.10.307

17. Wu X, Sui Z, Zhang H, Wang Y, Yu Z. Integrated analysis of lncRNA-Mediated ceRNA network in lung adenocarcinoma. *Front Oncol.* (2020) 10:554759. doi: 10.3389/fonc.2020.554759

18. Wu J, Cao J, Fan Y, Li C, Hu X. Comprehensive analysis of miRNA-mRNA regulatory network and potential drugs in chronic chagasic cardiomyopathy across human and mouse. *BMC Med Genomics.* (2021) 14:283. doi: 10.1186/s12920-021-01134-3

19. Wan Y, Zhang X, Leng H, Yin W, Zeng W, Zhang C. Identifying hub genes of papillary thyroid carcinoma in the TCGA and GEO database using bioinformatics analysis. *PeerJ.* (2020) 8:e9120. doi: 10.7717/peerj.9120

20. Mozaffarian D, Benjamin EJ, Go AS, Arnett DK, Blaha MJ, Cushman M, et al. Heart disease and stroke statistics-2016 update: a report from the American heart association. *Circulation.* (2016) 133:e38–360.

21. Zhang Y, Huo Y. Early reperfusion strategy for acute myocardial infarction: a need for clinical implementation. *J Zhejiang Univ Sci B.* (2011) 12:629–32. doi: 10.1631/jzus.B1101010

22. Hausenloy DJ, Yellon DM. Reperfusion injury salvage kinase signalling: taking a RISK for cardioprotection. *Heart Fail Rev.* (2007) 12:217–34. doi: 10.1007/s10741-007-9026-1

23. Toldo S, Abbate A. The NLRP3 inflammasome in acute myocardial infarction. *Nat Rev Cardiol.* (2018) 15:203–14. doi: 10.1038/nrcardio.2017.161

24. Xiao Z, Kong B, Fang J, Qin T, Dai C, Shuai W, et al. Ferrostatin-1 alleviates lipopolysaccharide-induced cardiac dysfunction. *Bioengineered.* (2021) 12:9367–76. doi: 10.1080/21655979.2021.2001913

25. Zheng PF, Zou QC, Chen LZ, Liu P, Liu ZY, Pan HW. Identifying patterns of immune related cells and genes in the peripheral blood of acute myocardial infarction patients using a small cohort. *J Transl Med.* (2022) 20:321. doi: 10.1186/s12967-022-03517-1

26. Sun Y, Wang Z, Hou J, Shi J, Tang Z, Wang C, et al. Shuangxinfang prevents S100A9-induced macrophage/microglial inflammation to improve cardiac function and depression-like behavior in rats after acute myocardial infarction. *Front Pharmacol.* (2022) 13:832590. doi: 10.3389/fphar.2022.832590

27. Xie J, Luo C, Mo B, Lin Y, Liu G, Wang X, et al. Inflammation and oxidative stress role of S100A12 as a potential diagnostic and therapeutic biomarker in acute myocardial infarction. *Oxid Med Cell Longev.* (2022) 2022:2633123. doi: 10.1155/2022/2633123

28. Kouassi KT, Gunasekar P, Agrawal DK, Jadhav GP. TREM-1; is it a pivotal target for cardiovascular diseases? *J Cardiovasc Dev Dis.* (2018) 5:45. doi: 10.3390/jcdd5030045

29. Ait-Oufella H, Yu M, Kotti S, Georges A, Vandestienne M, Joffre J, et al. Plasma and genetic determinants of soluble TREM-1 and major adverse cardiovascular events in a prospective cohort of acute myocardial infarction patients. Results from the FAST-MI 2010 Study. *Int J Cardiol.* (2021) 344:213–9. doi: 10.1016/j.ijcard.2021.09.018

30. Ong SB, Hernández-Reséndiz S, Crespo-Avilan GE, Mukhametshina RT, Kwek XY, Cabrera-Fuentes HA, et al. Inflammation following acute myocardial infarction: multiple players, dynamic roles, and novel therapeutic opportunities. *Pharmacol Ther.* (2018) 186:73–87. doi: 10.1016/j.pharmthera.2018.01.001

31. Paolisso P, Foà A, Bergamaschi L, Donati F, Fabrizio M, Chiti C, et al. Hyperglycemia, inflammatory response and infarct size in obstructive acute myocardial infarction and MINOCA. *Cardiovasc Diabetol.* (2021) 20:33. doi: 10.1186/s12933-021-01222-9

32. van Hout GP, Arslan F, Pasterkamp G, Hoefer IE. Targeting danger-associated molecular patterns after myocardial infarction. *Expert Opin Ther Targets.* (2016) 20:223–39. doi: 10.1517/14728222.2016.1088005

33. Arslan F, Smeets MB, O'Neill LA, Keogh B, McGuirk P, Timmers L, et al. Myocardial ischemia/reperfusion injury is mediated by leukocytic toll-like receptor-2 and reduced by systemic administration of a novel anti-toll-like receptor-2 antibody. *Circulation.* (2010) 121:80–90. doi: 10.1161/CIRCULATIONAHA.109.880187

34. Timmers L, Sluijter JP, van Keulen JK, Hoefer IE, Nederhoff MG, Goumans MJ, et al. Toll-like receptor 4 mediates maladaptive left ventricular remodeling and impairs cardiac function after myocardial infarction. *Circ Res.* (2008) 102:257–64. doi: 10.1161/CIRCRESAHA.107.158220

35. Kim EH, Wong SW, Martinez J. Programmed necrosis and disease: We interrupt your regular programming to bring you necroinflammation. *Cell Death Differ.* (2019) 26:25–40. doi: 10.1038/s41418-018-0179-3

36. Wen Q, Liu J, Kang R, Zhou B, Tang D. The release and activity of HMGB1 in ferroptosis. *Biochem Biophys Res Commun.* (2019) 510:278–83. doi: 10.1016/j.bbrc.2019.01.090

37. Stockwell BR, Friedmann Angeli JP, Bayir H, Bush AI, Conrad M, Dixon SJ, et al. Ferroptosis: a regulated cell death nexus linking metabolism, redox biology, and disease. *Cell.* (2017) 171:273–85. doi: 10.1016/j.cell.2017.09.021

38. Lee JJ, Ishihara K, Notomi S, Efstathiou NE, Ueta T, Maidana D, et al. Lysosome-associated membrane protein-2 deficiency increases the risk of reactive oxygen species-induced ferroptosis in retinal pigment epithelial cells. *Biochem Biophys Res Commun.* (2020) 521:414–9. doi: 10.1016/j.bbrc.2019.10.138

39. Yi J, Zhu J, Wu J, Thompson CB, Jiang X. Oncogenic activation of PI3K-AKT-mTOR signaling suppresses ferroptosis via SREBP-mediated lipogenesis. *Proc Natl Acad Sci USA.* (2020) 117:31189–97. doi: 10.1073/pnas.2017152117

40. Sun QY, Zhou HH, Mao XY. Emerging roles of 5-lipoxygenase phosphorylation in inflammation and cell death. *Oxid Med Cell Longev.* (2019) 2019:2749173. doi: 10.1155/2019/2749173

41. Karuppagounder SS, Alin L, Chen Y, Brand D, Bourassa MW, Dietrich K, et al. N-acetylcysteine targets 5 lipoxygenase-derived, toxic lipids and can synergize with prostaglandin E2 to inhibit ferroptosis and improve outcomes following hemorrhagic stroke in mice. *Ann Neurol.* (2018) 84:854–72. doi: 10.1002/ana.25356

42. Bao L, Zhao C, Feng L, Zhao Y, Duan S, Qiu M, et al. Ferritinophagy is involved in Bisphenol A-induced ferroptosis of renal tubular epithelial cells through the activation of the AMPK-mTOR-ULK1 pathway. *Food Chem Toxicol.* (2022) 163:112909. doi: 10.1016/j.fct.2022.112909

43. Li Q, Han X, Lan X, Gao Y, Wan J, Durham F, et al. Inhibition of neuronal ferroptosis protects hemorrhagic brain. *JCI Insight.* (2017) 2:e90777. doi: 10.1172/jci.insight.90777

44. Wang S, Yi X, Wu Z, Guo S, Dai W, Wang H, et al. CAMKK2 defines ferroptosis sensitivity of melanoma cells by regulating AMPKNRF2 pathway. *J Invest Dermatol.* (2022) 142:189–200.e8. doi: 10.1016/j.jid.2021.05.025

frontiers | Frontiers in Cardiovascular Medicine

TYPE Review
PUBLISHED 15 December 2022
DOI 10.3389/fcvm.2022.961991

OPEN ACCESS

EDITED BY
Michal Mokry,
University Medical Center Utrecht, Netherlands

REVIEWED BY
Daniel Gomari,
Stanford University, United States
Zhi-Ping Liu,
Shandong University, China
Miranda Witheford,
Toronto General Hospital, Canada

*CORRESPONDENCE
Shijie Xin
sjxin@cmu.edu.cn

SPECIALTY SECTION
This article was submitted to Atherosclerosis and Vascular Medicine, a section of the journal Frontiers in Cardiovascular Medicine

RECEIVED 05 June 2022
ACCEPTED 28 November 2022
PUBLISHED 15 December 2022

CITATION
Hao X, Cheng S, Jiang B and Xin S (2022) Applying multi-omics techniques to the discovery of biomarkers for acute aortic dissection.
Front. Cardiovasc. Med. 9:961991.
doi: 10.3389/fcvm.2022.961991

Applying multi-omics techniques to the discovery of biomarkers for acute aortic dissection

Xinyu Hao[1,2], Shuai Cheng[1,2], Bo Jiang[1,2] and Shijie Xin[1,2]*

[1]Department of Vascular Surgery, The First Affiliated Hospital of China Medical University, China Medical University, Shenyang, China, [2]Key Laboratory of Pathogenesis, Prevention and Therapeutics of Aortic Aneurysm, Shenyang, Liaoning, China

Acute aortic dissection (AAD) is a cardiovascular disease that manifests suddenly and fatally. Due to the lack of specific early symptoms, many patients with AAD are often overlooked or misdiagnosed, which is undoubtedly catastrophic for patients. The particular pathogenic mechanism of AAD is yet unknown, which makes clinical pharmacological therapy extremely difficult. Therefore, it is necessary and crucial to find and employ unique biomarkers for Acute aortic dissection (AAD) as soon as possible in clinical practice and research. This will aid in the early detection of AAD and give clear guidelines for the creation of focused treatment agents. This goal has been made attainable over the past 20 years by the quick advancement of omics technologies and the development of high-throughput tissue specimen biomarker screening. The primary histology data support and add to one another to create a more thorough and three-dimensional picture of the disease. Based on the introduction of the main histology technologies, in this review, we summarize the current situation and most recent developments in the application of multi-omics technologies to AAD biomarker discovery and emphasize the significance of concentrating on integration concepts for integrating multi-omics data. In this context, we seek to offer fresh concepts and recommendations for fundamental investigation, perspective innovation, and therapeutic development in AAD.

KEYWORDS

multi-omics, acute aortic dissection, biomarkers, high-throughput sequencing technology, mass spectrometry technology, diagnostics, integrated strategies

1 Introduction

1.1 Applying multi-omics concepts to biomedicine

Biomedicine is an important engineering field related to the improvement of medical diagnosis and human's own health. As science has advanced over the past few decades, it has become evident that many diseases, particularly those that are challenging to diagnose and cure, are frequently brought on by a confluence of genetic and environmental variables (1). When the idea of "omics" was first introduced, a new era had begun in which people were no longer constrained to using solitary factors to explain illness. This meant that we started to evaluate a set of molecules in a comprehensive way (2). One by one, the traditional ideas of genomics, transcriptomics, proteomics (3), and metabolomics were introduced. Single-omics methods, however, are only able to explain diseases at a single level (4) (e.g., at the gene, RNA, or protein level) and are unable to fully depict the complex biological processes involved (5), especially the regulatory and signaling mechanisms (6). In light of this, scientists' interest in the integration of several histology techniques has increased recently. It is a method that has the potential to broaden our understanding of biology and disease (1) as well as the diversity and depth of the biological sciences (7). The molecular underpinnings of complex diseases like cancer (8–10), immune system diseases (11, 12), infectious diseases (1, 13), and cardiovascular diseases (14) can be better understood by the analysis of multi-omics data. Thus, we can reveal disease-related etiological mechanisms, explore new biomarkers, and develop new targeted drugs for clinical research applications. To advance the development of clinical precision medicine (15) and bring benefits to patients (**Figure 1**).

1.2 Advantages and prospects of applying multi-omics concepts in AAD

Acute aortic dissection (AAD) is a cardiovascular disease with a high mortality risk, in which blood flow breaks through the intima of the aorta and enters the tunica media, forming a false lumen. The true lumen and the false lumen may or may not be connected, and blood flowing between them may form a thrombus. There has been an upsurge in AAD cases recently (16), with a trend toward younger ages (17). Aging, high blood pressure, atherosclerosis, and connective tissue-related genetic risk factors are among the many risk factors linked to AAD (18). Additionally, men are much more likely to experience it than women are (19) (**Figure 2**). AAD can be divided into acute type A dissection and acute type B dissection according to the anatomical location of the lesion. Acute type A dissection involves the ascending aorta and is treated clinically with emergency open surgery such as aortic replacement, while acute type B dissection involves only the thoracic descending aorta and its distal parts and is treated mainly with drugs or intervention (17). Clinically, patients with AAD tend to present with tearing-like pain, and the main site of pain correlates with the site of dissection, with chest pain being the most common. However, because the symptoms are not diagnostically specific, they are easily confused with other diseases such as acute coronary syndrome (ACS), acute myocardial infarction (AMI), and acute abdomen. And in about 6% of cases, no symptoms of chest pain are present (20), making AAD often misdiagnosed or missed (21). AAD rupture can have serious side effects, including extensive bleeding that quickly results in inadequate perfusion of several organs and eventual death (22). In patients with untreated symptoms caused by overlook or misdiagnosis, the mortality rate can range from 1 to 2% per hour following the beginning of symptoms to 50% at 48 h (19, 21).

Currently, the most common method used in hospitals for the diagnosis of AAD is laboratory tests combined with imaging (23). In order to further reduce the possibility of underdiagnosis and misdiagnosis, the use of omics techniques becomes an inevitable choice to drive technological innovation when we try to optimize the existing diagnostic protocols to discover new, biologically based, low-budget, easily accessible, highly sensitive, specific and non-invasive prognostic and diagnostic tools. We have gradually connected molecule-to-molecule and molecule-to-phenotype linkages in organisms by merging multi-omics, starting at the genetic level and moving up via nucleic acids, proteins, and tiny molecules of metabolism. At the same time, AAD, as a highly dynamic and changing disease, produces largely different specific biological indicators at each stage of its development. To develop a thorough biological model, more attention must be paid to longitudinal molecular alterations (i.e., various molecular layers) in the same or the same group of individuals (24). It also leads to a deeper comprehension of how signaling pathways and network interactions affect disease pathogenesis mechanisms (25). Additionally, these comprehensive data reveal several pathological features of AAD, which is crucial for patient risk classification and optimizing therapies to stop AAD progression (14).

2 Introduction of omics techniques

2.1 Genomics and transcriptomics

Since its inception more than ten years ago, genome-wide association analysis (GWAS) has significantly advanced our understanding of human susceptibility genes and their roles in common diseases. GWAS attempts to find locus variants associated with complex features in populations, and in particular to detect connections between common single nucleotide polymorphisms (SNPs) and a wide range of prevalent

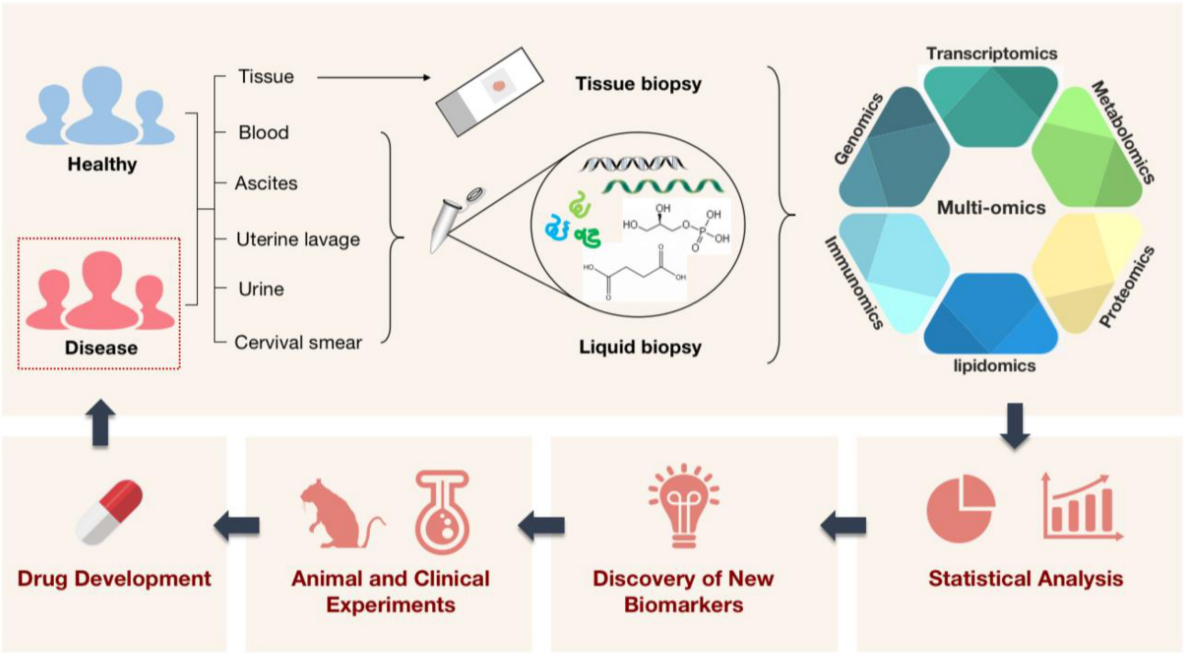

FIGURE 1
A schematic illustration of how multi-omics technologies are employed in biomedicine. Multi-omics technologies are used to process tissue samples from people, animals, and the environment for high-throughput quantitative analysis of molecules in biological systems. This aims to reveal disease-related etiological mechanisms, find new diagnostic markers, shed light on disease pathogenesis, and pave the way for the creation and application of new targeted therapeutic agents with the ultimate goal of treating diseased populations.

diseases (26). It inaugurated a new era in our understanding of the genetic origins of disease. Additionally, DNA microarrays (also known as genotyping microarrays) with known high-frequency SNPs are frequently used in such research (**Figure 3**). The number of variants that can be detected using genotyping microarrays has increased over the years, but even the high-density 5 million SNP microarray (Illumina OMNI5) (27) covers only a small fraction of the 3.3 billion bases in the human genome. Additionally, some SNPs with low frequency are frequently deleted after applying conventional quality control (QC) before association analysis, despite the fact that they could be crucial to understanding some rare diseases or phenotypes (28).

Following GWAS, sequencing technologies reached a historical turning point. Due to their reduced cost, broader detection range, and improved ability to discover uncommon genetic variants (e.g., point mutations, copy number variants, and structural variants) (29), high-throughput whole genome sequencing (WGS), whole exome sequencing (WES), and simplified genome sequencing (RRGS) are anticipated to displace microarray-based genotyping approaches in GWAS. In particular, WES technology allows better detection of pathogenic mutations present in coding regions or typical splice sites, allowing the study of up to 85% of Mendelian diseases (30). In the history of sequencing technology, second-generation sequencing (NGS) has been redefined in large part by improvements in microfabrication and high-resolution imaging that allow us to perform a large number of parallel sequencing responses at the micron scale (31). The division between NGS and third-generation sequencing (TGS) technologies is based on the development of real-time single-molecule sequencing (SMS) and nanopore sequencing (32). SMS makes it possible to directly sequence individual DNA molecules, doing away with the requirement for PCR amplification stages and cutting down on amplification-related mistakes. While this is happening, nanopore sequencing technology uses its own high accuracy, longer read length, and higher throughput of DNA or RNA molecules to apply to professional fields like genome assembly, full-length transcript detection, base modification detection, clinical diagnosis, and epidemic monitoring, greatly improving the quality and reliability of data (33).

If genomics is the study of the sequence and structural loci of the genes themselves, transcriptomics explores the function and structure of genes in an organism by looking at the level of gene expression regulation in turn. Transcriptome analysis focuses on gene expression levels and is crucial for understanding the structure and function of the genome, unraveling the genetic networks underlying disease, and discovering molecular biomarkers responsive to infections, medications, and disease states (34). RNA-seq technology enables more efficient, less expensive quantification of gene transcript levels. Most importantly, the discovery of novel genes

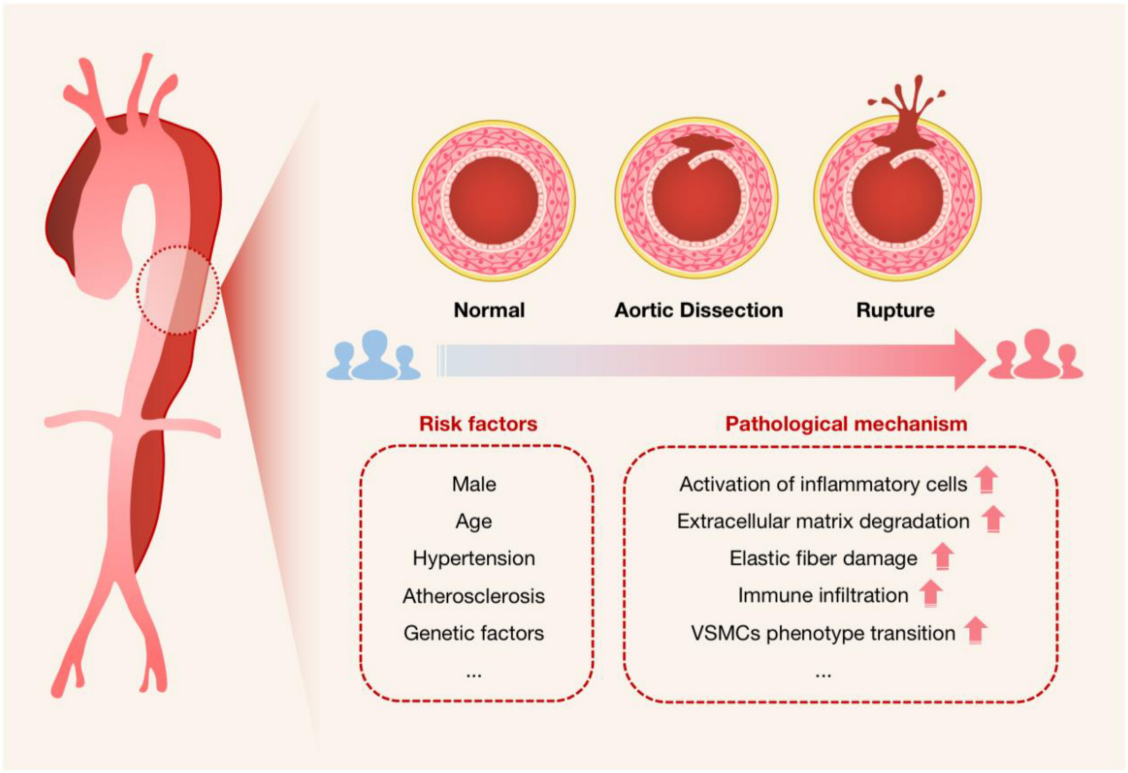

FIGURE 2
Schematic diagram used to characterize the onset of AAD. The cross-sectional schematics of a normal artery, an artery with aortic dissection, and an artery with dissection rupture are shown. It is intended to show the progression of AAD pathogenesis, i.e., the blood flow breaks through the intima of the aorta and enters the tunica media, forming a false lumen that will be at risk of rupture if not treated promptly, especially for Stanford type A dissection. Risk factors for AAD and possible associated pathological mechanisms are also listed.

and RNAs opens up new opportunities for the molecular biology sector to address clinical medical issues (35). Single cell RNA sequencing (scRNA-seq) enables transcriptome-wide analysis of individual cells, which can be used to study cell subpopulations (36) and uncommon cell types within tissues (37), involves isolating and lysing the individual cells, converting their RNA to cDNA, and amplifying the cDNA to produce high-throughput sequencing libraries (38).

By putting tissue sections on arrays of retrotransposon primers with specially placed barcodes, spatial transcriptomics enables the viewing and quantitative analysis of the transcriptome at spatial resolution in a single tissue section (39). It can replace the vacuum left by high-throughput techniques, which, since they cannot be used *in situ*, lose information about the spatial relationships between cataloged cell populations, by giving us unbiased maps of spatial composition for creating tissue atlases (40). Local networks of *in situ* intercellular communication can be better understood by spatial transcriptomics, and there is mounting proof that the tissue microenvironment of cells can affect their phenotypic. The molecular, cellular, and geographical structure of disease ecological niches (41) can be discovered by combining scRNA-seq with regionally resolved transcriptomics, multiplex *in situ* hybridization, *in situ* sequencing, and spatial barcoding approaches to localize RNA inside tissues (36).

2.2 Proteomics and metabolomics

Proteins have an irreplaceable role in exercising biological functions, and most of the functional information in an organism can be reflected by protein expression, structure, function, interactions and modifications (42). It can be said that proteins are the most direct presentation of the biological effects of a gene. Marc Wilkins coined the term "proteome" in 1996 (3), and it offers information that is complimentary to those of genomes and transcriptomics. However, proteomes are frequently substantially more complicated than their genomic and transcriptomic equivalents, and post-translational modifications (PTMs) in particular greatly contribute to the higher diversity of protein forms (43).

In the early days of proteomics research, reducing sample analysis time while increasing the depth of proteome coverage

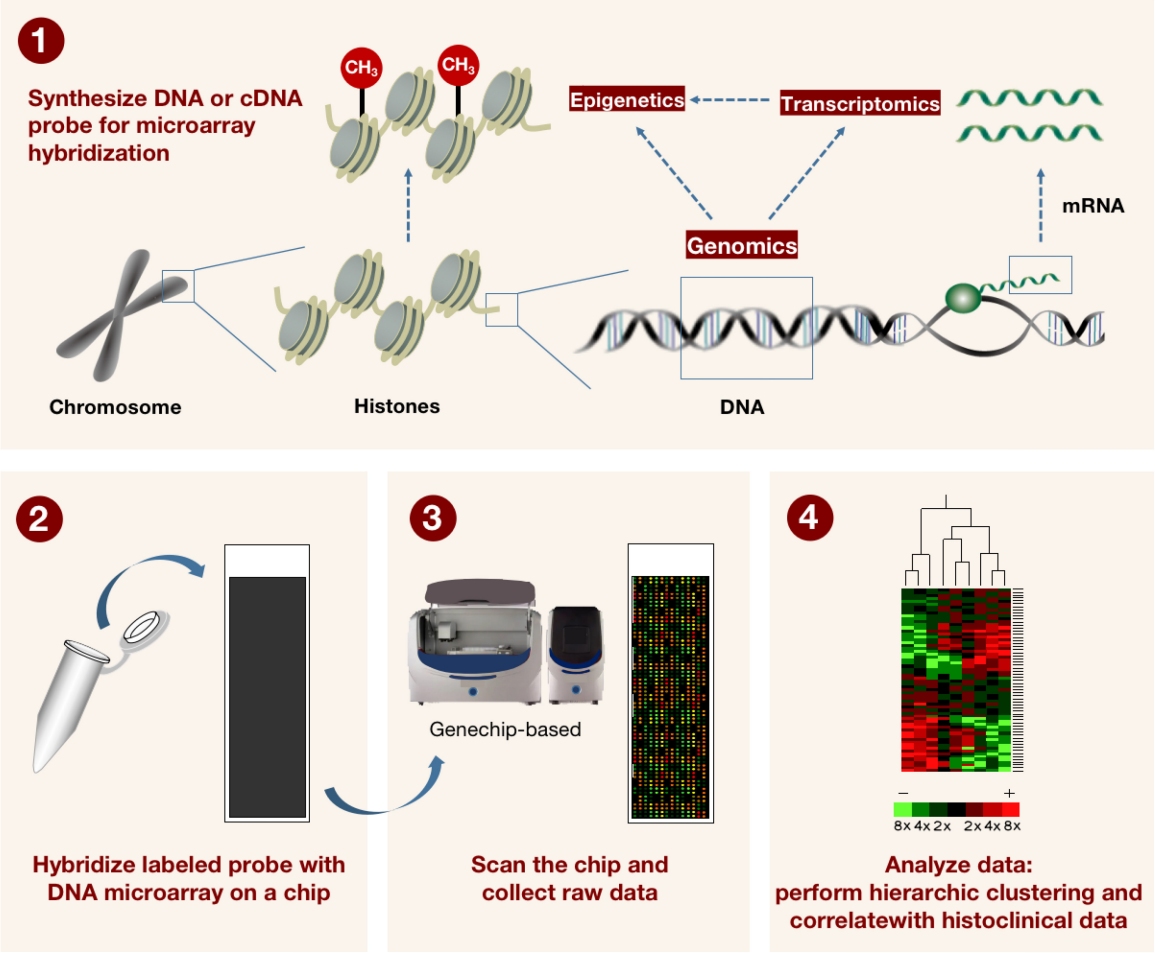

FIGURE 3
The method for describing how microarray technology is applied in genomics and transcriptomics. DNA or cDNA probes for microarray hybridization are first synthesized, and the labeled probes are subsequently hybridized to the DNA microarray on the microarray. The microarray is scanned by machine and raw data is collected. Finally, a hierarchical grouping and correlation with tissue clinical data was performed on the data. This in turn can be used to detect known gene sequences with high throughput.

was always the goal of scholars (44). The subsequent separation of complicated protein samples was made possible by the development of mass spectrometry (MS) and Edelman sequencing technologies. Then, isotope labeling, isobaric labeling, and metabolic labeling-based technologies called ICAT, iTRAQ (45), and SILAC (46) were introduced. The development of proteomics reached a pinnacle with the introduction of high-throughput sequencing technologies like X-ray crystallography (47), which can determine the three-dimensional structure of proteins as an anchor for structural biology, and NMR spectroscopy (48), which is used to resolve high-resolution protein structures (49). For decades, MS has been used extensively in the field of biomolecules, including high-throughput protein analyses that are both qualitative and quantitative, high-throughput analyses of protein post-translational modifications, identification of regulatory networks and protein-protein interactions, identification of protein-small molecule interactions, identification of biomarkers, and screening of potential drug targets (50). Tandem mass spectrometry combined with liquid chromatography (LC-MS/MS) has been used in a variety of settings. The fields which heavily relying on LC-MS/MS methods including clinical toxicology, clinical endocrinology, and validation of immunosuppressive medications (51).

In addition to being relevant to proteins and peptides, MS technique is crucial for the investigation of metabolic small molecules. The term "metabolome" was originally used by Oliver et al. in 1998 (52), and its analysis offers a novel method for the study of cellular metabolism and overall regulation in the fields of biochemistry and molecular biology. There are several ways to research metabolomics, however, at this point, nuclear magnetic resonance (NMR) spectroscopy and mass spectrometry (MS) metabolomics analysis are the most popular and encouraged methodologies. As a separation

technique, spectroscopy can separate compounds with similar structures, such as isomers, to reduce the complexity of biological extracts, and then send them to mass spectrometry for subsequent analysis, which will greatly improve the sensitivity and specificity of metabolomics analysis techniques. While metabolite culture supernatants are taken from tissues, biofluids, or cells, and then purified and injected by gas or liquid chromatography, MS is applied to metabolomics and proteomics in essentially the same ways. They are then measured for molecular mass-to-charge ratios and fragmentation patterns, which are compared to databases of known and anticipated compounds. Here, liquid chromatography-mass spectrometry (LC-MS) has been the method of choice for non-targeted metabolomics because it is the most adaptable and well-liked separation technology (53).

While the aforementioned analytical techniques are crucial, the choice of method and the development of the post-analytical data processing also significantly affect the outcomes (53). For currently tested metabolites, there are still major technical obstacles to data analysis and data integration (54). Recently, MetaboAnalyst's knowledge base was updated to include MS peak pathways, biomarker meta-analysis, a web-based resource manager for building networks of multi-omics technologies, and many other useful tools, opening up more possibilities for the future of metabolomics to have greater reproducibility and transparency in the interpretation of data analysis (55) (**Figure 4**).

3 Discovery of AAD biomarkers based on multi-omics technologies

Biomarker profiles are defined as indicators that can be measured in body fluids and tissues for the objective assessment of normal biology, pathological processes and pharmacological responses during actual treatment (56, 57). They have been divided into three major categories: molecular (e.g., chemicals, proteins, or genes), cellular (e.g., cell kinds, cell shape, and tissue histology), and imaging (e.g., X-ray, CT, PET or MRI features) (58). And in the clinical phase, a good biomarker must serve the purpose of "improving patient prognosis".

Most of the biomarkers for AAD at this stage have been discovered based on their possible pathological mechanisms. But regarding the pathogenic mechanisms underlying the development of AAD, there are currently a variety of conflicting and ambiguous views. Most researchers agree that two factors are primarily responsible for the pathogenesis of AAD: first, the pathological alterations in the vessel wall itself, including the activation of inflammatory cells, the breakdown of extracellular matrix, the destruction of elastic fibers, immune infiltration, and the loss and degeneration of smooth muscle cells (59), and second, the impact of mechanical shear stress on the vessel wall caused by blood flow (60), which is frequently closely related to unmanageable hypertension. Unfortunately, no diagnostic marker has been found to be as sensitive for AAD as BRCA for hereditary breast cancer or PSA for prostate cancer diagnosis and treatment. Therefore, the introduction of high-throughput histological technologies is particularly important for exploring and building a more complete network of AAD biologic diagnostic markers. In the following, we combine genomics, transcriptomics, proteomics and metabolomics with acute aortic coarctation in Pubmed, respectively, and summarize the biomarker findings in each panel, hoping to bring inspiration on the development of early diagnostic strategies for AAD.

3.1 Genomics and the discovery of AAD biomarkers

The risk factors for AAD contain many gene-related pathogenic mutations (61). Renard et al. (62) used the Clinical Genome Resource (ClinGen) framework to screen 11 genes from 53 candidates thought to be strongly associated with the development of hereditary thoracic aortic aneurysm and dissection (HTAAD), namely ACTA2, MYH11 [mainly involved in the smooth muscle cell contractile system (63)], MYLK, LOX and PRKG1 [aggressive in early onset (64) and associated with a reduced smooth muscle cell contractile phenotype (65)] associated with HTAAD; FBN1 associated with Marfan syndrome; COL3A1 associated with Ehlers-Danlos syndrome; and SMAD3, TGFB2, TGFBR1 and TGFBR2, which are associated with Loeys-Dietz syndrome and mainly involve components of the TGFβ signaling pathway (66). Of these, exome sequencing revealed that SMAD3 mutations cause 2% of familial thoracic aortic aneurysms and dissections (TAAD) (67). As a result of the identification of fresh missense mutations in SMAD3's evolutionarily conserved areas, Loeys-Dietz syndrome (LDS) type 3 has also been more precisely identified (68, 69). Similarly, a nonsense variant and four missense variants in the MH2 structural domain of SMAD2 (70) and a heterozygous missense variant in the MH1 structural domain of SMAD4 were detected by sequencing in patients with sporadic thoracic aortic disease and published as first reports (71), perhaps in relation to its important role in the proliferation of vascular smooth muscle cells (VSMCs), extracellular matrix maintenance and vascular remodeling related (72).

As a result, numerous modes of variation might appear when multiple susceptibility loci exist for the same gene, raising the risk of disease and making diagnosis more challenging (73). A pathogenic missense variation [c.6661T > C, p.(Cys2221Arg)] and two truncated variants [c.4786C > T, p.(Arg1596Ter)] and [c.6366C > CA, p.(Asp2123GlufsTer5)] of the FBN1 gene were found in three patients with Stanford B aortic dissection (74). Patients with truncating and splicing mutations were more likely to develop severe aortic dissection than those with

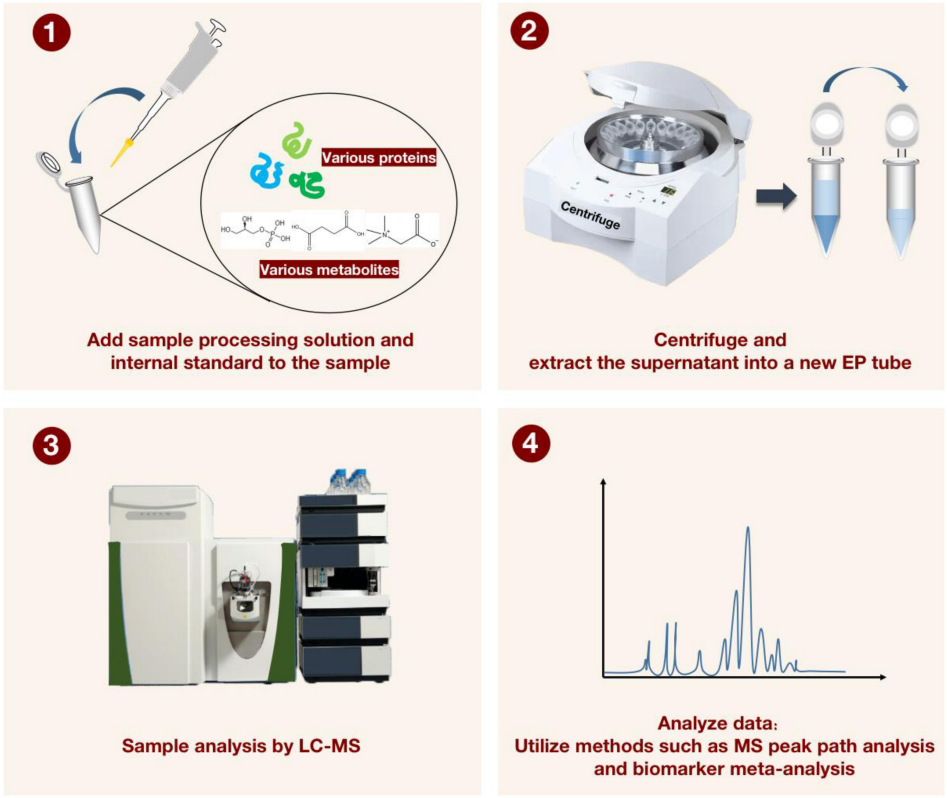

FIGURE 4
For characterizing the detection process of liquid chromatography-mass spectrometry (LC-MS) applied to proteomics and metabolomics. The sample processing solution and the internal standard solution are first added to the sample, and after vortexing and centrifugation, the supernatant is transferred to a new EP tube. The LC-MS instrument was then applied to manipulate the processed samples. Finally, MS peak path analysis and biomarker meta-analysis are performed to generate visualized data.

missense mutations, especially the shift mutations (82.76% vs. 42.86%) (75). Furthermore, there are also data showing that patients with AAD with FBN1 mutations develop the disease at a younger age than those without FBN1 mutations (76). There are many similar rare mutations in common pathogenic genes, with the identification of heterozygous rare variants c.839G > T (p.Ser280Arg) (77) and c.893T > G (p.Met298Arg) (78) missense mutations in LOX, encoding a lysyl oxidase, leading to the development of ascending aortic dissection. We also discovered 9 of 338 individuals with heterozygous uncommon LTBP3 variations in a previous study, including code-shifting variants, coding deletions, nonsense variants, and five missense replacements (79). Furthermore, mosaic variations have recently been found in NGS data from TAAD patients, while being frequently missed in routine molecular diagnosis (80).

In addition, the genetic heterogeneity of TAAD was confirmed by a study that identified multiple loci affected by rare copy number variants (CNVs) in one third of patients with early-onset TAAD (ETAAD) (81). The human genome contains many CNVs, which cover a lot more nucleotides than single nucleotide polymorphisms (SNPs) and dramatically increase the diversity of genetic variation seen in the genome. Though CNVs are challenging to find using standard NGS analysis, we found six CNVs using XHMM (an algorithm that hunts for CNVs in NGS data), including four intragenic (multiple) exon deletions in MYLK, TGFB2, SMAD3, and PRKG1 (82). And on the long arm of chromosome 10, one patient had a significant (>1,000,000 bp) CNV with 11 genes lost, including the full actin alpha 2 (ACTA2) gene (74). On the other hand, it has been discovered that 22 missense variants in ACTA2, which codes for α-smooth muscle actin (83), all increase the risk of AAD. Other genes, like the CDKN2A (cell cycle protein-dependent kinase inhibitor 2A) and CDKN2B genes on chromosome 9p21.3, which encode the senescence markers p16 and p15, have also been found to have genetic variations that have been linked to various vascular diseases and may contribute to aneurysm formation and aortic dissection (63).

Acute aortic dissections (AAD's) development and progression are also impacted by altered epigenetic control of genes. In tissue from patients with thoracic aortic dissection (TAD), analysis of cell-free DNA (cfDNA) by whole genome

bisulfite sequencing (WGBS) has revealed a number of differentially methylated regions (DMRs), with associated genes enriched in the vascular system and cardiac developmental regions. We also found that alterations in DNA methylation in TAD subsequently altered the expression of these genes. The expression levels of HOXA5, HOXB6 and HOXC6, for example, were significantly downregulated in TAD patients compared to healthy controls, with the expression levels of HOXA5 and HOXB6 significantly correlated with their methylation levels (84, 85). Moreover, Hox genes are known to play an important role not only in regulating cell proliferation, differentiation and migration, but also as regulators of phenotypic plasticity in VSMCs, which are closely associated with cardiovascular development and disease. The same enrichment of motifs involved in cellular component organization, enzyme-linked receptor protein signaling pathways (which may play a key role in the development of cardiopulmonary dysfunction), and revascularization was observed when MMP2, MMP14, and WNT2B genes were discovered in a different study. The MMP2 promoter's CpG site at position 2 was considerably more methylated in the TAD group (86). The deletion of methylation at non-CpG sites in AAD is caused by increased cell proliferation, which is linked to inflammatory vascular remodeling processes and environmental risk factors like smoking (87).

As more and more data are generated from the application of genomics to AAD, it is becoming clear that these mutated genes are often associated with pathological mechanisms of AAD pathogenesis. The risk of acute aortic events is complicated by a range of genetic variants affecting the development and remodeling of the thoracic aortic wall (88), and we also prefer to consider these pathogenic variants as genetic triggers of AAD. The likelihood of these genes being mutated to cause AAD increases when they are involved in the cell cycle (89), collagen metabolism (90), extracellular matrix maintenance (91, 92), vascular remodeling, smooth muscle cell proliferation, and the onset of hypertension (93). The occurrence of all these rare variants will need to be verified in the future by testing large samples and improving the precision of our technology. More interestingly, we discovered that carriers of pathogenic variants had significantly earlier onset of aortic dissection, higher rates of root aneurysms, lower rates of hypertension and smoking, and a higher incidence of aortic disease in family members when compared to patients without genetically pathogenic variants (94). High-throughput sequencing methods have made it possible to identify differentially expressed genes in AAD as well as in the general population. This is indicative of a variety of structural changes in the aorta that are largely genetic in origin. Gene-gene and gene-environment interactions can thus be investigated in relation to the risk of AAD by employing genetic determinants of human anatomy to comprehend cardiovascular development (95). A road map is also provided by improving the prognosis of thoracic aortic disease (96) (**Table 1**).

3.2 Transcriptomics and the discovery of AAD biomarkers

In recent years, transcriptomics has been applied to the study of AAD through the use of RNA-seq methods to identify differentially expressed genes (DEGs) between AAD patients and healthy or other disease populations, as well as bioinformatics methods like weighted gene correlation network analysis (WGCNA), GO functional annotation, KEGG pathway enrichment analysis, and regional variation analysis of genomic features. The data are then further mined, and a three-dimensional understanding of AAD begins to emerge.

The Hub gene screening method also aids in the quick identification of crucial genes, since hub genes are found at nodes in the gene network and typically play an important role in the onset of disease. The identification of crucial pathway targets can be aided by the prediction of hub genes using molecular complex assay (MCODE) and CytoHubber analysis, and the pathway's influence on disease can be more clearly determined by their knockdown or editing. Currently, many transcriptomics studies have used protein-protein interaction (PPI) networks to show the top-ranked hub genes by Cytohubber calculations, and when we statistically summarized the data, we found that the screening of hub genes did not overlap well in different datasets of different studies, which may be related to the ethnicity, type of disease, individual differences and screening conditions of the affected population. This might be related to variations in the affected population's ethnicity, disease type, individual factors, and screening conditions. Surprisingly, even though there was not much overlap between the independent genes, GO functional annotation and KEGG pathway enrichment analysis showed that these genes were primarily enriched in inflammatory cell activation, extracellular matrix degradation, endothelial cell apoptosis, vascular smooth muscle contraction, oxidative stress, adhesive plaques, protein kinase activity, adrenergic signaling, cell cycle-related, oocyte meiosis, luteinizing hormone mediated oocyte maturation and p53 signaling pathway among other related pathways (97–101).

Among them, inflammation takes place virtually constantly as AAD develops. According to earlier research, the pro-inflammatory and pro-apoptotic activity of myocardin-related transcription factor A (MRTF-A), which is induced by the hormone angiotensin II (Ang-II), aids in the development of AAD (102). FKBP11 promotes inflammation by allowing monocytes to colonize the aorta and degrade proteins (103). Activation of Janus kinase 2 (JAK2) (104, 105) and elevated plasma ANGPT2 levels (106, 107) are suggestive of upregulation of pro-inflammatory cytokines in AAD. In turn, these upregulated proinflammatory cytokines lead to activation of chemotactic and other immune cells, especially neutrophils and T cells, which can further secrete inflammatory factors and granzyme, exacerbating the medial lesion and leading to the

TABLE 1 Non-exhaustive list of biomarkers for AAD elucidated by genomics-based techniques.

Biomarker	Technology	Valuable considerations	References
ACTA2, MYH11, MYLK, LOX, PRKG1, FBN1, SMAD3, TGFB2, TGFBR1, TGFBR2, COL3A1	DNA sequencing, ClinGen framework	Some genes were found to have rare mutations in genetic loci and were considered to be closely related to HTAAD.	(62, 74, 78, 82, 83)
SMAD2, SMAD4	Genome sequencing	Rare mutations in genetic loci identified in sporadic AAD.	(70, 71)
LTBP3	WES	Rare mutations in genetic loci identified in sporadic AAD.	(79)
CDKN2A, CDKN2B	GWAS	Found to be involved in the pathogenesis of AAD and other arterial diseases.	(63)
HOXA5, HOXB6, HOXC6	WGBS	DMRs in tissues from patients with TAD, associated genes in the vasculature and Heart developing regions are enriched.	(84, 85)
MMP2, MMP14, WNT2B	Methylation microarray, Bisulfite pyrosequencing	The methylation of the second CpG site of the MMP2 promoter in the TAD group was significantly increased and an enrichment of loci involved in cellular component organization, enzyme-linked receptor protein signaling, and vascular remodeling was also observed.	(86)
USP15, SVIL	TWAS	The high expression of USP15 was associated with increased ascending aortic diameter, whereas high expression of SVIL was associated with increased diameter of the descending aorta.	(117)

development of aortic dissection (108). As for mesenchymal stem cells (MSC), because of their anti-inflammatory and repairing effects, whether they can be used in the treatment of AAD needs to be explored in more depth in the future. According to a specific study, RNA sequencing revealed that the genes CXCL1, CXCL5, HTR7, and SNAP25, which were upregulated, and EMX2, NCAM1, and IGFBP2, which were downregulated, were significantly differentially expressed in MSCs with aortic dissection. Adhesion-related signaling pathways were also significantly altered by enrichment analysis, indicating that MSCs treat AAD may involve adhesion function as well as anti-inflammatory mechanisms (109). Extracellular matrix degradation is also a significant pathogenic mechanism in AAD. Sequencing technology and genealogical co-isolation analysis identified 257 pathogenic or potentially pathogenic genes, accounting for 88.89% (64/72) of all genes encoding the collagen and matrix metalloproteinase systems, indicating that collagen loss and destruction as well as disruption of the matrix metalloproteinase system may be significant in the pathogenesis of AAD (90). In addition, LGMN (legumain), as a lysosomal cysteine protease, is mainly expressed in CD68-positive macrophages and has been shown to degrade extracellular matrix components directly or through activation of downstream signals. Besides, LGMN has also been shown to inhibit integrin αvβ3 by binding to it, reducing Rho GTPase activation, downregulating VSMC differentiation markers, and worsening the progression of thoracic aortic dissection (110).

Acute aortic dissection (AAD) has a reasonably diverse cellular landscape that is separated into immune and non-immune cells. Among them, immune cells include B cells, natural killer T cells, macrophages, dendritic cells, neutrophils, and mast cells; non-immune cells include endothelial cells, fibroblasts, and VSMC (111). With the help of single-cell RNA sequencing (scRNA-seq) technology, it is possible to understand the cellular composition of the aorta wall and the gene expression of specific cells. Major immune cell subset ratios have been observed to differ significantly between AAD and normal aorta tissues, with T cells, B cells, and natural killer (NK) cells ratios being higher in AAD tissue samples. Interestingly, macrophages were found to infiltrate only at the onset of entrapment, in contrast to the long-term infiltration of macrophages and chronic degradation of the extracellular matrix that can be observed in abdominal aortic aneurysms (AAA). At the same time, depletion of circulating monocytes significantly reduced the incidence of AAD, suggesting that macrophage infiltration in the aorta is more a cause than a consequence of AAD, suggesting that macrophage infiltration is more of a "triggering" event in AAD (108). The primary molecular traits of different cell types can also be further resolved, enabling higher resolution identification between different subtypes of the same cell to reveal functional differences. This can then lead to an in-depth study and interpretation of mechanisms that might be present in AAD, such as intercellular interactions (112). Another scRNA-seq-based investigation identified seven main DEGs (ACTA2, IL6, CTGF, BGN, ITGA8, THBS1, and CDH5) and significant alterations in the relative number of VSMCs. Additionally, we discovered that single cell trajectory analysis allowed VSMCs to differentiate into 8 distinct subtypes. And the up - regulation of genes associated with the synthetic phenotype, such as matrix metalloproteinase, inflammatory cytokines, and bone bridging protein, was also found in VSMCs (113), indicating that these cells underwent a transition from the contractile to the synthetic phenotype (111), with more abnormal proliferation and migration. The down-regulation of

integrin α9 (ITGA9) (114) and the up-regulation of tRF-1:30-chrM.Met-CAT (115) and CDK1 (98) facilitated exactly the occurrence of the VSMCs-related changes mentioned above. At the same time, morphological changes in endothelial cells in AAD patients, such as endothelial cell hyperplasia, loose cell junctions, and endothelial cell desquamation in aortic segments, suggest that endothelial cells are damaged in AAD patients, which may likewise underlie the pathogenesis of AAD (107). Interestingly, RBBP8/NOTCH1 was found to act as a linking molecule between DNA damage/repair and extracellular matrix (ECM) tissue, and we speculate that excessive DNA damage is a characteristic pathological change in sporadic aortic dissection (116), which may be associated with massive cellular damage and degeneration.

It should be noted that genes frequently express themselves in a selective manner and are influenced by environmental, temporal, and spatial factors. Awareness tissue function and pathological alterations requires an understanding of the biological positional context of gene expression. Scientists have also been working to address the problem of average transcriptome and spatial information loss in RNA-seq. The idea of spatial transcriptomics, which enables visualization and quantitative analysis of the transcriptome at spatial resolution in individual tissue sections and allows precise localization of gene expression events to particular locations in biological tissues, was only first introduced by STAHL et al. in 2016 (39). When spatial transcriptomics techniques are applied to AAD, it is possible to analyze individual genes' intra- and intercellular expression levels more thoroughly. These levels are influenced by the different anatomical regions of the aorta in which they are located (117) as well as by interactions between various cell types in the tissue microenvironment. This compensates for the lack of single-cell sequencing by enabling us to initially examine and visualize the heterogeneity of different anatomical parts of aorta and correlate cell type-specific gene expression to certain anatomical structural areas. By spatial transcriptomics, Li et al. measured differences between genes that were highly expressed in the Intima, media and adventitia of arteries, respectively (118). This finding may indicate that various cellular elements in the three aortic membranes each contribute in a unique way to the development of AAD (**Table 2**).

3.3 Proteomics and the discovery of AAD biomarkers

In proteomics research, some proteins that possess high abundance on their own are easy to detect but lack diagnostic specificity for diseases. To improve the fight against AAD in biomedical disciplines, it is crucial to apply quantitative protein technologies based on mass spectrometry and microarrays to identify and measure some low-abundance proteins that change throughout disease development (119). Future solutions to this technical issue are also anticipated, including multiplexing and targeted proteomics (120) combined with multidimensional and orthogonal separation techniques (121) to improve chromatographic resolution.

Looking around the cell, the extracellular matrix (ECM) is an insoluble structural component that makes up the matrix in the mesenchymal and epithelial capillaries and is mostly composed of collagen, elastin, proteoglycans and glycoproteins. Studies have demonstrated that ECM can impact biological processes such as cell differentiation, proliferation, adhesion, morphogenesis and phenotypic expression. An iTRAQ-based TAD proteomics study screened 36 differentially expressed proteins and validated them using western blotting for fibrillin-1, emilin-1, decorin, protein DJ-1 and histone H4. The results showed that the expression of protein DJ-1 and histone H4 was increased, while the expression of fibrillin-1, emilin-1 and decorin was decreased in TAD patients compared to controls. The results of differential proteomics screening and biological functional analysis also suggested that the major protein interaction networks involved in TAD are inflammation-interleukin 6 (IL-6) signaling, protein hydrolysis-extracellular matrix (ECM) remodeling, and cell adhesion-cell matrix interaction. These networks may be important in the pathogenesis of TAD when combined with the TGF-β signaling pathway (122). Also, by comparing aneurysmal tissue at the ascending aortic site in patients with and without Marfan syndrome (MFS), we demonstrated that microfibrillar-associated glycoprotein 4 (MFAP4) was present in high amounts in the aortic vessel wall of patients with MFS, and by 68 months of follow-up showed that type B entrapment occurred in 5 of the patients with high plasma MFAP4. At the same time, high plasma MFAP4 levels have been shown to be associated with low descending aortic dilatability, whereas the relationship between aortic dilatability in the thoracic descending aorta and type B entrapment has been previously studied (123). In addition, medial degeneration of thoracic aortic aneurysm and dissection (TAAD) is characterized by proteoglycan buildup, which is particularly damaging to the homeostasis of smooth muscle cells and predisposes to type A dissection. Aortic dissection/rupture is linked in Fbn1mgR/mgR mice to accumulation of aggregated proteoglycans and multifunctional proteoglycans in the ascending TAAD, which occurs through increased synthesis and/or impaired protein hydrolysis turnover (124). By using proteomics techniques, nine proteins, including Lumican, FGL1, PI16, MMP9, FBN1, MMP2, VWF, MMRN1, and PF4, that are linked to the pathophysiology of AAD, were also identified. Serum levels of these proteins were found to be considerably higher in AAD patients (125). Among these, Lumican, a tiny leucine-rich proteoglycan, is an essential part of the aorta wall's extracellular matrix and is crucial for cell division, migration, and differentiation as well as tissue healing. With a diagnostic sensitivity of 73.33% and a

TABLE 2 Non-exhaustive list of biomarkers for AAD elucidated by transcriptomics-based techniques.

Biomarker	Technology	Valuable considerations	References
CDC20, AURKA, RFC4, MCM4, TYMS, MCM2, DLGAP5, FANCI, BIRC5, POLE2	mRNA microarrays	qRT-PCR results showed that the expression levels of all hub genes in OA samples were significantly elevated in AAD.	(97)
SPP1, VEGFA, CCL20, GDF15, CXCL5, IGFBP3, CXCL14, HMOX1, CA9, CCL14	mRNA microarrays	CA9, CXCL5, GDF15, VEGFA, CCL20, HMOX1 and SPP1 were positively correlated with CD14 (corresponding to monocytes); CA9, CXCL5, GDF15 and VEGFA were positively correlated with CD68 (corresponding to macrophages).	(99)
CDK1, CDC20, CCNB2, CCNB1, MAD2L1, AURKA, C3AR1, NCAPG, CXCL12, ASPM	Microarray technology, MCODE, cytoHubba analyses	Inhibition of CDK1 reduces the proliferation and migration of VSMCs and protects blood vessels.	(98, 100)
RPS9, RPS18, RSRC1, DNAJC3, HBS1L, PRKCA, NCAM1, ITGB3, FTSJ3	GWAS, TWAS	Gene set enrichment analysis suggested that these hub genes mainly involved in mRNA catabolic process, focal adhesion and chemotaxis.	(101)
MRTF-A	Microarray technology	Plays a role in pro-inflammatory and pro-apoptotic processes and promotes AAD.	(102)
SLC20A1, GINS2, CNN1, FAM198B, MAD2L2, UBE2T, FKBP11, SLMAP, CCDC34, GALK1	Microarray technology, WGCNA	It has the strongest positive correlation with AAD	(103)
JAK2, PDGFA, TGFB1, VEGFA, TIMP3, TIMP4, SERPINE1	Microarray technology	Regulation of inflammatory response, growth factor activity and extracellular matrix	(104, 105)
ANGPT2	Microarray technology	ANGPT2 is significantly increased in the aortic intima of AAD patients	(107)
CXCL1, CXCL5, HTR7, SNAP25, EMX2, NCAM1, IGFBP2	RNA sequencing	Differentially expressed in mesenchymal stem cells, regulates the development of AAD	(109)
Legumain	Microarray technology	As an endogenous integrin αvβ3 modulator, Legumain promotes the development of TAD	(110)
ACTA2, IL6, CTGF, BGN, ITGA8, THBS1, CDH5	scRNA-seq	Among them, ITGA8, THBS1 and IL6 were enriched in four related signaling pathways, implying that these genes play a role in promoting metabolism, growth and angiogenesis in VSMC	(111)
ITGA9	Whole gene transcription microarrays	This gene is downregulated in AAD patients and is involved in regulating the phenotypic transition of VSMC from a contractile to a synthetic phenotype.	(114)

specificity of 98.33% for AAD, serum levels of Lumican were shown to be considerably higher in individuals with AAD in another investigation, making it a promising novel biomarker (126, 127). While the Lumican reflects aortic wall damage and repair of ECM proteins, the increased D-dimer indicates excessive fibrinolysis after AAD. The excellent specificity of Lumican for AAD and the excellent sensitivity of D-dimer can be coupled in the diagnosis of AAD, producing a better combined diagnosis with a sensitivity and specificity of 88.33% and 95% simultaneously (128). It was further demonstrated that the sensitivity and specificity could be adjusted to 79.49% and 98.46%, respectively, by combining ANGPTL8, hs-CRP, and D-dimer (126). ACAN proteoglycan was regarded as a trustworthy possible biomarker for ATAAD in plasma samples, with a sensitivity of 97% and specificity of 81% for the diagnosis of AAD, and is anticipated to be paired with additional markers (129). In the future, it is expected to be paired with additional biomarkers for combination diagnosis.

The maintenance of vascular homeostasis depends on the normal contractile function of vascular smooth muscle cells, which is closely related to cell-matrix adhesion. Cell adhesion makes up 27% of the primary biological functions of the proteins that differ in AAD, indicating that matrix remodeling and cell adhesion are significant pathophysiological mechanisms in AAD. The integrin family functions as cell adhesion molecules that mediate cell-extracellular matrix attachment. As biomarkers for the diagnosis of AAD, they include reduced expression of integrin α-3 (ITGA-3), integrin α-5 (ITGA-5) (22), and high expression of integrin α-IIb (ITGA2B), integrin α-M (ITGAM), integrin β-2 (ITGB2), and integrin β-3 (ITGB3) (130). Meanwhile, MMP-9, a key enzyme involved in the breakdown of extracellular matrix and the migration of inflammatory cells, was discovered to be enhanced by integrins in immortalized keratin-forming cells and its inhibitors were able to reduce the incidence of AAD by 40% (131). In the first 48 h after the onset of AAD, cytoskeletal proteins such vinculin have been discovered to sustain high levels, and they may play a part in early identification (132). Other cytoskeletal proteins like cofilin and LIMK are less expressed in thoracic aortic dissection than in healthy controls, which may contribute

to the weakening of the medial tissue of the thoracic aorta, increasing the diameter of the aorta and raising the risk of AAD development (133).

Similar to the enrichment findings from transcriptomic analysis, the majority of the differentially expressed proteins for proteins outside of cells showed functions primarily involved in cell migration and proliferation, inflammatory cell activation, cell contraction, oxidative stress, and muscle organ development (130). Extracellular superoxide dismutase, an enzyme involved in oxidative stress, was one of them. Its expression was more than 50% lower in AAD patient samples than in controls, and there was a rise in lipid peroxidation, both of which could point to the onset of AAD (134). Additionally, it has been discovered that many lipid-related proteins, including the carboxypeptidase N catalytic chain proteins (CPNs), complement component proteins, serum amyloid A protein (SAA), and complement component proteins, are differentially expressed in AAD (135). Circulating levels of LDL cholesterol and very low density lipoprotein (VLDL) small particles are also strongly linked to AAD (136).

Additionally, interesting biomarkers to distinguish TAD from emergency patients with significant chest pain included ITGA2, COL2A1, and MIF (137). Interestingly, a comparison of ascending aortic wall specimens from AAD, aneurysms and normal controls by differential in-gel electrophoresis (DIGE) analysis revealed that antitrypsin (A1AT) was found to be reduced in protein amounts in aortic tissue from aortic dissection compared to healthy aorta, but not in aneurysms (138). A1AT was, however, found to be considerably higher in aortic tissue samples from patients with thoracic aortic dissection and hypertension in another iTRAQ-based proteomics investigation (122). For the biological role performed by A1AT in AAD, further research and validation of this expression difference are still needed (**Table 3**).

3.4 Metabolomics and the discovery of AAD biomarkers

With the development of high performance liquid chromatography-mass spectrometry (HPLC-MS) technology, it is expanding from the field of drug metabolite analysis to the study of biological endogenous metabolites (139), allowing us to gradually study small molecule biomarkers. Peripheral blood metabolite analysis can also be utilized to help in the diagnosis of AAD because AAD changes the metabolome in the peripheral blood. Although peripheral blood testing is a rapid and less invasive technique, there is a lack of validated peripheral blood markers for AAD, especially small molecule metabolite markers (140). Large molecule proteins such smooth muscle myosin heavy chain (smMHC), creatine kinase-BB (CK-BB), D-dimer, MMPs, and elastin are the majority of the existing peripheral blood biomarkers of AAD (141, 142). Thus, it has become a research goal to discover more novel small molecule metabolic biomarkers of AAD.

Most of the entry points for the study of metabolomics were derived from the insights brought by transcriptomics and proteomics. We have discovered from earlier research that macrophages are crucial to the emergence of AAD. And because succinate triggers inflammatory changes in macrophages, Cui et al. found elevated plasma succinate concentrations in AAD patients compared to healthy controls, acute myocardial infarction (AMI) patients, and pulmonary embolism (PE) patients, leading to the idea that plasma succinate concentrations could distinguish AAD from the other three groups and the idea that succinate concentrations are regulated by p38α-CREB-OGDH axis in macrophages (143). Moreover, when macrophages undergo metabolic reprogramming, it leads to the accumulation of ferredoxin salts, which induces the activation of macrophage hypoxia-inducible factor 1-α (HIF-1α), which in turn exacerbates the development of AAD by increasing depolymerization and metallopeptidase structural domain 17 (ADAM17) triggering vascular inflammation, extracellular matrix degradation and elastic plate breakage (144). We also discovered, using multi-omics data in TAD, that elevated ceramide levels may be caused by accelerated ceramide *ab initio* production pathways in macrophages, with C18-ceramide, a key sphingolipid metabolite, being significantly different in TAD patients. Exogenous C18-ceramide is involved in the process of aortic injury by promoting smooth muscle cell contractile protein degradation, macrophage inflammation and MMP9 expression and exacerbating extracellular matrix degradation via the NLRP3-caspase 1 pathway (145, 146). Interestingly, another study found that sphingolipids (including sphingosine, phytosphingosine, sphingomyelin, and ceramide) were significantly reduced in the Stanford A AAD group but not in the Stanford B AAD group, making sphingolipids promising as potential biomarkers to differentiate Stanford A from Stanford B aortic dissection (147). Based on this study, the distinction between type A and type B dissection from a biochemical perspective is a promising finding. Also, on the basis of the theory that the descending segment of the thoracoabdominal aorta originated from the mesoderm in embryonic-based studies, whereas the aortic root and ascending aorta originated from the neural ridge, and that the different embryonic origins led to different gene expression and behavior of vascular smooth muscle cells in various regions of the aorta (88, 148). It also suggests that in the future we can pay more attention to whether the anatomical barrier of the aorta can be considered as a biological/metabolic/protein barrier and thus discover more of the different pathophysiological bases that may exist for type A and type B dissection. And the most variable lipid in AAD, lysophosphatidylcholine (LPC), is reduced in each subtype of the disease and is located at the center of the network

TABLE 3 Non-exhaustive list of biomarkers for AAD elucidated by proteomic-based techniques.

Biomarker	Technology	Valuable considerations	References
Fibrillin-1, emilin-1, decorin, protein DJ-1 and histone H4	iTRAQ technique	Their differential expression in TAD was identified by protein blotting.	(122)
MFAP4	MS	High plasma MFAP4 levels and more diverse N-glycosylation are associated with a higher incidence of type B aortic coarctation	(123)
Lumican, FGL1, PI16, MMP9, FBN1, MMP2, VWF, MMRN1, PF4	iTRAQ technique	Serum levels of FGL1, PI16 and MMP9 were significantly elevated in AAD patients.	(125)
Lumican	iTRAQ technique	The combined detection of D-dimer and Lumican has better diagnostic value for AAD.	(127)
ACAN	MS	ACAN protein concentration is enhanced in plasma of patients with acute type A aortic dissection.	(129)
ITGA-3, ITGA-5	Amine-reactive tandem mass tag (TMT) labeling, MS	the IOD of ITGA-3 and ITGA-5 in AAD patients was significantly lower than that in healthy donors.	(22)
ITGA2B, ITGAM, ITGB2, ITGB3	MS, 4D-LFQ	These proteins were significantly upregulated in the ascending aorta tissue of AAD patients.	(130)
Vinculin	label-free proteomics approach	Vinculin were found to maintain high levels within 48 h before the onset of AAD.	(132)
Cofilin, LIMK	previous proteomic research	The protein expression of cofilin and LIMK was significantly decreased in thoracic aortic dissection tissue compared with normal control.	(133)
Extracellular superoxide dismutase	MS	Its expression in AAD patient samples is more than 50% lower than that in the control group.	(134)
SAAs, complement component proteins, CPNs	iTRAQ technique	B2-GP1, CPN1, F9, LBP, SAA1, and SAA2, were validated by ELISA.	(135)
FGF6, FGF9, HGF, BCL2L1, VEGFA, ECM1, SPOCK3, IL1b, LDL-C, VLDL-C	GWAS, pQTL	Circulating levels of all these proteins are associated with AAD.	(136)
ITGA2, MIF, COL2A1	label-free quantification proteomics method	It can discriminating TAD from emergency patients with severe chest pain.	(137)
A1AT	iTRAQ technique	One study said it was decreased in AAD, while another study showed it was increased.	(122, 138)

linked to lipid changes (149). In recent years, lipidomics has emerged in multi-omics studies of AAD, and more and more biomarkers are beginning to be identified. In addition to the sphingolipids and LPC already mentioned, significant changes in lipid and polar metabolites were discovered in AAD patients by untargeted metabolomic analysis. This was followed by changes in the phosphatidylcholine metabolic pathways observed with targeted metabolomics, which further revealed significantly higher trimethylamine N-oxide (TMAO) levels and lower carnitine, choline, and betaine levels in AAD (150).

Overall, the tryptophan, histidine, glycerophospholipids, ether lipids, choline metabolism (140), and galactose metabolic pathways (151) are largely affected by the metabolites differently expressed in AAD. Among them, AFMK, glycerophosphatidylcholine and ergot sulfur were more than 50-fold elevated in peripheral blood of AAD patients compared to the healthy population (140). With reduced plasma glutamate levels and increased plasma phenylalanine levels in patients with AAD, metabolomics analysis of plasma amino acid profiles also revealed differences in amino acid levels between acute and chronic aortic dissection (152), which may point to a potential role for amino acid levels in the acute pathogenesis of aortic dissection.

In order to reverse the lethal effects of AAD, it is crucial to apply metabolomics techniques to the study of AAD pathogenesis and the identification of specific biomarkers, especially to more precisely and acutely identify changes in the levels of some transient metabolites, which, like the butterfly effect, may reveal a number of significant cascading responses that have not been focused on (**Table 4**).

4 Integration strategies for turning multiple "omics" into "multi-omics"

From each of the omics levels, gene networks associated with the AAD disease can be built using studies from the four primary fields of genomics, transcriptomics, proteomics, and

TABLE 4 Non-exhaustive list of biomarkers for AAD elucidated by metabolomics-based techniques.

Biomarker	Technology	Valuable considerations	References
Succinate	MS	Plasma succinate concentrations were elevated in AAD patients compared with healthy controls, acute myocardial infarction (AMI) patients, and pulmonary embolism (PE) patients.	(143)
C18-ceramide	UPLC-MS/MS	It is significantly increased in patients with TAD but not significantly different in patients with TAA.	(145)
Sphingolipids(including sphingosine, phytosphingosine, and ceramides)	UPLC-MS	They are significantly reduced in the Stanford type A AAD group but not in the Stanford type B AAD group.	(147)
Lysophosphatidylcholine(LPC)	HPLC-MS	Decreased in different types of AAD.	(149)
TMAO, carnitine, choline and betaine	HPLC	The level of TMAO was significantly increased, while the levels of carnitine, choline and betaine were decreased.	(150)
AFMK, glycerophosphocholine, ergothioneine	HPLC-MS	Those levels in AD patient peripheral sera that were more than 50 times higher than in normal human peripheral sera.	(140)
Histidine, Glycine, Serine, Citrate, Ornithine, Hydroxyproline, Proline, Creatine, GABA, Glutamic Acid, Cysteine, Phenylalanine	LC-MS/MS	Pairwise comparison of differences in plasma amino acid levels between acute dissection, chronic dissection, and coronary heart disease.	(152)

metabolomics. Network level overlap can then be computed. A common study strategy now involves using methods and ideas from systems biology and bioinformatics to find pathways that are enriched, identify Hub genes, and validate them (101, 153). Although separate omics approaches have made a significant contribution to our understanding of AAD, we have yet to identify integrated signaling pathways and networks. The problem of low translation rate in clinical practice continues, and the heterogeneity in sample extraction and data collecting also contributes to a significant gap between clinical and basic research. To better improve the predictive power of basic research for clinical practice, we have gradually focused our attention on more advanced data processing. The use of web-based integrated techniques is growing in popularity quickly, with advantages that go much beyond the simple association of various unfiltered datasets or differentially enriched molecules from several layers. Such integrated approaches (inclusive methods) provide insights not available from any single layer of omics data by exploring causal links between histological candidates and disease conditions/pathways using advanced analysis.

Here, we should focus on the longitudinal integration strategy (154), which is to examine multiple omics variables on the same sample. Denoising, downscaling, and normalizing the dataset beforehand can make it more standard and practical for us, and the data will be more accurate and rigorous. However, it has been a significant problem to combine and interpret numerous noisy and high-dimensional data into a single biological model, which has been a considerable challenge. Prior to analyzing multi-omics data, this necessitates not only performing dimensionality reduction operations based on feature selection or feature extraction on the dataset (155), but also having a solid grasp of the fundamentals of data integration and visualization techniques to make sure the right techniques are applied for the relevant dataset. We must take the matching of multi-omics data into account while selecting a data integration method. For single-cell sequencing, whether measurements are made on the same cells is particularly important for integrated analysis of the data (156). Also, the selection of the dataset is highly related to the main objectives of the analysis and the analysis method that the researcher envisages before collecting the data. If a satisfactory number of samples and depth of coverage cannot be achieved simultaneously, the choice of dataset should be based on the analysis objectives. If the aim is to identify differentially expressed genes between cases and controls, the power provided by more samples is usually preferable to the higher accuracy provided by a higher sequencing depth. However, if the main purpose of the analysis is to identify novel transcripts, or to examine the expression of specific alleles, the deeper the coverage, the better. On the other hand, for the selection of model species, the advantages of using animal models include reproducibility, controllability of environmental factors, availability of relevant tissues, accurate phenotypes, an almost unlimited number of exact biological replicates, and the ability to follow hypotheses experimentally. However, animal models also have limitations. Many gene-specific models are limited to one genetic background, mouse models may not encapsulate the human biology of complex diseases, and some manifestations of human disease may be difficult to test in mouse models. We can help us validate the biological relevance of the models themselves in advance by comparing the histological data between human and animal models, which requires actually specific analysis and selection based on the disease the investigator is studying (2).

In order to analyze complicated data, machine learning (ML) models are frequently utilized. These models can be broadly categorized into supervised learning and unsupervised learning. Unsupervised learning for cluster analysis learning is one of them and is based on data similarity. Five multi-omics

integration techniques—JIVE, MCCA, MCIA, MFA, and SNF—representing multivariate, tandem-based, and transformation-based approaches have been chosen to compare their capacity to combine more than two omics data in an unsupervised manner (157), providing us with a benchmark for choosing future multi-omics research techniques in the area of AAD. Deep learning (DL), a branch of machine learning, is an unsupervised learning technique based on model structural variations that enables computers to carry out an automated learning process. Due to their ability to capture non-linear and hierarchical features as well as their predictive accuracy, DL algorithms are among the most promising methods in multi-omics data processing (158). There are also studies that classify integration strategies into five categories: early integration, hybrid integration, intermediate strategies, late integration and hierarchical integration (159). They integrate datasets in different ways at different stages of data processing, and each has its own advantages and disadvantages, requiring us to make specific decisions for different datasets and research purposes. The objectives we always work toward include, however, limiting the amount of data loss and noise while lowering dataset heterogeneity, conserving the properties of unique histological datasets, and recording interactions between various histologies.

In recent years, numerous innovative and distinctive computational modeling frameworks and R programming packages (160, 161) have been created, and academics frequently choose integrated tools or platforms that mix interactive visuals with integrated analytical workflows (28). Examples include the DeepProg methodological model (162), which can explicitly model patient survival as a goal and predict the survival risk of new patients, and the DIABLO methodological model (163), which allows for module-based analysis and cross-sectional study design. It will be more convenient for non-data analysis professions like clinical researchers and will promote interdisciplinary development and collaboration.

5 Current shortcomings and future prospects

It is encouraging to see how quickly systems biology technologies are developing, and the idea of using them to treat AAD is become more and more appealing. The development of multi-omics has been aided by the big data era, and applying multi-omics technology to biomedicine is both an opportunity and a challenge. The identification of biomarkers using multi-omics data can aid in stratifying patients, improving prevention, early diagnosis, and prediction, monitoring progression, interpreting patterns and endophenotypes, and creating individualized treatment plans (158, 164).

However, the current state of AAD research demonstrates that multi-omics integration for biomarker exploration is still notably lacking. The only studies available have focused on the combined analysis of genomics and transcriptomics (101). For example, based on the fact that the increased risk of AAD rupture is mostly associated with aortic enlargement and aneurysm development, some scholars screened some potential gene targets based on the integration of genome-wide association studies (GWAS), transcriptome-wide association studies (TWAS), and rare variant analysis, and analyzed their associated cell types in combination with single-cell RAN sequencing, and identified a number of potential targets including VSMCs, fibroblasts, three different types of endothelial cells, macrophage and lymphocyte populations, and examined the precise gene expression patterns in each cell type (117). Another study combined differentially expressed genes (DEGs) of AAD and differentially methylated m6A genes from other datasets, obtained differentially expressed m6A-related genes by gene crossover results, and analyzed the relationship between these genes and immune cell infiltration. This study also explored in greater detail epigenetic mechanisms through DNA/chromatin and histone modifications, and the association with cell that brings new insights into the potential influence of externa. However, as noted in numerous studies, gene expression patterns are frequently utilized to research disease states, despite the fact that proteins are the primary functional components causing the disease. At the same time, the advent of metabolomics and macrogenomics, which integrate the impacts of food intake, utilization, and flow, represents an extra complexity of disease (165). It follows that our future focus and effort in the field of AAD research will be integrated studies combining proteomics, metabolomics, and other histological concepts. We anticipate finding more drug-targeting protein families in the future thanks to multi-omics integration approaches, which will allow us to investigate the molecular targets and potential pharmacological action mechanisms on AAD (166). The future therapy pathway for AAD will also include a critical stage involving the screening of biomarkers for acute pharmacological inhibitors, which may also serve as a model for the construction of drug resistance profiles. At the same time, we should also actively apply and integrate some of the newly emerged omics concepts in the future. For example, using the concept of radiomics to digitize image information, merge it with sequencing information and establish correlation, it may be possible to propose new molecular biology-based pathological typing for AAD based on large sample multi-omics sequencing (167).

Each of these new concepts will significantly advance our understanding of the biological networks and linkages in AAD. As a result of their strong interconnections, clusters of similar pathways naturally occur, giving us the opportunity to gather the key biological themes in each stage or layer of the disease. In particular, the resulting pathway networks could offer a global view of the various processes involved in the disease (168). This would be especially important for

a disease like AAD, which has multiple sites of pathogenesis and is very dynamic. We will be able to learn more about the pathogenic mechanisms of AAD by enhancing routes and building interaction networks. This indicates that in the future, employing multi-omics technologies for their bioinformatic analysis and validation, we can more frequently draw new inspiration and insights into AAD research from other diseases with similar pathophysiology or risk factors for its development. For instance, using microarray and bioinformatics analysis, we discovered that ALDH2 deficiency downregulates miR-31-5p, which further modifies cardiac myosin mRNA levels and attenuates abnormal VSMC phenotypic transition to achieve the impact of avoiding the formation of AAD (169). However, inactivating mutations in ALDH2 (called ALDH2*2 or rs671 mutants) are risk factors for the development and poor prognosis of atherosclerotic cardiovascular disease. By using RNA-seq, proteomics, and immunoprecipitation experiments, we later discovered and verified Rac2 as its downstream target, demonstrating the crucial function of the ALDH2-Rac2 axis in mediating cytokinesis during atherosclerosis (170). As a result, many genes are present in the body as a "double-edged sword," and even in diseases that are linked to specific mutations, they can have opposing effects. To create more dependable, scientific, and accountable healthcare decisions, it is crucial to evaluate them more thoroughly using multi-omics technology.

In addition to the above mentioned shortcomings in the application of multi-omics technologies, there is also much room for development and enhancement of the omics technologies themselves. One of them is the advent of single-cell analysis, which promises a deeper exploration in the field of proteins and allows for the quantification of more than 1000 proteins from a single mammalian cell, has the potential to advance biomedical research and provide a new degree of granularity in our understanding of biological systems. Future proteomics technologies, which have the ability to do away with the necessity for antibodies and open up paths for minimally biased research into single cell protein expression, are equally promising (171). And when it comes to operational standards, the species specificity should be carefully taken into account throughout the whole multi-omics study process (172, 173), particularly during screening and validation, as failure to do so could result in an inadequately enriched analysis of various datasets. Orthometry, machine learning, and signaling networks are being used in computational methods being actively developed to increase the translatability of omics datasets between preclinical models and humans (174). To produce findings that can be applied, technical histological expertise must be paired with fundamental biological knowledge. In the future, we anticipate being able to standardize and rigorize studies to the fullest extent possible in order to produce data with a higher signal-to-noise ratio and a more comprehensive integrated analysis. Meanwhile, massive data sharing systems like MarkerDB (58) will also accelerate this field's development. We anticipate that by addressing the aforementioned concerns, precision medicine will be able to move beyond the traditional approach of signs and symptoms and create more individualized treatment plans for patients based on diagnoses that incorporate clinical, lifestyle, genetic, and other biomarkers.

6 Conclusion

Using the idea of multi-omics integration and gathering data from all levels, we have employed and attempted to develop more advanced systems biology methodologies to investigate the underlying molecular mechanisms of AAD from surface to deeper levels. To lower the missed diagnosis rate of AAD and enhance illness prognosis, we will look into new medication treatment targets with the aim of identifying better bio-diagnostic indicators. Our initial goal in attempting to find solutions to all issues will always be to cure the condition and, ideally, in the future, improve patient quality of life.

Author contributions

XH conducted the literature review, drafted the manuscript, and prepared the figures. SC and BJ revised the manuscript. All authors have substantially contributed to the article and approved the submitted version.

Funding

This work was supported by the National Natural Science Foundation of China (grant number: 81974049).

Conflict of interest

The authors declare that the research was conducted in the absence of any commercial or financial relationships that could be construed as a potential conflict of interest.

Publisher's note

References

1. Zhou M, Varol A, Efferth T. Multi-omics approaches to improve malaria therapy. *Pharmacol Res.* (2021) 167:105570. doi: 10.1016/j.phrs.2021.105570

2. Hasin Y, Seldin M, Lusis A. Multi-omics approaches to disease. *Genome Biol.* (2017) 18:83. doi: 10.1186/s13059-017-1215-1

3. Wilkins MR, Sanchez JC, Gooley AA, Appel RD, Humphery-Smith I, Hochstrasser DF, et al. Progress with proteome projects: why all proteins expressed by a genome should be identified and how to do it. *Biotechnol Genet Eng Rev.* (1996) 13:19–50. doi: 10.1080/02648725.1996.10647923

4. Chakraborty S, Hosen MI, Ahmed M, Shekhar HU. Onco-multi-OMICS approach: a new frontier in cancer research. *Biomed Res Int.* (2018) 2018:9836256. doi: 10.1155/2018/9836256

5. Karczewski KJ, Snyder MP. Integrative omics for health and disease. *Nat Rev Genet.* (2018) 19:299–310. doi: 10.1038/nrg.2018.4

6. Yang TL, Shen H, Liu A, Dong SS, Zhang L, Deng FY, et al. A road map for understanding molecular and genetic determinants of osteoporosis. *Nat Rev Endocrinol.* (2020) 16:91–103. doi: 10.1038/s41574-019-0282-7

7. Fukushima A, Kanaya S, Nishida K. Integrated network analysis and effective tools in plant systems biology. *Front Plant Sci.* (2014) 5:598. doi: 10.3389/fpls.2014.00598

8. Dwivedi S, Purohit P, Misra R, Lingeswaran M, Vishnoi JR, Pareek P, et al. Single cell omics of breast cancer: an update on characterization and diagnosis. *Indian J Clin Biochem.* (2019) 34:3–18. doi: 10.1007/s12291-019-0811-0

9. Liu G, Dong C, Liu L. Integrated multiple "-omics" data reveal subtypes of hepatocellular carcinoma. *PLoS One.* (2016) 11:e0165457. doi: 10.1371/journal.pone.0165457

10. Xiao Y, Bi M, Guo H, Li M. Multi-omics approaches for biomarker discovery in early ovarian cancer diagnosis. *EBioMedicine.* (2022) 79:104001. doi: 10.1016/j.ebiom.2022.104001

11. Ghosh D, Bernstein JA, Khurana Hershey GK, Rothenberg ME, Mersha TB. Leveraging multilayered "omics" data for atopic dermatitis: a road map to precision medicine. *Front Immunol.* (2018) 9:2727. doi: 10.3389/fimmu.2018.02727

12. Hou X, Qu H, Zhang S, Qi X, Hakonarson H, Xia Q, et al. The multi-omics architecture of juvenile idiopathic arthritis. *Cells.* (2020) 9:2301. doi: 10.3390/cells9102301

13. Bernardes JP, Mishra N, Tran F, Bahmer T, Best L, Blase JI, et al. Longitudinal multi-omics analyses identify responses of megakaryocytes, erythroid cells, and plasmablasts as hallmarks of severe COVID-19. *Immunity.* (2020) 53:1296–314.e9. doi: 10.1016/j.immuni.2020.11.017

14. Doran S, Arif M, Lam S, Bayraktar A, Turkez H, Uhlen M, et al. Multi-omics approaches for revealing the complexity of cardiovascular disease. *Brief Bioinform.* (2021) 22:bbab061. doi: 10.1093/bib/bbab061

15. Olivier M, Asmis R, Hawkins GA, Howard TD, Cox LA. The need for multi-omics biomarker signatures in precision medicine. *Int J Mol Sci.* (2019) 20:4781. doi: 10.3390/ijms20194781

16. Aboyans V, Boukhris M. Dissecting the epidemiology of aortic dissection. *Eur Heart J Acute Cardiovasc Care.* (2021) 10:710–1. doi: 10.1093/ehjacc/zuab065

17. Zeng T, Shi L, Ji Q, Shi Y, Huang Y, Liu Y, et al. Cytokines in aortic dissection. *Clin Chim Acta* (2018) 486:177–82. doi: 10.1016/j.cca.2018.08.005

18. Tchana-Sato V, Sakalihasan N, Defraigne JO. [Aortic dissection]. *Rev Med Liege.* (2018) 73:290–5.

19. Gawinecka J, Schönrath F, von Eckardstein A. Acute aortic dissection: pathogenesis, risk factors and diagnosis. *Swiss Med Wkly.* (2017) 147:w14489. doi: 10.4414/smw.2017.14489

20. Manea MM, Dragos D, Antonescu F, Sirbu AG, Tiron AT, Dobri AM, et al. Aortic dissection: an easily missed diagnosis when pain doesn't hold the stage. *Am J Case Rep.* (2019) 20:1788–92. doi: 10.12659/AJCR.917179

21. Silaschi M, Byrne J, Wendler O. Aortic dissection: medical, interventional and surgical management. *Heart.* (2017) 103:78–87. doi: 10.1136/heartjnl-2015-308284

22. Xing L, Xue Y, Yang Y, Wu P, Wong CCL, Wang H, et al. Proteomic analysis identification of integrin alpha 3 and integrin alpha 5 as novel biomarkers in pathogenesis of acute aortic dissection. *Biomed Res Int.* (2020) 2020:1068402. doi: 10.1155/2020/1068402

23. Moore AG, Eagle KA, Bruckman D, Moon BS, Malouf JF, Fattori R, et al. Choice of computed tomography, transesophageal echocardiography, magnetic resonance imaging, and aortography in acute aortic dissection: international registry of acute aortic dissection (IRAD). *Am J Cardiol.* (2002) 89:1235–8. doi: 10.1016/s0002-9149(02)02316-0

24. Kristensen VN, Lingjærde OC, Russnes HG, Vollan HK, Frigessi A, ørresen-Dale ALB. Principles and methods of integrative genomic analyses in cancer. *Nat Rev Cancer.* (2014) 14:299–313. doi: 10.1038/nrc3721

25. Kopczynski D, Coman C, Zahedi RP, Lorenz K, Sickmann A, Ahrends R. Multi-OMICS: a critical technical perspective on integrative lipidomics approaches. *Biochim Biophys Acta Mol Cell Biol Lipids.* (2017) 1862:808–11. doi: 10.1016/j.bbalip.2017.02.003

26. Visscher PM, Brown MA, McCarthy MI, Yang J. Five years of GWAS discovery. *Am J Hum Genet.* (2012) 90:7–24. doi: 10.1016/j.ajhg.2011.11.029

27. Xing C, Huang J, Hsu YH, DeStefano AL, Heard-Costa NL, Wolf PA, et al. Evaluation of power of the illumina humanomni5M-4v1 beadchip to detect risk variants for human complex diseases. *Eur J Hum Genet.* (2016) 24:1029–34. doi: 10.1038/ejhg.2015.244

28. Chu X, Zhang B, Koeken V, Gupta MK, Li Y. Multi-omics approaches in immunological research. *Front Immunol.* (2021) 12:668045. doi: 10.3389/fimmu.2021.668045

29. McMahon A, Lewis E, Buniello A, Cerezo M, Hall P, Sollis E, et al. Sequencing-based genome-wide association studies reporting standards. *Cell Genom.* (2021) 1:100005. doi: 10.1016/j.xgen.2021.100005

30. Milewicz DM, Regalado ES, Shendure J, Nickerson DA, Guo DC. Successes and challenges of using whole exome sequencing to identify novel genes underlying an inherited predisposition for thoracic aortic aneurysms and acute aortic dissections. *Trends Cardiovasc Med.* (2014) 24:53–60. doi: 10.1016/j.tcm.2013.06.004

31. Mardis ER. Next-generation DNA sequencing methods. *Annu Rev Genomics Hum Genet.* (2008) 9:387–402.

32. Heather JM, Chain B. The sequence of sequencers: the history of sequencing DNA. *Genomics.* (2016) 107:1–8. doi: 10.1016/j.ygeno.2015.11.003

33. Wang Y, Zhao Y, Bollas A, Wang Y, Au KF. Nanopore sequencing technology, bioinformatics and applications. *Nat Biotechnol.* (2021) 39:1348–65. doi: 10.1038/s41587-021-01108-x

34. Jiang Z, Zhou X, Li R, Michal JJ, Zhang S, Dodson MV, et al. Whole transcriptome analysis with sequencing: methods, challenges and potential solutions. *Cell Mol Life Sci.* (2015) 72:3425–39.

35. Soon WW, Hariharan M, Snyder MP. High-throughput sequencing for biology and medicine. *Mol Syst Biol.* (2013) 9:640.

36. Longo SK, Guo MG, Ji AL, Khavari PA. Integrating single-cell and spatial transcriptomics to elucidate intercellular tissue dynamics. *Nat Rev Genet.* (2021) 22:627–44. doi: 10.1038/s41576-021-00370-8

37. van der Wijst MGP, Brugge H, de Vries DH, Deelen P, Swertz MA, Franke L. Single-cell RNA sequencing identifies celltype-specific cis-eQTLs and co-expression QTLs. *Nat Genet.* (2018) 50:493–7. doi: 10.1038/s41588-018-0089-9

38. Ziegenhain C, Vieth B, Parekh S, Reinius B, Guillaumet-Adkins A, Smets M, et al. Comparative analysis of single-cell RNA sequencing methods. *Mol Cell.* (2017) 65:631–43.e4.

39. Ståhl PL, Salmén F, Vickovic S, Lundmark A, Navarro JF, Magnusson J, et al. Visualization and analysis of gene expression in tissue sections by spatial transcriptomics. *Science.* (2016) 353:78–82.

40. Rao A, Barkley D, França GS, Yanai I. Exploring tissue architecture using spatial transcriptomics. *Nature.* (2021) 596:211–20. doi: 10.1038/s41586-021-03634-9

41. Baccin C, Al-Sabah J, Velten L, Helbling PM, Grünschläger F, Hernández-Malmierca P, et al. Combined single-cell and spatial transcriptomics reveal the molecular, cellular and spatial bone marrow niche organization. *Nat Cell Biol.* (2020) 22:38–48. doi: 10.1038/s41556-019-0439-6

42. Domon B, Aebersold R. Mass spectrometry and protein analysis. *Science.* (2006) 312:212–7. doi: 10.1016/s1570-0232(02)00125-3

43. Smith LM, Kelleher NL. Proteoform: a single term describing protein complexity. *Nat Methods.* (2013) 10:186–7. doi: 10.1038/nmeth.2369

44. Zhang Z, Wu S, Stenoien DL, Paša-Tolić L. High-throughput proteomics. *Annu Rev Anal Chem (Palo Alto Calif).* (2014) 7:427–54. doi: 10.1146/annurev-anchem-071213-020216

45. Butler GS, Dean RA, Morrison CJ, Overall CM. Identification of cellular MMP substrates using quantitative proteomics: isotope-coded affinity tags (ICAT)

and isobaric tags for relative and absolute quantification (iTRAQ). *Methods Mol Biol.* (2010) 622:451–70. doi: 10.1007/978-1-60327-299-5_26

46. Chen X, Wei S, Ji Y, Guo X, Yang F. Quantitative proteomics using SILAC: principles, applications, and developments. *Proteomics.* (2015) 15:3175–92.

47. Shi Y. A glimpse of structural biology through X-ray crystallography. *Cell.* (2014) 159:995–1014.

48. Breindel L, Burz DS, Shekhtman A. Interaction proteomics by using in-cell NMR spectroscopy. *J Proteomics.* (2019) 191:202–11.

49. Aslam B, Basit M, Nisar MA, Khurshid M, Rasool MH. Proteomics: technologies and their applications. *J Chromatogr Sci.* (2017) 55:182–96.

50. Altelaar AF, Munoz J, Heck AJ. Next-generation proteomics: towards an integrative view of proteome dynamics. *Nat Rev Genet.* (2013) 14:35–48. doi: 10.1038/nrg3356

51. Seger C, Salzmann L. After another decade: LC-MS/MS became routine in clinical diagnostics. *Clin Biochem.* (2020) 82:2–11. doi: 10.1016/j.clinbiochem.2020.03.004

52. Oliver SG, Winson MK, Kell DB, Baganz F. Systematic functional analysis of the yeast genome. *Trends Biotechnol.* (1998) 16:373–8. doi: 10.1016/S0167-7799(98)01214-1

53. Gertsman I, Barshop BA. Promises and pitfalls of untargeted metabolomics. *J Inherit Metab Dis.* (2018) 41:355–66.

54. Bauermeister A, Mannochio-Russo H, Costa-Lotufo LV, Jarmusch AK, Dorrestein PC. Mass spectrometry-based metabolomics in microbiome investigations. *Nat Rev Microbiol.* (2022) 20:143–60.

55. Chong J, Soufan O, Li C, Caraus I, Li S, Bourque G, et al. MetaboAnalyst 4.0: towards more transparent and integrative metabolomics analysis. *Nucleic Acids Res.* (2018) 46:W486–94. doi: 10.1093/nar/gky310

56. Vasan RS. Biomarkers of cardiovascular disease: molecular basis and practical considerations. *Circulation.* (2006) 113:2335–62.

57. Rifai N, Gillette MA, Carr SA. Protein biomarker discovery and validation: the long and uncertain path to clinical utility. *Nat Biotechnol.* (2006) 24:971–83. doi: 10.1038/nbt1235

58. Wishart DS, Bartok B, Oler E, Liang KYH, Budinski Z, Berjanskii M, et al. MarkerDB: an online database of molecular biomarkers. *Nucleic Acids Res.* (2021) 49:D1259–67. doi: 10.1093/nar/gkaa1067

59. Zhou Z, Liu Y, Zhu X, Tang X, Wang Y, Wang J, et al. Exaggerated Autophagy in stanford type A aortic dissection: a transcriptome pilot analysis of human ascending aortic tissues. *Genes.* (2020) 11:1187. doi: 10.3390/genes11101187

60. Sen I, Erben YM, Franco-Mesa C, DeMartino RR. Epidemiology of aortic dissection. *Semin Vasc Surg.* (2021) 34:10–7.

61. Gago-Díaz M, Ramos-Luis E, Zoppis S, Zorio E, Molina P, Braza-Boïls A, et al. Postmortem genetic testing should be recommended in sudden cardiac death cases due to thoracic aortic dissection. *Int J Legal Med.* (2017) 131:1211–9. doi: 10.1007/s00414-017-1583-9

62. Renard M, Francis C, Ghosh R, Scott AF, Witmer PD, Adès LC, et al. Clinical validity of genes for heritable thoracic aortic aneurysm and dissection. *J Am Coll Cardiol.* (2018) 72:605–15.

63. Grond-Ginsbach C, Pjontek R, Aksay SS, Hyhlik-Dürr A, Böckler D, Gross-Weissmann ML. Spontaneous arterial dissection: phenotype and molecular pathogenesis. *Cell Mol Life Sci.* (2010) 67:1799–815. doi: 10.1007/s00018-010-0276-z

64. Gago-Díaz M, Blanco-Verea A, Teixidó G, Huguet F, Gut M, Laurie S, et al. PRKG1 and genetic diagnosis of early-onset thoracic aortic disease. *Eur J Clin Invest.* (2016) 46:787–94. doi: 10.1111/eci.12662

65. Guo DC, Regalado E, Casteel DE, Santos-Cortez RL, Gong L, Kim JJ, et al. Recurrent gain-of-function mutation in PRKG1 causes thoracic aortic aneurysms and acute aortic dissections. *Am J Hum Genet.* (2013) 93:398–404. doi: 10.1016/j.ajhg.2013.06.019

66. Van Laer L, Dietz H, Loeys B. Loeys-Dietz syndrome. *Adv Exp Med Biol.* (2014) 802:95–105. doi: 10.1007/978-94-007-7893-1_7

67. Regalado ES, Guo DC, Villamizar C, Avidan N, Gilchrist D, McGillivray B, et al. Exome sequencing identifies SMAD3 mutations as a cause of familial thoracic aortic aneurysm and dissection with intracranial and other arterial aneurysms. *Circ Res.* (2011) 109:680–6. doi: 10.1161/CIRCRESAHA.111.248161

68. Blinc A, Maver A, Rudolf G, Tasič J, Pretnar Oblak J, Berden P, et al. Clinical exome sequencing as a novel tool for diagnosing Loeys-dietz syndrome type 3. *Eur J Vasc Endovasc Surg.* (2015) 50:816–21. doi: 10.1016/j.ejvs.2015.08.003

69. Engström K, Vánky F, Rehnberg M, Trinks C, Jonasson J, Green A, et al. Novel SMAD3 p.Arg386Thr genetic variant co-segregating with thoracic aortic aneurysm and dissection. *Mol Genet Genomic Med.* (2020) 8:e1089. doi: 10.1002/mgg3.1089

70. Cannaerts E, Kempers M, Maugeri A, Marcelis C, Gardeitchik T, Richer J, et al. Novel pathogenic SMAD2 variants in five families with arterial aneurysm and dissection: further delineation of the phenotype. *J Med Genet.* (2019) 56:220–7. doi: 10.1136/jmedgenet-2018-105304

71. Duan XY, Guo DC, Regalado ES, Shen H, Coselli JS, Estrera AL, et al. SMAD4 rare variants in individuals and families with thoracic aortic aneurysms and dissections. *Eur J Hum Genet.* (2019) 27:1054–60. doi: 10.1038/s41431-019-0357-x

72. Wang Y, Huang HY, Bian GL, Yu YS, Ye WX, Hua F, et al. of SMAD4 enhances thoracic aortic aneurysm and dissection risk through promoting smooth muscle cell apoptosis and proteoglycan degradation. *EBioMedicine.* (2017) 21:197–205. doi: 10.1016/j.ebiom.2017.06.022

73. Xu S, Li L, Fu Y, Wang X, Sun H, Wang J, et al. Increased frequency of FBN1 frameshift and nonsense mutations in Marfan syndrome patients with aortic dissection. *Mol Genet Genomic Med.* (2020) 8:e1041. doi: 10.1002/mgg3.1041

74. Erhart P, Gieldon L, Ante M, Körfer D, Strom T, Grond-Ginsbach C, et al. Acute Stanford type B aortic dissection-who benefits from genetic testing? *J Thorac Dis.* (2020) 12:6806–12. doi: 10.21037/jtd-20-2421

75. Li J, Yang L, Diao Y, Zhou L, Xin Y, Jiang L, et al. Genetic testing and clinical relevance of patients with thoracic aortic aneurysm and dissection in northwestern China. *Mol Genet Genomic Med.* (2021) 9:e1800. doi: 10.1002/mgg3.1800

76. Chen ZR, Bao MH, Wang XY, Yang YM, Huang B, Han ZL, et al. Genetic variants in Chinese patients with sporadic Stanford type A aortic dissection. *J Thorac Dis.* (2021) 13:4008–22. doi: 10.21037/jtd-20-2758

77. Guo DC, Regalado ES, Gong L, Duan X, Santos-Cortez RL, Arnaud P, et al. LOX mutations predispose to thoracic aortic aneurysms and dissections. *Circ Res.* (2016) 118:928–34.

78. Lee VS, Halabi CM, Hoffman EP, Carmichael N, Leshchiner I, Lian CG, et al. Loss of function mutation in LOX causes thoracic aortic aneurysm and dissection in humans. *Proc Natl Acad Sci U.S.A.* (2016) 113:8759–64. doi: 10.1073/pnas.1601442113

79. Guo DC, Regalado ES, Pinard A, Chen J, Lee K, Rigelsky C, et al. LTBP3 pathogenic variants predispose individuals to thoracic aortic aneurysms and dissections. *Am J Hum Genet.* (2018) 102:706–12. doi: 10.1016/j.ajhg.2018.03.002

80. Yang H, Zhu G, Zhou W, Luo M, Zhang Y, Zhang Y, et al. A systematic study of mosaicism in heritable thoracic aortic aneurysm and dissection. *Genomics.* (2022) 114:196–201. doi: 10.1016/j.ygeno.2021.12.002

81. Prakash S, Kuang SQ, Regalado E, Guo D, Milewicz D. Recurrent rare genomic copy number variants and bicuspid aortic valve are enriched in early onset thoracic aortic aneurysms and dissections. *PLoS One.* (2016) 11:e0153543. doi: 10.1371/journal.pone.0153543

82. Overwater E, Marsili L, Baars MJH, Baas AF, van deBeek I, Dulfer E, et al. Results of next-generation sequencing gene panel diagnostics including copy-number variation analysis in 810 patients suspected of heritable thoracic aortic disorders. *Hum Mutat.* (2018) 39:1173–92. doi: 10.1002/humu.23565

83. Bergeron SE, Wedemeyer EW, Lee R, Wen KK, McKane M, Pierick AR, et al. Allele-specific effects of thoracic aortic aneurysm and dissection alpha-smooth muscle actin mutations on actin function. *J Biol Chem.* (2011) 286:11356–69. doi: 10.1074/jbc.M110.203174

84. Liu P, Zhang J, Du D, Zhang D, Jin Z, Qiu W, et al. Altered DNA methylation pattern reveals epigenetic regulation of Hox genes in thoracic aortic dissection and serves as a biomarker in disease diagnosis. *Clin Epigenet.* (2021) 13:124. doi: 10.1186/s13148-021-01110-9

85. Maredia A, Guzzardi D, Aleinati M, Iqbal F, Khaira A, Madhu A, et al. Aorta-specific DNA methylation patterns in cell-free DNA from patients with bicuspid aortic valve-associated aortopathy. *Clin Epigenet.* (2021) 13:147. doi: 10.1186/s13148-021-01137-y

86. Li N, Lin H, Zhou H, Zheng D, Xu G, Shi H, et al. Efficient detection of differentially methylated regions in the genome of patients with thoracic aortic dissection and association with MMP2 hypermethylation. *Exp Ther Med.* (2020) 20:1073–81. doi: 10.3892/etm.2020.8753

87. Pan S, Lai H, Shen Y, Breeze C, Beck S, Hong T, et al. DNA methylome analysis reveals distinct epigenetic patterns of ascending aortic dissection and bicuspid aortic valve. *Cardiovasc Res.* (2017) 113:692–704. doi: 10.1093/cvr/cvx050

88. Fletcher AJ, Syed MBJ, Aitman TJ, Newby DE, Walker NL. Inherited thoracic aortic disease: new insights and translational targets. *Circulation.* (2020) 141:1570–87. doi: 10.1161/CIRCULATIONAHA.119.043756

89. Zhang X, Yang Z, Li X, Liu X, Wang X, Qiu T, et al. Bioinformatics analysis reveals cell cycle-related gene upregulation in ascending aortic tissues from murine models. *Front Genet.* (2022) 13:823769. doi: 10.3389/fgene.2022.823769

90. Li Z, Zhou C, Tan L, Chen P, Cao Y, Li C, et al. Variants of genes encoding collagens and matrix metalloproteinase system increased the risk of aortic dissection. *Sci China Life Sci.* (2017) 60:57–65. doi: 10.1007/s11427-016-0333-3

91. Chen Y, Sun Y, Li Z, Li C, Xiao L, Dai J, et al. Identificationof COL3A1 variants associated with sporadic thoracic aortic dissection: a case-control study. *Front Med.* (2021) 15:438–47. doi: 10.1007/s11684-020-0826-1

92. Guo DC, Grove ML, Prakash SK, Eriksson P, Hostetler EM, LeMaire SA, et al. Genetic variants in LRP1 and ULK4 are associated with acute aortic dissections. *Am J Hum Genet.* (2016) 99:762–9. doi: 10.1016/j.ajhg.2016.06.034

93. Chai T, Tian M, Yang X, Qiu Z, Lin X, Chen L. Association of circulating cathepsin B levels with blood pressure and aortic dilation. *Front Cardiovasc Med.* (2022) 9:762468. doi: 10.3389/fcvm.2022.762468

94. Wolford BN, Hornsby WE, Guo D, Zhou W, Lin M, Farhat L, et al. Clinical implications of identifying pathogenic variants in individuals with thoracic aortic dissection. *Circ Genom Precis Med.* (2019) 12:e002476.

95. Chang Y, Yuan Q, Jiang P, Sun L, Ma Y, Ma X. Association of gene polymorphisms in MYH11 and TGF-β signaling with the susceptibility and clinical outcomes of DeBakey type III aortic dissection. *Mamm Genome.* (2022) 33:555–63. doi: 10.1007/s00335-021-09929-6

96. Tcheandjieu C, Xiao K, Tejeda H, Lynch JA, Ruotsalainen S, Bellomo T, et al. High heritability of ascending aortic diameter and trans-ancestry prediction of thoracic aortic disease. *Nat Genet.* (2022) 54:772–82. doi: 10.1038/s41588-022-01070-7

97. Wang W, Wang T, Wang Y, Piao H, Li B, Zhu Z, et al. Integration of Gene expression profile data to verify hub genes of patients with Stanford A aortic dissection. *Biomed Res Int.* (2019) 2019:3629751. doi: 10.1155/2019/3629751

98. Wang W, Liu Q, Wang Y, Piao H, Li B, Zhu Z, et al. Verification of hub genes in the expression profile of aortic dissection. *PLoS One.* (2019) 14:e0224922. doi: 10.1371/journal.pone.0224922

99. Gao H, Sun X, Liu Y, Liang S, Zhang B, Wang L, et al. Analysis of Hub genes and the mechanism of immune infiltration in Stanford type A aortic dissection. *Front Cardiovasc Med.* (2021) 8:680065. doi: 10.3389/fcvm.2021.680065

100. Jiang T, Si L. Identification of the molecular mechanisms associated with acute type A aortic dissection through bioinformatics methods. *Braz J Med Biol Res.* (2019) 52:e8950. doi: 10.1590/1414-431X20198950

101. Zhang Y, Li L, Ma L. Integrative analysis of transcriptome-wide association study and mRNA expression profile identified candidate genes and pathways associated with aortic aneurysm and dissection. *Gene.* (2022) 808:145993. doi: 10.1016/j.gene.2021.145993

102. Ito S, Hashimoto Y, Majima R, Nakao E, Aoki H, Nishihara M, et al. MRTF-A promotes angiotensin II-induced inflammatory response and aortic dissection in mice. *PLoS One.* (2020) 15:e0229888. doi: 10.1371/journal.pone.0229888

103. Wang T, He X, Liu X, Liu Y, Zhang W, Huang Q, et al. Weighted Gene Co-expression network analysis identifies FKBP11 as a key regulator in acute aortic dissection through a NF-kB dependent pathway. *Front Physiol.* (2017) 8:1010. doi: 10.3389/fphys.2017.01010

104. Kimura N, Futamura K, Arakawa M, Okada N, Emrich F, Okamura H, et al. Gene expression profiling of acute type A aortic dissection combined with in vitro assessment. *Eur J Cardiothorac Surg.* (2017) 52:810–7. doi: 10.1093/ejcts/ezx095

105. Pan S, Wu D, Teschendorff AE, Hong T, Wang L, Qian M, et al. JAK2-centered interactome hotspot identified by an integrative network algorithm in acute Stanford type A aortic dissection. *PLoS One.* (2014) 9:e89406. doi: 10.1371/journal.pone.0089406

106. Weis-Müller BT, Modlich O, Drobinskaya I, Unay D, Huber R, Bojar H, et al. Gene expression in acute Stanford type A dissection: a comparative microarray study. *J Transl Med.* (2006) 4:29.

107. Huang B, Tian L, Chen Z, Zhang L, Su W, Lu T, et al. Angiopoietin 2 as a novel potential biomarker for acute aortic dissection. *Front Cardiovasc Med.* (2021) 8:743519. doi: 10.3389/fcvm.2021.743519

108. Liu Y, Zou L, Tang H, Li J, Liu H, Jiang X, et al. Single-cell sequencing of immune cells in human aortic dissection tissue provides insights into immune cell heterogeneity. *Front Cardiovasc Med.* (2022) 9:791875.

109. Yang J, Zou S, Liao M, Qu L. Transcriptome sequencing revealed candidate genes relevant to mesenchymal stem cells' role in aortic dissection patients. *Mol Med Rep.* (2018) 17:273–83. doi: 10.3892/mmr.2017.7851

110. Pan L, Bai P, Weng X, Liu J, Chen Y, Chen S, et al. Legumain is an endogenous modulator of integrin αvβ3 triggering vascular degeneration, dissection, and rupture. *Circulation.* (2022) 145:659–74. doi: 10.1161/CIRCULATIONAHA.121.056640

111. Xu C, Liu X, Fang X, Yu L, Lau HC, Li D, et al. Single-cell RNA sequencing reveals smooth muscle cells heterogeneity in experimental aortic dissection. *Front Genet.* (2022) 13:836593. doi: 10.3389/fgene.2022.836593

112. Chen Y, Zhang T, Yao F, Gao X, Li D, Fu S, et al. Dysregulation of interaction between LOX(high) fibroblast and smooth muscle cells contributes to the pathogenesis of aortic dissection. *Theranostics.* (2022) 12:910–28. doi: 10.7150/thno.66059

113. Shao Y, Li G, Huang S, Li Z, Qiao B, Chen D, et al. Effects of extracellular matrix softening on vascular smooth muscle cell dysfunction. *Cardiovasc Toxicol.* (2020) 20:548–56. doi: 10.1007/s12012-020-09580-8

114. Huang B, Niu Y, Chen Z, Yang Y, Wang X. Integrin α9 is involved in the pathopoiesis of acute aortic dissection via mediating phenotype switch of vascular smooth muscle cell. *Biochem Biophys Res Commun.* (2020) 533:519–25. doi: 10.1016/j.bbrc.2020.08.095

115. Fu X, He X, Yang Y, Jiang S, Wang S, Peng X, et al. Identification of transfer RNA-derived fragments and their potential roles in aortic dissection. *Genomics.* (2021) 113:3039–49. doi: 10.1016/j.ygeno.2021.06.039

116. Zhou Z, Liu Y, Gao S, Zhou M, Qi F, Ding N, et al. Excessive DNA damage mediates ECM degradation via the RBBP8/NOTCH1 pathway in sporadic aortic dissection. *Biochim Biophys Acta Mol Basis Dis.* (2022) 1868:166303. doi: 10.1016/j.bbadis.2021.166303

117. Pirruccello JP, Chaffin MD, Chou EL, Fleming SJ, Lin H, Nekoui M, et al. Deep learning enables genetic analysis of the human thoracic aorta. *Nat Genet.* (2022) 54:40–51. doi: 10.1038/s41588-021-00962-4

118. Li YH, Cao Y, Liu F, Zhao Q, Adi D, Huo Q, et al. Visualization and analysis of gene expression in Stanford type A aortic dissection tissue section by spatial transcriptomics. *Front Genet.* (2021) 12:698124. doi: 10.3389/fgene.2021.698124

119. Wu J, Wang W, Chen Z, Xu F, Zheng Y. Proteomics applications in biomarker discovery and pathogenesis for abdominal aortic aneurysm. *Expert Rev Proteomics.* (2021) 18:305–14.

120. Pappireddi N, Martin L, Wühr M. A review on quantitative multiplexed proteomics. *Chembiochem.* (2019) 20:1210–24.

121. Antberg L, Cifani P, Sandin M, Levander F, James P. Critical comparison of multidimensional separation methods for increasing protein expression coverage. *J Proteome Res.* (2012) 11:2644–52. doi: 10.1021/pr201257y

122. Zhang K, Pan X, Zheng J, Xu D, Zhang J, Sun L. Comparative tissue proteomics analysis of thoracic aortic dissection with hypertension using the iTRAQ technique. *Eur J Cardiothorac Surg.* (2015) 47:431–8. doi: 10.1093/ejcts/ezu171

123. Yin 殷晓科 X, Wanga S, Fellows AL, Barallobre-Barreiro J, Lu R, Davaapil H, et al. Glycoproteomic analysis of the aortic extracellular matrix in marfan patients. *Arterioscler Thromb Vasc Biol.* (2019) 39:1859–73. doi: 10.1161/ATVBAHA.118.312175

124. Cikach FS, Koch CD, Mead TJ, Galatioto J, Willard BB, Emerton KB, et al. Massive aggrecan and versican accumulation in thoracic aortic aneurysm and dissection. *JCI Insight.* (2018) 3:e97167. doi: 10.1172/jci.insight.97167

125. Deng T, Liu Y, Gael A, Fu X, Deng X, Liu Y, et al. Study on proteomics-based aortic dissection molecular markers using iTRAQ combined with label free techniques. *Front Physiol.* (2022) 13:862732. doi: 10.3389/fphys.2022.862732

126. Yang Y, Jiao X, Li L, Hu C, Zhang X, Pan L, et al. Increased circulating angiopoietin-like protein 8 levels are associated with thoracic aortic dissection and higher inflammatory conditions. *Cardiovasc Drugs Ther.* (2020) 34:65–77.

127. Gu G, Cheng W, Yao C, Yin J, Tong C, Rao A, et al. Quantitative proteomics analysis by isobaric tags for relative and absolute quantitation identified Lumican as a potential marker for acute aortic dissection. *J Biomed Biotechnol.* (2011) 2011:920763.

128. Xiao Z, Xue Y, Yao C, Gu G, Zhang Y, Zhang J, et al. Acute aortic dissection biomarkers identified using isobaric tags for relative and absolute quantitation. *Biomed Res Int.* (2016) 2016:6421451.

129. König KC, Lahm H, Dreßen M, Doppler SA, Eichhorn S, Beck N, et al. Aggrecan: a new biomarker for acute type A aortic dissection. *Sci Rep.* (2021) 11:10371.

130. Wang MM, Wang BZ, Adi D, Shao MH, Zhang D, Lu CF, et al. [Analysis on tissue-related biomarkers in patients with acute aortic dissection]. *Zhonghua Xin Xue Guan Bing Za Zhi.* (2021) 49:1108–16. doi: 10.3760/cma.j.cn112148-20210929-00839

131. Li X, Liu D, Zhao L, Wang L, Li Y, Cho K, et al. Targeted depletion of monocyte/macrophage suppresses aortic dissection with the spatial regulation of MMP-9 in the aorta. *Life Sci.* (2020) 254:116927. doi: 10.1016/j.lfs.2019.116927

132. Wang HQ, Yang H, Tang Q, Gong YC, Fu YH, Wan F, et al. Identification of vinculin as a potential diagnostic biomarker for acute aortic dissection using

label-free proteomics. *Biomed Res Int.* (2020) 2020:7806409. doi: 10.1155/2020/7806409

133. Tian L, Liao MF, Zhang L, Lu QS, Jing ZP. A study of the expression and interaction of Destrin, cofilin, and LIMK in Debakey I type thoracic aortic dissection tissue. *Scand J Clin Lab Invest.* (2010) 70:523–8. doi: 10.3109/00365513.2010.521572

134. Liao M, Liu Z, Bao J, Zhao Z, Hu J, Feng X, et al. A proteomic study of the aortic media in human thoracic aortic dissection: implication for oxidative stress. *J Thorac Cardiovasc Surg.* (2008) 136:65–72, 72.e1–3. doi: 10.1016/j.jtcvs.2007.11.017

135. Cheng N, Wang H, Zhang W, Wang H, Jin X, Ma X, et al. Comparative proteomic investigation of plasma reveals novel potential biomarker groups for acute aortic dissection. *Dis Markers.* (2020) 2020:4785068. doi: 10.1155/2020/4785068

136. Chai T, Tian M, Yang X, Qiu Z, Lin X, Chen L. Genome-wide identification of associations of circulating molecules with spontaneous coronary artery dissection and aortic aneurysm and dissection. *Front Cardiovasc Med.* (2022) 9:874912. doi: 10.3389/fcvm.2022.874912

137. Qiu P, Yang M, Pu H, Hou J, Chen X, Wu Z, et al. Potential clinical value of biomarker-guided emergency triage for thoracic aortic dissection. *Front Cardiovasc Med.* (2021) 8:777327. doi: 10.3389/fcvm.2021.777327

138. Schachner T, Golderer G, Sarg B, Lindner HH, Bonaros N, Mikuz G, et al. The amounts of alpha 1 antitrypsin protein are reduced in the vascular wall of the acutely dissected human ascending aorta. *Eur J Cardiothorac Surg.* (2010) 37:684–90. doi: 10.1016/j.ejcts.2009.07.025

139. Lu X, Zhao X, Bai C, Zhao C, Lu G, Xu G, et al. LC-MS-based metabonomics analysis. *J Chromatogr B Analyt Technol Biomed Life Sci.* (2008) 866:64–76. doi: 10.1016/j.jchromb.2007.10.022

140. Ren Y, Tang Q, Liu W, Tang Y, Zhu R, Li B. Serum biomarker identification by mass spectrometry in acute aortic dissection. *Cell Physiol Biochem.* (2017) 44:2147–57.

141. Suzuki T, Katoh H, Watanabe M, Kurabayashi M, Hiramori K, Hori S, et al. Novel biochemical diagnostic method for aortic dissection. Results of a prospective study using an immunoassay of smooth muscle myosin heavy chain. *Circulation.* (1996) 93:1244–9. doi: 10.1161/01.cir.93.6.1244

142. Apostolakis E, Akinosoglou K. What's new in the biochemical diagnosis of acute aortic dissection: problems and perspectives. *Med Sci Monit.* (2007) 13:Ra154–8.

143. Cui H, Chen Y, Li K, Zhan R, Zhao M, Xu Y, et al. Untargeted metabolomics identifies succinate as a biomarker and therapeutic target in aortic aneurysm and dissection. *Eur Heart J.* (2021) 42:4373–85. doi: 10.1093/eurheartj/ehab605

144. Lian G, Li X, Zhang L, Zhang Y, Sun L, Zhang X, et al. Macrophage metabolic reprogramming aggravates aortic dissection through the HIF1α-ADAM17 pathway (☆). *EBioMedicine.* (2019) 49:291–304. doi: 10.1016/j.ebiom.2019.09.041

145. Yang H, Yang F, Luo M, Chen Q, Liu X, Zhang Y, et al. Metabolomic profile reveals that ceramide metabolic disturbance plays an important role in thoracic aortic dissection. *Front Cardiovasc Med.* (2022) 9:826861. doi: 10.3389/fcvm.2022.826861

146. Doppler C, Arnhard K, Dumfarth J, Heinz K, Messner B, Stern C, et al. Metabolomic profiling of ascending thoracic aortic aneurysms and dissections - Implications for pathophysiology and biomarker discovery. *PLoS One.* (2017) 12:e0176727. doi: 10.1371/journal.pone.0176727

147. Zhou X, Wang R, Zhang T, Liu F, Zhang W, Wang G, et al. Identification of lysophosphatidylcholines and sphingolipids as potential biomarkers for acute aortic dissection via serum metabolomics. *Eur J Vasc Endovasc Surg.* (2019) 57:434–41. doi: 10.1016/j.ejvs.2018.07.004

148. Murillo H, Lane MJ, Punn R, Fleischmann D, Restrepo CS. Imaging of the aorta: embryology and anatomy. *Semin Ultrasound CT MR.* (2012) 33:169–90.

149. Huang H, Ye G, Lai SQ, Zou HX, Yuan B, Wu QC, et al. Plasma lipidomics identifies unique lipid signatures and potential biomarkers for patients with aortic dissection. *Front Cardiovasc Med.* (2021) 8:757022. doi: 10.3389/fcvm.2021.757022

150. Zeng Q, Rong Y, Li D, Wu Z, He Y, Zhang H, et al. Identification of serum biomarker in acute aortic dissection by global and targeted metabolomics. *Ann Vasc Surg.* (2020) 68:497–504.

151. Zhang K, Pan X, Zheng J, Liu Y, Sun L. The metabolic analysis in human aortic tissues of aortic dissection. *J Clin Lab Anal.* (2022) 36:e24623.

152. Wang L, Liu S, Yang W, Yu H, Zhang L, Ma P, et al. Plasma amino acid profile in patients with aortic dissection. *Sci Rep.* (2017) 7:40146.

153. Yin F, Zhang H, Guo P, Wu Y, Zhao X, Li F, et al. Comprehensive analysis of key m6A modification related genes and immune infiltrates in human aortic dissection. *Front Cardiovasc Med.* (2022) 9:831561. doi: 10.3389/fcvm.2022.831561

154. Zitnik M, Nguyen F, Wang B, Leskovec J, Goldenberg A, Hoffman MM. Machine learning for integrating data in biology and medicine: principles, practice, and opportunities. *Inf Fusion.* (2019) 50:71–91. doi: 10.1016/j.inffus.2018.09.012

155. Meng C, Zeleznik OA, Thallinger GG, Kuster B, Gholami AM, Culhane AC. Dimension reduction techniques for the integrative analysis of multi-omics data. *Brief Bioinform.* (2016) 17:628–41. doi: 10.1093/bib/bbv108

156. Miao Z, Humphreys BD, McMahon AP, Kim J. Multi-omics integration in the age of million single-cell data. *Nat Rev Nephrol.* (2021) 17:710–24. doi: 10.1038/s41581-021-00463-x

157. Tini G, Marchetti L, Priami C, Scott-Boyer MP. Multi-omics integration-a comparison of unsupervised clustering methodologies. *Brief Bioinform.* (2019) 20:1269–79.

158. Kang M, Ko E, Mersha TB. A roadmap for multi-omics data integration using deep learning. *Brief Bioinform.* (2022) 23:bbab454.

159. Picard M, Scott-Boyer MP, Bodein A, Périn O, Droit A. Integration strategies of multi-omics data for machine learning analysis. *Comput Struct Biotechnol J.* (2021) 19:3735–46.

160. Ulfenborg B. Vertical and horizontal integration of multi-omics data with miodin. *BMC Bioinformatics.* (2019) 20:649. doi: 10.1186/s12859-019-3224-4

161. Bodein A, Scott-Boyer MP, Perin O, Lê Cao KA, Droit A. timeOmics: an R package for longitudinal multi-omics data integration. *Bioinformatics.* (2021) 38:577–9. doi: 10.1093/bioinformatics/btab664

162. Poirion OB, Jing Z, Chaudhary K, Huang S, Garmire LX. DeepProg: an ensemble of deep-learning and machine-learning models for prognosis prediction using multi-omics data. *Genome Med.* (2021) 13:112.

163. Singh A, Shannon CP, Gautier B, Rohart F, Vacher M, Tebbutt SJ, et al. DIABLO: an integrative approach for identifying key molecular drivers from multi-omics assays. *Bioinformatics.* (2019) 35:3055–62.

164. Reel PS, Reel S, Pearson E, Trucco E, Jefferson E. Using machine learning approaches for multi-omics data analysis: a review. *Biotechnol Adv.* (2021) 49:107739.

165. Leon-Mimila P, Wang J, Huertas-Vazquez A. Relevance of multi-omics studies in cardiovascular diseases. *Front Cardiovasc Med.* (2019) 6:91. doi: 10.3389/fcvm.2019.00091

166. Liang Z, Zhang Y, Chen Q, Hao J, Wang H, Li Y, et al. Analysis of MCM proteins' role as a potential target of statins in patients with acute type A aortic dissection through bioinformatics. *Genes.* (2021) 12:387.

167. Gillies RJ, Kinahan PE, Hricak H. Radiomics: images are more than pictures. They are data. *Radiology.* (2016) 278:563–77.

168. Schlotter F, Halu A, Goto S, Blaser MC, Body SC, Lee LH, et al. Spatiotemporal multi-omics mapping generates a molecular atlas of the aortic valve and reveals networks driving disease. *Circulation.* (2018) 138:377–93.

169. Yang K, Ren J, Li X, Wang Z, Xue L, Cui S, et al. Prevention of aortic dissection and aneurysm via an ALDH2-mediated switch in vascular smooth muscle cell phenotype. *Eur Heart J.* (2020) 41:2442–53.

170. Zhang J, Zhao X, Guo Y, Liu Z, Wei S, Yuan Q, et al. Macrophage ALDH2 (aldehyde dehydrogenase 2) stabilizing Rac2 is required for efferocytosis internalization and reduction of atherosclerosis development. *Arterioscler Thromb Vasc Biol.* (2022) 42:700–16.

171. Vistain LF, Tay S. Single-cell proteomics. *Trends Biochem Sci.* (2021) 46:661–72. doi: 10.1016/j.tibs.2021.01.013

172. Shen H, Lu S, Dong L, Xue Y, Yao C, Tong C, et al. hsa-miR-320d and hsa-miR-582, miRNA biomarkers of aortic dissection, regulate apoptosis of vascular smooth muscle cells. *J Cardiovasc Pharmacol.* (2018) 71:275–82. doi: 10.1097/FJC.0000000000000568

173. Wineinger NE, Patki A, Meyers KJ, Broeckel U, Gu CC, Rao DC, et al. Genome-wide joint SNP and CNV analysis of aortic root diameter in African Americans: the HyperGEN study. *BMC Med Genomics.* (2011) 4:4. doi: 10.1186/1755-8794-4-4

174. Blaser MC, Kraler S, Lüscher TF, Aikawa E. Multi-omics approaches to define calcific aortic valve disease pathogenesis. *Circ Res.* (2021) 128:1371–97. doi: 10.1161/CIRCRESAHA.120.317979

frontiers | Frontiers in Cardiovascular Medicine

TYPE Original Research
PUBLISHED 10 February 2023
DOI 10.3389/fcvm.2023.1042272

OPEN ACCESS

EDITED BY
Ying Wang,
University of British Columbia,
Canada

REVIEWED BY
Ying Wang,
Mayo Clinic,
United States
Feng Xu,
University of British Columbia,
Canada

*CORRESPONDENCE
Shu-Yang Li
✉ lishuyang1990@hotmail.com
Takaki Hiwasa
✉ hiwasa_takaki@faculty.chiba-u.jp

SPECIALTY SECTION
This article was submitted to Atherosclerosis and Vascular Medicine, a section of the journal Frontiers in Cardiovascular Medicine

RECEIVED 12 September 2022
ACCEPTED 11 January 2023
PUBLISHED 10 February 2023

CITATION
Li S-Y, Yoshida Y, Kubota M, Zhang B-S, Matsutani T, Ito M, Yajima S, Yoshida K, Mine S, Machida T, Hayashi A, Takemoto M, Yokote K, Ohno M, Nishi E, Kitamura K, Kamitsukasa I, Takizawa H, Sata M, Yamagishi K, Iso H, Sawada N, Tsugane S, Iwase K, Shimada H, Iwadate Y and Hiwasa T (2023) Utility of atherosclerosis-associated serum antibodies against colony-stimulating factor 2 in predicting the onset of acute ischemic stroke and prognosis of colorectal cancer. *Front. Cardiovasc. Med.* 10:1042272. doi: 10.3389/fcvm.2023.1042272

Utility of atherosclerosis-associated serum antibodies against colony-stimulating factor 2 in predicting the onset of acute ischemic stroke and prognosis of colorectal cancer

Shu-Yang Li[1,2]*, Yoichi Yoshida[1,3], Masaaki Kubota[1,2], Bo-Shi Zhang[1], Tomoo Matsutani[1], Masaaki Ito[4], Satoshi Yajima[5], Kimihiko Yoshida[5], Seiichiro Mine[1,6,7], Toshio Machida[1,7,8], Aiko Hayashi[9], Minoru Takemoto[9,10], Koutaro Yokote[9], Mikiko Ohno[11,12], Eiichiro Nishi[11,12], Kenichiro Kitamura[13], Ikuo Kamitsukasa[14], Hirotaka Takizawa[15], Mizuki Sata[16,17], Kazumasa Yamagishi[16], Hiroyasu Iso[18], Norie Sawada[19], Shoichiro Tsugane[19], Katsuro Iwase[2], Hideaki Shimada[4,5], Yasuo Iwadate[1,3] and Takaki Hiwasa[1,2,3,4]*

[1]Department of Neurological Surgery, Graduate School of Medicine, Chiba University, Chiba, Japan, [2]Department of Biochemistry and Genetics, Graduate School of Medicine, Chiba University, Chiba, Japan, [3]Comprehensive Stroke Center, Chiba University Hospital, Chiba, Japan, [4]Department of Clinical Oncology, Toho University Graduate School of Medicine, Tokyo, Japan, [5]Department of Gastroenterological Surgery, Toho University Graduate School of Medicine, Tokyo, Japan, [6]Department of Neurological Surgery, Chiba Prefectural Sawara Hospital, Chiba, Japan, [7]Department of Neurological Surgery, Chiba Cerebral and Cardiovascular Center, Chiba, Japan, [8]Department of Neurosurgery, Eastern Chiba Medical Center, Chiba, Japan, [9]Department of Endocrinology, Hematology and Gerontology, Graduate School of Medicine, Chiba University, Chiba, Japan, [10]Department of Diabetes, Metabolism and Endocrinology, School of Medicine, International University of Health and Welfare, Chiba, Japan, [11]Department of Cardiovascular Medicine, Graduate School of Medicine, Kyoto University, Kyoto, Japan, [12]Department of Pharmacology, Shiga University of Medical Science, Otsu, Shiga, Japan, [13]Kitakurihama Takuchi Clinic, Yokosuka, Kanagawa, Japan, [14]Department of Neurology, Chiba Rosai Hospital, Chiba, Japan, [15]Port Square Kashiwado Clinic, Kashiwado Memorial Foundation, Chiba, Japan, [16]Department of Public Health Medicine, Faculty of Medicine, and Health Services Research and Development Center, University of Tsukuba, Tsukuba, Japan, [17]Department of Preventive Medicine and Public Health, Keio University School of Medicine, Tokyo, Japan, [18]Public Health, Department of Social Medicine, Osaka University Graduate School of Medicine, Suita, Japan, [19]Division of Cohort Research, National Cancer Center Institute for Cancer Control, Tokyo, Japan

Introduction: Autoantibodies against inflammatory cytokines may be used for the prevention of atherosclerosis. Preclinical studies consider colony-stimulating factor 2 (CSF2) as an essential cytokine with a causal relationship to atherosclerosis and cancer. We examined the serum anti-CSF2 antibody levels in patients with atherosclerosis or solid cancer.

Methods: We measured the serum anti-CSF2 antibody levels *via* amplified luminescent proximity homogeneous assay-linked immunosorbent assay based on the recognition of recombinant glutathione S-transferase-fused CSF2 protein or a CSF2-derived peptide as the antigen.

Results: The serum anti-CSF2 antibody (s-CSF2-Ab) levels were significantly higher in patients with acute ischemic stroke (AIS), acute myocardial infarction (AMI), diabetes mellitus (DM), and chronic kidney disease (CKD) compared with healthy donors (HDs). In addition, the s-CSF2-Ab levels were associated with intima-media thickness and hypertension. The analyzes of samples obtained from a Japan Public

Health Center-based prospective study suggested the utility of s-CSF2-Ab as a risk factor for AIS. Furthermore, the s-CSF2-Ab levels were higher in patients with esophageal, colorectal, gastric, and lung cancer than in HDs but not in those with mammary cancer. In addition, the s-CSF2-Ab levels were associated with unfavorable postoperative prognosis in colorectal cancer (CRC). In CRC, the s-CSF2-Ab levels were more closely associated with poor prognosis in patients with p53-Ab-negative CRC despite the lack of significant association of the anti-p53 antibody (p53-Ab) levels with the overall survival.

Conclusion: S-CSF2-Ab was useful for the diagnosis of atherosclerosis-related AIS, AMI, DM, and CKD and could discriminate poor prognosis, especially in p53-Ab-negative CRC.

KEYWORDS

colony-stimulating factor 2, acute ischemic stroke, colorectal cancer, antibody biomarker, atherosclerosis

1. Introduction

Cytokines, such as interleukins, tumor necrosis factor, interferons, and colony-stimulating factors, contribute to the presence and development of a variety of diseases (1, 2), including cancer (3), acute ischemic stroke (AIS; 4), and acute myocardial infarction (AMI; 5). As a cytokine, colony-stimulating factor 2 (CSF2, also known as granulocyte-macrophage colony-stimulating factor) deficiency has been reported to be associated with increased atherogenesis under hypercholesterolemic conditions in mouse models (6), and the administration of CSF2 can prevent the progression of atherosclerosis through changes in the composition of atherosclerotic lesions (7). Atherosclerosis is intimately linked to and accompanied by diabetes mellitus (DM) and chronic kidney disease (CKD) (8). Several reports have demonstrated that atherosclerosis mainly contributes to the emergence of AIS and AMI (9, 10).

Intriguingly, growing evidence supports that atherosclerosis and cancer are closely related based on the shared pathophysiology of inflammation as a disease promoter (11, 12). Furthermore, CSF2 has been shown to exert antitumor activity in gastrointestinal tract cancers, such as esophageal cancer (EC; 13), colorectal cancer (CRC) (14), and gastric cancer (GC; 15). CSF2 upregulation was associated with increased aggressiveness of various tumor types, including head and neck cancers (16), glioblastomas (17), and bladder cancer (18). The utility of widely used serum biomarkers, such as carcinoembryonic antigen (CEA) (19), carbohydrate antigen 19–9 (CA19-9) (20), and anti-p53 antibody (p53-Ab; 21–23), for the early diagnosis and prognosis prediction of gastrointestinal tract cancers is limited (24, 25). The discovery of novel biomarkers in gastrointestinal tract cancers is required for the prognostic prediction and development of targeted therapeutics.

Recent studies have reported the production of serum autoantibodies against secreted proteins (25–32). Autoantibodies produced against cytokines circulating in the peripheral blood can potentially impact their binding to target membrane receptors and the subsequent disease progression. We have previously identified autoantibodies against CSF2 in the sera of patients with acute cardiac syndrome (33). In this study, we examined the serum anti-CSF2 antibody levels in patients with AIS, AMI, DM, CKD, and cancer.

2. Materials and methods

2.1. Selection of patients and healthy donors

The sera of patients with AIS and transient ischemic attack (TIA), which were collected within 2 weeks after disease onset, were obtained from Chiba Prefectural Sawara Hospital and Chiba Rosai Hospital. The stroke subtypes were determined according to the criteria of the Trial of ORG 10172 in Acute Stroke Treatment classification system (34), and large-artery atherosclerosis and small-arterial occlusion (lacuna) were included as AIS or ischemic stroke. The sera of patients with DM and AMI were obtained from Chiba University Hospital and Kyoto University Hospital, respectively. The sera of patients with CKD were obtained from the Kumamoto cohort (35, 36). The Department of Surgery, Toho University Hospital, collected sera from patients with EC, GC, CRC, lung cancer (LC), and mammary cancer (MC; 37) between June 2010 and February 2016, and all patients were followed up until July 2018 or death. EC was analyzed in 91 cases, GC was analyzed in 57 cases and CRC was analyzed in 113 cases, of which all cases were underwent radical surgery. Patients who underwent neoadjuvant chemotherapy and had a double cancer were excluded from the study. According to the Japanese Classification of Colorectal, Appendiceal, and Anal Carcinoma, 3d English Edition (Secondary Publication; 38), the numbers of patients with colorectal cancer were as follows: five patients in stage 0, 29 in stage I, 32 in stage II, 31 in stage III, and 16 in stage IV. In addition, the sera of healthy donors (HDs) were selected from people who underwent a medical checkup at Chiba University, Port Square Kashiwado Clinic, and Chiba Prefectural Sawara Hospital. Clinicopathological characteristics and prognoses were obtained retrospectively. Individuals with no history of cancer, autoimmune disease, or cerebrovascular disease and those without any abnormalities on cranial MRI were enrolled as HDs.

Serum samples of AIS, TIA, DM, CKD, and HD were collected at the time of hospital admission. Serum samples of the cancers were collected before treatment. All serum samples were centrifuged at 3,000 g for 10 min, and the supernatants were stored at −80°C until use. To preserve sample integrity, repeated freezing/thawing of serum samples was avoided.

2.2. Clinical data

Clinical data of all patients; e.g., maximum intima-media thickness (max-IMT; 39), were the maximum values of the intima-media thickness for both left and right sides of the carotid ultrasound results performed using a high-frequency line array probe. The plaque score was computed by summing the maximum thickness (millimeters) of the plaques in each segment on both sides (40, 41). The cardio-ankle vascular index (CAVI; 42), which is independent of blood pressure, was developed using CAVI = a{(2ρ/ΔP) x ln(Ps/Pd)PWV2} + b, where Ps is the systolic blood pressure, Pd is the diastolic blood pressure, PWV is the pulse wave velocity, ΔP is Ps–Pd, ρ is blood density, and a and b are scale conversion constants. Scale conversion constants were determined to match CAVI with PWV (Hasegawa's method). All these measurements and calculations were made at the same time automatically in VaSera (Fukuda Denshi Co. LTD, Tokyo). All data were collected by Japanese clinical professionals and were written in the patient's clinical record. Data regarding the risk factors for atherosclerosis, including hypertension, diabetes, hyperlipidemia, cardiovascular disease (CVD), smoking, and alcohol usage were defined as previously described (43, 44) and the levels of serum p53 antibodies (p53-Abs; 22), serum CEA (45) and CA19-9 (46) were also evaluated as previously described. The cutoff values for serum p53-Ab, CEA, and CA19-9 levels were set at 1.3 IU/ml, 10 ng/ml, and 37.0 ng/ml, respectively.

2.3. Expression and purification of CSF2 protein

The cDNA containing the amino-terminal (first 145 amino-acid residues) of CSF2 (NM_000758.4) was inserted into the *Bam*HI/*Not*I site of pGEX-4 T-1 to obtain the pGEX-4 T-1-CSF2 plasmid (GenScript, Piscataway, NJ). The expression of the cDNA product was induced by treating pGEX-4 T-1-CSF2-transformed *Escherichia coli* BL-21 with 0.1-mM isopropyl-β-D-thiogalactoside (Wako Pure Chemicals, Osaka, Japan) for 4 h at 37°C. The cells were subsequently lysed in BugBuster Master Mix (Merck KGaA, Darmstadt, Germany). Glutathione S-transferase (GST)-tagged CSF2 protein was purified using Glutathione-Sepharose® (Cytiva, Pittsburgh, PA column chromatography according to the manufacturer's protocols, as previously described) (43, 47).

2.4. Generation of the CSF2 peptide antigen

The potential antigenic epitopes in CSF2 were predicted through the examination of the full-length CSF2 protein using an online tool[1], as previously described (48, 49). An *N*-terminal biotinylated 18-mer peptide encompassing the amino-acid residues between 77 and 94 of CSF2 was designed (33), and the synthetic peptide with a purity >95.93% was manufactured by Eurofins Genomics K.K. (Tokyo, Japan). The amino-acid sequence of the peptide, designated as bCSF2-77, is as follows: biotin-LYKQGLRGSLTKLKGPLT-COOH.

1 http://www.imtech.res.in/raghava/propred/

2.5. Western blotting

Purified GST-CSF2 and control GST proteins were electrophoresed using 11% sodium dodecyl-sulfate (SDS)–polyacrylamide gels, followed by transfer to nitrocellulose membranes (Advantec, Tokyo, Japan). The membranes were blocked with 0.1% dry milk in Tris-buffered saline [150 mM NaCl, 20 mM Tris–HCl (pH 7.6), and 0.1% Tween-20; TBS-T] and subsequently incubated with anti-GST antibodies (goat, ab6613, Abcam, Cambridgeshire, United Kingdom), anti-CSF2 antibodies (rabbit, sc-37,753, Santa Cruz Biotechnology, Dallas, TX), or HD and patient sera diluted at 1:1000. Thereafter, the membranes were washed five times with TBS-T and incubated with horseradish peroxidase-conjugated second antibodies (anti-goat IgG, anti-rabbit IgG, and antihuman IgG; Santa Cruz Biotechnology, Santa Cruz, CA) for 20 min. After washing with TBS-T five times, Immobilon Western Chemiluminescent Substrate (Merck KGaA) was added to the membranes, and luminescence was detected using LuminoGraph II (Atto, Tokyo, Japan), as previously described (30, 44, 50).

2.6. Measurement of serum anti-CSF2 and anti-bCSF2-77 peptide antibody levels

Amplified luminescence proximity homogeneous assay-linked immunosorbent assay (AlphaLISA) was employed to measure the serum anti-CSF2 antibody (s-CSF2-Ab) and serum anti-bCSF2-77-peptide antibody (s-CSF2pep-Ab) levels. The reaction mixture containing 2.5 µL of serum samples diluted at 1:100 in AlphaLISA buffer (25 mM HEPES pH 7.4, 0.1% casein, 0.5% Triton X-100, 1 mg/mL of dextran-500, and 0.05% Proclin-300) and 2.5 µL of GST or GST-CSF2 proteins (10 µg/ml) or 400 ng/mL of bCSF2-77 was incubated in 384-well white opaque OptiPlate microtiter plates (PerkinElmer, Beaconsfield, United Kingdom) at room temperature for 6–8 h. Next, 2.5 µL of anti-human immunoglobulin G (IgG)-conjugated acceptor beads (40 µg/ml) and 2.5-µL glutathione-conjugated donor beads (40 µg/ml) or 2.5 µL of streptavidin-conjugated donor beads (40 µg/ml) were added. After incubation in the dark for 7–28 days at room temperature, chemical emission was measured using an EnSpire Alpha microplate reader (PerkinElmer), as previously described (48, 51, 52). Specific reactions were calculated by subtracting the emitted alpha photon counts of the GST and buffer controls from those of the GST-CSF2 protein and the bCSF2-77 peptide, respectively.

2.7. Japan public health center cohort analysis

The longitudinal correlation between plasma s-CSF2pep-Ab levels and AIS in the Japan Public Health Center (JPHC)-based prospective study was investigated using AlphaLISA. The study nested within the JPHC cohort (53, 54) included approximately 30,000 Japanese individuals aged 40–69 years at the baseline period of 1990–1994 with stored plasma samples. The s-CSF2pep-Ab levels were measured in 202 cases who were included in the cohort between the baseline period and 2008 and in 202 controls whose sex, age (within 2 years), date of blood sampling (within 3 months), time since the last meal (within 4 h), and study location were matched with the cases. We used conditional logistic regression

model to estimate the odds ratios (ORs) with 95% confidence intervals (CIs) for estimating the risk of AIS based on s-CSF2pep-Ab levels.

2.8. Cell culture

LoVo cells, a human CRC line expressing wild-type p53 (55), and DLD1 cells, a human CRC line expressing mutant p53 (56), were cultured at 37°C in a humidified atmosphere containing 5% CO_2. LoVo cells were cultured in Ham's F-12 (Ham's F-12, NACALAI TESQUE, Inc., Kyoto, Japan) supplemented with 10% heat-inactivated fetal bovine serum (Thermo Fisher Scientific, Waltham, MA) and 100 μg/ml of kanamycin (Meiji Pharmaceutical, Kyoto, Japan). DLD1 cells were cultured in Dulbecco's Modified Eagle's Medium (NACALAI TESQUE) and supplemented with 10% fetal bovine serum and 100 μg/ml of kanamycin.

2.9. MTS assay

The effects of CSF2 and s-CSF2-Ab on the proliferation and viability of LoVo and DLD1 cells were evaluated using 3-(4,5-dimethylthiazol-2-yl)-5-(3-carboxymethoxyphenyl)-2-(4-sulfophenyl)-2H-tetrazolium (MTS, Promega, Madison, WI) assay, as previously reported (57, 58). Briefly, the cells were seeded into 96-well plates at a density of 2×10^3 cells/well. Next, rabbit anti-CSF2 antibody (10 μg/ml; Cusabio Technology, Houston, TX), CSF2 (1 μg/ml; PeproTech, Rocky Hill, NJ), or anti-CSF2 antibody (10 μg/ml) plus CSF2 (1 μg/ml) was added, and the plates were incubated for 72 h at 37°C in a humidified atmosphere containing 5% CO_2. For the MTS assay, 20 μl of the 20:1 MTS (1.9 mg/ml)-PMS (phenazine methosulfate, Promega; 44 μg/ml) dye solution (CellTiter 96 AQueous Nonradioactive Cell Proliferation Assay, Promega) was directly added to each well, and the cells were incubated for 3–4 h. The absorbance at 490 nm was measured using a microplate reader (Emax, Molecular Devices, Sunnyvale, CA), and the data were expressed as relative cell viability ratios, i.e., absorbance of each experimental group versus the drug-free control.

2.10. Luciferase reporter assay

LoVo cells (1×10^5 cells/well) seeded into 24-well plates were transfected with pCMV-p53WT plasmid (0.5 μg), a plasmid expressing wild-type p53, together with pGL3-p21-Luc (0.1 μg), a firefly luciferase reporter plasmid containing the promoter region of *p21/Cip1*, and pRL-SV40 (0.01 μg; Promega), a control *Renilla* luciferase reporter plasmid, using Lipofectamine Plus (Thermo Fisher Scientific). pCMV-p53WT was generously provided by Dr. Bert Vogelstein (Howard Hughes Medical Institute), and pGL3-p21-Luc (59) was kindly provided by Dr. Mian Wu (University of Science and Technology of China; 60). After 24 h of incubation, ultrapure water, rabbit anti-CSF2 antibody (10 μg/ml), or CSF2 (1 μg/ml) was added to each well. Two days after the transfection, firefly and *Renilla* luciferase activities were determined using the Dual-Luciferase Assay System (Promega) and a luminescence reader (Atto, Tokyo, Japan), as previously reported (49, 60). The firefly luciferase activity was normalized to the luciferase activity of the *Renilla* control plasmid.

2.11. Analysis of phosphorylated p53 levels

LoVo cells were treated with 1 μg/ml of CSF2 or 10 μg/ml of anti-CSF2 antibody for 4 h, followed by washing with phosphate-buffered saline. The cells were lysed in 2% SDS, 10% glycerol, 50-mM Tris-Cl (pH 6.8), 0.01% bromophenol blue, and 1% β-mercaptoethanol. The lysates were incubated at 100°C for 3 min, sonicated for 10 min, separated on 9% SDS–polyacrylamide gels, and transferred to nitrocellulose membranes. The following primary antibodies were used with 1:1000 dilution in TBS-T: rabbit anti-Ser-46 phospho-specific p53 antibody (sc-101,764, Santa Cruz Biotechnology), rabbit anti-Ser-392 phospho-specific p53 antibody (sc-7,997-R, Santa Cruz Biotechnology), mouse anti-Ser-315 phospho-specific p53 antibody (K0059-3, Medical & Biological Laboratories, Nagoya, Japan), rabbit anti-Thr-81 phospho-p53 antibody (2,676, Cell Signaling Technology, Danvers, MA), and rabbit anti-β-actin antibody (sc-8,432, Santa Cruz Biotechnology).

2.12. Statistical analysis

The Mann–Whitney *U* test and Student's *t*-test (two-sided) were employed to determine significant differences between the two groups, and the Kruskal–Wallis test (Mann–Whitney *U* with Bonferroni's correction applied) was employed to evaluate the differences among three or more groups. Correlations were determined using Spearman's correlation and logistic regression analyzes. All statistical analyzes were conducted using GraphPad Prism 5 (GraphPad, San Diego, CA) and the EZR software (61). Western blotting analysis was conducted using the ImageJ software (NIH, Bethesda, MD). A repeated-measured analysis of variance (ANOVA) with Tukey's *post hoc* comparisons was performed on the MTS assay results and luciferase reporter assay results. The predictive values of the putative disease markers were evaluated using receiver operating characteristic (ROC) curve analysis, and the cutoff values were set to maximize the sums of sensitivity plus specificity. Furthermore, the analyzes of patient survival were evaluated using the Kaplan–Meier method and compared using the log-rank test. All tests were two-tailed, and P values <0.05 were considered to indicate statistically significant differences.

3. Results

3.1. Presence of serum antibodies against purified proteins in patients with AIS, DM, EC, and CRC

We performed western blotting to confirm the presence of serum autoantibodies against CSF2 in the sera of patients with AIS, DM, EC, and CRC. As presented in Figure 1, the recombinant GST-CSF2 protein reacted with the commercial anti-GST and anti-CSF2 antibodies, whereas the control GST protein reacted with the anti-GST but not with the anti-CSF2 antibody. The GST-CSF2 protein was also recognized by serum IgG antibodies from patients with AIS (#07544 and #07684), DM (#22226), EC (#EC-6), and CRC (#Co-58) but not by the sera of the HD (#09101). To avoid contingency, we performed western blotting for more serum samples. The GST-CSF2 protein was also recognized by serum IgG antibodies from patients with AIS (#007303, #07344, and #07684), TIA (#02291, #07278, and #07642), DM (#22297, #22370, and #22375), EC (#EC-3, #EC-4, and #EC-6), and CRC (#Co-3, #Co-5, and #Co-12), but not by the sera of the HDs (#09101, #07547, and #07572;

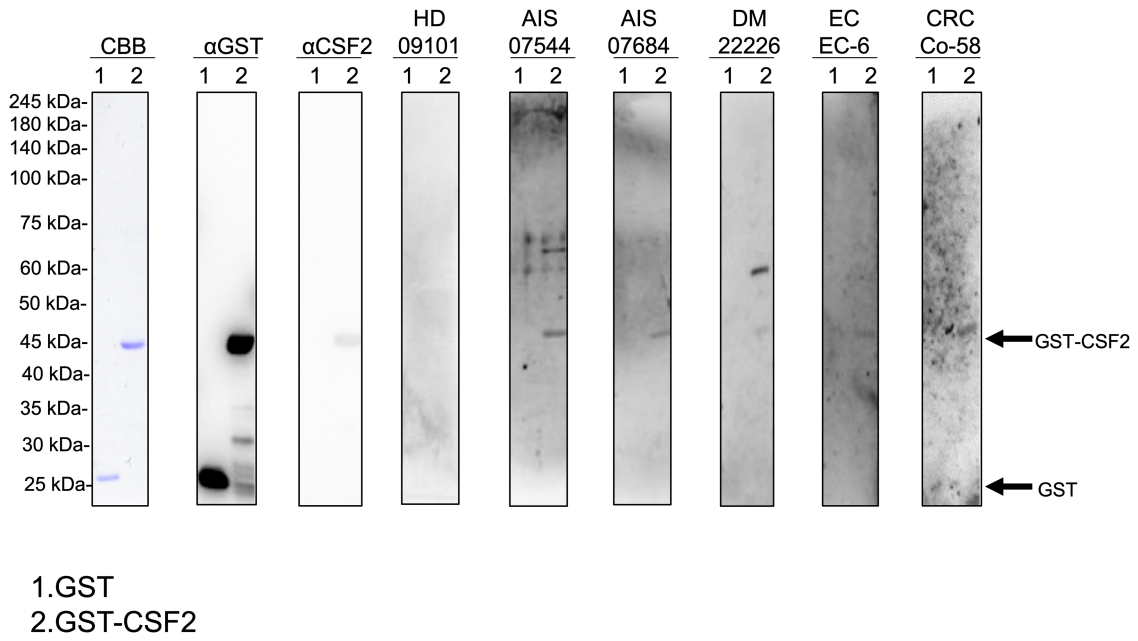

FIGURE 1
Detection of serum antibodies against CSF2. Presence of antibodies against CSF2 in the serum samples of patients with acute ischemic stroke (AIS), diabetes mellitus (DM), esophageal cancer (EC), and colorectal cancer (CRC). Purified GST-CSF2 (lane 1) and GST (lane 2) proteins were separated on sodium dodecyl sulfate–polyacrylamide gels, followed by staining with Coomassie Brilliant Blue (CBB) or western blotting using anti-GST (αGST), anti-CSF2 (αCSF2), and serum samples from patients with AIS (07544, 07684), DM (22226), EC (EC-6), and CRC (Co-58) and from a healthy donor (HD)(09101). The full, non-adjusted image of Figure 1 is shown in the Supplementary Figure S1. Molecular weights are presented in the left lane. Arrows indicate the positions of GST-CSF2 (44.6kDa) and GST (26kDa). CSF2, colony-stimulating factor 2.

Supplementary Figure S2). And the GST protein alone did not demonstrate observable reactivity with any of these serum samples (data not shown).

3.2. The s-CSF2-Ab and s-CSF2pep-Ab levels are elevated In patients with AIS and TIA

Next, we examined the s-CSF2-Ab levels in HDs and patients with AIS and TIA using AlphaLISA. As presented in Figure 2A, the s-CSF2-Ab levels were significantly higher in patients with AIS than in HDs (Figure 2A). Similarly, the s-CSF2pep-Ab levels were significantly higher in patients with AIS and TIA than in HDs (Figure 2B). Based on the cutoff s-CSF2-Ab level, defined as two standard deviations (SDs) above the average s-CSF2-Ab level in HDs, the s-CSF2-Ab positivity rates were 5.5% in HDs and 12.2% in patients with AIS (Table 1). Using the same approach to define the cutoff s-CSF2pep-Ab level, the rates of s-CSF2pep-Ab positivity were 5.6, 18.1, and 10.9% in HDs and in patients with AIS and TIA, respectively. Furthermore, the ROC analysis revealed that the areas under the curve (AUCs) for s-CSF2-Ab vs. AIS, s-CSF2pep-Ab vs. AIS, and s-CSF2pep-Ab vs. TIA were 0.576, 0.658, and 0.647, respectively (Figures 2C–E), suggesting that the s-CSF2pep-Ab level was more closely associated with AIS than the s-CSF2-Ab level.

3.3. The s-CSF2-Ab and s-CSF2pep-Ab levels are elevated in patients with AMI and DM

Next, we measured the s-CSF2-Ab and s-CSF2pep-Ab levels in patients with AMI and DM. The average (±SD) ages of HDs and patients with AMI and DM were 58.29 ± 5.63, 58.20 ± 8.50, and 58.48 ± 9.17 years, respectively (Table 2). The s-CSF2-Ab and s-CSF2pep-Ab levels were significantly higher in patients with AMI and DM than in HDs (Figures 3A,B). Based on the cutoff s-CSF2-Ab and s-CSF2pep-Ab levels, defined as two SDs above the average levels in HDs, the rates of s-CSF2-Ab and s-CSF2pep-Ab positivity were 2.3 and 1.6% in HDs, 10.2 and 11.7% in patients with AMI, and 13.3 and 10.2% in patients with DM, respectively (Table 2). The ROC analysis revealed that the AUCs for s-CSF2-Ab were 0.650 and 0.638 for AMI and DM, respectively. Similarly, the ROC analysis revealed that the AUCs for s-CSF2pep-Ab were 0.785 and 0.740 for AMI and DM, respectively. The higher AUCs for both s-CSF2-Ab and s-CSF2pep-Ab in AMI and DM than in AIS and TIA (Figures 3D–G) suggested that s-CSF2-Ab and s-CSF2pep-Ab might be more closely associated with AMI and DM than with AIS and TIA.

The patients with DM, who were followed up for 100 months after serum collection, were categorized into positive and negative groups based on the cutoff s-CSF2-Ab and s-CSF2pep-Ab levels determined using the ROC analysis (Figures 3E,G). Albeit not correlated with age, sex, obesity, and the onset of cerebrovascular events or cancer, the s-CSF2pep-Ab positivity was significantly correlated with the onset of cardiovascular events (Supplementary Table S1). Furthermore, both the s-CSF2-Ab-and s-CSF2pep-Ab-positive groups had poor DM prognosis compared with the antibody-negative groups ($P = 0.019$ and $P = 0.034$, respectively; Figures 3C,H). Importantly, the difference in the overall survival between the antibody-positive and antibody-negative groups was most striking after 80 months.

3.4. Association of the s-CSF2-Ab and s-CSF2pep-Ab levels with CKD

We also examined the s-CSF2-Ab and s-CSF2pep-Ab levels in the sera of 82 HDs and 300 patients with CKD, including 145 patients with

10.3389/fcvm.2023.1042272

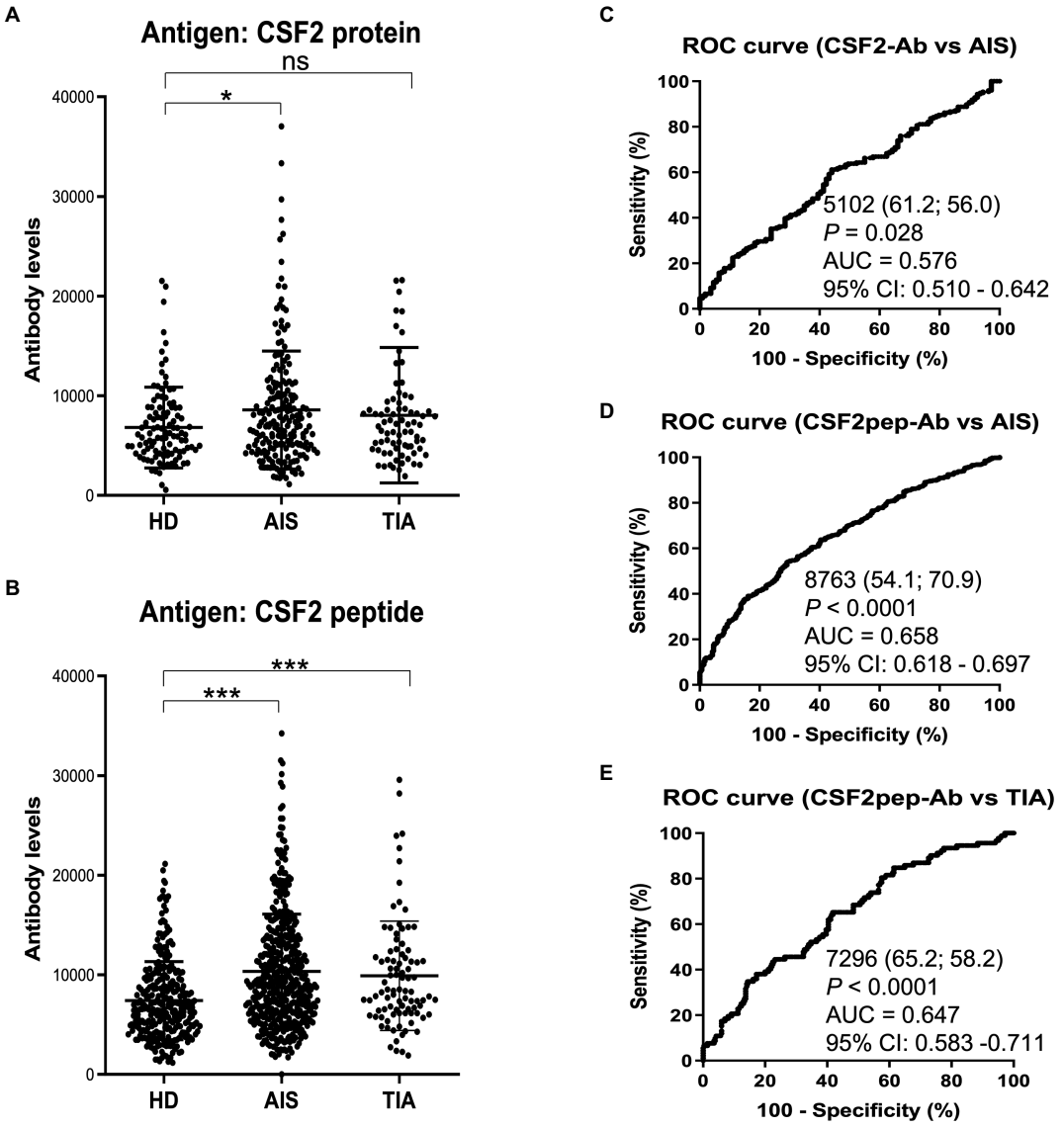

FIGURE 2
Comparison of the s-CSF2-Ab and s-CSF2pep-Ab levels in patients with AIS and TIA and in HDs. **(A–B)** Levels of serum antibodies against **(A)** s-CSF2-Ab and **(B)** s-CSF2pep-Ab determined using amplified luminescence proximity homogeneous assay-linked immunosorbent assay (AlphaLISA), calculated by subtracting the levels of antibodies against the control GST. Scatter dot plots of the s-CSF2-Ab and s-CSF2pep-Ab levels are also presented. Bars represent averages ± standard deviation (SD). $^{**}P<0.05$; $^{*}P<0.01$; ns, not significant, Kruskal–Wallis test. **(C–E)** A receiver operating characteristic (ROC) curve analysis was conducted to assess the ability of s-CSF2-Ab to detect AIS **(C)** and that of s-CSF2pep-Ab to detect AIS **(D)** and TIA **(E)**. The numbers indicate the cutoff values for the indicated markers, and the numbers in parentheses indicate sensitivity (left) and specificity (right). The areas under the ROC curve (AUC) and 95% confidence intervals (CIs) are also shown. AIS, acute ischemic stroke; HD, healthy donor; CSF2-Ab, CSF2 antibody; CSF2pep-Ab, CSF2 peptide antibody; TIA, transient ischemic attack.

diabetic kidney disease (CKD type 1), 32 patients with nephrosclerosis (CKD type 2), and 123 patients with glomerulonephritis (CKD type 3). The s-CSF2-Ab and s-CSF2pep-Ab levels were significantly higher in patients with CKD types 1, 2, and 3 than in HDs (Figures 4A,B). Based on the cutoff antibody levels, defined as two SDs above the average levels in HDs, the s-CSF2-Ab positivity rates were 4.8, 22.1, 28.1, and 22%, and the s-CSF2pep-Ab positivity rates were 1.2, 18.6, 21.9, and 14.6% in HDs and patients with CKD types 1, 2, and 3, respectively (Table 3). The ROC analysis revealed that the AUCs for s-CSF2-Ab were 0.644, 0.683, and 0.593 (Figures 4C–E), and the AUCs for s-CSF2pep-Ab were 0.657, 0.669, and 0.631 (Figures 4F–H) in patients with CKD types 1, 2, and 3, respectively. The AUC for the s-CSF2-Ab level was higher in patients with CKD type 2 than in those with CKD type 1.

3.5. Correlation analysis

We conducted a comparative analysis of the s-CSF2-Ab levels and participant characteristics in a cohort of 384 participants from Chiba Prefectural Sawara Hospital, including 196 patients with AIS, 79 patients with TIA, and 109 HDs. The baseline characteristics of the cohort are summarized in Supplementary Table S2. The Mann–Whitney *U* test was employed to compare the s-CSF2-Ab levels between males and females;

TABLE 1 Comparison of the s-CSF2-Ab and s-CSF2pep-Ab levels in HDs versus those in patients with AIS and TIA.

Sample information		HD	AIS	TIA
Total sample number		109	196	79
Male/Female		62/47	122/74	46/33
Age (Average ± SD)		59.82 ± 7.90	75.13 ± 7.28	70.67 ± 12.75
		s-CSF2-Ab	s-CSF2pep-Ab	
HD	Average	5,944	7,406	
	SD	4,315	3,929	
	Cutoff values	14,575	15,264	
	Total number	109	285	
	Positive number	6	16	
	Positive (%)	5.5%	5.6%	
AIS	Average	7,753	10,334	
	SD	6,299	5,764	
	Total number	196	464	
	Positive number	24	84	
	Positive (%)	**12.2%**	**18.1%**	
	P value (*vs* HD)	**<0.05**	**<0.0001**	
TIA	Average	6,980	9,903	
	SD	7,680	5,477	
	Total number	79	92	
	Positive number	7	10	
	Positive (%)	8.9%	**10.9%**	
	P value (*vs* HD)	ns	**<0.0001**	

The upper panel indicates the number of total samples, samples from male and female participants, and ages [average ± standard deviation (SD)]. The lower panel summarizes the serum antibody levels examined by amplified luminescence proximity homogeneous assay-linked immunosorbent assay (AlphaLISA). Purified CSF2-GST proteins and CSF2 peptides were used as antigens. The cutoff values were determined as the average HD values plus two SDs, and positive samples for which the Alpha counts exceeded the cutoff value were scored. *P* values were calculated using the Kruskal–Wallis test (Mann–Whitney U test with Bonferroni's correction applied). *P* values lower than 0.05 and positive rates higher than 10% are marked in bold. These data are plotted and shown in Figures 2A,B. CSF2, colony-stimulating factor 2; s-CSF2-Abs, the serum anti-CSF2 antibodies; s-CSF2pep-Abs, the serum anti-CSF2 peptide antibodies; HDs, healthy donors; AIS, acute ischemic stroke; TIA, transient ischemic attack.

obese or not (body mass index, < or ≥ 25 kg/m^2); those with (+) or without (−) another disease including DM, hypertension, CVD, and dyslipidemia; and those with or without smoking and alcohol intake habits. Significantly higher s-CSF2-Ab levels were observed in patients with hypertension than in those without hypertension ($P = 0.020$; Table 4). Contrarily, the s-CSF2-Ab levels were inversely associated with dyslipidemia ($P = 0.027$) possibly because the patients but not the HDs were taking cholesterol-lowering drugs, such as statins. However, s-CSF2-Ab showed lower levels in participants with CVD, probably because only 15 positive cases with CVD complications were compared with 369 negative cases with CVD complications ($P = 0.976$).

Furthermore, Spearman's rank-order correlation analysis was conducted to determine the correlation between the serum antibody levels and participant characteristics, including general information (e.g., age, body height, weight, body mass index, and degree of artery stenosis) and blood tests (sodium, chloride, white and red blood cell counts, hematocrit, etc.). The s-CSF2-Ab levels were significantly correlated with age, blood pressure (BP), smoking duration, and max-IMT (Table 5). However, the s-CSF2-Ab levels were inversely correlated with the levels of total cholesterol, cholinesterase, and albumin. The observed correlation with max-IMT suggested that s-CSF2-Ab levels were associated with early atherosclerosis prior to stenosis (62–64).

Spearman's rank-order correlation analysis of the CKD cohort consisting of 300 participants also revealed a significant correlation with plaque score, max-IMT, and cardio-ankle vascular index (left and right; Supplementary Table S3), which reflect the degree of atherosclerosis (65). Furthermore, C-reactive protein was associated with the s-CSF2-Ab levels in the CKD cohort, supporting the role of s-CSF2-Ab in inflammation in CKD.

Logistic regression analysis was conducted to determine the predictors of AIS in the Chiba Prefectural Sawara Hospital cohort (Supplementary Table S2). The univariate logistic regression analysis revealed that elevated s-CSF2-Ab levels were associated with increased risk of AIS ($P < 0.0001$). Moreover, the multivariate logistic regression analysis demonstrated that age, hypertension, and s-CSF2-Ab level were independent predictors of AIS (Supplementary Table S4).

3.6. Japan public health center cohort analysis

To determine whether s-CSF2pep-Ab can be used as a marker to predict the onset of AIS, we examined the JPHC cohort samples, which were obtained as previously described (30). The s-CSF2pep-Ab levels were strongly associated with the risk of AIS. The ORs (95% CI) were 1.72 (0.91–3.24), 2.47 (1.31–4.65), and 3.03 (1.58–5.80) for the samples with the second, third, and fourth quartiles of the s-CSF2pep-Ab levels, respectively, compared with the first quartile (Table 6). Consistently, the s-CSF2pep-Ab levels were significantly higher in patients with TIA (Figure 2E), which can be a prodromal stage of AIS (66), compared with HDs. These results indicated that s-CSF2pep-Ab might be a useful marker in predicting the onset of AIS.

3.7. Elevated s-CSF2-Ab levels in patients with cancer

Based on previous reports suggesting that CSF2 could inhibit the development of cancer (13–15, 67), we further investigated the serum samples from patients with EC, CRC, GC, LC, and MC. The s-CSF2-Ab levels were significantly higher in patients with EC, CRC, GC, and LC, but not in those with MC, compared with HDs (Figure 5; Table 7). The highest rates of s-CSF2-Ab positivity were observed in patients with EC and CRC (Table 7). The AUCs for s-CSF2-Ab were 0.816 and 0.714 versus EC and CRC, respectively (Figures 5B,D), which were much higher than versus AIS (0.576), AMI (0.650), DM (0.638), type-1 CKD (0.644), type-2 CKD (0.683), type-3 CKD (0.593), GC (0.659), and LC

TABLE 2 Comparing the s-CSF2-Ab and s-CSF2pep-Ab levels between HDs and patients with AMI or DM.

Sample information		HD	AMI	DM
Total sample number		128	128	128
Male/Female		72/56	105/23	72/56
Age (Average ± SD)		58.29 ± 5.63	58.20 ± 8.50	58.48 ± 9.17
		s-CSF2-Ab	s-CSF2pep-Ab	
HD	Average	27,010	3,006	
	SD	19,725	2,234	
	Cutoff values	66,460	7,474	
	Total number	128	128	
	Positive number	3	2	
	Positive (%)	2.3%	1.6%	
AMI	Average	37,075	4,979	
	SD	22,495	2,503	
	Total number	128	128	
	Positive number	13	15	
	Positive (%)	**10.2%**	**11.7%**	
	P value (*vs* HD)	**<0.0001**	**<0.0001**	
DM	Average	40,329	4,851	
	SD	36,680	4,096	
	Total number	128	128	
	Positive number	17	13	
	Positive (%)	**13.3%**	**10.2%**	
	P value (*vs* HD)	**<0.0001**	**<0.0001**	

The upper panel indicates the number of total samples, samples from male and female participants, and ages (average ± SD). The lower panel summarizes the s-CSF2-Ab and s-CSF2pep-Ab levels examined using AlphaLISA. Numbers are as shown in Table 1; *P* values of <0.05 and positive rates of >10% are marked in bold font. The plots for these data are shown in Figures 3A,B. AMI, acute myocardial infarction; DM, diabetes mellitus.

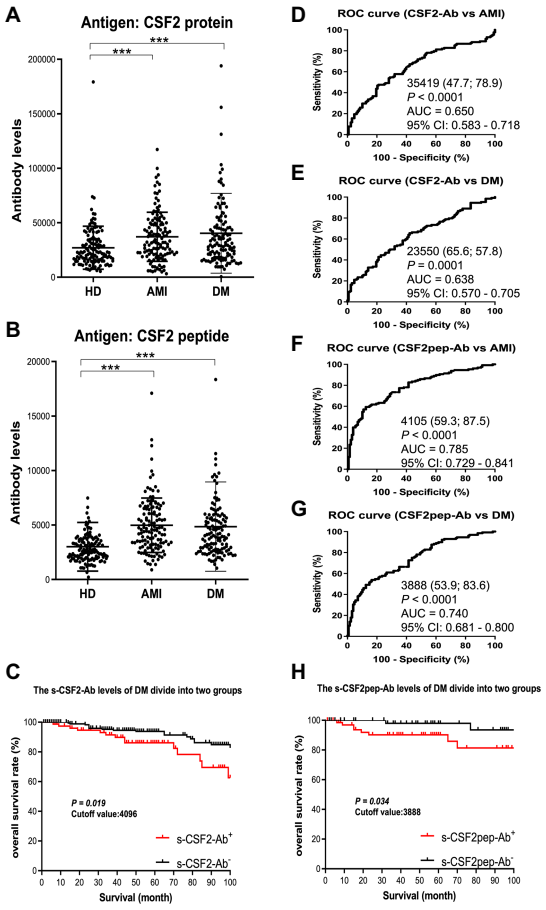

FIGURE 3
Comparison of the s-CSF2-Ab and s-CSF2pep-Ab levels between HDs and patients with AMI and DM. (**A,B**) The levels of s-CSF2-Ab and s-CSF2pep-Ab in HDs and patients with acute myocardial infarction (AMI) (**A**) and diabetes mellitus (DM) (**B**) were determined using AlphaLISA. The bars represent averages±SD. *** *P*<0.001, Mann–Whitney *U* test. (**D,E**) The ROC curves to assess the ability of s-CSF2-Ab to predict AMI and DM are presented in (**D**) and (**E**), respectively. (**F,G**) The ability of s-CSF2pep-Ab to predict AMI (**E**) and DM (**F**) was also evaluated *via* ROC analysis. Comparison of the overall survival in patients with DM between the s-CSF2-Ab positive (s-CSF2-Ab$^+$) and s-CSF2-Ab negative (s-CSF2-Ab$^-$) groups (*P*=0.019; **C**) and between the s-CSF2pep-Ab positive (s-CSF2-Ab$^+$) and s-CSF2pep-Ab negative (s-CSF2-Ab$^-$) groups (*P*=0.034; **C**). Statistical analyzes were performed by the Log-Rank test between two groups.

(0.636; Figures 2C, 3D,E, 4C–E, 5B–E). This may indicate that s-CSF2-Ab levels are more closely associated with EC and CRC compared to others.

The patients with CRC were divided into the positive and negative groups based on the cutoff s-CSF2-Ab levels determined using the ROC analysis (Figure 5D) to evaluate the association of the s-CSF2-Ab levels with postoperative survival and all of whom underwent radical surgery. The overall survival was significantly different between the s-CSF2-Ab-positive and s-CSF2-Ab-negative patients with CRC (*P*=0.011; Figure 6A). Moreover, we analyzed the correlation between s-CSF2-Ab and the age or the stage in patients with CRC. The result revealed that the s-CSF2-Ab was independent of the age or the stage (Supplementary Table S5). The comparison of the overall survival in patients with CRC categorized according to serum p53-Ab positivity (i.e., serum p53-Ab ≥1.3 IU/ml) did not reveal a significant difference (*P*=0.952; Figure 6B).

The correlation analysis of patients with CRC indicated that the s-CSF2-Ab levels were associated with the serum p53-Ab level (*P*=0.039) but not with the serum CEA or CA19-9 levels (Table 8), suggesting a degree of functional relevance between the serum CSF2 and p53 levels. Next, we categorized the patients with CRC into p53-Ab-positive and p53-Ab-negative populations. Within the p53-Ab-negative group, the prognosis of the s-CSF2-Ab-positive patients was significantly worse than that of the s-CSF2-Ab-negative patients (*P*=0.004), which was not observed within the p53-Ab-positive group (Figures 6C,D). Serum p53-Ab-negative cancers may be maintaining functional wild-type p53; therefore, these results raised the possibility that s-CSF2-Ab and CSF2 could influence the development of CRC *via* wild-type p53. Of note, the overall survival based on the s-CSF2-Ab levels did not

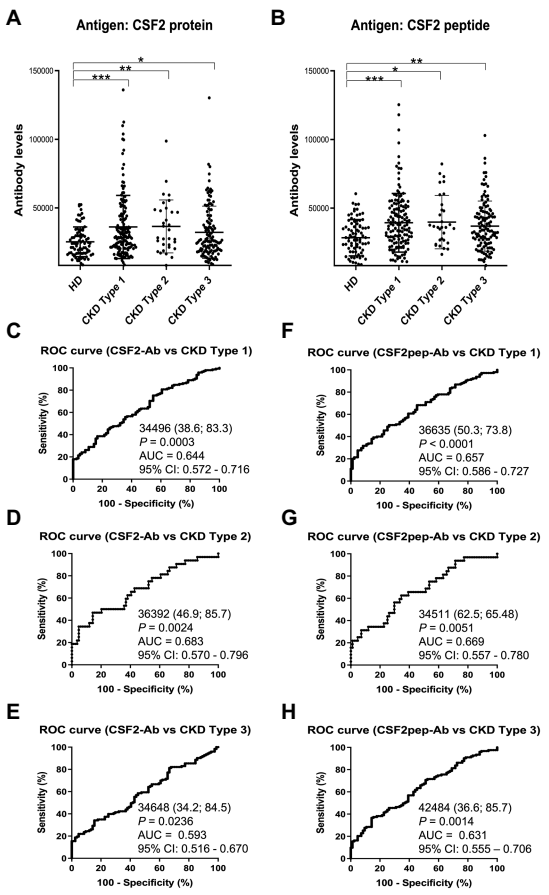

FIGURE 4
Association of the s-CSF2-Ab and s-CSF2pep-Ab levels with CKD. The levels of s-CSF-Ab (**A**) and s-CSF2pep-Ab (**B**) in HDs and in patients with diabetic CKD (CKD type 1), nephrosclerosis (CKD type 2), and glomerulonephritis (CKD type 3) were examined using AlphaLISA. The bars represent averages ± SD. **P*<0.05; ***P*<0.01; ****P*<0.001, Kruskal–Wallis test. The data are summarized in Table 3. (**C–E**) ROC analysis to determine the ability of s-CSF2-Ab to predict CKD type 1 (**C**), type 2 (**D**), and type 3 (**E**). (**F–H**) ROC analysis to determine the ability of s-CSF2pep-Ab to predict CKD type 1 (**F**), type 2 (**G**), and type 3 (**H**). The numbers in the graphs are the same as those presented Figure 2. CKD, chronic kidney disease.

exhibit significant differences in patients with EC and GC (Supplementary Figures 3A,B).

3.8. Effect of CSF2 and anti-CSF2 antibodies on cell replication and transactivation ability of p53 in CRC cells

We evaluated the effects of the CSF2 and anti-CSF2 antibodies on cell replication using LoVo cells, a human CRC line harboring wild-type p53 (55). LoVo cells were treated with CSF2 and/or a commercial rabbit polyclonal anti-CSF2 antibody (Cusabio Technology) to examine their impact on cell replication using the MTS assay. As presented in Supplementary Figure S4, treatment with CSF2 for 72 h led to a slight decrease in cell replication, whereas the presence of the anti-CSF2 antibody significantly promoted the proliferation of LoVo cells. Moreover, the replication-promoting effect of the anti-CSF2 antibody was reversed by the simultaneous addition of an excess quantity of antigenic CSF2 (PeproTech), suggesting that the stimulation of proliferation by the anti-CSF2 antibody was attributed mainly to the suppression of CSF2 in the medium and not to other effects due to impurities. Contrarily, none of the effects of CSF2 and the anti-CSF2 antibody observed in LoVo cells were detected in DLD1 harboring mutant p53 (Supplementary Figure S4).

Next, we used pGL3-p21-Luc containing the promoter sequence of *p21/Cip1*, a p53-target gene, to evaluate the p53 activity after the addition of CSF2 and/or the anti-CSF2 antibody using a luciferase reporter assay. In LoVo cells, p21-Luc, which was partially preactivated by cotransfection of wild-type p53, was further activated by treatment with CSF2 but significantly attenuated by treatment with the anti-CSF2 antibody ($P < 0.01$; Supplementary Figure S5). The decrease in the activation of p21-Luc by the anti-CSF2 antibody was reversed by the concurrent addition of excess antigenic CSF2, indicating that the reduction of p21-Luc activation by the anti-CSF2 antibody was caused by the suppression of CSF2 in the medium rather than its effects related to other impurities in the CSF2 antibody preparation. Therefore, these results indicate that CSF2 might induce the p53 transactivation ability, leading to the inhibition of tumor cell proliferation.

To determine p53-mediated transactivation, we measured the phosphorylation of p53 at Ser-46 using western blotting (68). The levels of Ser-46-phosphorylated p53 were reduced after treatment with the rabbit anti-CSF2 antibody and increased after treatment with CSF2 (Supplementary Figure S6). No apparent changes were observed in the levels of p53 phosphorylated at other sites, including Ser-392, Ser-315, and Thr-81 (data not shown). Thus, these results indicated that the rabbit anti-CSF2 antibody and the serum autoantibodies against CSF2 promoted tumor progression by suppressing p53 activity, which was preactivated by endogenous CSF2.

4. Discussion

In the present study, we investigated the relationship between CSF2 and atherosclerosis-related diseases, including AIS, AMI, DM, CKD, and cancer based on data from previous studies. We confirmed the presence of anti-CSF antibodies in patient sera using western blotting with recombinant full-length GST-tagged CSF2 (Figure 1). Subsequently, we measured the serum antibody levels using GST-CSF2 and the *N*-terminal biotinylated 18-mer peptide, bCSF2-77, as antigens in AlphaLISA. We found that both the s-CSF2-Ab and s-CSF2pep-Ab levels were higher in patients with AIS, AMI, DM, and CKD than those with HDs (Figures 2, 3, 5; Tables 1–3). The s-CSF2-Ab levels were closely correlated with max-IMT, plaque score, and cardio-ankle vascular index (Table 5; Supplementary Table S3), which are typical indices of atherosclerosis leading to AIS and AMI (62–65). CSF2 has been demonstrated to have a protective impact on atherogenesis (6), and the administration of CSF2 has been reported to prevent the progression of atherosclerosis *via* changes in the composition of atherosclerotic lesions (7). We observed that both the s-CSF2-Ab and s-CSF2pep-Ab levels were highly correlated with atherosclerosis-related diseases, such as AIS, AMI, CKD, and DM. Intriguingly, we also found that the levels of s-CSF2pep-Ab but not s-CSF2-Ab were associated with TIA. It is possible that the CSF2 peptide with a single epitope can be specifically recognized by anti-CSF2 antibodies, whereas the CSF2 protein with multiple epitopes can also cross-react with other non-specific antibodies in addition to being recognized by specific anti-CSF2 antibodies. Furthermore, we found that

TABLE 3 The s-CSF2-Ab and s-CSF2pep levels associated with CKD.

Sample information		HD	CKD type 1	CKD type 2	CKD type 3
Total sample number		82	145	32	123
Male/Female		44/38	106/39	21/11	70/53
Age (Average ± SD)		44.10 ± 11.19	66.04 ± 10.38	76.03 ± 9.78	61.98 ± 11.69
		s-CSF2-Ab	s-CSFpep-Ab		
HD	Average	25,266	28,353		
	SD	10,846	13,215		
	Cutoff value	46,958	54,783		
	Total number	84	84		
	Positive number	4	1		
	Positive (%)	4.8%	1.2%		
CKD type 1	Average	36,041	39,262		
	SD	22,993	21,382		
	Total number	145	145		
	Positive number	32	27		
	Positive (%)	**22.1%**	**18.6%**		
	P value (*vs* HD)	**<0.001**	**<0.001**		
CKD type 2	Average	36,425	39,778		
	SD	19,287	19,499		
	Total number	32	32		
	Positive number	9	7		
	Positive (%)	**28.1%**	**21.9%**		
	P value (*vs* HD)	**<0.01**	**<0.05**		
CKD type 3	Average	32,164	36,810		
	SD	19,073	18,290		
	Total number	123	123		
	Positive number	27	18		
	Positive (%)	**22.0%**	**14.6%**		
	P value (*vs* HD)	**<0.05**	**<0.01**		

The upper panel indicates the number of total samples, samples from male and female participants, and ages (average ± SD). The lower panel summarizes the s-CSF2-Ab and s-CSF2pep-Ab levels examined using AlphaLISA. Numbers are as shown in Table 1; *P* values of <0.05 and positive rates of >10% are marked in bold font. The plots for these data are shown in Figures 4A,B. CKD, chronic kidney disease; CKD type 1, diabetic CKD; CKD type 2, nephrosclerosis; CKD type-3, glomerulonephritis.

TABLE 4 Association between s-CSF2-Ab levels and the data from participants in the Sawara Hospital cohort.

Data analysis of s-CSF2-Ab levels			
Sex		Male	Female
Sample number		230	154
s-CSF2-Ab level	Average	7,553	6,374
	SD	6,771	5,083
P value (*vs* Male)			0.166
Obesity		BMI < 25	BMI ≥25
Sample number		263	121
s-CSF2-Ab level	Average	7,288	6,628
	SD	6,622	5,046
P value (*vs* BMI < 25)			0.270
Complication		DM-	DM+
Sample number		303	81
s-CSF2-Ab level	Average	7,062	7,150
	SD	5,900	7,129
P value (*vs* DM-)			0.909
Complication		Hypertension-	Hypertension+
Sample number		144	240
s-CSF2-Ab level	Average	6,105	7,666
	SD	4,927	6,750
P value (*vs* Hypertension-)			**0.020**
Complication		CVD-	CVD+
Sample number		369	15
s-CSF2-Ab level	Average	7,124	5,999
	SD	6,271	2,498
P value (*vs* CVD-)			0.976
Complication		Dyslipidemia-	Dyslipidemia+
Sample number		267	117
s-CSF2-Ab level	Average	7,608	5,876
	SD	6,862	3,950
P value (*vs* Dyslipidemia-)			**0.027**
Lifestyle		Non-smoker	Smoker
Sample number		187	197
s-CSF2-Ab level	Average	6,705	7,493
	SD	6,580	5,675
P value (*vs* Non-smoker)			0.091
Lifestyle		Alcohol-	Alcohol+
Sample number		173	211
s-CSF2-Ab level	Average	7,258	6,935
	SD	5,486	6,688
P value (*vs* Alcohol-)			0.128

Participants were divided into two groups according to the following classifications: sex (male and female); obesity (body mass index, < or ≥ 25 kg/m^2); with (+) or without (−) other disease including DM, hypertension, CVD, and dyslipidemia; and with (+) or without (−) smoking and alcohol intake habits. The Mann–Whitney *U* test was used to compare the s-CSF2-Ab levels of the two groups. Sample numbers, averages, and SDs of counts, as well as *P* values are shown. Significant correlations ($P < 0.05$) are marked in bold.

10.3389/fcvm.2023.1042272

TABLE 5 Correlation analysis of s-CSF2-Ab levels with data from subjects in the Sawara Hospital cohort.

	s-CSF2-Ab	
Category	*r* value	*P* value
Age	0.0969	**0.0381**
Height (cm)	0.0478	0.3522
Weight (kg)	−0.0502	0.3276
BMI	−0.0961	0.0609
max IMT	0.1579	**0.0056**
A/G	−0.0964	0.0681
AST (GOT)	−0.0576	0.2620
ALT (GPT)	−0.0732	0.1535
ALP	0.0522	0.3302
LDH	0.0395	0.4483
tBil	−0.0543	0.2955
CHE	−0.1560	**0.0081**
gamma-GTP	−0.0916	0.0822
albumin	−0.1140	**0.0263**
BUN	0.0490	0.3391
creatinin	0.0770	0.1332
eGFR	−0.0583	0.2700
UA	0.0628	0.3008
AMY	−0.0735	0.2724
T-CHO	−0.1889	**0.0006**
HDL-c	−0.0512	0.4406
TG	−0.0315	0.6219
Na	−0.0025	0.9608
Cl	−0.0477	0.3554
WBC	0.0575	0.2633
RBC	0.0370	0.4726
HGB	−0.1067	**0.0377**
HCT	−0.1096	**0.0326**
MCV	−0.0581	0.2584
MCH	−0.0023	0.9636
MCHC	−0.0583	0.2572
PLT	−0.0071	0.8896
MPV	0.0222	0.6658
PCT	0.0414	0.4303
PDW	−0.0129	0.8027
Blood glucose	0.0995	0.0632
HbA1c	−0.0444	0.4478
BP	0.1069	**0.0439**
Smoking duration (year)	0.1139	**0.0288**
Alcohol Freq (time/w)	0.0791	0.1297

Correlation coefficients (*r* values), and *P* values obtained by Spearman correlation analysis are shown. Subjects' data used were age, height, weight, BMI, body mass index; max-IMT, maximum intima–media thickness; A/G, albumin/globulin ratio; AST, aspartate aminotransferase; ALT, alanine amino transferase; ALP, alkaline phosphatase; LDH, lactate dehydrogenase; tBil, total bilirubin; CHE, cholinesterase; gamma-GTP, γ-glutamyl transpeptidase; ALB, albumin; BUN, blood urea nitrogen; creatinine; eGFR, estimated glomerular filtration rate; UA, uric acid; AMY, amylase; T-CHO, total cholesterol; HDL-c, high-density lipoprotein cholesterol; TG, triglyceride; Na, sodium; Cl, chloride; WBC, white blood cell number; RBC, red blood cell number; HGB, hemoglobin; HCT, hematocrit; MCV, mean corpuscular volume; MCH, mean corpuscular hemoglobin; MCHC, MCH concentration; PLT, platelet number; MPV, mean platelet volume; PCT, procalcitonin; PDW, platelet distribution width; HbA1c, blood glucose, glycated hemoglobin; smoking duration (year), and alcohol intake frequency (times/week).

the AUC of s-CSF2pep-Ab in patients with AIS, AMI, DM, and CKD were all higher than the AUC of s-CSF2-Ab in patients, except for type-2 CKD. Consistent with this, it was reported that using peptide epitopes would be beneficial with respect to assay specificity, while recombinant proteins also included many cross-reactive epitopes that would react with low specificity antibodies, leading to a lower specificity of the test (48, 69). Therefore, the use of s-CSF2pep-Ab as an antibody marker may be more accurate for the diagnosis of diseases. The s-CSF2-Ab levels were correlated well with hypertension (Table 4) and weakly with BP (Table 5) but were not correlated with glycated hemoglobin and blood glucose, which are typical DM markers. Patients with diabetic CKD (CKD type 1) and those with nephrosclerosis (CKD type 2) exhibited equally higher s-CSF2-Ab and s-CSF2pep-Ab levels than the HDs (Figures 4A, B). The AUCs of CKD type 2 were higher than those of CKD type 1. These results indicate that the s-CSF2-Ab levels do not directly reflect DM but are associated with DM-induced atherosclerotic disorders. Furthermore, using multivariate logistic regression analysis, we identified age, hypertension, and s-CSF2-Ab as independent predictors of AIS (Supplementary Table S4). Thus, s-CSF2-Ab may be able to discriminate atherosclerosis caused by hypertension, which leads to the onset of AIS and AMI. These findings, subsequently validated by the analysis of the JPHC cohort (Table 6), indicate that s-CSF2-Ab should be considered as a risk factor for AIS.

TABLE 6 Analysis of JPHC cohort subjects.

s-CSF2pep-Ab *vs* AIS	Case/control	Matched OR (95% CI)
1st	28/51	1.00
2nd	40/50	1.72 (0.91–3.24)
3rd	61/51	2.47 (1.31–4.65)
4th	73/50	3.03 (1.58–5.80)

The odds ratios (ORs) and 95% CI of the 1st, 2nd, 3rd, and the highest (4th) quartiles versus the lowest (1st) quartile are shown for AIS with respect to anti-CSF2 peptide antibody (CSF2pep-Ab) levels. Age-, sex-, and area-matched, conditional odds ratios, and 95% confidence intervals (CIs) of AIS according to CSF2 peptide antibody markers. OR: odds ratios.

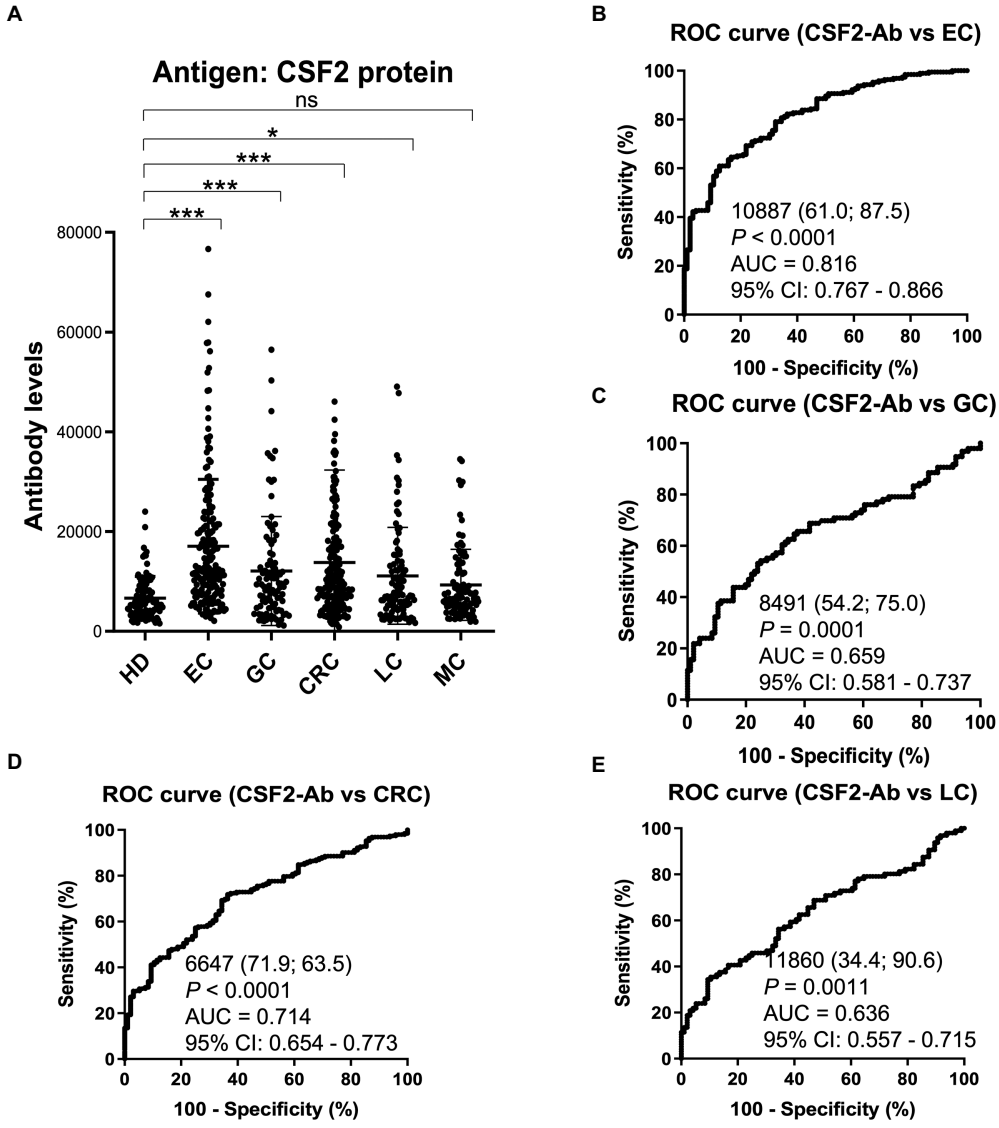

FIGURE 5
Comparison of the s-CSF2-Ab levels between HDs and patients with cancers. (**A**) Scatter dot plots of the s-CSF2-Ab levels in HDs and in patients with EC, gastric cancer (GC), CRC, lung cancer (LC), and mammary cancer (MC). The results are presented as described in the legend of Figure 2. ***P*<0.01; ****P*<0.001; ns, not significant. ROC analysis was conducted to assess the ability of s-CSF2-Abs to detect EC (**B**), GC (**C**), CRC (**D**), and LC (**E**).

TABLE 7 Association of s-CSF2-Ab levels with cancer development.

Sample information		HD	EC	GC	CC	LC	MC
Total sample number		96	192	96	192	96	96
Male/Female		51/45	155/37	68/28	119/74	42/54	58/38
Age (Average ± SD)		57.9 ± 6.0	67.4 ± 9.8	68.7 ± 10.6	66.7 ± 11.7	60.9 ± 13.3	68.1 ± 9.6
		s-CSF2-Ab					
HD	Average	6,678					
	SD	4,312					
	Cutoff value	15,301					
	Total number	96					
	Positive number	5					
	Positive (%)	5.2%					
EC	Average	17,068					
	SD	13,393					
	Total number	192					
	Positive number	82					
	Positive (%)	**42.7%**					
	P value (*vs* HD)	**<0.0001**					
GC	Average	12,095					
	SD	10,906					
	Total number	96					
	Positive number	23					
	Positive (%)	**24.0%**					
	P value (*vs* HD)	**<0.0001**					
CRC	Average	13,779					
	SD	18,560					
	Total number	192					
	Positive number	58					
	Positive (%)	**30.2%**					
	P value (*vs* HD)	**<0.0001**					
LC	Average	11,127					
	SD	9,695					
	Total number	96					
	Positive number	23					
	Positive (%)	**24.0%**					
	P value (*vs* HD)	**<0.05**					
MC	Average	9,320					
	SD	7,120					
	Total number	96					
	Positive number	15					
	Positive (%)	**15.6%**					
	P value (*vs* HD)	ns					

Types of cancer diagnoses included. EC, esophageal cancer; GC, gastric cancer; CRC, colorectal carcinoma; LC, lung cancer; MC, mammary cancer. The upper panel indicates the numbers of all samples and samples from males and females as well as age (average ± SD). The lower panel summarizes the serum antibody levels examined by AlphaLISA using purified CSF2-GST proteins as the antigens, as described in the legend of Table 1. *P* values of < 0.05 and positive rates of > 10% are marked in bold font. The plots for these data are shown in Figure 5A.

In addition, the s-CSF2-Ab levels were associated with several cancers, including EC, CRC, GC, and LC (Figure 5; Table 7). As presented in Table 8, the s-CSF2-Ab and p53-Ab levels were correlated. Among the patients with CRC whose serum p53-Ab levels were below the cutoff, the prognosis was worse in those with high s-CSF2-Ab levels than in those with low s-CSF2-Ab levels. Furthermore, the *P* value of Figure 6D was even lower than that of Figure 6A in the survival analysis of patients with CRC. After transactivation by the wild-type p53, the protein product of

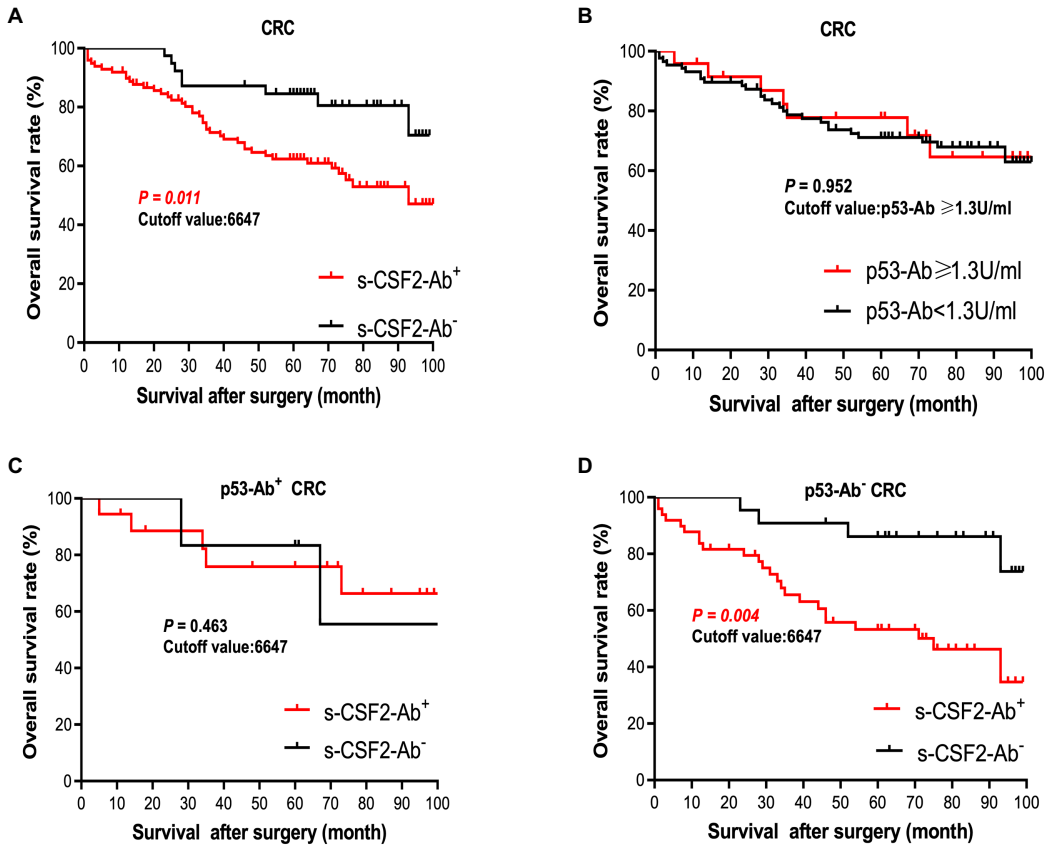

FIGURE 6
Comparison of survival according to s-CSF2-Ab positivity in patients with CRC after surgery. (**A**) Comparison of the postoperative survival between the s-CSF2-Ab$^+$ and s-CSF2-Ab$^-$ patients with CRC (P=0.011). (**B**) Comparison of the overall survival between the p53-Ab$^+$ (≥1.3U/ml) and p53-Ab$^-$ (<1.3U/ml) patients with CRC (P=0.952). (**C**) Comparison of the overall survival between the s-CSF2-Ab$^+$ and s-CSF2-Ab$^-$ patients with CRC among those with p53-Ab ≥1.3U/ml (P=0.463). (**D**) Comparison of the overall survival between the s-CSF2-Ab$^+$ and s-CSF2-Ab$^-$ patients with CRC among those with p53-Ab <1.3U/ml (P=0.004). The cutoff values in patients with CRC were determined *via* the ROC analysis presented in Figure 5D. Statistical analyzes were performed by the Log-Rank test between two groups.

mouse double minute 2 homolog (*MDM2*) preferentially polyubiquitinates p53 protein, leading to its degradation (68, 70). Contrarily, in the presence of mutant p53, the MDM2 levels are maintained at low levels, and the degradation of p53 is limited, leading to the high p53 expression (71). Therefore, most of the anti-p53 autoantibodies in patients with CRC are formed in response to p53 mutations (72), and patients without p53-Ab harbor wild-type p53. Based on the observed effect of p53-Ab status, we used wild-type p53-harboring LoVo cells to investigate the relationship of CSF2 and CSF2-Ab with p53 (Supplementary Figures S4, S5). We found that anti-CSF2-Ab reduced the p53 transactivation ability, leading to the increased proliferation of LoVo cells (Supplementary Figures S4, S5). Consistently, the levels of Ser-46-phosphorylated p53 were increased by treatment with CSF2 and reduced by treatment with anti-CSF2-Ab (Supplementary Figure S6). Interestingly, it was previously reported that the anti-CSF2 antibodies decreased CSF2 cytokine bioavailability, possibly by disrupting their binding to receptors (73–75), and the expression of p53 was significantly increased in neutrophils cultured with CSF2 (76). These results indicate that the high levels of CSF2-Ab may reduce p53 activity *via* adsorption of CSF2 in the circulation, leading to an increase in the proliferation of cancer cells and unfavorable prognosis in patients with CRC (Figure 6D). Gene therapy using wild-type p53, delivered using physical methods or viral vectors, was reported to significantly suppress CRC (77), but not MC (78), in preclinical and clinical models. Therefore, CRC might be more sensitive to the tumor suppressor p53 than MC, which might partially explain our findings that the s-CSF2-Ab levels were not associated with MC (Figure 5; Table 7).

Numerous lines of evidence support the presence of a relationship between atherosclerosis and cancer, which share inflammation as an underlying pathophysiology (11, 12). p53 deficiency not only leads to accelerated atherosclerosis (79–81) but also increases BP, heart rate, and sympathetic activity of the heart and blood vessels, thus contributing to the development of hypertension (82). In the present study, we found that the s-CSF2-Ab levels were significantly associated with hypertension, which is a major risk factor for not only atherosclerosis (9, 83–85) but also AIS and AMI (35, 86–88). Therefore, based on the current study findings, we hypothesize that the s-CSF2-Ab levels may contribute to atherosclerosis through the elevated hypertension caused by reduced p53 activity. Therefore, based on the current study findings, we hypothesize that the s-CSF2-Ab may directly contribute to the development of cancer by reducing p53 activity, and indirectly contribute to the onset of atherosclerosis-related AIS, AMI, and CKD through p53-mediated regulation of hypertension. This may explain the overall higher positive rate of s-CSF2-Ab in patients with solid cancer than those in patients with atherosclerosis-related AIS, AMI, DM, and CKD (Tables 1–3, 7).

The overview diagram (Figure 7) summarizes the relationship between s-CSF2-Ab and wild-type p53 in cancer and atherosclerosis-related diseases. Consistently, the high s-CSF2-Ab levels in patients with DM indicated unfavorable prognosis, which was especially pronounced after 80 months (Figures 3C,H). Thus, s-CSF2-Ab might have a causal relationship with the development of atherosclerosis and cancer.

Results of this study suggest that the measurement of serum s-CSF2-Ab levels can provide valuable information for diagnosing atherosclerosis-related AIS and solid cancers. The serum s-CSF2pep-Ab levels can be used for diagnosing TIA. Investigations showed that approximately 15% of patients with ischemic stroke experience a TIA before the onset of AIS (89), and approximately 50% of the patients with TIA visited medical facilities after their symptoms completely disappeared (90, 91). However, it is sometimes difficult for physicians to diagnose a TIA only by taking the patient's history into consideration, as half of the TIA patients visit the hospital after the symptoms have completely disappeared. Although tests such as MRI and carotid artery angiography can be used to improve diagnoses, they are generally expensive, time consuming, and inconvenient. In the case of solid cancers, early diagnoses can greatly improve the survival time of patients and reduce the financial burden caused by medical treatments. Therefore, if s-CSF2pep-Ab can be applied as a biomarker in combination with other risk factors and biomarkers for AIS, TIA or solid cancers to diagnose the occurrence of the disease, this will greatly facilitate clinical practice and contribute to the medical economy. Cytokines and cytokine antibodies in the serum are the ideal targets for the development of preventative and therapeutic approaches due to drug accessibility. The administration of CSF2 has been demonstrated to prevent the progression of atherosclerosis (7). Alternatively, the development decoy molecules that can bind to and adsorb s-CSF2-Ab might be effective for disease prevention.

5. Limitation

We acknowledge that the current study has several limitations. First, atherosclerosis risk factors, such as hypercholesterolemia, were not associated with the elevated levels of s-CSF2-Ab in the present study. Antihypertensive drugs, cholesterol-lowering statins, and antiplatelet agents are considered to influence the pathogenesis of atherosclerosis (92–95). Because detailed statistics on medications taken by patients prior to hospital admission are not available, we were unable to study the specific effects of drugs on s-CSF2-Ab levels, and further studies are needed in patients who were not taking drugs that could affect atherosclerosis and cancer. In future studies, the potential modulating effects of these drugs on the s-CSF2-Ab levels should be considered. Second, the blood samples were collected at the time of hospital admission and the period of stroke onset and admission differed depending on the patient, which is another limitation. Third, as we used specimens obtained from hospitals and universities in Japan, it is unclear whether our conclusions are applicable to other populations. Thus, it is essential for general practical use in the world to conduct more international collaborative research using specimens from many countries. Fourth, the cutoff values we used were average+2SD and Youden index of ROC analysis. However, other methods should also be considered to optimize the cutoff values, improving the ability of s-CSF2-Ab as a biomarker to discriminate normal individuals from patients and favorable prognosis from unfavorable prognosis.

6. Conclusion

It is possible to predict the onset of atherosclerotic AIS and AMI by using s-CSF2-Ab as a marker. Moreover, high s-CSF2-Ab levels exhibited poor

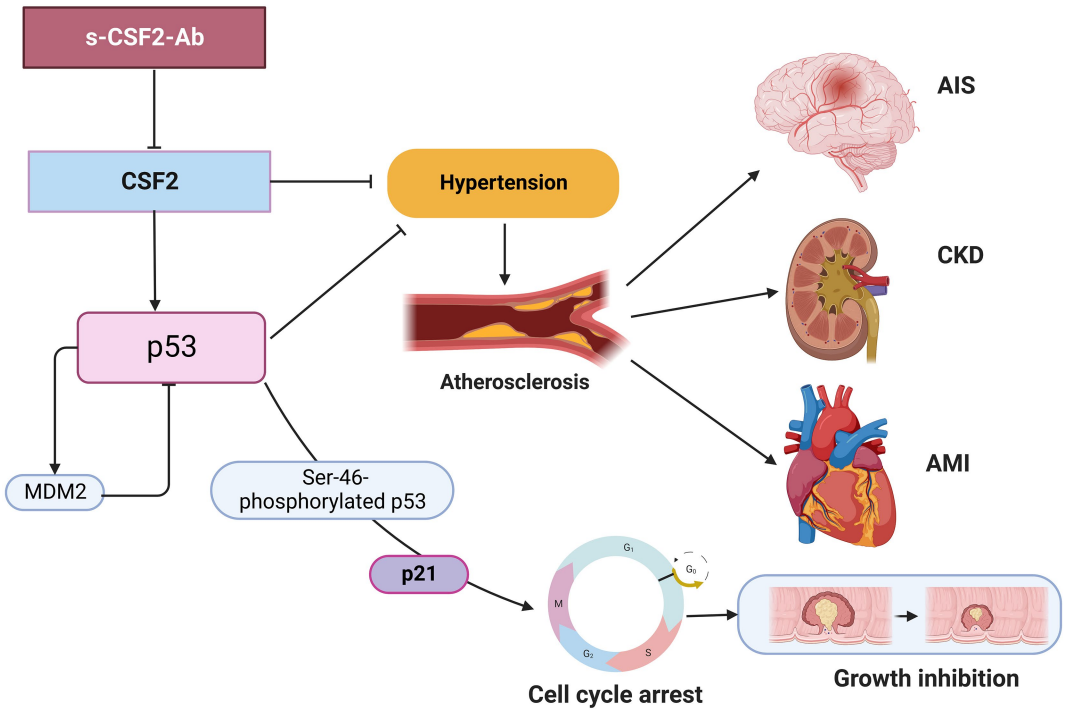

FIGURE 7
Diagram of the relationship between s-CSF2-Ab and p53 in cancer and atherosclerosis-related diseases. Arrows represent the downstream activation, and blocked arrows represent inhibitory action. Created with BioRender.com. *MDM2*, mouse double minute 2 homolog.

TABLE 8 Association between s-CSF2-Ab levels and data from participants in the Toho University Hospital cohort.

Data analysis of s-CSF2-Ab levels			
Sex		Male	Female
Sample number		45	68
s-CSF2-Ab level	Average	10,178	6,374
	SD	7,451	5,083
P value (*vs* Male)			**0.010**
CEA		CEA ≥10 ng/ml	CEA <10 ng/ml
Sample number		29	84
s-CSF2-Ab level	Average	14,744	12,333
	SD	11,892	8,825
P value (*vs* CEA < 10 ng/ml)			0.428
CA19-9		CA19-9 ≥ 37 ng/ml	CA19-9 < 37 ng/ml
Sample number		58	55
s-CSF2-Ab level	Average	13,525	12,347
	SD	10,331	9,052
P value (*vs* CA19-9 < 37 ng/ml)			0.436
p53-Abs		p53-Ab ≥1.3 U/ml	p53-Ab <1.3 U/ml
Sample number		24	89
s-CSF2-Ab level	Average	17,158	11,818
	SD	11,977	8,732
P value (*vs* p53-Ab<1.3 U/ml)			**0.039**
Organizational type		Tubular	None-Tubular
Sample number		50	63
s-CSF2-Ab level	Average	13,355	12,632
	SD	10,182	9,379
P value (*vs* none-tubular)			0.555

Participants were divided into two groups according to the following parameters: sex (male and female), obesity, BMI, body mass index; CEA, carcinoembryonic antigen; CA19-9, carbohydrate antigen 19–9; p53-Ab, and organizational type. The Mann–Whitney *U* test was used to compare the s-CSF2-Ab levels of the two groups. Sample numbers, averages, and SDs of counts, as well as *P* values are shown. Significant correlations ($P < 0.05$) are marked in bold.

overall survival in patients with CRC who may be harboring wild-type p53. Taken together, these results indicate s-CSF2-Ab as a potentially valuable therapeutic target for the prevention of atherosclerosis and solid cancers.

Data availability statement

The original contributions presented in the study are included in the article/Supplementary material, further inquiries can be directed to the corresponding authors.

Ethics statement

The studies involving human participants were reviewed and approved by Local Ethics Review Board of Chiba University, Graduate School of Medicine in Chiba, Japan (no. 2018–320), Toho University Graduate School of Medicine in Tokyo, Japan (no. A19033). The patients/participants provided their written informed consent to participate in this study.

Author contributions

SYL, TMac, YI, and TH conceived and designed the study. SYL, MK, TMac, KYa, MO, MT, and KI conducted the experiments and acquired the data. YY, SM, MI, KYos, AH, KYok, HI, KK, NS, ST, and HT contributed to the reagents, materials, analysis tools, or the patient data. YY, SY, MS, EN, and IK analyzed and interpreted the data. BSZ, TMat, MI, HS, and MT performed the statistical analyzes. SYL, YI, and TH drafted the manuscript. All authors contributed to the article and approved the submitted version.

Funding

This work was supported, in part, by research grants from the Japan Science and Technology Agency (JST), JSPS KAKENHI Grant Number 20 K17953, 19 K09451, 17 K19810, 20 K07810, 16 K10520, 21 K08695, and 15 K10117. The Japan Public Health Center-based Prospective Study was supported by (National Cancer Center Research and Development Fund since 2011) and a Grant-in-Aid for Cancer Research from the Ministry of Health, Labour and Welfare of Japan (from 1989 to 2010).

Acknowledgments

The authors would like to thank Masaki Takiguchi (Department of Biochemistry and Genetics, Graduate School of Medicine, Chiba University) for valuable discussions. We are grateful to Bert Vogelstein (Howard Hughes Medical Institute) and Mian Wu (University of Science and Technology of China) for providing expression and reporter plasmids.

Conflict of interest

The authors declare that the research was conducted in the absence of any commercial or financial relationships that could be construed as a potential conflict of interest.

Publisher's note

Supplementary material

The Supplementary material for this article can be found online at: https://www.frontiersin.org/articles/10.3389/fcvm.2023.1042272/full#supplementary-material

References

1. Jiang, YX, Yang, SW, Li, PA, Luo, X, Li, ZY, Hao, YX, et al. The promotion of the transformation of quiescent gastric cancer stem cells by IL-17 and the underlying mechanisms. *Oncogene*. (2017) 36:1256–64. doi: 10.1038/onc.2016.291
2. Matsubara, T, Furukawa, S, and Yabuta, K. Serum levels of tumor necrosis factor, interleukin 2 receptor, and interferon-gamma in Kawasaki disease involved coronary-artery lesions. *Clin Immunol Immunopathol*. (1990) 56:29–36. doi: 10.1016/0090-1229(90)90166-n
3. Tong, Y, Song, Y, and Deng, S. Combined analysis and validation for DNA methylation and gene expression profiles associated with prostate cancer. *Cancer Cell Int*. (2019) 19:50. doi: 10.1186/s12935-019-0753-x
4. Qin, C, Liu, Q, Hu, ZW, Zhou, LQ, Shang, K, Bosco, DB, et al. Microglial TLR4-dependent autophagy induces ischemic white matter damage via STAT1/6 pathway. *Theranostics*. (2018) 8:5434–51. doi: 10.7150/thno.27882
5. Lebedeva, A, Fitzgerald, W, Molodtsov, I, Shpektor, A, Vasilieva, E, and Margolis, L. Differential clusterization of soluble and extracellular vesicle-associated cytokines in myocardial infarction. *Sci Rep*. (2020) 10:21114. doi: 10.1038/s41598-020-78004-y
6. Ditiatkovski, M, Toh, BH, and Bobik, A. GM-CSF deficiency reduces macrophage PPAR-gamma expression and aggravates atherosclerosis in ApoE-deficient mice. *Arterioscler Thromb Vasc Biol*. (2006) 26:2337–44. doi: 10.1161/01.Atv.0000238357.60338.90
7. Shindo, J, Ishibashi, T, Yokoyama, K, Nakazato, K, Ohwada, T, Shiomi, M, et al. Granulocyte-macrophage colony–stimulating factor prevents the progression of atherosclerosis via changes in the cellular and extracellular composition of atherosclerotic lesions in watanabe heritable hyperlipidemic rabbits. *Circulation*. (1999) 99:2150–6. doi: 10.1161/01.CIR.99.16.2150
8. Valdivielso, JM, Rodríguez-Puyol, D, Pascual, J, Barrios, C, Bermúdez-López, M, Sánchez-Niño, MD, et al. Atherosclerosis in chronic kidney disease: more, kess, or just different? *Arterioscler Thromb Vasc Biol*. (2019) 39:1938–66. doi: 10.1161/atvbaha.119.312705
9. Libby, P, Buring, JE, Badimon, L, Hansson, GK, Deanfield, J, Bittencourt, MS, et al. *Atheroscler Nat Rev Dis Primers*. (2019) 5:56. doi: 10.1038/s41572-019-0106-z
10. Agarwal, S, Sud, K, Thakkar, B, Menon, V, Jaber, WA, and Kapadia, SR. Changing trends of atherosclerotic risk factors among patients with acute myocardial infarction and acute ischemic stroke. *Am J Cardiol*. (2017) 119:1532–41. doi: 10.1016/j.amjcard.2017.02.027
11. Barrera, G, Pizzimenti, S, and Dianzani, MU. Lipid peroxidation: control of cell proliferation, cell differentiation and cell death. *Mol Asp Med*. (2008) 29:1–8. doi: 10.1016/j.mam.2007.09.012
12. Thanan, R, Oikawa, S, Hiraku, Y, Ohnishi, S, Ma, N, Pinlaor, S, et al. Oxidative stress and its significant roles in neurodegenerative diseases and cancer. *Int J Mol Sci*. (2014) 16:193–217. doi: 10.3390/ijms16010193
13. Zhang, J, Liu, Q, Qiao, L, Hu, P, Deng, G, Liang, N, et al. Novel role of granulocyte-macrophage colony-stimulating factor: antitumor effects through inhibition of epithelial-to-mesenchymal transition in esophageal cancer. *Onco Targets Ther*. (2017) 10:2227–37. doi: 10.2147/ott.S133504
14. Urdinguio, RG, Fernandez, AF, Moncada-Pazos, A, Huidobro, C, Rodriguez, RM, Ferrero, C, et al. Immune-dependent and independent antitumor activity of GM-CSF aberrantly expressed by mouse and human colorectal tumors. *Cancer Res*. (2013) 73:395–405. doi: 10.1158/0008-5472.Can-12-0806
15. Liu, H, Lin, C, Shen, Z, Zhang, H, He, H, Li, H, et al. Decreased expression of granulocyte-macrophage colony-stimulating factor is associated with adverse clinical outcome in patients with gastric cancer undergoing gastrectomy. *Oncol Lett*. (2017) 14:4701–7. doi: 10.3892/ol.2017.6738
16. Hong, IS. Stimulatory versus suppressive effects of GM-CSF on tumor progression in multiple cancer types. *Exp Mol Med*. (2016) 48:e242. doi: 10.1038/emm.2016.64
17. Albulescu, R, Codrici, E, Popescu, ID, Mihai, S, Necula, LG, Petrescu, D, et al. Cytokine patterns in brain tumour progression. *Mediat Inflamm*. (2013) 2013:979748. doi: 10.1155/2013/979748
18. Perez, FA, Fligner, CL, and Yu, EY. Rapid clinical deterioration and leukemoid reaction after treatment of urothelial carcinoma of the bladder: possible effect of granulocyte colony-stimulating factor. *J Clin Oncol*. (2009) 27:e215–7. doi: 10.1200/jco.2009.22.4931
19. Thomas, DS, Fourkala, EO, Apostolidou, S, Gunu, R, Ryan, A, Jacobs, I, et al. Evaluation of serum CEA, CYFRA21-1 and CA125 for the early detection of colorectal cancer using longitudinal preclinical samples. *Br J Cancer*. (2015) 113:268–74. doi: 10.1038/bjc.2015.202
20. Amoura, Z, Duhaut, P, Huong, DL, Wechsler, B, Costedoat-Chalumeau, N, Francès, C, et al. Tumor antigen markers for the detection of solid cancers in inflammatory myopathies. *Cancer Epidemiol Biomark Prev*. (2005) 14:1279–82. doi: 10.1158/1055-9965.Epi-04-0624
21. Shimada, H, Arima, M, Nakajima, K, Koide, Y, Okazumi, S, Matsubara, H, et al. Detection of serum p53 antibodies in mucosal esophageal cancer and negative conversion after treatment. *Am J Gastroenterol*. (1998) 93:1388–9. doi: 10.1111/j.1572-0241.1998.1388a.x
22. Shimada, H, Ochiai, T, and Nomura, F. Titration of serum p53 antibodies in 1,085 patients with various types of malignant tumors: a multiinstitutional analysis by the Japan p53 antibody research group. *Cancer*. (2003) 97:682–9. doi: 10.1002/cncr.11092
23. Mattioni, M, Soddu, S, Porrello, A, D'Alessandro, R, Spila, A, and Guadagni, F. Serum anti-p53 antibodies as a useful marker for prognosis of gastric carcinoma. *Int J Biol Markers*. (2007) 22:302–6. doi: 10.5301/jbm.2008.1415
24. Chu, DZ, Erickson, CA, Russell, MP, Thompson, C, Lang, NP, Broadwater, RJ, et al. Prognostic significance of carcinoembryonic antigen in colorectal carcinoma. Serum levels before and after resection and before recurrence. *Arch Surg*. (1991) 126:314–6. doi: 10.1001/archsurg.1991.01410270054010
25. Zhang, G, Xu, Q, Wang, Z, Sun, L, Lv, Z, Liu, J, et al. p53 protein expression affected by TP53 polymorphism is associated with the biological behavior and prognosis of low rectal cancer. *Oncol Lett*. (2019) 18:6807–21. doi: 10.3892/ol.2019.10999
26. Browne, SK. Anticytokine autoantibody–associated immunodeficiency. *Annu Rev Immunol*. (2014) 32:635–57. doi: 10.1146/annurev-immunol-032713-120222
27. Browne, SK, and Holland, SM. Immunodeficiency secondary to anticytokine autoantibodies. *Curr Opin Allergy Clin Immunol*. (2010) 10:534–41. doi: 10.1097/ACI.0b013e3283402b41
28. Palmer, JP, Asplin, CM, Clemons, P, Lyen, K, Tatpati, O, Raghu, PK, et al. Insulin antibodies in insulin-dependent diabetics before insulin treatment. *Science*. (1983) 222:1337–9. doi: 10.1126/science.6362005
29. Matsumura, T, Terada, J, Kinoshita, T, Sakurai, Y, Yahaba, M, Tsushima, K, et al. Circulating autoantibodies against neuroblastoma suppressor of tumorigenicity 1 (NBL1): a potential biomarker for coronary artery disease in patients with obstructive sleep apnea. *PLoS One*. (2018) 13:e0195015. doi: 10.1371/journal.pone.0195015
30. Hiwasa, T, Wang, H, Goto, K-i, Mine, S, Machida, T, Kobayashi, E, et al. Serum anti-DIDO1, anti-CPSF2, and anti-FOXJ2 antibodies as predictive risk markers for acute ischemic stroke. *BMC Med*. (2021) 19:131. doi: 10.1186/s12916-021-02001-9
31. Hiwasa, T, Machida, T, Zhang, X-M, Kimura, R, Wang, H, Iwase, K, et al. Elevated levels of autoantibodies against ATP2B4 and BMP-1 in sera of patients with atherosclerosis-related diseases. *Immunome Res*. (2015) 11:097. doi: 10.4172/1745-7580.1000097
32. Kubota, M, Yoshida, Y, Kobayashi, E, Matsutani, T, Li, SY, Zhang, BS, et al. Serum anti-SERPINE1 antibody as a potential biomarker of acute cerebral infarction. *Sci Rep*. (2021) 11:21772. doi: 10.1038/s41598-021-01176-8
33. Chen, PM, Ohno, M, Hiwasa, T, Nishi, K, Saijo, S, Sakamoto, J, et al. Nardilysin is a promising biomarker for the early diagnosis of acute coronary syndrome. *Int J Cardiol*. (2017) 243:1–8. doi: 10.1016/j.ijcard.2017.04.047
34. Adams, HP, Bendixen, BH, Kappelle, LJ, Biller, J, Love, BB, Gordon, DL, et al. Classification of subtype of acute ischemic stroke. Definitions for use in a multicenter clinical trial. TOAST. Trial of org 10172 in acute stroke treatment. *Stroke*. (1993) 24:35–41. doi: 10.1161/01.STR.24.1.35
35. Nishiura, R, Fujimoto, S, Sato, Y, Yamada, K, Hisanaga, S, Hara, S, et al. Elevated osteoprotegerin levels predict cardiovascular events in new hemodialysis patients. *Am J Nephrol*. (2009) 29:257–63. doi: 10.1159/000157629
36. Komatsu, H, Fujimoto, S, Hara, S, Fukuda, A, Fukudome, K, Yamada, K, et al. Recent therapeutic strategies improve renal outcome in patients with IgA nephropathy. *Am J Nephrol*. (2009) 30:19–25. doi: 10.1159/000197116
37. Ito, M, Hiwasa, T, Oshima, Y, Yajima, S, Suzuki, T, Nanami, T, et al. Identification of serum anti-striatin 4 antibodies as a common marker for esophageal cancer and other solid cancers. *Mol Clin Oncol*. (2021) 15:237. doi: 10.3892/mco.2021.2399
38. Japanese Classification of Colorectal. Appendiceal, and anal carcinoma: the 3d English edition secondary publication. *J Anus Rectum Colon*. (2019) 3:175–95. doi: 10.23922/jarc.2019-018. PMID:31768468
39. Terminology and Diagnostic Criteria Committee, Japan Society of Ultrasonics in Medicine. Standard method for ultrasound evaluation of carotid artery lesions. *J Med Ultrason (2001)*. (2009) 36:219–26. doi: 10.1007/s10396-009-0238-y
40. Nakahashi, T, Tada, H, Sakata, K, Nomura, A, Ohira, M, Mori, M, et al. Additive prognostic value of carotid plaque score to enhance the age, creatinine, and ejection fraction score in patients with acute coronary syndrome. *J Atheroscler Thromb*. (2018) 25:709–19. doi: 10.5551/jat.42317
41. Handa, N, Matsumoto, M, Maeda, H, Hougaku, H, Ogawa, S, Fukunaga, R, et al. Ultrasonic evaluation of early carotid atherosclerosis. *Stroke*. (1990) 21:1567–72. doi: 10.1161/01.str.21.11.1567
42. Shirai, K, Utino, J, Otsuka, K, and Takata, M. A novel blood pressure-independent arterial wall stiffness parameter; cardio-ankle vascular index (CAVI). *J Atheroscler Thromb*. (2006) 13:101–7. doi: 10.5551/jat.13.101
43. Yoshida, Y, Wang, H, Hiwasa, T, Machida, T, Kobayashi, E, Mine, S, et al. Elevation of autoantibody level against PDCD11 in patients with transient ischemic attack. *Oncotarget*. (2018) 9:8836–48. doi: 10.18632/oncotarget.23653
44. Wang, H, Zhang, XM, Tomiyoshi, G, Nakamura, R, Shinmen, N, Kuroda, H, et al. Association of serum levels of antibodies against MMP1, CBX1, and CBX5 with transient ischemic attack and cerebral infarction. *Oncotarget*. (2018) 9:5600–13. doi: 10.18632/oncotarget.23789
45. Hashiguchi, Y, Kasai, M, Fukuda, T, Ichimura, T, Yasui, T, and Sumi, T. Serum carcinoembryonic antigen as a tumour marker in patients with endometrial cancer. *Curr Oncol*. (2016) 23:e439–42. doi: 10.3747/co.23.3153

46. Kambara, Y, Miyake, H, Nagai, H, Yoshioka, Y, Shibata, K, Asai, S, et al. CA19-9 is a significant prognostic marker of patients with stage III gastric cancer. *Eur J Surg Oncol*. (2020) 46:1918–24. doi: 10.1016/j.ejso.2020.05.003

47. Sugimoto, K, Hiwasa, T, Shibuya, K, Hirano, S, Beppu, M, Isose, S, et al. Novel autoantibodies against the proteasome subunit PSMA7 in amyotrophic lateral sclerosis. *J Neuroimmunol*. (2018) 325:54–60. doi: 10.1016/j.jneuroim.2018.09.013

48. Hiwasa, T, Tomiyoshi, G, Nakamura, R, Shinmen, N, Kuroda, H, Kunimatsu, M, et al. Serum SH3BP5-specific antibody level is a biomarker of atherosclerosis. *Immunome Res*. (2017) 9:18559–69. doi: 10.18632/oncotarget.24963

49. Liu, TL, Shimada, H, Ochiai, T, Shiratori, T, Lin, SE, Kitagawa, M, et al. Enhancement of chemosensitivity toward peplomycin by calpastatin-stabilized NF-kappaB p65 in esophageal carcinoma cells: possible involvement of Fas/Fas-L synergism. *Apoptosis*. (2006) 11:1025–37. doi: 10.1007/s10495-006-6353-y

50. Yoshida, Y, Zhang, XM, Wang, H, Machida, T, Mine, S, Kobayashi, E, et al. Elevated levels of autoantibodies against DNAJC2 in sera of patients with atherosclerotic diseases. *Heliyon*. (2020) 6:e04661. doi: 10.1016/j.heliyon.2020.e04661

51. Li, SY, Yoshida, Y, Kobayashi, E, Adachi, A, Hirono, S, Matsutani, T, et al. Association between serum anti-ASXL2 antibody levels and acute ischemic stroke, acute myocardial infarction, diabetes mellitus, chronic kidney disease and digestive organ cancer, and their possible association with atherosclerosis and hypertension. *Int J Mol Med*. (2020) 46:1274–88. doi: 10.3892/ijmm.2020.4690

52. Li, SY, Yoshida, Y, Kobayashi, E, Kubota, M, Matsutani, T, Mine, S, et al. Serum anti-AP3D1 antibodies are risk factors for acute ischemic stroke related with atherosclerosis. *Sci Rep*. (2021) 11:13450. doi: 10.1038/s41598-021-92786-9

53. Tsugane, S, and Sawada, N. The JPHC study: design and some findings on the typical Japanese diet. *Jpn J Clin Oncol*. (2014) 44:777–82. doi: 10.1093/jjco/hyu096

54. Ikeda, A, Iso, H, Sasazuki, S, Inoue, M, and Tsugane, S. The combination of helicobacter pylori-and cytotoxin-associated gene-a seropositivity in relation to the risk of myocardial infarction in middle-aged Japanese: the Japan public health center-based study. *Atherosclerosis*. (2013) 230:67–72. doi: 10.1016/j.atherosclerosis.2013.06.013

55. Ahmed, D, Eide, PW, Eilertsen, IA, Danielsen, SA, Eknæs, M, Hektoen, M, et al. Epigenetic and genetic features of 24 colon cancer cell lines. *Oncogenesis*. (2013) 2:e71. doi: 10.1038/oncsis.2013.35

56. Nita, ME, Nagawa, H, Tominaga, O, Tsuno, N, Fujii, S, Sasaki, S, et al. 5-fluorouracil induces apoptosis in human colon cancer cell lines with modulation of Bcl-2 family proteins. *Br J Cancer*. (1998) 78:986–92. doi: 10.1038/bjc.1998.617

57. Couture, C, Desjardins, P, Zaniolo, K, Germain, L, and Guérin, SL. Enhanced wound healing of tissue-engineered human corneas through altered phosphorylation of the CREB and AKT signal transduction pathways. *Acta Biomater*. (2018) 73:312–25. doi: 10.1016/j.actbio.2018.04.021

58. Zhu, Y, Zhang, X, Qi, L, Cai, Y, Yang, P, Xuan, G, et al. HULC long noncoding RNA silencing suppresses angiogenesis by regulating ESM-1 via the PI3K/Akt/mTOR signaling pathway in human gliomas. *Oncotarget*. (2016) 7:14429–40. doi: 10.18632/oncotarget.7418

59. Jiang, P, Du, W, Heese, K, and Wu, M. The bad guy cooperates with good cop p53: bad is transcriptionally up-regulated by p53 and forms a bad/p53 complex at the mitochondria to induce apoptosis. *Mol Cell Biol*. (2006) 26:9071–82. doi: 10.1128/mcb.01025-06

60. Shinmen, N, Koshida, T, Kumazawa, T, Sato, K, Shimada, H, Matsutani, T, et al. Activation of NFAT signal by p53-K120R mutant. *FEBS Lett*. (2009) 583:1916–22. doi: 10.1016/j.febslet.2009.04.041

61. Kanda, Y. Investigation of the freely available easy-to-use software 'EZR' for medical statistics. *Bone Marrow Transplant*. (2013) 48:452–8. doi: 10.1038/bmt.2012.244

62. Tran, LT, Park, HJ, and Kim, HD. Is the carotid intima-media thickness really a good surrogate marker of atherosclerosis? *J Atheroscler Thromb*. (2012) 19:680–90. doi: 10.5551/jat.11767

63. Zureik, M, Ducimetière, P, Touboul, PJ, Courbon, D, Bonithon-Kopp, C, Berr, C, et al. Common carotid intima-media thickness predicts occurrence of carotid atherosclerotic plaques: longitudinal results from the aging vascular study (EVA) study. *Arterioscler Thromb Vasc Biol*. (2000) 20:1622–9. doi: 10.1161/01.atv.20.6.1622

64. Koivistoinen, T, Virtanen, M, Hutri-Kähönen, N, Lehtimäki, T, Jula, A, Juonala, M, et al. Arterial pulse wave velocity in relation to carotid intima-media thickness, brachial flow-mediated dilation and carotid artery distensibility: the cardiovascular risk in young finns study and the health 2000 survey. *Atherosclerosis*. (2012) 220:387–93. doi: 10.1016/j.atherosclerosis.2011.08.007

65. Nakamura, K, Tomaru, T, Yamamura, S, Miyashita, Y, Shirai, K, and Noike, H. Cardio-ankle vascular index is a candidate predictor of coronary atherosclerosis. *Circ J*. (2008) 72:598–604. doi: 10.1253/circj.72.598

66. Rothwell, PM, and Warlow, CP. Timing of TIAs preceding stroke: time window for prevention is very short. *Neurology*. (2005) 64:817–20. doi: 10.1212/01.Wnl.0000152985.32732.Ee

67. Selvarajan, V, Bidkar, AP, Shome, R, Banerjee, A, Chaubey, N, Ghosh, SS, et al. Studying in vitro phagocytosis of apoptotic cancer cells by recombinant GMCSF-treated RAW 264.7 macrophages. *Int J Biol Macromol*. (2017) 102:1138–45. doi: 10.1016/j.ijbiomac.2017.05.003

68. Levine, AJ. p53 and the immune response: 40 years of exploration-a plan for the future. *Int J Mol Sci*. (2020) 21:21. doi: 10.3390/ijms21020541

69. Pandey, S, Malviya, G, and Chottova, DM. Role of peptides in diagnostics. *Int J Mol Sci*. (2021) 22:22. doi: 10.3390/ijms22168828

70. Wu, X, Bayle, JH, Olson, D, and Levine, AJ. The p53-mdm-2 autoregulatory feedback loop. *Genes Dev*. (1993) 7:1126–32. doi: 10.1101/gad.7.7a.1126

71. Lukashchuk, N, and Vousden, KH. Ubiquitination and degradation of mutant p53. *Mol Cell Biol*. (2007) 27:8284–95. doi: 10.1128/mcb.00050-07

72. Levine, AJ, Momand, J, and Finlay, CA. The p53 tumour suppressor gene. *Nature*. (1991) 351:453–6. doi: 10.1038/351453a0

73. Piccoli, L, Campo, I, Fregni, CS, Rodriguez, BM, Minola, A, Sallusto, F, et al. Neutralization and clearance of GM-CSF by autoantibodies in pulmonary alveolar proteinosis. *Nat Commun*. (2015) 6:7375. doi: 10.1038/ncomms8375

74. Shibata, Y, Berclaz, PY, Chroneos, ZC, Yoshida, M, Whitsett, JA, and Trapnell, BC. GM-CSF regulates alveolar macrophage differentiation and innate immunity in the lung through PU.1. *Immunity*. (2001) 15:557–67. doi: 10.1016/s1074-7613(01)00218-7

75. Jarrell, JA, Baker, MC, Perugino, CA, Liu, H, Bloom, MS, Maehara, T, et al. Neutralizing anti-IL-1 receptor antagonist autoantibodies induce inflammatory and fibrotic mediators in IgG4-related disease. *J Allergy Clin Immunol*. (2022) 149:358–68. doi: 10.1016/j.jaci.2021.05.002

76. Zahran, N, Sabry, O, and Raafat, M. Granulocyte macrophage colony stimulating factor as an adjuvant in ESRD at high risk of bacterial infection. *J Med Sci*. (2019) 19:17–23. doi: 10.3923/jms.2019.17.23

77. Baek, JH, Agarwal, ML, Tubbs, RR, Vladisavljevic, A, Tomita, H, Bukowski, RM, et al. In vivo recombinant adenovirus-mediated p53 gene therapy in a syngeneic rat model for colorectal cancer. *J Korean Med Sci*. (2004) 19:834–41. doi: 10.3346/jkms.2004.19.6.834

78. Parker, LP, Wolf, JK, and Price, JE. Adenoviral-mediated gene therapy with Ad5CMVp53 and Ad5CMVp21 in combination with standard therapies in human breast cancer cell lines. *Ann Clin Lab Sci*. (2000) 30:395–405. PMID: 11045764

79. Guevara, NV, Kim, HS, Antonova, EI, and Chan, L. The absence of p53 accelerates atherosclerosis by increasing cell proliferation in vivo. *Nat Med*. (1999) 5:335–9. doi: 10.1038/6585

80. Merched, AJ, Williams, E, and Chan, L. Macrophage-specific p53 expression plays a crucial role in atherosclerosis development and plaque remodeling. *Arterioscler Thromb Vasc Biol*. (2003) 23:1608–14. doi: 10.1161/01.Atv.0000084825.88022.53

81. van Vlijmen, BJ, Gerritsen, G, Franken, AL, Boesten, LS, Kockx, MM, Gijbels, MJ, et al. Macrophage p53 deficiency leads to enhanced atherosclerosis in APOE*3-Leiden transgenic mice. *Circ Res*. (2001) 88:780–6. doi: 10.1161/hh0801.089261

82. Liu, J, Li, W, Li, Y, Chen, T, El-Dahr, S, Feng, Y, et al. Abstract 15: loss of tumor suppressor protein p53 is linked to high blood pressure. *Hypertension*. (2013) 62:A15. doi: 10.1161/hyp.62.suppl_1.A15

83. Hollander, W. Role of hypertension in atherosclerosis and cardiovascular disease. *Am J Cardiol*. (1976) 38:786–800. doi: 10.1016/0002-9149(76)90357-x

84. Kannel, WB, Neaton, JD, Wentworth, D, Thomas, HE, Stamler, J, Hulley, SB, et al. Overall and coronary heart disease mortality rates in relation to major risk factors in 325,348 men screened for the MRFIT. Multiple risk factor intervention trial. *Am Heart J*. (1986) 112:825–36. doi: 10.1016/0002-8703(86)90481-3

85. Stamler, J, Neaton, JD, and Wentworth, DN. Blood pressure (systolic and diastolic) and risk of fatal coronary heart disease. *Hypertension*. (1989) 13:I2–I12. doi: 10.1161/01.hyp.13.5_suppl.i2

86. Goldstein, LB, Bushnell, CD, Adams, RJ, Appel, LJ, Braun, LT, Chaturvedi, S, et al. Guidelines for the primary prevention of stroke: a guideline for healthcare professionals from the American Heart Association/American Stroke Association. *Stroke*. (2011) 42:517–84. doi: 10.1161/STR.0b013e3181fcb238

87. Alloubani, A, Saleh, A, and Abdelhafiz, I. Hypertension and diabetes mellitus as a predictive risk factors for stroke. *Diabetes Metab Syndr*. (2018) 12:577–84. doi: 10.1016/j.dsx.2018.03.009

88. Atabek, ME, Akyürek, N, Eklioglu, BS, and Alp, H. Impaired systolic blood dipping and nocturnal hypertension: an independent predictor of carotid intima-media thickness in type 1 diabetic patients. *J Diabetes Complicat*. (2014) 28:51–5. doi: 10.1016/j.jdiacomp.2013.09.007

89. Johnston, SC, Fayad, PB, Gorelick, PB, Hanley, DF, Shwayder, P, van Husen, D, et al. Prevalence and knowledge of transient ischemic attack among US adults. *Neurology*. (2003) 60:1429–34. doi: 10.1212/01.wnl.0000063309.41867.0f

90. Rothwell, PM, Giles, MF, Chandratheva, A, Marquardt, L, Geraghty, O, Redgrave, JN, et al. Effect of urgent treatment of transient ischaemic attack and minor stroke on early recurrent stroke (EXPRESS study): a prospective population-based sequential comparison. *Lancet*. (2007) 370:1432–42. doi: 10.1016/s0140-6736(07)61448-2

91. Zock, E, Kerkhoff, H, and Kleyweg, RP. Initial reactions of patients after a stroke: more than half undertake no action. *Ned Tijdschr Geneeskd*. (2012) 156:A4336. PMID: 22748365

92. Kang, BY, Wang, W, Palade, P, Sharma, SG, and Mehta, JL. Cardiac hypertrophy during hypercholesterolemia and its amelioration with rosuvastatin and amlodipine. *J Cardiovasc Pharmacol*. (2009) 54:327–34. doi: 10.1097/FJC.0b013e3181b76713

93. Aude, YW, and Mehta, JL. Nonplatelet-mediated effects of aspirin. *Drugs Today (Barc)*. (2002) 38:501–7. doi: 10.1358/dot.2002.38.7.820117

94. Hörl, G, Froehlich, H, Ferstl, U, Ledinski, G, Binder, J, Cvirn, G, et al. Simvastatin efficiently lowers small LDL-IgG immune complex levels: a therapeutic quality beyond the lipid-lowering effect. *PLoS One*. (2016) 11:e0148210. doi: 10.1371/journal.pone.0148210

95. Hadi, NR, Mohammad, BI, Ajeena, IM, and Sahib, HH. Antiatherosclerotic potential of clopidogrel: antioxidant and anti-inflammatory approaches. *Biomed Res Int*. (2013) 2013:790263. doi: 10.1155/2013/790263

frontiers | Frontiers in Cardiovascular Medicine

TYPE Original Research
PUBLISHED 03 May 2023
DOI 10.3389/fcvm.2023.1161761

OPEN ACCESS

EDITED BY
Ying Wang,
University of British Columbia, Canada

REVIEWED BY
Joshua Dubland,
Provincial Health Services Authority, Canada
Xiaofeng Yang,
Temple University, United States
Baiba Vilne,
Riga Stradiņš University, Latvia

*CORRESPONDENCE
Farideh Razi
f-razi@tums.ac.ir
Bagher Larijani
emrc@tums.ac.ir

†These authors have contributed equally to this work

RECEIVED 08 February 2023
ACCEPTED 17 April 2023
PUBLISHED 03 May 2023

CITATION
Dehghanbanadaki H, Dodangeh S, Parhizkar Roudsari P, Hosseinkhani S, Khashayar P, Noorchenarboo M, Rezaei N, Dilmaghani-Marand A, Yoosefi M, Arjmand B, Khalagi K, Najjar N, Kakaei A, Bandarian F, Aghaei Meybodi H, Larijani B and Razi F (2023) Metabolomics profile and 10-year atherosclerotic cardiovascular disease (ASCVD) risk score.
Front. Cardiovasc. Med. 10:1161761.
doi: 10.3389/fcvm.2023.1161761

Metabolomics profile and 10-year atherosclerotic cardiovascular disease (ASCVD) risk score

Hojat Dehghanbanadaki[1†], Salimeh Dodangeh[1†], Peyvand Parhizkar Roudsari[2], Shaghayegh Hosseinkhani[3], Pouria Khashayar[4], Mohammad Noorchenarboo[5], Negar Rezaei[6], Arezou Dilmaghani-Marand[6], Moein Yoosefi[6], Babak Arjmand[7], Kazem Khalagi[8,9], Niloufar Najjar[10], Ardeshir Kakaei[9], Fatemeh Bandarian[10], Hamid Aghaei Meybodi[11], Bagher Larijani[1*] and Farideh Razi[10*]

[1]Endocrinology and Metabolism Research Center, Endocrinology and Metabolism Clinical Sciences Institute, Tehran University of Medical Sciences, Tehran, Iran, [2]Diabetes Research Center, Endocrinology and Metabolism Clinical Sciences Institute, Tehran University of Medical Sciences, Tehran, Iran, [3]Metabolic Disorders Research Center, Endocrinology and Metabolism Molecular—Cellular Sciences Institute, Tehran University of Medical Sciences, Tehran, Iran, [4]Institute of Cardiovascular and Medical Sciences, University of Glasgow, Glasgow, United Kingdom, [5]Department of Epidemiology and Biostatistics, School of Public Health, Tehran University of Medical Sciences, Tehran, Iran, [6]Non-Communicable Diseases Research Center, Endocrinology and Metabolism Population Sciences Institute, Tehran University of Medical Sciences, Tehran, Iran, [7]Cell Therapy and Regenerative Medicine Research Center, Endocrinology and Metabolism Molecular-Cellular Sciences Institute, Tehran, Iran, [8]Obesity and Eating Habits Research Center, Endocrinology and Metabolism Clinical Sciences Institute, Tehran University of Medical Sciences, Tehran, Iran, [9]Osteoporosis Research Center, Endocrinology and Metabolism Clinical Sciences Institute, Tehran University of Medical Sciences, Tehran, Iran, [10]Metabolomics and Genomics Research Center, Endocrinology and Metabolism Molecular-Cellular Sciences Institute, Tehran University of Medical Sciences, Tehran, Iran, [11]Personalized Medicine Research 10-Center, Endocrinology and Metabolism Clinical Sciences Institute, Tehran University of Medical Sciences, Tehran, Iran

Background: The intermediate metabolites associated with the development of atherosclerotic cardiovascular disease (ASCVD) remain largely unknown. Thus, we conducted a large panel of metabolomics profiling to identify the new candidate metabolites that were associated with 10-year ASCVD risk.

Methods: Thirty acylcarnitines and twenty amino acids were measured in the fasting plasma of 1,102 randomly selected individuals using a targeted FIA-MS/MS approach. The 10-year ASCVD risk score was calculated based on 2013 ACC/AHA guidelines. Accordingly, the subjects were stratified into four groups: low-risk ($n = 620$), borderline-risk ($n = 110$), intermediate-risk ($n = 225$), and high-risk ($n = 147$). 10 factors comprising collinear metabolites were extracted from principal component analysis.

Results: C_4DC, $C_{8:1}$, $C_{16}OH$, citrulline, histidine, alanine, threonine, glycine, glutamine, tryptophan, phenylalanine, glutamic acid, arginine, and aspartic acid were significantly associated with the 10-year ASCVD risk score (p-values $\leq$ 0.044). The high-risk group had higher odds of factor 1 (12 long-chain acylcarnitines, OR = 1.103), factor 2 (5 medium-chain acylcarnitines, OR = 1.063), factor 3 (methionine, leucine, valine, tryptophan, tyrosine, phenylalanine, OR = 1.074), factor 5 (6 short-chain acylcarnitines, OR = 1.205), factor 6 (5 short-chain

Abbreviations
CVD, cardiovascular disease; ASCVD, atherosclerotic cardiovascular disease; ACC, American college of cardiology; AHA, American heart association; HDL-C, high-density lipoprotein cholesterol; KMO, Kaiser-Meyer-Olkin; PCA, principal component analysis; KEGG, kyoto encyclopedia of genes and genomes; BMI, body mass index; BCAA, branched-chain amino acid; AAA, aromatic amino acid; WC, waist circumference; HC, hip circumference; SBP, systolic blood pressure; DBP, diastolic blood pressure; TG, triglyceride; Non-HDL-C, non-high-density lipoprotein cholesterol; HbA1c, hemoglobin A1c; FPG, fasting plasma glucose; OR, odds ratio.

acylcarnitines, OR = 1.229), factor 7 (alanine, proline, OR = 1.343), factor 8 ($C_{18:2}$OH, glutamic acid, aspartic acid, OR = 1.188), and factor 10 (ornithine, citrulline, OR = 1.570) compared to the low-risk ones; the odds of factor 9 (glycine, serine, threonine, OR = 0.741), however, were lower in the high-risk group. "D-glutamine and D-glutamate metabolism", "phenylalanine, tyrosine, and tryptophan biosynthesis", and "valine, leucine, and isoleucine biosynthesis" were metabolic pathways having the highest association with borderline/intermediate/high ASCVD events, respectively.

Conclusions: Abundant metabolites were found to be associated with ASCVD events in this study. Utilization of this metabolic panel could be a promising strategy for early detection and prevention of ASCVD events.

KEYWORDS

cardiovascular disease, ASCVD, metabolomics, amino acids, acylcarnitine

Introduction

Cardiovascular disease (CVD) is a disorder of the heart/vessels known as the most important reason behind global mortality. The contribution of CVD to the death rate has increased continuously (1, 2). Therefore, it is crucial to identify high-risk individuals to prevent CVD and its associated complications and reduce the burden of the disease and mortality (3). To this purpose, different CVD risk assessment scoring systems have been developed so far (4). One of the recent most-applied tools is the 10-year atherosclerotic CVD (ASCVD) risk index that was presented by the American Heart Association (AHA)/ the American College of Cardiology (ACC) (5). This risk score was calculated based on several characteristics of individuals including age, sex, race, total cholesterol, high-density lipoprotein cholesterol (HDL-C), systolic blood pressure, antihypertensive treatment, smoking status, and diabetes mellitus history (6, 7).

Although there have been many advances in the development of predictive CVD risk assessment tools, the underlying molecular pathomechanisms of ASCVD events are largely unrecognized. This issue revealed the necessity for conducting metabolomics analysis (8). The metabolomics approach allows for a better understanding of the intermediate metabolites associated with ASCVD events and leads to the identification of new diagnostic and therapeutic strategies (9, 10). Indeed, physiologic perturbations, particularly in individuals at high risk of ASCVD events, can rapidly affect metabolite profiling, which can be targeted for disease management (11). Herein, several metabolomics studies have been conducted to determine the association between metabolic profiles and CVD risk, which showed that branched-chain amino acids and urea cycle-related metabolites, were associated with higher cardiovascular risk (12, 13). However, these studies identified the association between a number of acylcarnitines/amino acids and CVD risk, but the results are not easily comparable, e.g., isoleucine, leucine, and glutamine were associated with cardiovascular events in one study (13) while these metabolites were not associated with an increased incidence of cardiovascular events in another study (12). So, intermediate metabolites associated with developing ASCVD events remain largely unknown. Thus, to better understand the pathogenesis of the disease, in this study, we conducted the comprehensive metabolomics profiling of plasma in a large-scale Iranian population and determined the association between plasma metabolite levels and the 10-year ASCVD risk score.

Methods

Study subjects

1,102 individuals aged between 40 and 79 years old with LDL levels less than 190 mg/dl and no pre-existing coronary artery disease or myocardial infarction were randomly selected from a survey of Surveillance of Risk Factors of Non-Communicable Diseases in Iran (STEPs 2016). In brief, the STEPs 2016 protocol, previously published, includes 31,050 individuals older than 18 years from the rural and urban areas of 389 Iranian districts selected using a systematic cluster random sampling (14). The study protocol conforms to the ethical guidelines of the 1975 Declaration of Helsinki. The Ethics Committee of Tehran University of Medical Sciences and Endocrine & Metabolism Research Institute approved the study protocol with the ID number IR.TUMS.EMRI.REC.1395.00141, and written informed consent was obtained before participation.

Blood sampling and laboratory assessment

The blood was sampled from peripheral venous following at least 12 h of overnight fasting and stored in sodium fluoride plus EDTA tubes. A part of the whole blood was used for HbA1c measurement and the plasma of the remaining blood was isolated for other biochemical laboratory testing using commercial Roche kits (Roche Diagnostics, Mannheim, Germany) and Cobas C311 auto analyzer.

Plasma metabolic profiling

The concentration of 30 acylcarnitines and 20 amino acids were measured in plasma using flow injection tandem mass

spectrometry (triple quadrupole SCIEX API 3,200 with electrospray ionization) equipped with a Thermo Scientific Dionex UltiMate 3,000 standard HPLC system and a derivatization method with butanol-HCL (15). Briefly, the mixture of plasma samples and internal standard were centrifuged at 4°C. Supernatant fluids were collected in new vials and dried with nitrogen 99.9% at 45°C. Derivatization solution, a combination of 1-butanol and acetyl chloride, was then added to the vials with the aim of protein precipitation. Also, derivatization with butanol-HCL has the benefit of simultaneous derivatization of amino acids and acylcarnitines which makes the measurement, faster and cheaper. After vortexing, they were incubated at 65°C for 15 min with the advantage of the effective destruction of phospholipids. The samples were dried with nitrogen 99.9% at 45°C, then dissolved in 100 µl of mobile phase solution, a mix of water and acetonitrile, before injection. Ratios of the signals of the metabolites relative to the internal standards were used to make calibration curves and calculate analyte concentrations in the QC materials and samples.

10-year ASCVD risk score assessment

The 10-year risk for primary atherosclerotic cardiovascular disease was calculated based on pooled cohort equations in the 2013 ACC/AHA Guidelines (16). The equation predicts the risk of stroke, nonfatal myocardial infarction, and coronary artery disease death within 10 years in subjects aged between 40 and 79 years old with LDL < 190 mg/dl and no pre-existing ASCVD events. The equation takes into account age, gender, race, HDL cholesterol, total cholesterol, systolic blood pressure, the use of hypertension drugs, smoking habits, and diabetes. The individuals were stratified into four groups according to their 10-year ASCVD risk score and the threshold was determined based on the special report from AHA/ACC (6): (1) Low-risk group ($n = 620$) with a score of 0% to 5%, (2) Borderline-risk group ($n = 110$) with a score of 5% to 7.5%, (3) Intermediate-risk group ($n = 225$) with a score of 7.5% to 20%, and (4) High-risk group ($n = 147$) with a score of 20% or more.

Statistical analysis

SPSS version 19.0 was used for statistical analyses. The workflow diagram of the statistical analysis is presented in **Additional File S1**. After checking the normality by Kolmogorov–Smirnov test, mean (± standard deviation) and median (interquartile range) were applied to describe continuous variables with and without normal distributions, respectively. Number and percentage (%) were applied to describe categorical variables. Chi-squared test was used to compare the frequency of categorical variables between the groups. ANOVA test and Bonferroni *post hoc* test were used to compare normally distributed variables between the groups. The Kruskal-Wallis and Mann–Whitney U tests were used to compare non-normally distributed variables between the groups. Benjamini-Hochberg method was applied for the adjustment of *p*-values obtained from the Kruskal-Wallis H test of the metabolite concentrations. The correlation between the metabolite concentrations and the 10-year ASCVD risk was determined using the Spearman correlation coefficient and the stepwise multiple linear regression analysis methods. To standardize the data on metabolite level, we calculated the natural logarithm of metabolite concentration and considered their Z value for logistic regression analysis and factor analysis. Binary logistic regression analysis was used to determine the odds ratio (OR) of metabolite profile in the borderline/intermediate/high-risk groups compared to the low-risk one. For factor analysis, the Kaiser-Meyer-Olkin (KMO) test and Bartlett's Test of Sphericity were used to investigate the adequacy of sample size and for statistical comparison of the correlation matrix with the identity matrix. KMO values ≥ 0.80 were considered credible. Principal component analysis (PCA) with varimax rotation was performed to reduce the metabolites into a smaller subclass of orthogonal (uncorrelated) factors. The extracted factors with eigenvalues higher than 1.0 and metabolites with loading scores more than 0.4 were considered important for the given PCA. The factor score was calculated through the sum of obtained metabolite concentrations multiplied by their loading matrix which was obtained from the rotated component matrix with the rotation method of Varimax with Kaiser Normalization (**Additional File S2**). Furthermore, MetaboAnalyst (Version 5.0) based on the metabolic Kyoto Encyclopedia of Genes and Genomes (KEGG) database was used for enrichment pathway analysis of metabolic alterations between study groups that were identified from logistic regression analysis. The enrichment ratio is calculated based on the observed hits divided by expected hits. A *p*-value less than 0.05 was considered significant in all analyses.

Results

General characteristics of the study population

The study population comprised 1,102 participants with a mean age of 54.41 ± 10.22 years and a female percentage of 53.27%. The sociodemographic and laboratory characteristics of the low/borderline/intermediate/high ASCVD risk groups are shown in **Table 1**. The groups had no significant difference with regard to BMI and cholesterol levels (*p*-value ≥ 0.056).

Metabolite profile as a 10-year ASCVD risk score predictor

Tables 2, **3** demonstrate the median (interquartile range) of plasma concentration of 30 acylcarnitines and 20 amino acids in

TABLE 1 The general characteristics of participants stratified by 10-year ASCVD risk score.

Variables		Low-risk ($n = 620$)	Borderline-risk ($n = 110$)	Intermediate-risk ($n = 225$)	High-risk ($n = 147$)	*p*-value
Age (year)		48.32 ± 5.98	55.15 ± 7.05	60.34 ± 7.33	70.53 ± 6.64	**<0.001**
Female, *n* (%)		425 (69)	47 (43)	72 (32)	43 (29)	**<0.001**
BMI (kg/m^2)		28.24 ± 5.32	28.17 ± 4.97	27.15 ± 4.73	27.50 ± 4.81	0.056
WC (cm)		93.92 ± 13.27	96.17 ± 13.00	96.11 ± 12.89	98.03 ± 13.02	**<0.001**
HC (cm)		103.54 ± 11.59	103.27 ± 10.84	101.25 ± 9.79	101.13 ± 10.82	**0.002**
WC/HC		0.91 ± 0.09	0.93 ± 0.09	0.95 ± 0.08	0.97 ± 0.10	**<0.001**
SBP (mm Hg)		124.44 ± 16.01	131.25 ± 18.53	138.80 ± 21.37	151.34 ± 20.31	**<0.001**
DBP (mm Hg)		78.79 ± 10.63	80.19 ± 11.20	84.21 ± 12.63	84.79 ± 13.33	**<0.001**
HDL-C (mg/dl)		42.91 ± 11.31	39.51 ± 10.88	38.82 ± 11.37	39.16 ± 11.56	**<0.001**
TG (mg/dl)		126.19 ± 74.98	147.81 ± 85.08	166.96 ± 158.20	138.94 ± 79.30	**<0.001**
Cholesterol (mg/dl)		167.24 ± 33.65	169.13 ± 33.84	171.78 ± 38.93	167.92 ± 38.95	0.414
Non-HDL-C (mg/dl)		124.34 ± 33.22	129.62 ± 34.27	132.96 ± 39.57	128.76 ± 36.12	**0.025**
HbA1c (%)		5.56 ± 0.71	5.93 ± 1.26	6.15 ± 1.35	6.57 ± 1.53	**<0.001**
FPG (mg/dl)		95.80 ± 23.37	109.16 ± 53.20	110.13 ± 44.08	119.07 ± 51.05	**<0.001**
10-year ASCVD risk		2.05 ± 1.26	6.11 ± 0.68	12.70 ± 3.65	33.67 ± 12.09	**<0.001**
Area of living, *n* (%)	Rural	201 (32)	36 (33)	85 (38)	45 (31)	**<0.001**
	Urban	419 (68)	74 (67)	140 (62)	102 (69)	
Education (years), *n* (%)	<1	113 (18)	23 (21)	77 (34)	57 (39)	**<0.001**
	1 to 6	216 (35)	39 (35)	74 (33)	51 (35)	
	7 to 12	215 (35)	37 (34)	46 (20)	17 (12)	
	>12	76 (12)	11 (10)	28 (12)	22 (15)	
Smoking, *n* (%)		46 (7)	21 (19)	61 (27)	31 (21)	**<0.001**
Diabetes, *n* (%)		36 (6)	22 (20)	52 (23)	71 (48)	**<0.001**

BMI, body mass index; WC, waist circumference; HC, hip circumference; SBP, systolic blood pressure; DBP, diastolic blood pressure; HDL-C, high density lipoprotein cholesterol; TG, triglyceride; Non-HDL-C, non-high-density lipoprotein cholesterol; HbA1c, hemoglobin A1c; FPG, fasting plasma glucose.

TABLE 2 The plasma concentration for acylcarnitines stratified by 10-year ASCVD risk score.

Acylcarnitines (μmol/l)	Low-risk	Borderline-risk	Intermediate-risk	High-risk	FDR*
C_0	54.251 (45.854–61.755)	56.876 (48.720–66.211)	58.995 (50.103–66.252)	55.313 (47.701–66.281)	**<0.001**
C_2	13.547 (11.317–16.249)	14.232 (11.583–16.534)	13.665 (11.762–16.310)	14.752 (12.163–17.516)	**0.014**
C_3	0.734 (0.571–0.955)	0.856 (0.666–1.180)	0.878 (0.695–1.117)	0.934 (0.697–1.172)	**<0.001**
C_3DC	0.072 (0.055–0.099)	0.079 (0.063–0.101)	0.080 (0.057–0.106)	0.090 (0.067–0.117)	**<0.001**
C_4	0.363 (0.286–0.490)	0.393 (0.307–0.556)	0.412 (0.334–0.515)	0.437 (0.346–0.536)	**<0.001**
C_4OH	0.049 (0.038–0.065)	0.053 (0.043–0.065)	0.052 (0.040–0.067)	0.057 (0.045–0.075)	**<0.001**
C_4DC	0.062 (0.048–0.078)	0.070 (0.057–0.084)	0.071 (0.058–0.087)	0.075 (0.059–0.101)	**<0.001**
C_5	0.197 (0.155–0.256)	0.221 (0.174–0.269)	0.239 (0.187–0.304)	0.237 (0.192–0.296)	**<0.001**
$C_{5:1}$	0.035 (0.027–0.052)	0.040 (0.029–0.052)	0.037 (0.030–0.054)	0.041 (0.031–0.058)	**0.002**
C_5OH	0.060 (0.051–0.072)	0.068 (0.056–0.078)	0.066 (0.057–0.077)	0.069 (0.061–0.079)	**<0.001**
C_5DC	0.283 (0.229–0.366)	0.318 (0.266–0.386)	0.325 (0.253–0.401)	0.351 (0.277–0.449)	**<0.001**
C_6	0.164 (0.120–0.239)	0.169 (0.129–0.230)	0.170 (0.123–0.242)	0.183 (0.136–0.260)	0.140
C_8	0.245 (0.167–0.353)	0.253 (0.188–0.372)	0.251 (0.175–0.370)	0.275 (0.192–0.415)	0.080
$C_{8:1}$	0.284 (0.199–0.408)	0.329 (0.258–0.458)	0.290 (0.216–0.416)	0.322 (0.225–0.408)	**0.009**
C_{10}	0.315 (0.215–0.481)	0.331 (0.245–0.491)	0.323 (0.212–0.483)	0.358 (0.242–0.567)	0.057
$C_{10:1}$	0.320 (0.230–0.441)	0.340 (0.257–0.453)	0.315 (0.224–0.458)	0.340 (0.251–0.502)	0.150
C_{12}	0.120 (0.092–0.173)	0.135 (0.101–0.172)	0.137 (0.104–0.183)	0.151 (0.104–0.207)	**<0.001**
C_{14}	0.049 (0.039–0.064)	0.055 (0.043–0.068)	0.056 (0.045–0.073)	0.061 (0.045–0.081)	**<0.001**
$C_{14:1}$	0.109 (0.081–0.162)	0.116 (0.090–0.158)	0.111 (0.082–0.167)	0.125 (0.088–0.187)	0.080
$C_{14:2}$	0.085 (0.063–0.116)	0.086 (0.071–0.115)	0.088 (0.065–0.121)	0.096 (0.072–0.135)	0.161
C_{14}OH	0.011 (0.008–0.014)	0.012 (0.009–0.015)	0.013 (0.010–0.016)	0.014 (0.010–0.018)	**<0.001**
C_{16}	0.168 (0.142–0.203)	0.175 (0.157–0.214)	0.184 (0.152–0.224)	0.189 (0.160–0.231)	**<0.001**
C_{16}OH	0.010 (0.008–0.012)	0.011 (0.008–0.013)	0.012 (0.010–0.014)	0.013 (0.010–0.016)	**<0.001**
$C_{16:1}$OH	0.015 (0.012–0.020)	0.016 (0.013–0.021)	0.017 (0.013–0.024)	0.018 (0.014–0.026)	**<0.001**
$C_{16:1}$	0.042 (0.032–0.058)	0.044 (0.033–0.056)	0.044 (0.034–0.061)	0.050 (0.036–0.068)	**0.005**
C_{18}	0.060 (0.049–0.073)	0.065 (0.052–0.077)	0.067 (0.056–0.086)	0.068 (0.056–0.084)	**<0.001**
$C_{18:1}$	0.169 (0.135–0.218)	0.177 (0.138–0.222)	0.177 (0.143–0.231)	0.174 (0.145–0.230)	0.068
C_{18}OH	0.008 (0.006–0.010)	0.008 (0.007–0.010)	0.009 (0.007–0.011)	0.010 (0.008–0.012)	**<0.001**
$C_{18:1}$OH	0.011 (0.009–0.014)	0.012 (0.010–0.015)	0.012 (0.010–0.016)	0.013 (0.010–0.017)	**<0.001**
$C_{18:2}$OH	0.027 (0.021–0.035)	0.029 (0.022–0.037)	0.029 (0.022–0.038)	0.029 (0.024–0.039)	**0.015**

*FDR: False Discovery Rate (Adjusted P-value).

TABLE 3 The plasma concentration for amino acids stratified by a 10-year ASCVD risk score.

Amino acids (μmol/l)	Low-risk	Borderline-risk	Intermediate-risk	High-risk	FDR*
Alanine	401.30 (337.65–471.10)	426.40 (363.60–494.50)	426.50 (374.40–479.20)	423.00 (373.20–499.10)	**<0.001**
Aspartic acid	12.45 (10.10–14.75)	12.65 (10.40–15.00)	12.50 (10.60–14.70)	12.40 (10.00–14.60)	0.844
Glutamic acid	65.50 (57.90–72.20)	68.55 (62.50–75.20)	68.80 (61.90–77.20)	67.30 (61.90–76.00)	**<0.001**
Leucine	118.65 (102.85–134.40)	131.95 (109.50–146.60)	130.20 (115.40–150.70)	126.40 (115.30–147.30)	**<0.001**
Methionine	27.50 (24.60–31.70)	28.40 (24.50–31.90)	27.80 (24.80–31.90)	27.60 (24.40–30.50)	0.455
Phenylalanine	61.85 (55.00–69.20)	62.30 (55.30–69.30)	66.30 (59.20–73.50)	67.40 (60.20–73.60)	**<0.001**
Tyrosine	68.70 (59.80–79.10)	71.75 (65.10–80.30)	70.70 (63.90–82.00)	70.80 (63.30–80.50)	**0.005**
Valine	249.75 (220.95–282.30)	266.80 (236.50–303.60)	274.70 (239.00–310.10)	269.50 (237.80–299.20)	**<0.001**
Arginine	67.95 (56.00–83.65)	72.00 (60.10–82.30)	70.30 (54.40–83.50)	68.10 (55.50–80.70)	0.694
Citrulline	35.65 (30.20–40.70)	39.85 (34.50–45.20)	39.60 (33.20–45.10)	40.80 (35.30–48.20)	**<0.001**
Glycine	256.80 (211.0–327.55)	253.25 (222.60–298.00)	233.90 (203.10–284.00)	240.30 (206.40–293.60)	**0.003**
Ornithine	85.70 (73.20–100.00)	88.30 (76.00–105.60)	93.00 (81.30–111.50)	89.50 (76.70–104.40)	**<0.001**
Proline	230.30 (191.50–278.60)	253.75 (206.90–305.60)	257.60 (208.50–310.10)	251.00 (206.50–307.30)	**<0.001**
Threonine	138.24 (116.70–158.40)	136.45 (117.90–156.40)	138.24 (117.10–157.10)	123.90 (105.10–146.70)	**0.005**
Serine	102.05 (84.50–122.00)	99.65 (86.80–111.90)	96.90 (80.40–116.30)	93.80 (78.70–108.00)	**0.002**
Histidine	83.65 (74.85–94.60)	84.75 (76.40–96.20)	81.70 (71.90–92.90)	77.60 (69.30–87.00)	**<0.001**
Lysine	179.65 (148.25–204.45)	179.05 (155.80–206.90)	177.30 (148.60–207.50)	173.50 (145.00–206.30)	0.848
Tryptophan	69.85 (60.25–80.05)	71.30 (60.20–83.60)	71.60 (61.20–83.20)	66.60 (56.90–77.40)	**0.034**
Asparagine	46.70 (35.30–57.40)	47.51 (40.70–58.60)	44.70 (33.00–54.70)	44.00 (31.30–55.80)	0.087
Glutamine	516.95 (430.25–578.80)	506.65 (446.50–590.10)	518.07 (439.60–578.90)	512.90 (431.30–598.20)	0.925

*FDR: False Discovery Rate (Adjusted P-value).

the four study groups, respectively. For ease of visualization of the data scatter, the concentration of acylcarnitines/amino acids in the four study groups is plotted in **Additional File S3**. The correlation matrix between metabolites and general features of participants is shown in **Figure 1**. The significantly altered metabolites between male and female participants for the four study groups are shown in **Additional File S4**.

The result of the logistic regression on metabolites to discriminate borderline/intermediate/high ASCVD risk patients from low-risk ones is presented in **Additional File S5**. Patients with high ASCVD risk score were more likely to have an increase in the concentration of 24 acylcarnitines and nine amino acids (p-value ≤ 0.041) and were less likely to have an increase in five amino acids than low ASCVD risk group (p-value ≤ 0.010). Furthermore, an increase in 18 acylcarnitines and 13 amino acids was more likely to occur in intermediate ASCVD risk patients than in low ASCVD risk patients (p-value ≤ 0.044). However, an increase in two amino acids was less likely to occur in intermediate ASCVD risk patients than in low ASCVD risk patients (p-value ≤ 0.013). Patients with borderline ASCVD risk score were more likely to have an increase in 24 acylcarnitines and nine amino acids than low ASCVD risk patients (p-value ≤ 0.041) and were less likely to have an increase in five amino acids than low ASCVD risk patients (p-value ≤ 0.010). The logistic regression analysis was repeated after adjustment for BMI; in the new analysis, the significant p-values remained significant, and non-significant ones remained non-significant.

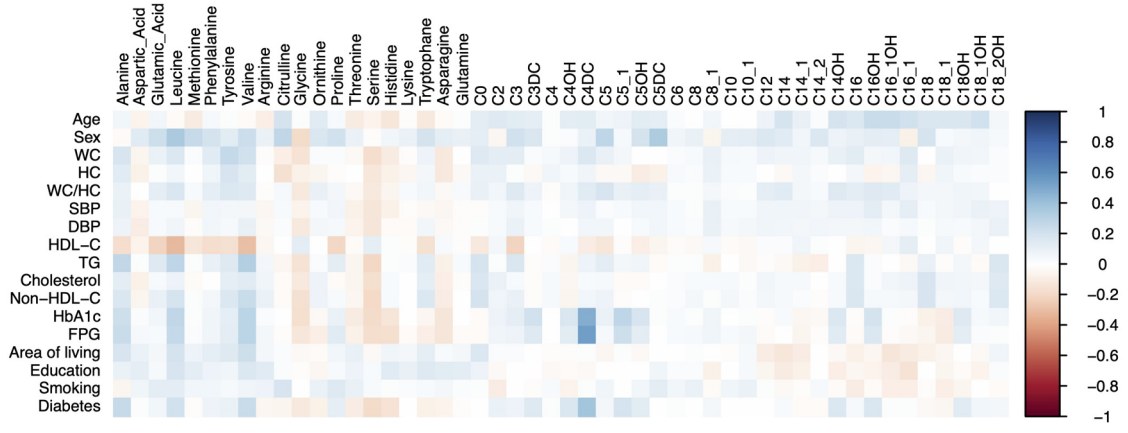

FIGURE 1
Correlation matrix between metabolites and general features of participants.

Metabolite profile and 10-year ASCVD risk

Additional File S6 shows the correlation between the metabolite profile and the 10-year ASCVD risk score. Thirty acylcarnitines and nine amino acids were positively associated with the ASCVD risk score ($p \leq 0.034$) and four amino acids were inversely related to it ($p \leq 0.026$). The strongest associations belonged to 3-OH-hexadecanoylcarnitine ($C_{16}OH$, $r = 0.279$, $p < 0.001$), propionyl carnitine (C_3, $r = 0.262$, $p < 0.001$), leucine ($r = 0.256$, $p < 0.001$), isovaleryl carnitine (C_5, $r = 0.251$, $p < 0.001$), and 3-OH-isovalerylcarnitine (C_5OH, $r = 0.250$, $p < 0.001$). The multiple linear regression on all measured metabolites is summarized in **Table 4**. Three acylcarnitines (methylmalonyl-/succinyl carnitine [C_4DC], octenoyl carnitine [$C_{8:1}$], and 3-OH-hexadecanoylcarnitine [$C_{16}OH$]) and 11 amino acids (citrulline, histidine, alanine, threonine, glycine, glutamine, tryptophan, phenylalanine, glutamic acid, arginine, aspartic acid) were concluded as possible predictors of the 10-year ASCVD risk score.

Metabolite-derived factors and ASCVD risk

In the factor analysis, the KMO coefficient was 0.874, indicating adequate sampling of data. A p-value of <0.001 from Bartlett's sphericity test suggested a statistical difference between the correlation and the identity matrix. Both tests revealed the data to be appropriate for factor analysis.

PCA analysis on the standardized metabolites resulted in 11 factors with an eigenvalue of more than one in the screen plot (**Additional File S7**). The logistic regression analysis of the borderline/intermediate/high-risk groups compared to the low-risk group is illustrated in **Table 5**. Patients with high ASCVD risk score were more likely to have an increase in factors 1, 2, 3, 5, 6, 7, 8, and 10 than low ASCVD risk group (p-value ≤ 0.009) and were less likely to have an increase in factor nine (p-value < 0.001). The

TABLE 5 The logistic regression between the factors extracted by PCA and 10-year ASCVD risk score.

Indices	Groups	OR	95% CI	*p*-value*
Factor 1	Borderline-risk	1.021	(0.984–1.059)	0.271
	Intermediate-risk	1.061	(1.034–1.089)	**0.000**
	High-risk	1.103	(1.072–1.134)	**0.000**
Factor 2	Borderline-risk	1.040	(0.984–1.099)	0.164
	Intermediate-risk	1.011	(0.965–1.060)	0.645
	High-risk	1.063	(1.015–1.112)	**0.009**
Factor 3	Borderline-risk	1.082	(1.020–1.147)	**0.009**
	Intermediate-risk	1.106	(1.058–1.156)	**0.000**
	High-risk	1.074	(1.019–1.132)	**0.008**
Factor 4	Borderline-risk	1.033	(0.960–1.112)	0.384
	Intermediate-risk	0.985	(0.930–1.042)	0.593
	High-risk	0.971	(0.907–1.039)	0.395
Factor 5	Borderline-risk	1.146	(1.061–1.238)	**0.001**
	Intermediate-risk	1.193	(1.125–1.265)	**0.000**
	High-risk	1.205	(1.128–1.287)	**0.000**
Factor 6	Borderline-risk	1.195	(1.077–1.327)	**0.001**
	Intermediate-risk	1.146	(1.055–1.245)	**0.001**
	High-risk	1.229	(1.121–1.348)	**<0.001**
Factor 7	Borderline-risk	1.346	(1.121–1.617)	**0.001**
	Intermediate-risk	1.294	(1.123–1.491)	**<0.001**
	High-risk	1.343	(1.140–1.582)	**<0.001**
Factor 8	Borderline-risk	1.184	(1.004–1.396)	0.045
	Intermediate-risk	1.275	(1.127–1.443)	**<0.001**
	High-risk	1.188	(1.025–1.377)	**0.022**
Factor 9	Borderline-risk	0.922	(0.795–1.070)	0.286
	Intermediate-risk	0.828	(0.737–0.930)	**0.001**
	High-risk	0.741	(0.642–0.856)	**<0.001**
Factor 10	Borderline-risk	1.473	(1.231–1.762)	**<0.001**
	Intermediate-risk	1.534	(1.336–1.762)	**<0.001**
	High-risk	1.570	(1.338–1.841)	**<0.001**
Factor 11	Borderline-risk	1.101	(0.801–1.513)	0.554
	Intermediate-risk	0.980	(0.770–1.247)	0.868
	High-risk	0.918	(0.690–1.223)	0.560

The reference category is the low-risk group.
*After adjustment for BMI, the significant p-values remain significant and non-significant p-values remain non-significant.

TABLE 4 The multiple linear regression of the metabolites influencing 10-year ASCVD risk score.

Metabolites	Unstandardized coefficients		Standardized coefficients	t	*p*-value
	β	Standard error	beta		
(Constant)	−0.265	2.922		−0.091	0.928
C_4DC	27.122	10.384	0.079	2.612	**0.009**
$C_{8:1}$	−5.143	1.886	−0.079	−2.727	**0.007**
$C_{16}OH$	426.657	76.198	0.166	5.599	**<0.001**
Citrulline	0.281	0.037	0.239	7.515	**<0.001**
Histidine	−0.14	0.025	−0.204	−5.503	**<0.001**
Alanine	0.015	0.004	0.129	4.232	**<0.001**
Threonine	−0.037	0.011	−0.111	−3.37	**0.001**
Glycine	−0.014	0.004	−0.098	−3.395	**0.001**
Glutamine	0.013	0.003	0.139	3.882	**<0.001**
Tryptophane	−0.097	0.022	−0.144	−4.468	**<0.001**
Phenylalanine	0.109	0.032	0.114	3.405	**0.001**
Glutamic acid	0.089	0.031	0.099	2.901	**0.004**
Arginine	−0.038	0.018	−0.065	−2.076	**0.038**
Aspartic acid	−0.213	0.106	−0.069	−2.017	**0.044**

intermediate-risk group was more likely to have an increase in factors 1, 3, 5, 6, 7, 8, and 10 than the low-risk group (p-value ≤ 0.001) and was less likely to have an increase in factor 9 than the low-risk group (p-value = 0.001). Patients with borderline ASCVD risk score were more likely to have an increase in factors 3, 5, 6, 7, and 10 than the low-risk group (p-value ≤ 0.009).

The enriched metabolic pathways mediated between study groups

The results of pathway enrichment analysis of altered metabolites in low ASCVD risk group with borderline/intermediate/high ASCVD risk groups are summarized in **Additional File S8**. The differential metabolites between the low ASCVD risk group and borderline/intermediate/high ASCVD risk groups were mainly associated with the biological processes of "aminoacyl-tRNA biosynthesis", "arginine biosynthesis", "D-glutamine and D-glutamate metabolism", "valine, leucine and isoleucine biosynthesis", and "phenylalanine, tyrosine, and tryptophan biosynthesis" (**Figures 2A–C**). The metabolic pathways with the highest enrichment ratio in explaining the differences in metabolic profile between the low ASCVD risk group and the borderline/intermediate/high ASCVD risk groups were "D-glutamine and D-glutamate metabolism", "phenylalanine, tyrosine, and tryptophan biosynthesis", and "valine, leucine, and isoleucine biosynthesis", respectively. The working model of the metabolic perturbance is shown in **Figure 3**.

Discussion

It has been discovered that the metabolite profile has a significant correlation with ASCVD risk such as coronary artery disease. Moreover, certain metabolic features can be considered independent and valuable predictors of cardiovascular events with regard to early diagnosis, treatment strategies, and better risk stratification (13). In this study, the 10-year ASCVD risk score was used to classify individuals into four groups: low-, borderline-, intermediate-, and high-risk of ASCVD events. Consequently, their metabolite profile (the plasma concentration of 30 acylcarnitines and 20 amino acids) was measured to determine the association between metabolite profile and the risk of 10-year ASCVD events.

The results of our study indicated a positive correlation between all 30 acylcarnitines, alanine, glutamic acid, leucine, phenylalanine, tyrosine, valine, citrulline, ornithine, and proline and the 10-year ASCVD risk score and a negative correlation of glycine, threonine, serine, and histidine with this score. In accordance with our findings, Würtz P et al. (12) showed a positive correlation between the circulating concentrations of phenylalanine and tyrosine and cardiovascular risk. Ruiz-Canela M et al. (17) in a case-cohort study have shown the direct correlation between higher concentrations of branched-chain amino acids (BCAAs) including leucine and valine, and higher CVD risk. The important role of BCAAs as the predictive markers of cardiovascular events has been also suggested in another study by Hu W et al. (18). Vaarhorst AA et al. (19) reported that blood concentrations of valine, ornithine, and glutamate were associated with coronary heart disease. Shah SH et al. (13) found a considerable association between the plasma levels of glutamate, leucine, isoleucine, citrulline, C_2, C_8, $C_{10:1}$, $C_{14:2}$ and CVD risk in the same direction that we found in the current study. Besides, the elevated levels of serum C2 and C8 acylcarnitines are in relation to higher cardiovascular death risk. They could also be correlated with a modest increase in the risk of fatal/nonfatal acute myocardial infarction in patients with stable angina pectoris (20). As shown in **Table 6**, these findings from the previous studies are in line with our findings.

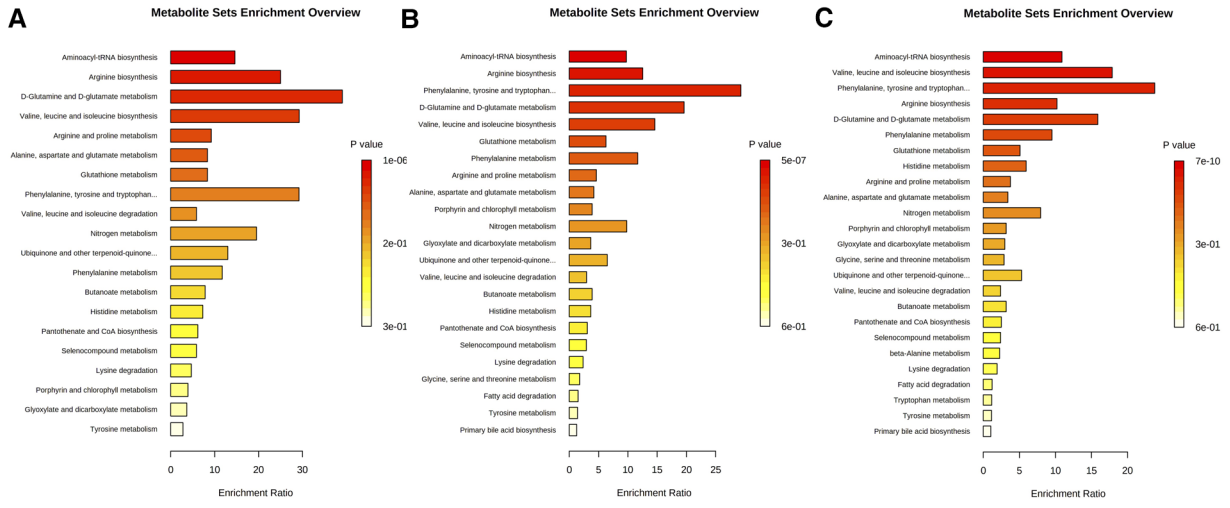

FIGURE 2
Pathway enrichment analysis between (**A**) low ASCVD risk group and borderline ASCVD risk group, (**B**) low ASCVD risk group and intermediate ASCVD risk group, and (**C**) low ASCVD risk group and high ASCVD risk group. The color of each pathway is based on the p-value [-log(p): logarithm of the p-value, Fisher's test p-value].

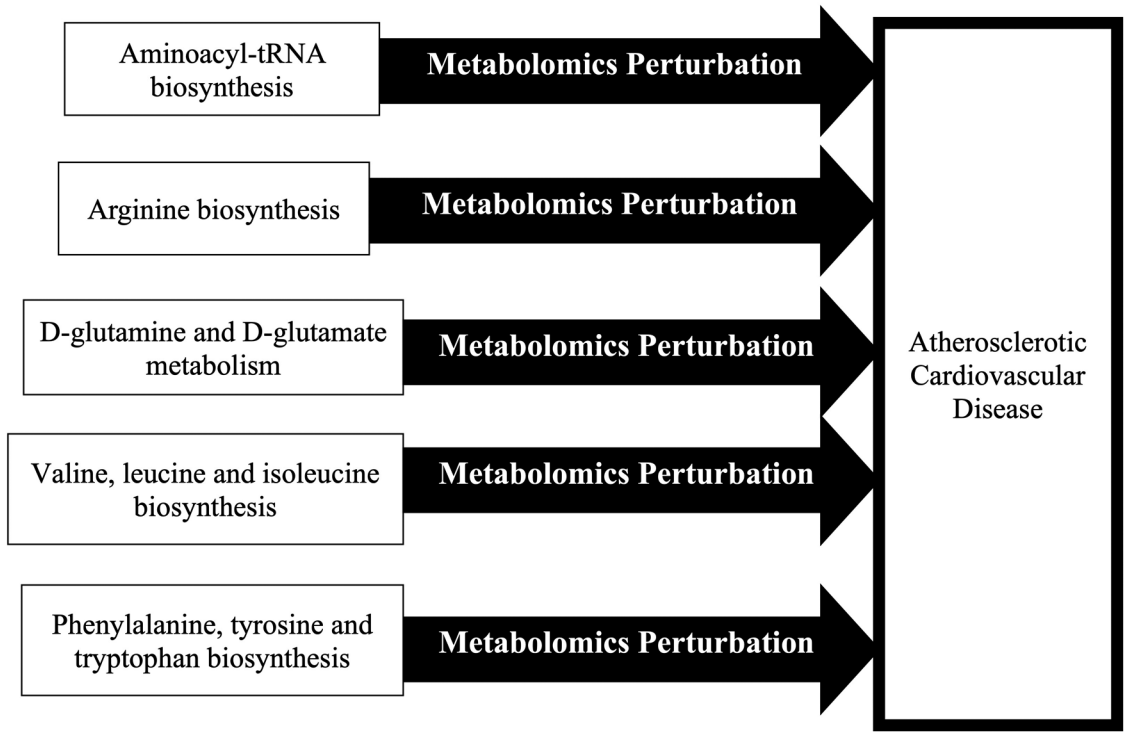

FIGURE 3
Working model of metabolomic perturbance and ASCVD.

TABLE 6 Comparisons between results of metabolomic studies and current study.

Metabolomic study	Metabolite alteration in high CVD risk	Results of current study
Würtz P et al. (12)	Higher phenylalanine and tyrosine	Higher phenylalanine and tyrosine
Ruiz-Canela M et al. (17)	Higher leucine and valine	Higher leucine and valine
Hu W et al. (18)	Higher leucine, isoleucine, valine	Higher leucine and valine
Vaarhorst AA et al. (19)	Higher valine, ornithine, and glutamate	Higher valine, ornithine, and glutamic acid
Shah SH et al. (13)	Higher glutamate, leucine, isoleucine, citrulline, C_2, C_8, $C_{10:1}$, $C_{14:2}$	Higher glutamic acid, leucine, citrulline, C_2, $C_{14.2}$
Strand E et al. (20)	Higher C_2, C_8, and C_{16}	Higher C_2 and C_{16}

This study has also found from multiple linear analysis that C_4DC, $C_{8:1}$, and C_{16}OH, citrulline, histidine, alanine, threonine, glycine, glutamine, tryptophan, phenylalanine, glutamic acid, arginine, and aspartic acid could be considered as new candidate biomarkers for the 10-year ASCVD risk. Based on a study by Hu W et al. (18), there is an independent association between BCAAs and intima-media thickness as a marker of coronary artery disease. Several other studies have also indicated a strong association between acylcarnitines and cardiovascular events (21, 22). In addition, metabolite disturbances can also contribute to the CVD risk factors such as diabetes mellitus as found in many studies (23–27). In this regard, plasma levels of BCAA and aromatic amino acids (AAAs) particularly tyrosine, phenylalanine, and isoleucine can predict both diabetes mellitus and CVD events (28, 29).

Metabolomics can help us identify new intermediate metabolites to better understand the underlying mechanisms responsible for higher 10-year ASCVD risk. For instance, the odds ratio between low- and high/intermediate-risk patients can be explained by certain underlying pathways including aminoacyl-tRNA biosynthesis, valine, leucine, and isoleucine biosynthesis, arginine biosynthesis, phenylalanine, tyrosine, and tryptophan biosynthesis, D-glutamine and D-glutamate metabolism, phenylalanine metabolism, and glutathione metabolism. The role of these underlying mechanisms in the development of cardiovascular events has been stated in previous studies (30–32). For instance, the aminoacyl-tRNA synthetases are found to have an important role in modifying the function of regulatory proteins in different cellular processes. The effects of aminoacyl-tRNA synthetase pathways on coronary arteries, aorta, cardiomyocytes, and fibroblasts and their strong association with angiogenesis and cardiomyopathy have been identified previously, and it suggested the potential role of aminoacyl-tRNA synthetase pathways as therapeutic/diagnostic targets of ASCVDs (30). In addition, the disturbed mechanisms of valine, leucine, isoleucine, and their α-keto acids were reported in animals suffering from cardiac events (31, 32). Arginine is another amino acid with an important role in different cellular processes such as protein biosynthesis. Furthermore, it is also involved in vascular tone and endothelial function affecting cardiovascular function (33).

Another study has also introduced phenylalanine, tyrosine, and tryptophan biosynthesis (using multi-omics approaches) to be involved in vascular function alterations (34). Phenylalanine metabolism has also been shown to have considerable effects on predicting poor outcomes in critically ill patients presenting with heart failure (35). The pathogenic role of high phenylalanine levels in cardiac aging has also been found (36). On the other hand, glutathione metabolism is also known to have considerable effects on various cell functions during CVD events such as cytokine production and protein synthesis. In this regard, it has been stated that glutathione deficiency can be associated with heart attack and stroke (37). Besides, glutathione metabolism is associated with poor outcomes such as death or re-hospitalization in heart failure patients (38).

Published articles regarding the metabolomics analysis of CVD risk, particularly those on amino acids or acylcarnitines mainly utilize the Framingham risk score for risk estimation of CVD events (13, 18). Despite the effectiveness of the ASCVD risk score and its preference in many cases (39), there are not many articles that have used the ASCVD risk score for that purpose. On the other hand, there have been fewer investigations on acylcarnitines compared with other metabolites like amino acids. The other strength of this study is its large population and broad list of investigated metabolites, which makes its results more valuable. Besides, various acylcarnitines generally showed a stronger association with CVD risk in fasting subjects than in nonfasting subjects (20); so, we measured the concentration of metabolites in fasting plasma. However, this study also has some limitations. The cross-sectional nature of the study prevents us from finding any temporality and actual causality associations between the 10-year ASCVD risk and metabolite profile. This study was conducted on Iranian individuals, which limits the generalization of the results to different populations. Also, the risk of actual ASCVD events according to the metabolic profile was not investigated. Additionally, meaningful differences in the studied patient groups might have affected the metabolite levels. Although these variabilities were adjusted in the risk score estimation equation, their existence is one of the limitations of the present study. Despite all the benefits of metabolic profiling in predictive strategies, its generalizability and reproducibility have to be investigated through comprehensive studies to establish its potential usefulness in the clinical setting (40). Thus, longitudinal studies are needed to confirm the predictive value of the metabolite profile on the ASCVD risk.

Conclusions

This study identified many amino acids and acylcarnitines as metabolite fingerprints of individuals at higher risk of 10-year ASCVD events. Among them, our results suggest C_4DC, $C_{8:1}$, $C_{16}OH$, citrulline, histidine, alanine, threonine, glycine, glutamine, tryptophan, phenylalanine, glutamic acid, arginine, and aspartic acid be associated with the 10-year ASCVD risk score and thus could be used as potential predictive biomarkers for the ASCVD events. Furthermore, several metabolic pathways associated with the development of 10-year ASCVD events were identified. Among them, "D-glutamine and D-glutamate metabolism", "phenylalanine, tyrosine, and tryptophan biosynthesis", and "valine, leucine, and isoleucine biosynthesis" showed the most influential pathways in this pathogenesis. These findings allow for a better understanding of mechanisms underlying ASCVD events and then were used in diagnostic and therapeutic strategies. However, more studies are still required to confirm this association in larger populations.

Acylcarnitines name: Free carnitine (C_0), Acetyl carnitine (C_2), Propionyl carnitine (C_3), Malonyl carnitine (C_3DC), Butyryl carnitine (C_4), Methylmalonyl-/succinyl carnitine (C_4DC), 3-OH-iso-/butyryl carnitine (C_4OH), Isovaleryl carnitine (C_5), Tiglylcarnitine ($C_{5:1}$), 3-OH-isovalerylcarnitine (C_5OH), Glutaryl carnitine (C_5DC), Hexanoyl carnitine (C_6), Octanoyl carnitine (C_8), Octenoyl carnitine ($C_{8:1}$), Decanoyl carnitine (C_{10}), Decenoyl carnitine ($C_{10:1}$), Dodecanoyl carnitine (C_{12}), Tetradecanoyl carnitine (C_{14}), Tetradecenoyl carnitine ($C_{14:1}$), Tetradecadienoyl carnitine ($C_{14:2}$), 3-OH-tetradecanoylcarnitine ($C_{14}OH$), Hexadecanoyl carnitine (C_{16}), 3-OH-hexadecanoylcarnitine ($C_{16}OH$), 3-OH-hexadecenoylcarnitine ($C_{16:1}OH$), Hexadecenoyl carnitine ($C_{16:1}$), Octadecanoyl carnitine (C_{18}), Octadecenoyl carnitine ($C_{18:1}$), 3-OH-octadecanoyl carnitine ($C_{18}OH$), 3-OH-octadecenoyl carnitine ($C_{18:1}OH$), Octadecadienoyl carnitine ($C_{18:2}$).

Data availability statement

The original contributions presented in the study are included in the article/**Supplementary Material**, further inquiries can be directed to the corresponding author/s.

Ethics statement

The studies involving human participants were reviewed and approved by Tehran University of Medical Sciences and Endocrine & Metabolism Research Institute. The patients/participants provided their written informed consent to participate in this study.

Author contributions

Study idea, HD, BL and FR; supervision, BL and FR; project administration, HD; data curation, FR; data collection, HD, SD, PR, SH, PK, MN, NR, AD, MY, BA, KK, NN, AK, FB and HAM; methodology, HD, BL and FR; data analyses, HD, SD, SH and FR; visualization, SH; writing—original draft, HD, SD and PR; All authors reviewed, edited, and approved the final manuscript. All authors contributed to the article and approved the submitted version.

Conflict of interest

The authors declare that the research was conducted in the absence of any commercial or financial relationships that could be construed as a potential conflict of interest.

Publisher's note

All claims expressed in this article are solely those of the authors and do not necessarily represent those of their affiliated organizations, or those of the publisher, the editors and the reviewers. Any product that may be evaluated in this article, or claim that may be made by its manufacturer, is not guaranteed or endorsed by the publisher.

Supplementary material

The Supplementary Material for this article can be found online at: https://www.frontiersin.org/articles/10.3389/fcvm.2023.1161761/full#supplementary-material.

References

1. Fu X, Xu J, Zhang R, Yu J. The association between environmental endocrine disruptors and cardiovascular diseases: a systematic review and meta-analysis. *Environ Res*. (2020) 187:109464. doi: 10.1016/j.envres.2020.109464

2. Münzel T, Hahad O, Sørensen M, Lelieveld J, Duerr GD, Nieuwenhuijsen M, et al. Environmental risk factors and cardiovascular diseases: a comprehensive expert review. *Cardiovasc Res*. (2022) 118(14):2880–902. doi: 10.1093/cvr/cvab316

3. Piko P, Kosa Z, Sandor J, Adany R. Comparative risk assessment for the development of cardiovascular diseases in the Hungarian general and roma population. *Sci Rep*. (2021) 11(1):3085. doi: 10.1038/s41598-021-82689-0

4. Sarrafzadegan N, Hassannejad R, Marateb HR, Talaei M, Sadeghi M, Roohafza HR, et al. PARS Risk charts: a 10-year study of risk assessment for cardiovascular diseases in eastern Mediterranean region. *PLoS One*. (2017) 12(12):e0189389. doi: 10.1371/journal.pone.0189389

5. Cauwenberghs N, Hedman K, Kobayashi Y, Vanassche T, Haddad F, Kuznetsova T. The 2013 ACC/AHA risk score and subclinical cardiac remodeling and dysfunction: complementary in cardiovascular disease prediction. *Int J Cardiol*. (2019) 297:67–74. doi: 10.1016/j.ijcard.2019.09.061

6. Lloyd-Jones DM, Braun LT, Ndumele CE, Smith Jr SC, Sperling LS, Virani SS, et al. Use of risk assessment tools to guide decision-making in the primary prevention of atherosclerotic cardiovascular disease: a special report from the American heart association and American college of cardiology. *Circulation*. (2019) 139(25):e1162–e77. doi: 10.1161/CIR.0000000000000638

7. Karmali KN, Goff DC, Ning H, Lloyd-Jones DM. A systematic examination of the 2013 ACC/AHA pooled cohort risk assessment tool for atherosclerotic cardiovascular disease. *J Am Coll Cardiol*. (2014) 64(10):959–68. doi: 10.1016/j.jacc.2014.06.1186

8. McGarrah RW, Crown SB, Zhang G-F, Shah SH, Newgard CB. Cardiovascular metabolomics. *Circ Res*. (2018) 122(9):1238–58. doi: 10.1161/CIRCRESAHA.117.311002

9. Kordalewska M, Markuszewski MJ. Metabolomics in cardiovascular diseases. *J Pharm Biomed Anal*. (2015) 113:121–36. doi: 10.1016/j.jpba.2015.04.021

10. Shah SH, Hauser ER, Bain JR, Muehlbauer MJ, Haynes C, Stevens RD, et al. High heritability of metabolomic profiles in families burdened with premature cardiovascular disease. *Mol Syst Biol*. (2009) 5(1):258. doi: 10.1038/msb.2009.11

11. Ussher JR, Elmariah S, Gerszten RE, Dyck JR. The emerging role of metabolomics in the diagnosis and prognosis of cardiovascular disease. *J Am Coll Cardiol*. (2016) 68(25):2850–70. doi: 10.1016/j.jacc.2016.09.972

12. Würtz P, Havulinna AS, Soininen P, Tynkkynen T, Prieto-Merino D, Tillin T, et al. Metabolite profiling and cardiovascular event risk: a prospective study of 3 population-based cohorts. *Circulation*. (2015) 131(9):774–85. doi: 10.1161/CIRCULATIONAHA.114.013116

13. Shah SH, Bain JR, Muehlbauer MJ, Stevens RD, Crosslin DR, Haynes C, et al. Association of a peripheral blood metabolic profile with coronary artery disease and risk of subsequent cardiovascular events. *Circ: Cardiovasc Genet*. (2010) 3(2):207–14. doi: 10.1161/CIRCGENETICS.109.852814

14. Djalalinia S, Modirian M, Sheidaei A, Yoosefi M, Zokaiee H, Damirchilu B, et al. Protocol design for large-scale cross-sectional studies of surveillance of risk factors of non-communicable diseases in Iran: STEPs 2016. *Arch Iran Med*. (2017) 20(9):608–16. doi: 10.34172/aim.2022.99

15. Arjmand B, Dehghanbanadaki H, Yoosefi M, Rezaei N, Mohammadi Fateh S, Ghodssi-Ghassemabadi R, et al. Association of plasma acylcarnitines and amino acids with hypertension: a nationwide metabolomics study. *PloS One*. (2023) 18(1):e0279835. doi: 10.1371/journal.pone.0279835

16. Goff Jr DJ, Lloyd-Jones DM, Bennett G, Coady S, D'Agostino RB, Gibbons R, et al. 2013 ACC/AHA guideline on the assessment of cardiovascular risk: a report of the American College of Cardiology/American Heart Association Task Force on Practice Guidelines. *Circulation*. (2014) 129(25 Suppl 2):S49–73. doi: 10.1161/01.cir.0000437741.48606.98

17. Ruiz-Canela M, Toledo E, Clish CB, Hruby A, Liang L, Salas-Salvadó J, et al. Plasma branched-chain amino acids and incident cardiovascular disease in the PREDIMED trial. *Clin Chem*. (2016) 62(4):582–92. doi: 10.1373/clinchem.2015.251710

18. Hu W, Sun L, Gong Y, Zhou Y, Yang P, Ye Z, et al. Relationship between branched-chain amino acids, metabolic syndrome, and cardiovascular risk profile in a Chinese population: a cross-sectional study. *Int J endocrinol*. (2016) 2016:8173905. doi: 10.1155/2016/8173905

19. Vaarhorst AA, Verhoeven A, Weller CM, Böhringer S, Göraler S, Meissner A, et al. A metabolomic profile is associated with the risk of incident coronary heart disease. *Am Heart J*. (2014) 168(1):45–52. e7. doi: 10.1016/j.ahj.2014.01.019

20. Strand E, Pedersen ER, Svingen GFT, Olsen T, Bjørndal B, Karlsson T, et al. Serum acylcarnitines and risk of cardiovascular death and acute myocardial infarction in patients with stable angina pectoris. *J Am Heart Assoc*. (2017) 6(2):e003620. doi: 10.1161/JAHA.116.003620

21. Deda O, Panteris E, Meikopoulos T, Begou O, Mouskeftara T, Karagiannidis E, et al. Correlation of Serum acylcarnitines with clinical presentation and severity of coronary artery disease. *Biomolecules*. (2022) 12(3):354. doi: 10.3390/biom12030354

22. Kalim S, Clish CB, Wenger J, Elmariah S, Yeh RW, Deferio JJ, et al. A plasma long-chain acylcarnitine predicts cardiovascular mortality in incident dialysis patients. *J Am Heart Assoc*. (2013) 2(6):e000542. doi: 10.1161/JAHA.113.000542

23. Wang TJ, Larson MG, Vasan RS, Cheng S, Rhee EP, McCabe E, et al. Metabolite profiles and the risk of developing diabetes. *Nat Med*. (2011) 17(4):448–53. doi: 10.1038/nm.2307

24. Wang-Sattler R, Yu Z, Herder C, Messias AC, Floegel A, He Y, et al. Novel biomarkers for pre-diabetes identified by metabolomics. *Mol Syst Biol*. (2012) 8(1):615. doi: 10.1038/msb.2012.43

25. Guasch-Ferré M, Ruiz-Canela M, Li J, Zheng Y, Bulló M, Wang DD, et al. Plasma acylcarnitines and risk of type 2 diabetes in a Mediterranean population at high cardiovascular risk. *J Clin Endocrinol Metab*. (2018) 104(5):1508–19. doi: 10.1210/jc.2018-01000

26. Storesund S, Svardal A, Lonnebakken M, Strand E, Berge R, Nygard O, et al. The associations of serum acylcarnitines with long term cardiovascular prognosis in patients with non-obstructive coronary artery disease. *Atherosclerosis*. (2021) 331:e204–e5. doi: 10.1016/j.atherosclerosis.2021.06.627

27. Gao F, Kovalik J-P, Zhao X, Chow VJ, Chew H, Teo LL, et al. Exacerbation of cardiovascular ageing by diabetes mellitus and its associations with acyl-carnitines. *Aging*. (2021) 13(11):14785–805. doi: 10.18632/aging.203144

28. Magnusson M, Lewis GD, Ericson U, Orho-Melander M, Hedblad B, Engström G, et al. A diabetes-predictive amino acid score and future cardiovascular disease. *Eur Heart J*. (2012) 34(26):1982–9. doi: 10.1093/eurheartj/ehs424

29. Tillin T, Hughes AD, Wang Q, Würtz P, Ala-Korpela M, Sattar N, et al. Diabetes risk and amino acid profiles: cross-sectional and prospective analyses of ethnicity, amino acids and diabetes in a south Asian and European cohort from the SABRE (southall and brent REvisited) study. *Diabetologia*. (2015) 58(5):968–79. doi: 10.1007/s00125-015-3517-8

30. Zou Y, Yang Y, Fu X, He X, Liu M, Zong T, et al. The regulatory roles of aminoacyl-tRNA synthetase in cardiovascular disease. *Mol Ther Nucleic Acids*. (2021) 25:372–87. doi: 10.1016/j.omtn.2021.06.003

31. Walejko JM, Christopher BA, Crown SB, Zhang G-F, Pickar-Oliver A, Yoneshiro T, et al. Branched-chain α-ketoacids are preferentially reaminated and activate protein synthesis in the heart. *Nat Commun*. (2021) 12(1):1680. doi: 10.1038/s41467-021-21962-2

32. Bhattacharya S, Granger CB, Craig D, Haynes C, Bain J, Stevens RD, et al. Validation of the association between a branched chain amino acid metabolite profile and extremes of coronary artery disease in patients referred for cardiac catheterization. *Atherosclerosis*. (2014) 232(1):191–6. doi: 10.1016/j.atherosclerosis.2013.10.036

33. Gambardella J, Khondkar W, Morelli MB, Wang X, Santulli G, Trimarco V. Arginine and endothelial function. *Biomedicines*. (2020) 8(8):277. doi: 10.3390/biomedicines8080277

34. Tam C-CF, Chan Y-H, Wong Y-K, Li Z, Zhu X, Su K-J, et al. Multi-omics signatures link to ticagrelor effects on vascular function in patients with acute coronary syndrome. *Arterioscler Thromb Vasc Biol*. (2022) 42(6):789–98. doi: 10.1161/ATVBAHA.121.317513

35. Chen W-S, Wang C-H, Cheng C-W, Liu M-H, Chu C-M, Wu H-P, et al. Elevated plasma phenylalanine predicts mortality in critical patients with heart failure. *ESC Heart Failure*. (2020) 7(5):2884–93. doi: 10.1002/ehf2.12896

36. Czibik G, Mezdari Z, Altintas DM, Bréhat J, Pini M, d'Humières T, et al. Dysregulated phenylalanine catabolism plays a key role in the trajectory of cardiac aging. *Circulation*. (2021) 144(7):559–74. doi: 10.1161/CIRCULATIONAHA.121.054204

37. Wu G, Fang Y-Z, Yang S, Lupton JR, Turner ND. Glutathione metabolism and its implications for health. *J Nutr*. (2004) 134(3):489–92. doi: 10.1093/jn/134.3.489

38. Cao TH, Jones DJL, Voors AA, Quinn PA, Sandhu JK, Chan DCS, et al. Plasma proteomic approach in patients with heart failure: insights into pathogenesis of disease progression and potential novel treatment targets. *Eur J Heart Fail*. (2020) 22(1):70–80. doi: 10.1002/ejhf.1608

39. Wang H, Sun Y, Wang S, Tao Y, Zhang L. Comparisons of the framingham and ASCVD risk scores for coronary heart disease risk prediction in Chinese men. *Int J Cardiol*. (2018) 266:269. doi: 10.1016/j.ijcard.2018.03.061

40. Bagheri M, Djazayery A, Farzadfar F, Qi L, Yekaninejad MS, Aslibekyan S, et al. Plasma metabolomic profiling of amino acids and polar lipids in Iranian obese adults. *Lipids Health Dis*. (2019) 18(1):1–9. doi: 10.1186/s12944-019-1037-0

frontiers | Frontiers in Cardiovascular Medicine

TYPE Mini Review
PUBLISHED 26 May 2023
DOI 10.3389/fcvm.2023.1202187

OPEN ACCESS

EDITED BY
Louis Maximilian Buja,
University of Texas Health Science Center at Houston, United States

REVIEWED BY
Jon Homeister,
University of North Carolina at Chapel Hill, United States

*CORRESPONDENCE
Kathryn L. Howe
✉ kathryn.howe@uhn.ca

RECEIVED 07 April 2023
ACCEPTED 20 April 2023
PUBLISHED 26 May 2023

CITATION
Patel S, Guo MK, Abdul Samad M and Howe KL (2023) Extracellular vesicles as biomarkers and modulators of atherosclerosis pathogenesis. Front. Cardiovasc. Med. 10:1202187. doi: 10.3389/fcvm.2023.1202187

Extracellular vesicles as biomarkers and modulators of atherosclerosis pathogenesis

Sarvatit Patel[1,2,3], Mandy Kunze Guo[1,2], Majed Abdul Samad[1] and Kathryn L. Howe[1,2,3,4]*

[1]Toronto General Hospital Research Institute, University Health Network, Toronto, ON, Canada, [2]Institute of Medical Science, University of Toronto, Toronto, ON, Canada, [3]Division of Vascular Surgery, Department of Surgery, University of Toronto, Toronto, ON, Canada, [4]Peter Munk Cardiac Centre, University Health Network, Toronto, ON, Canada

Extracellular vesicles (EVs) are small, lipid bilayer-enclosed structures released by various cell types that play a critical role in intercellular communication. In atherosclerosis, EVs have been implicated in multiple pathophysiological processes, including endothelial dysfunction, inflammation, and thrombosis. This review provides an up-to-date overview of our current understanding of the roles of EVs in atherosclerosis, emphasizing their potential as diagnostic biomarkers and their roles in disease pathogenesis. We discuss the different types of EVs involved in atherosclerosis, the diverse cargoes they carry, their mechanisms of action, and the various methods employed for their isolation and analysis. Moreover, we underscore the importance of using relevant animal models and human samples to elucidate the role of EVs in disease pathogenesis. Overall, this review consolidates our current knowledge of EVs in atherosclerosis and highlights their potential as promising targets for disease diagnosis and therapy.

KEYWORDS

extracellular vesicles, atherosclerosis, biomarkers, therapeutics, EV tracking models

1. Introduction

Atherosclerosis is a significant cause of cardiovascular disease (CVD) that can lead to heart attack, stroke, kidney failure, and major amputation (1–4). Approximately 17.9 million people die from CVD annually (5). Atherosclerosis is a chronic inflammatory process characterized by endothelial activation, accumulation of lipoproteins, and recruitment of inflammatory cells that leads to plaques that gradually enlarge and either restrict blood flow or embolize, damaging the heart or peripheral tissues (6). The current diagnostic methods for atherosclerosis are associated with rare but significant procedure-related consequences and considerable cost (7, 8). The classical biomarkers, such as total cholesterol, low-density lipoprotein (LDL), or serum triglyceride levels, are the gold standard diagnostic tests for atherosclerosis (9). C-reactive protein, a non-specific inflammatory marker, has emerged as a clinical marker for residual risk in atherosclerosis patients with good cholesterol control (10, 11). Many of these biomarkers can diagnose CVD but cannot definitively predict stroke or myocardial infarction (MI) risk. There is a need for new CVD biomarkers that are cost-effective, improve detection, and identify novel treatment targets. As we enter the era of precision medicine, we need a more granular understanding of biomarkers that can be used as reliable screening tools with metrics to guide personalized intervention to prevent devastating clinical events.

The American Heart Association proposed seven metrics in 2010 to define and monitor cardiovascular health (12). Managing the disease involves non-pharmacological methods (healthy diet, regular physical activity, and tobacco abstinence) (1) and pharmacological interventions such as statins to control lipoprotein levels (13–15), with newer options such as cholesterol-binding agents (e.g., ezetimibe) (16) and proprotein convertase subtilisin/kexin type 9 (PCSK9, lowers LDL) inhibitors (e.g., evolocumab) (17–19) also available. Notably, several studies have highlighted challenges in achieving therapeutic goals for serum lipids despite high-intensity statin therapy (20–22). In some cases, surgery or stent-based therapies are required to manage more severe atherosclerosis. While current strategies can slow the progression of atherosclerosis and/or prevent clinical events (23), further research is needed to understand the specific cellular and molecular mechanisms underpinning plaque progression to identify targets for stabilization and/or plaque regression. One area of promise includes delineating cellular communication during atherosclerotic plaque development and progression. In this regard, extracellular vesicles (EVs) have been identified as essential cell-cell communicators that may hold promise in improving our understanding of atherosclerotic disease—from biomarkers to disease pathogenesis (24–26) (**Figure 1**).

2. Extracellular vesicles

2.1. Biogenesis, cargo, and functions

EVs are lipid bilayer-bound particles that all cell types release into the extracellular space. They can be classified into three major types based on their biogenesis, morphological, and biochemical properties: exosomes (form as intraluminal vesicles within multivesicular bodies that fuse with the plasma membrane, 30–100 nm), microvesicles (directly bud off from healthy plasma membrane/also referred to as ectosomes, 100–1,000 nm) and apoptotic bodies (form during apoptosis, 1–5 μm) (27, 28). Furthermore, EVs carry cargo that contains biologically active materials, such as DNA, microRNA, messenger RNA, proteins, lipids, and carbohydrates. Once released into the extracellular space, EVs may directly interact with nearby cells (28). EVs can enter biological fluids *via* transcytosis or by breaching biological barriers, where they can travel throughout the body *via* the circulation—either blood or lymphatics (28, 29). EVs can then be taken up by recipient cells *via* endocytosis, fusion with the recipient cell plasma membrane, or binding to target cell membrane proteins (30, 31). The transferred cargo to recipient cells can affect molecular and cellular signalling pathways and functions.

Current EV isolation permits classification based on size, density and surface markers but does not discriminate based on biogenesis (28). That said, proteomic analysis has revealed distinct protein composition for EV subtypes (32), with some markers helping to distinguish EVs by biogenesis pathways. For example, exosome markers include endosomal sorting complexes required for transport (ESCRT) proteins, Alix and tetraspanins, while ectosome markers include Annexin A2/A5, ARF6 and Enolase 1 (32). Although advanced technology will undoubtedly yield more discrimination between EV populations, some promise exists in using inhibition of EV biogenesis by pharmacological therapies. For example, inhibitors of cancer exosome secretion may impact cancer progression and metastasis (33). Ultimately, the ideal strategy will be to find specific inhibitors that can impact EVs associated with pathology but not those that play critical physiological roles (34). To do this, we will need a more nuanced understanding of the kinetics of EV release from the host cell, travel within the circulation, recipient cell uptake, and EV clearance.

EV cargo is biologically active. In cancer, EV cargo can promote neoplastic transformation and cell proliferation, contributing to cancer initiation and progression (35–38). During atherogenesis, EVs released from endothelial cells (ECs) and immune cells promote leukocyte infiltration and plaque maturation (39–41). This suggests that EVs circulating in the plasma could serve as non-invasive disease biomarkers. Both *in vitro* and *in vivo* studies have shown that circulating EVs carry microRNA, which can be biomarkers for neurodegenerative diseases (42–45) and CVD (46). EVs possess several unique advantages compared to traditional biomarkers (47). EVs are stably circulated in almost all bodily fluids, they can represent the current disease state by carrying specific cargo from parental cells, and they can be collected sequentially. As a result, EVs have significant potential as clinically valuable biomarkers capable of providing multiple, minimally intrusive assessments of the disease state.

EVs can also be used as a stable drug delivery system that protects cargo from degradation (48–54). EVs have numerous advantages over cell-based therapies in regenerative medicine, such as long shelf life, ease of transportation, long-term storage, and lack of replication (55–57). As drug delivery vehicles, they outperform synthetic drug carriers by crossing tissue and cellular barriers (48). In preclinical studies, EVs have been used as a drug delivery system. For instance, exosome-mediated siRNA delivery has been used in Alzheimer's disease (45), while mesenchymal stem cell-derived exosomes have been used to treat ischemic lung injury (58) and eye disorders (59). However, further understanding of EV circulation dynamics, targeting, internalization, and intracellular trafficking pathways is needed to fully capitalize on the therapeutic potential.

2.2. Characterization

EV isolation is divided into three main approaches based on size, density, and surface markers (31). Size-exclusion chromatography (SEC) is one commonly used technique for EV isolation based on size, while differential ultracentrifugation exploits the distinct density gradients of EVs (60). Finally, magnetic beads/affinity chromatography or flow cytometry uses surface markers to extract EVs with high specificity but low yield (31). There is no single gold standard. Although

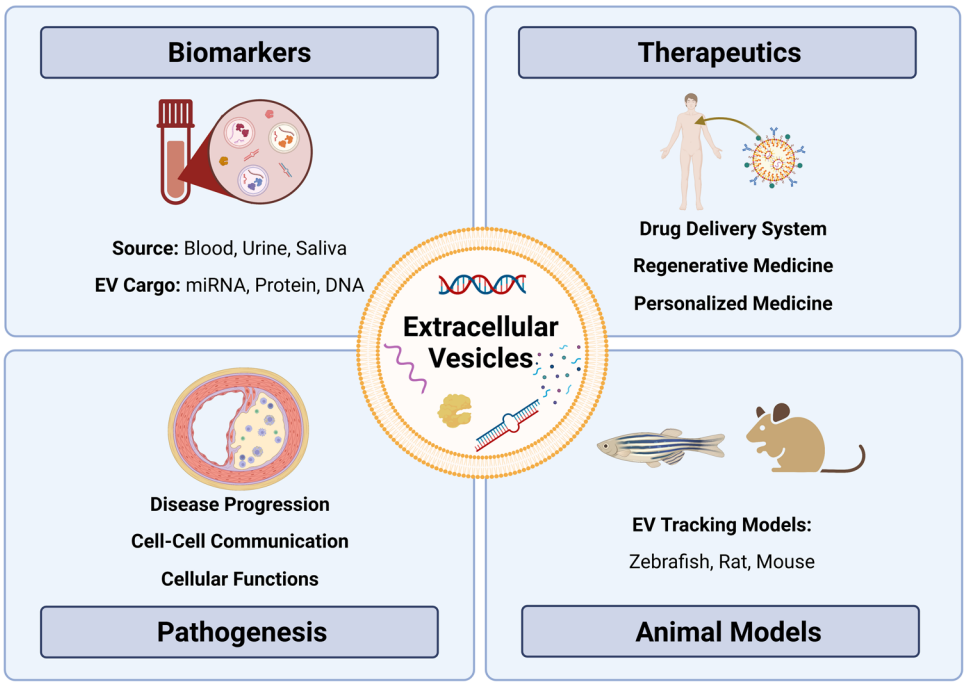

FIGURE 1
Exploring the role of extracellular vesicles in atherosclerosis: insights from biomarkers, therapeutics, pathobiology, and translational models. Extracellular vesicles (EVs) as versatile entities for various applications. EVs, small membrane-bound particles, have emerged as promising biomarkers for diagnostic and prognostic purposes in various diseases. They have also shown great potential as therapeutic agents for their ability to carry and deliver bioactive molecules. Moreover, EVs have been implicated in the pathogenesis of many diseases, including cancer, neurodegenerative diseases, and atherosclerosis. Animal studies have contributed significantly to our understanding of the biology and functions of EVs, paving the way for their clinical translation.

ultracentrifugation has been widely used in the past, there has been a shift towards SEC attributed in part to the higher EV yield and functionality obtained through SEC (61, 62).

The Minimal Information for Studies of Extracellular Vesicles (MISEV) 2018 provides a key tool for standardizing EV research (31) and has helped to establish rigour in a rapidly emerging field of research by outlining criteria for EV quantification and characterization. Suggestions include EV quantification by nanoparticle tracking analysis (NTA) (63), characterization by surface marker protein expression using western blot (31), and purity control to detect the presence of non-vesicular contamination, such as apolipoprotein A1 and albumin in EVs enriched from plasma (64). Imaging EVs *via* electron microscopy is recommended (63), while flow cytometry detecting surface markers can be used to characterize the cellular origin of EVs (65, 66). In this way, rigorous determination of cell-specific EVs holds promise as highly specific biomarkers for a disease state. EVs can be further characterized by analyzing their cargo. Mass spectrometry has been used to study EV proteomics in biofluids and tissues (67, 68). Similarly, transcriptomics has been employed to investigate the nucleic acid cargo of EVs, specifically microRNA cargo, primarily through microarrays and RT-qPCR, which are limited to a particular RNA panel (69).

Despite the considerable advancement in technology for EV isolation and characterization, limitations and challenges remain. However, as developing technology continues to refine EV research, it is becoming clear that EVs play crucial roles in biological processes, govern disease, and have emerged as a new avenue in atherosclerosis research.

3. EVs in atherosclerosis

3.1. EVs in plasma

EVs might serve as diagnostic and therapeutic tools for many CVD conditions. EV levels in the blood, urine and saliva have been linked to clinical risk in patients with stable CVD (70) (**Table 1**). Elevated EVs are associated with risk factors such as smoking, diabetes, and hypercholesteremia (84). The abundance of EVs carried in plasma reflects the potential for utilizing these EVs as biomarkers for CVD, and notably that EVs derived from specific cell types, such as ECs, leukocytes and platelets, correlate with CVD (85). A previous study exploited the surface markers expressed on EVs to purify and isolate cell-specific EVs, followed by enrichment and analysis of EV cargo. In EVs isolated from plasma, CD14 upregulation was linked to a higher risk of ischemic stroke occurrence (80), while increased cystatin C and polygenic immunoglobin receptors were linked to acute coronary syndrome (77).

Circulating EVs from different cellular origins and their distinct cargo (e.g., microRNA, protein) have been linked to

Table 1 Potential biomarkers for cardiovascular diseases.

Disease	Sample	Biomarker	Levels	Study Design	Potential application	Reference
Heart Failure (HF)	Plasma	miR-1254, miR-1306	↑	2203 patients with HF	Prognosis	(71)
		Galectin-3	↑	1329 patients with HF	Prognosis	(72)
	Saliva	Galectin-3	↑	64 patients with HF; 51 healthy controls	Diagnosis	(73)
	Plasma-EVs	miR-425, miR-744	↓	31 patients with HF; 31 healthy controls	Diagnosis	(74)
	Serum-EVs	mir-92B-5P	↑	28 patients with HF; 30 healthy controls	Diagnosis	(75)
Acute Coronary Syndrome (ACS)	Plasma	miR-208b, miR-133a	↑	444 patients with ACS	Diagnosis	(76)
	Serum-EVs	pIgR, cystatin C	↑	471 ACS-suspected patients	Diagnosis	(77)
Coronary Artery Disease (CAD)	Urine	collagen α1 (I and III)	↑	67 patients presenting with symptoms suspicious for CAD	Diagnosis	(78)
	Plasma-EVs	miR-126, miR-199a	↑	181 patients with stable CAD	Prognosis	(79)
Vascular Disease	Plasma-EVs	Cystatin C, Serpin F2, CD14	↑	1060 patients with vascular disease and severe vascular risk factors	Prognosis	(80)
Myocardial Infarction (MI)	Plasma	miR-499-5p, miR-208b	↑	424 patients with suspected ACS	Prognosis	(81)
	Serum-EVs	miR-192, miR-194, miR-34a	↑	21 patients with MI; 65 matched controls	Prognosis	(82)
Atherosclerosis	Plasma	PIGR, IGHA2, APOA, HPT, HEP2	↑	222 patients with atherosclerosis; 222 matched controls	Prognosis	(83)

pathological conditions such as dyslipidemia, diabetes (86–88), CVD (60, 79), and inflammatory disorders (89–91). This suggests that EVs play a role in the immune response, vascular remodelling, endothelial dysfunction, and apoptosis, all of which underlie atherosclerosis (92, 93). Studies have shown that leukocyte-derived, neutrophil-derived, and activated platelet-derived EVs were significantly higher in patients with atherosclerosis (94, 95). EVs carried in plasma may be helpful as biomarkers for atherosclerosis, but accuracy must be improved to detect changes in EV count from specific cell types. As EVs are heterogeneous in size, composition, and cellular origin, it makes identifying specific populations and correlating them to disease challenging (46). In addition to EV heterogeneity, clinical variables (e.g., age, sex), comorbidities (e.g., obesity), and clinical history (e.g., cancer, medications) affect circulating EVs in plasma (31).

Furthermore, laboratory standardization will be critical before employing EVs as a biomarker: lack of standard protocols for EV isolation, quantification, and characterization leads to variability in results and negates their utility as a biomarker or clinical assessment tool. EV biomarkers lack a standard reference range, making it difficult to compare among populations and studies. No EV-based biomarker has been adopted for CVD, and more research is needed to develop standard protocols to study plasma EVs. Work is ongoing, as the International Society for Extracellular Vesicles has a specific blood task force focused on standardizing plasma and serum-derived EVs (96).

To address the challenges in EV detection, standardization, and clinical translation, technological improvements, standardized protocols, and prospective large clinical trials are needed (97, 98). Precision medicine EV research has recently become more prominent. It is a potential path that enables physicians and researchers to use patient data to develop personalized treatments. For instance, a multi-biomarker approach may incorporate EV evaluation for screening/diagnosis, prognosis, and monitoring of people at risk of atherosclerotic CVD (97). Several subsets of EV biomarkers can be exploited for patient risk evaluations, reclassification, and disease stage diagnosis (97). Applying transcriptomic and proteomic analysis plus artificial intelligence algorithms to clinical data can help identify high-risk individuals and administer preventive strategies quickly (98).

3.2. EVs in plaque

As EVs protect their molecular cargo from degradation and carry surface markers identifying their parent cell, plasma EVs a unique opportunity to study disease states (diagnostic potential). On the other hand, EVs in tissue can contribute to the pathophysiology or progression of plaques (therapeutic targets) (99). At this time, however, screening and tracing EVs released from cells or tissues *in vivo* remains challenging. EVs are found in early and advanced plaques, suggesting they are involved in both the initiation and advanced phases of plaque development in humans (100–102). Patients with atherosclerosis demonstrated enrichment of proatherogenic EV cargo, such as vascular cell adhesion molecule-1, von Willebrand Factor, endothelial nitric oxide synthase, and angiopoietin-1, compared to healthy control participants (103, 104). Athough EV production, function, and quantity in atherosclerotic lesions still needs more delineatation, some granularity is emerging, with human atherosclerotic plaques containing EVs derived from leukocytes, macrophages, erythrocytes, lymphocytes, and smooth muscle cells (SMCs) (101, 102, 105).

Most of our current understanding of the role of EVs in atherosclerosis has been obtained from studies using EVs derived from cell cultures, which may not accurately represent EVs found *in vivo*. Nonetheless, EVs have been found to exert significant

influence over a range of pro-atherogenic processes, such as inflammation, thrombosis, and angiogenesis (84). In particular, EC-derived EVs have been implicated in endothelial dysfunction (106, 107) and vascular inflammation (108), which may contribute to the development of early atherosclerotic plaques. Moreover, EC-derived EVs can communicate with macrophages (109, 110) and SMCs (111–113) to regulate vascular disease, while monocyte-derived EVs have been found to modulate vascular inflammation and cell death (114–116). Additionally, foam cell-derived EVs have been shown to regulate SMC migration, thereby potentially accelerating the progression of atherosclerotic lesions (117). EVs produced from a range of cell types, including T-cells, platelets, dendritic cells, and monocytic cells, have also been shown to cause macrophage apoptosis (118–122), that may contribute to the development and progression of atherosclerosis. Moreover, EVs have been found to play various multifaceted and environment-dependent roles in other cellular processes, such as endothelial permeability (123), pro- and anti-inflammatory signaling (124–126), leukocyte transmigration and lipid accumulation (127–129), SMC proliferation (130), intravascular calcification (131), extracellular matrix remodeling (132), and plaque rupture. Collectively, the evidence suggests a substantial role for EVs in atherosclerosis pathogenesis, emphasizing the need for additional research into the mechanisms underlying EV-mediated intercellular communication in this disease. New technologies such as flow cytometry and single EV analysis will increase detection precision and provide more detail on cell-specific EV phenotypes, their cargo, and their role in disease regulation. Until then, an emerging resource for EV studies is the development of multicellular models for tracking.

4. EV tracking animal models

Despite recent discoveries, it is still challenging to understand the spatiotemporal distribution and physiological activities of EVs *in vivo*. Little is known about the biological activities of EVs *in vivo*, including tissue distribution, blood levels, and clearance dynamics. EVs have been investigated in several disease-simulating animal models, including mouse, rats, and zebrafish.

The transparent nature of zebrafish makes them an ideal model (133, 134). The transgenic zebrafish model was recently established, enabling in vivo identification, tracking, and isolation of endogenous EVs produced by different cell types (135). A cell membrane-tethered fluorophore reporter system in the zebrafish allows cell-specific EV tracking and the potential to track EVs in cell-cell communication within the cardiovascular system (135). *In vivo*, a live EV tracking model of zebrafish demonstrated inter-organ communication by endogenous exosomes (136). Despite these successes, zebrafish EV tracking models have technological limitations (136) and consequently, more complex models are needed.

EVs have also been studied using more advanced organisms for models of diseases such as cancer (137, 138) and neurological disorders (139–141). For example, a murine model was used to determine the therapeutic effects of immunity and matrix regulatory cell-derived EVs on idiopathic pulmonary fibrosis (142). Several studies have used the rat model to study the role of EVs in spinal cord injuries (143, 144) and repetitive stress (145). Rat models have also been used to investigate the therapeutic potential of EVs to treat diseases such as small cerebral vessel disease (146), colo-cutaneous post-surgical fistula (147), and congenital diaphragmatic hernia (148).

EVs and their relevance to various disease processes have been investigated over the past decade, but EV tracking *in vivo* remains challenging. Understanding EV biodistribution throughout an organism will be essential before use in clinical practice. Using an EV tracking mouse model, a few studies have demonstrated EV-mediated cell-cell communication and the effects of EVs produced from tumour cells on distant organs (149–151). Investigators used Cre-LoxP mouse models to study cell or tissue-specific EVs by crossing CD9/CD63-GFPf/f exosome reporter mice with Cre-mice (αMHC-MerCreMer for cardiomyocytes, Pax8-Cre for renal tubular epithelial cells, Cdh5-CreERT2 for ECs, villin-Cre for intestine, and alb-Cre for liver) (152–154). In addition, a transgenic rat model (GFP-tagged human CD63) was employed to determine intercellular and mother-to-child EV transfer *in vivo* (155). However, a complete understanding of the role of cell-specific EVs in atherosclerotic diseases remains elusive. To investigate the potential of EVs as biomarkers or disease modulators, novel animal models that allow for the tracking, characterization, and evaluation of cell-specific EVs are required.

5. Perspectives for future studies

EVs, known to carry biologically active cargoes, appear to play an important role in the pathogenesis of atherosclerosis. However, studying plaque-derived EVs is challenging due to limited accessibility and the complex composition of plaques. Thus, researchers have turned to studying EVs in circulation, particularly in those carried in plasma, to gain insights into atherosclerosis biology. Although plasma is easily accessible, identifying reliable biomarkers is challenging, and pairing biomarkers with clinical events may not reflect the disease state entirely. Therefore, it is necessary to determine whether disease regions release EVs into circulation, which could serve as a potential biomarker. The paired assessment of EVs from circulation and plaques of the same patient is one possible approach, representing a promising and meaningful strategy for an atherosclerosis study.

Further research must elucidate the precise mechanisms by which plaque-derived EVs contribute to atherosclerosis pathogenesis to identify potential therapeutic targets. The primary challenge in studying EVs within the plaque is determining their source (cell-specific EVs) and their functions on neighbouring cells. Transgenic zebrafish models have demonstrated the feasibility of tracking EVs within the cardiovascular system (135). More sophisticated animal models

are essential to enable EV-tracking into plaques, better comprehend EV biogenesis and metabolism, and investigate cell-specific EV roles and functions during disease progression. Plasma-derived EVs (e.g., leukocyte origin) have demonstrated potential as biomarkers for assessing plaque vulnerability in patients (156, 157). The potential for EVs carried in plasma to shed light on the biology of atherosclerotic plaque vulnerability to rupture (leading to clinical events such as MI and stroke) is promising and requires further investigation. Using EVs as therapeutic targets for atherosclerosis is a growing area of interest, given their stability as drug-delivery vehicles (158, 159). Overall, EVs represent a promising area for future research in the field of atherosclerosis.

6. Conclusions

EVs have been recognized as important components in the pathogenesis of atherosclerosis. EVs derived from immune and ECs are implicated in developing and destabilizing atherosclerotic plaques. Plasma EVs carry the potential for conveying information related to the vulnerability of atherosclerotic plaques and can serve as potential biomarkers for atherosclerosis and its associated complications, such as MI and stroke. Moreover, the prospect of utilizing EVs as therapeutic targets for atherosclerosis has recently gained substantial interest. While work remains to improve the tools and standardization of EV research, EVs nonetheless represent an encouraging area for future research in the field of atherosclerosis and hold the potential to provide novel insights into the diagnosis, treatment, and prevention of this chronic inflammatory disease.

Author contributions

SP and KH designed the topic of this review article. SP wrote the manuscript with MKG and MS. SP, MKG, and MS performed the literature review and designed the table. SP created the figure. KH participated in editing and provided conceptual input to the manuscript. All authors contributed to the article and approved the submitted version.

Funding

SP is supported by the Toronto General Hospital Research Institute Postdoctoral Fellowship Award. KH is supported by a Canadian Institutes of Health Research (CIHR) Project Grant PJT178006, the Heart and Stroke Foundation of Canada (New Investigator Award), Vascular Cures (Wylie Scholar Award), Blair Early Career Professorship in Vascular Surgery, Peter Munk Cardiac Centre, and University Health Network.

Acknowledgments

BioRender.com was used in the creation of the figure for this review.

Conflict of interest

The authors declare that the research was conducted in the absence of any commercial or financial relationships that could be construed as a potential conflict of interest.

Publisher's note

References

1. Libby P, Buring JE, Badimon L, Hansson GK, Deanfield J, Bittencourt MS, et al. Atherosclerosis. *Nat Rev Dis Primer*. (2019) 5(1):56. doi: 10.1038/s41572-019-0106-z

2. Dichgans M, Pulit SL, Rosand J. Stroke genetics: discovery, biology, and clinical applications. *Lancet Neurol*. (2019) 18(6):587–99. doi: 10.1016/S1474-4422(19)30043-2

3. Valdivielso JM, Rodríguez-Puyol D, Pascual J, Barrios C, Bermúdez-López M, Sánchez-Niño MD, et al. Atherosclerosis in chronic kidney disease. *Arterioscler Thromb Vasc Biol*. (2019) 39(10):1938–66. doi: 10.1161/ATVBAHA.119.312705

4. Behroozian A, Beckman JA. Microvascular disease increases amputation in patients with peripheral artery disease. *Arterioscler Thromb Vasc Biol*. (2020) 40(3):534–40. doi: 10.1161/ATVBAHA.119.312859

5. Cardiovascular diseases (CVDs). (cited 2022 Nov 3). Available at: https://www.who.int/news-room/fact-sheets/detail/cardiovascular-diseases-(cvds)

6. Berliner JA, Navab M, Fogelman AM, Frank JS, Demer LL, Edwards PA, et al. Atherosclerosis: basic mechanisms. *Circulation*. (1995) 91(9):2488–96. doi: 10.1161/01.CIR.91.9.2488

7. Nelson AJ, Ardissino M, Psaltis PJ. Current approach to the diagnosis of atherosclerotic coronary artery disease: more questions than answers. *Ther Adv Chronic Dis*. (2019) 10:2040622319884819. doi: 10.1177/2040622319884819

8. Knaapen P. Computed tomography to replace invasive coronary angiography? *Circ Cardiovasc Imaging*. (2019) 12(2):e008710. doi: 10.1161/CIRCIMAGING.119.008710

9. Upadhyay RK. Emerging risk biomarkers in cardiovascular diseases and disorders. *J Lipids*. (2015) 2015:971453. doi: 10.1155/2015/971453

10. Badimon L, Peña E, Arderiu G, Padró T, Slevin M, Vilahur G, et al. C-Reactive protein in atherothrombosis and angiogenesis. *Front Immunol*. (2018) 9:430. doi: 10.3389/fimmu.2018.00430

11. Ridker PM, Everett BM, Thuren T, MacFadyen JG, Chang WH, Ballantyne C, et al. Antiinflammatory therapy with canakinumab for atherosclerotic disease. *N Engl J Med*. (2017) 377(12):1119–31. doi: 10.1056/NEJMoa1707914

12. Sacco RL. The new American heart association 2020 goal: achieving ideal cardiovascular health. *J Cardiovasc Med*. (2011) 12(4):255. doi: 10.2459/JCM.0b013e328343e986

13. Cholesterol Treatment Trialists' (CTT) Collaboration, Baigent C, Blackwell L, Emberson J, Holland LE, Reith C, Bhala N, et al. Efficacy and safety of more intensive lowering of LDL cholesterol: a meta-analysis of data from 170,000 participants in 26 randomised trials. *Lancet Lond Engl*. (201) 376(9753):1670–81. doi: 10.1016/S0140-6736(10)61350-5

14. Baigent C, Keech A, Kearney PM, Blackwell L, Buck G, Pollicino C, et al. Efficacy and safety of cholesterol-lowering treatment: prospective meta-analysis of data from 90,056 participants in 14 randomised trials of statins. *Lancet Lond Engl*. (2005) 366 (9493):1267–78. doi: 10.1016/S0140-6736(05)67394-1

15. Cholesterol Treatment Trialists' (CTT) Collaborators. The effects of lowering LDL cholesterol with statin therapy in people at low risk of vascular disease: meta-analysis of individual data from 27 randomised trials. *Lancet*. (2012) 380 (9841):581–90. doi: 10.1016/S0140-6736(12)60367-5

16. Hammersley D, Signy M. Ezetimibe: an update on its clinical usefulness in specific patient groups. *Ther Adv Chronic Dis*. (2017 Jan) 8(1):4–11. doi: 10.1177/2040622316672544

17. Sabatine MS, Giugliano RP, Keech AC, Honarpour N, Wiviott SD, Murphy SA, et al. Evolocumab and clinical outcomes in patients with cardiovascular disease. *N Engl J Med*. (2017) 376(18):1713–22. doi: 10.1056/NEJMoa1615664

18. Farmaki P, Damaskos C, Garmpis N, Garmpi A, Savvanis S, Diamantis E. PCSK9 Inhibitors and cardiovascular disease: impact on cardiovascular outcomes. *Curr Drug Discov Technol*. (2020) 17(2):138–46. doi: 10.2174/1570163816666181211112358

19. Sobati S, Shakouri A, Edalati M, Mohammadnejad D, Parvan R, Masoumi J, et al. PCSK9: a key target for the treatment of cardiovascular disease (CVD). *Adv Pharm Bull*. (2020) 10(4):502–11. doi: 10.34172/apb.2020.062

20. Unni SK, Quek RGW, Biskupiak J, Lee VC, Ye X, Gandra SR. Assessment of statin therapy, LDL-C levels, and cardiovascular events among high-risk patients in the United States. *J Clin Lipidol*. (2016) 10(1):63–71. e3. doi: 10.1016/j.jacl.2015.09.008

21. Danchin N, Almahmeed W, Al-Rasadi K, Azuri J, Berrah A, Cuneo CA, et al. Achievement of low-density lipoprotein cholesterol goals in 18 countries outside Western Europe: the international ChoLesterol management practice study (ICLPS). *Eur J Prev Cardiol*. (2018) 25(10):1087–94. doi: 10.1177/2047487318777079

22. García-Gil M, Blanch J, Comas-Cufí M, Daunis-i-Estadella J, Bolíbar B, Martí R, et al. Patterns of statin use and cholesterol goal attainment in a high-risk cardiovascular population: a retrospective study of primary care electronic medical records. *J Clin Lipidol*. (2016) 10(1):134–42. doi: 10.1016/j.jacl.2015.10.007

23. Raggi P, Genest J, Giles JT, Rayner KJ, Dwivedi G, Beanlands RS, et al. Role of inflammation in the pathogenesis of atherosclerosis and therapeutic interventions. *Atherosclerosis*. (2018) 276:98–108. doi: 10.1016/j.atherosclerosis.2018.07.014

24. Xiang D, Li Y, Cao Y, Huang Y, Zhou L, Lin X, et al. Different effects of endothelial extracellular vesicles and LPS-induced endothelial extracellular vesicles on vascular smooth muscle cells: role of curcumin and its derivatives. *Front Cardiovasc Med*. (2021) 8:649352. Available at: doi: 10.3389/fcvm.2021.649352

25. Njock MS, Cheng HS, Dang LT, Nazari-Jahantigh M, Lau AC, Boudreau E, et al. Endothelial cells suppress monocyte activation through secretion of extracellular vesicles containing antiinflammatory microRNAs. *Blood*. (2015) 125(20):3202–12. doi: 10.1182/blood-2014-11-611046

26. Jansen F, Stumpf T, Proebsting S, Franklin BS, Wenzel D, Pfeifer P, et al. Intercellular transfer of miR-126-3p by endothelial microparticles reduces vascular smooth muscle cell proliferation and limits neointima formation by inhibiting LRP6. *J Mol Cell Cardiol*. (2017) 104:43–52. doi: 10.1016/j.yjmcc.2016.12.005

27. Gustafson D, Veitch S, Fish JE. Extracellular vesicles as protagonists of diabetic cardiovascular pathology. *Front Cardiovasc Med*. (2017) 4:71. doi: 10.3389/fcvm.2017.00071

28. van Niel G, Carter DRF, Clayton A, Lambert DW, Raposo G, Vader P. Challenges and directions in studying cell-cell communication by extracellular vesicles. *Nat Rev Mol Cell Biol*. (2022) 23(5):369–82. doi: 10.1038/s41580-022-00460-3

29. Milasan A, Tessandier N, Tan S, Brisson A, Boilard E, Martel C. Extracellular vesicles are present in mouse lymph and their level differs in atherosclerosis. *J Extracell Vesicles*. (2016) 5:31427. doi: 10.3402/jev.v5.31427

30. Mulcahy LA, Pink RC, Carter DRF. Routes and mechanisms of extracellular vesicle uptake. *J Extracell Vesicles*. (2014) 3:10.3402/jev.v3.24641. doi: 10.3402/jev.v3.24641

31. Théry C, Witwer KW, Aikawa E, Alcaraz MJ, Anderson JD, Andriantsitohaina R, et al. Minimal information for studies of extracellular vesicles 2018 (MISEV2018): a position statement of the international society for extracellular vesicles and update of the MISEV2014 guidelines. *J Extracell Vesicles*. (2018) 7(1):1535750. doi: 10.1080/20013078.2018.1535750

32. Brás IC, Khani MH, Riedel D, Parfentev I, Gerhardt E, van RC, et al. Ectosomes and exosomes are distinct proteomic entities that modulate spontaneous activity in neuronal cells. *bioRxiv*. (2021):2021.06.24.449731. doi: 10.1101/2021.06.24.449731v1

33. Kim JH, Lee CH, Baek MC. Dissecting exosome inhibitors: therapeutic insights into small-molecule chemicals against cancer. *Exp Mol Med*. (2022) 54(11):1833–43. doi: 10.1038/s12276-022-00898-7

34. Catalano M, O'Driscoll L. Inhibiting extracellular vesicles formation and release: a review of EV inhibitors. *J Extracell Vesicles*. (2020) 9(1):1703244. doi: 10.1080/20013078.2019.1703244

35. Bongiovanni L, Andriessen A, Wauben MHM, Nolte-'t Hoen ENM, de Bruin A. Extracellular vesicles: novel opportunities to understand and detect neoplastic diseases. *Vet Pathol*. (2021) 58(3):453–71. doi: 10.1177/0300985821999328

36. Santos JC, Lima NdS, Sarian LO, Matheu A, Ribeiro ML, Derchain SFM. Exosome-mediated breast cancer chemoresistance via miR-155 transfer. *Sci Rep*. (2018) 8(1):829. doi: 10.1038/s41598-018-19339-5

37. Felicetti F, De Feo A, Coscia C, Puglisi R, Pedini F, Pasquini L, et al. Exosome-mediated transfer of miR-222 is sufficient to increase tumor malignancy in melanoma. *J Transl Med*. (2016) 14(56):1–15. doi: 10.1186/s12967-016-0811-2

38. Sánchez CA, Andahur EI, Valenzuela R, Castellón EA, Fullá JA, Ramos CG, et al. Exosomes from bulk and stem cells from human prostate cancer have a differential microRNA content that contributes cooperatively over local and pre-metastatic niche. *Oncotarget*. (2016) 7(4):3993–4008. doi: 10.18632/oncotarget.6540

39. Akhmerov A, Parimon T. Extracellular vesicles, inflammation, and cardiovascular disease. *Cells*. (2022) 11(14):2229. doi: 10.3390/cells11142229

40. Buffolo F, Monticone S, Camussi G, Aikawa E. Role of extracellular vesicles in the pathogenesis of vascular damage. *Hypertension*. (2022) 79(5):863–73. doi: 10.1161/HYPERTENSIONAHA.121.17957

41. Huber J, Vales A, Mitulovic G, Blumer M, Schmid R, Witztum JL, et al. Oxidized membrane vesicles and blebs from apoptotic cells contain biologically active oxidized phospholipids that induce monocyte-endothelial interactions. *Arterioscler Thromb Vasc Biol*. (2002) 22(1):101–7. doi: 10.1161/hq0102.101525

42. Hill AF. Extracellular vesicles and neurodegenerative diseases. *J Neurosci Off J Soc Neurosci*. (2019) 39(47):9269–73. doi: 10.1523/JNEUROSCI.0147-18.2019

43. Cervenakova L, Saá P, Yakovleva O, Vasilyeva I, de Castro J, Brown P, et al. Are prions transported by plasma exosomes? *Transfus Apher Sci Off J World Apher Assoc Off J Eur Soc Haemapheresis*. (2016) 55(1):70–83. doi: 10.1016/j.transci.2016.07.013

44. Saá P, Yakovleva O, de Castro J, Vasilyeva I, De Paoli SH, Simak J, et al. First demonstration of transmissible spongiform encephalopathy-associated prion protein (PrPTSE) in extracellular vesicles from plasma of mice infected with mouse-adapted variant creutzfeldt-jakob disease by in vitro amplification. *J Biol Chem*. (2014) 289 (42):29247–60. doi: 10.1074/jbc.M114.589564

45. Cheng L, Doecke JD, Sharples RA, Villemagne VL, Fowler CJ, Rembach A, et al. Prognostic serum miRNA biomarkers associated with Alzheimer's disease shows concordance with neuropsychological and neuroimaging assessment. *Mol Psychiatry*. (2015) 20(10):1188–96. doi: 10.1038/mp.2014.127

46. Chong SY, Lee CK, Huang C, Ou YH, Charles CJ, Richards AM, et al. Extracellular vesicles in cardiovascular diseases: alternative biomarker sources, therapeutic agents, and drug delivery carriers. *Int J Mol Sci*. (2019) 20(13):3272. doi: 10.3390/ijms20133272

47. Martin-Ventura JL, Roncal C, Orbe J, Blanco-Colio LM. Role of extracellular vesicles as potential diagnostic and/or therapeutic biomarkers in chronic cardiovascular diseases. *Front Cell Dev Biol*. (2022) 10:81. doi: 10.3389/fcell.2022.813885

48. Elsharkasy OM, Nordin JZ, Hagey DW, de Jong OG, Schiffelers RM, Andaloussi SE, et al. Extracellular vesicles as drug delivery systems: why and how? *Adv Drug Deliv Rev*. (2020) 159:332–43. doi: 10.1016/j.addr.2020.04.004

49. Herrmann IK, Wood MJA, Fuhrmann G. Extracellular vesicles as a next-generation drug delivery platform. *Nat Nanotechnol*. (2021) 16(7):748–59. doi: 10.1038/s41565-021-00931-2

50. de Jong OG, Kooijmans SAA, Murphy DE, Jiang L, Evers MJW, Sluijter JPG, et al. Drug delivery with extracellular vesicles: from imagination to innovation. *Acc Chem Res*. (2019) 52(7):1761–70. doi: 10.1021/acs.accounts.9b00109

51. Zhang F, Guo J, Zhang Z, Duan M, Wang G, Qian Y, et al. Application of engineered extracellular vesicles for targeted tumor therapy. *J Biomed Sci*. (2022) 29 (1):14. doi: 10.1186/s12929-022-00798-y

52. Niu W, Xiao Q, Wang X, Zhu J, Li J, Liang X, et al. A biomimetic drug delivery system by integrating grapefruit extracellular vesicles and doxorubicin-loaded heparin-based nanoparticles for glioma therapy. *Nano Lett*. (2021) 21(3):1484–92. doi: 10.1021/acs.nanolett.0c04753

53. Yong T, Zhang X, Bie N, Zhang H, Zhang X, Li F, et al. Tumor exosome-based nanoparticles are efficient drug carriers for chemotherapy. *Nat Commun*. (2019) 10 (1):3838. doi: 10.1038/s41467-019-11718-4

54. Zhang J, Yuan ZF, Wang Y, Chen WH, Luo GF, Cheng SX, et al. Multifunctional envelope-type mesoporous silica nanoparticles for tumor-triggered targeting drug delivery. *J Am Chem Soc*. (2013) 135(13):5068–73. doi: 10.1021/ja312004m

55. Murphy DE, de Jong OG, Brouwer M, Wood MJ, Lavieu G, Schiffelers RM, et al. Extracellular vesicle-based therapeutics: natural versus engineered targeting and trafficking. *Exp Mol Med*. (2019) 51(3):1–12. doi: 10.1038/s12276-019-0223-5

56. Li M, Fang F, Sun M, Zhang Y, Hu M, Zhang J. Extracellular vesicles as bioactive nanotherapeutics: an emerging paradigm for regenerative medicine. *Theranostics*. (2022) 12(11):4879–903. doi: 10.7150/thno.72812

57. De Jong OG, Van Balkom BWM, Schiffelers RM, Bouten CVC, Verhaar MC. Extracellular vesicles: potential roles in regenerative medicine. *Front Immunol*. (2014) 5:608. doi: 10.3389/fimmu.2014.00608

58. Li Jw, Wei L, Han Z, Chen Z. Mesenchymal stromal cells-derived exosomes alleviate ischemia/reperfusion injury in mouse lung by transporting anti-apoptotic miR-21-5p. *Eur J Pharmacol*. (2019) 852:68–76. doi: 10.1016/j.ejphar.2019.01.022

59. Rad LM, Yumashev AV, Hussen BM, Jamad HH, Ghafouri-Fard S, Taheri M, et al. Therapeutic potential of microvesicles in cell therapy and regenerative medicine of ocular diseases with an especial focus on mesenchymal stem cells-derived microvesicles. *Front Genet*. (2022) 13:570. dodoi: i: 10.3389/fgene.2022.847679

60. Dickhout A, Koenen RR. Extracellular vesicles as biomarkers in cardiovascular disease; chances and risks. *Front Cardiovasc Med*. (2018) 5:113. doi: 10.3389/fcvm.2018.00113

61. Takov K, Yellon DM, Davidson SM. Comparison of small extracellular vesicles isolated from plasma by ultracentrifugation or size-exclusion chromatography: yield, purity and functional potential. *J Extracell Vesicles*. (2019) 8(1):1560809. doi: 10.1080/20013078.2018.1560809

62. Mol EA, Goumans MJ, Doevendans PA, Sluijter JPG, Vader P. Higher functionality of extracellular vesicles isolated using size-exclusion chromatography compared to ultracentrifugation. *Nanomedicine Nanotechnol Biol Med*. (2017) 13 (6):2061–5. doi: 10.1016/j.nano.2017.03.011

63. van der Pol E, Coumans FaW, Grootemaat AE, Gardiner C, Sargent IL, Harrison P, et al. Particle size distribution of exosomes and microvesicles determined by transmission electron microscopy, flow cytometry, nanoparticle tracking analysis, and resistive pulse sensing. *J Thromb Haemost JTH*. (2014) 12(7):1182–92. doi: 10.1111/jth.12602

64. Karimi N, Cvjetkovic A, Jang SC, Crescitelli R, Hosseinpour Feizi MA, Nieuwland R, et al. Detailed analysis of the plasma extracellular vesicle proteome after separation from lipoproteins. *Cell Mol Life Sci CMLS*. (2018) 75(15):2873–86. doi: 10.1007/s00018-018-2773-4

65. Bernal-Mizrachi L, Jy W, Jimenez JJ, Pastor J, Mauro LM, Horstman LL, et al. High levels of circulating endothelial microparticles in patients with acute coronary syndromes. *Am Heart J*. (2003) 145(6):962–70. doi: 10.1016/S0002-8703(03)00103-0

66. Chiva-Blanch G, Bratseth V, Ritschel V, Andersen GØ, Halvorsen S, Eritsland J, et al. Monocyte-derived circulating microparticles (CD14+, CD14+/CD11b+ and CD14+/CD142+) are related to long-term prognosis for cardiovascular mortality in STEMI patients. *Int J Cardiol*. (2017) 227:876–81. doi: 10.1016/j.ijcard.2016.11.302

67. Bandu R, Oh JW, Kim KP. Mass spectrometry-based proteome profiling of extracellular vesicles and their roles in cancer biology. *Exp Mol Med*. (2019 51 (3):1–10. doi: 10.1038/s12276-019-0218-2

68. Schey KL, Luther JM, Rose KL. Proteomics characterization of exosome cargo. *Methods San Diego Calif*. (2015) 87:75–82. doi: 10.1016/j.ymeth.2015.03.018

69. Turchinovich A, Drapkina O, Tonevitsky A. Transcriptome of extracellular vesicles: state-of-the-art. *Front Immunol*. (2019) 10:202. doi: 10.3389/fimmu.2019.00202

70. Nozaki T, Sugiyama S, Koga H, Sugamura K, Ohba K, Matsuzawa Y, et al. Significance of a multiple biomarkers strategy including endothelial dysfunction to improve risk stratification for cardiovascular events in patients at high risk for coronary heart disease. *J Am Coll Cardiol*. (2009) 54(7):601–8. doi: 10.1016/j.jacc.2009.05.022

71. Bayés-Genis A, Lanfear DE, de Ronde MWJ, Lupón J, Leenders JJ, Liu Z, et al. Prognostic value of circulating microRNAs on heart failure-related morbidity and mortality in two large diverse cohorts of general heart failure patients. *Eur J Heart Fail*. (2018) 20(1):67–75. doi: 10.1002/ejhf.984

72. van der Velde AR, Gullestad L, Ueland T, Aukrust P, Guo Y, Adourian A, et al. Prognostic value of changes in galectin-3 levels over time in patients with heart failure: data from CORONA and COACH. *Circulation: Heart Failure*. (2013) 6(2):219–26. doi: 10.1161/CIRCHEARTFAILURE.112.000129

73. Zhang X, Wan Y, Chata R, Brazzale A, Atherton JJ, Kostner K, et al. A pilot study to demonstrate diagnostic potential of galectin-3 levels in saliva. *J Clin Pathol*. (2016 69(12):1100–4. doi: 10.1136/jclinpath-2016-203631

74. Wang L, Liu J, Xu B, Liu YL, Liu Z. Reduced exosome miR-425 and miR-744 in the plasma represents the progression of fibrosis and heart failure. *Kaohsiung J Med Sci*. (2018v) 34(11):626–33. doi: 10.1016/j.kjms.2018.05.008

75. Wu T, Chen Y, Du Y, Tao J, Li W, Zhou Z, et al. Circulating exosomal miR-92b-5p is a promising diagnostic biomarker of heart failure with reduced ejection fraction patients hospitalized for acute heart failure. *J Thorac Dis*. (2018) 10(11):6211–20. doi: 10.21037/jtd.2018.10.52

76. Widera C, Gupta SK, Lorenzen JM, Bang C, Bauersachs J, Bethmann K, et al. Diagnostic and prognostic impact of six circulating microRNAs in acute coronary syndrome. *J Mol Cell Cardiol*. (2011) 51(5):872–5. doi: 10.1016/j.yjmcc.2011.07.011

77. de Hoog VC, Timmers L, Schoneveld AH, Wang JW, van de Weg SM, Sze SK, et al. Serum extracellular vesicle protein levels are associated with acute coronary syndrome. *Eur Heart J Acute Cardiovasc Care*. (2013) 2(1):53–60. doi: 10.1177/2048872612471212

78. von zur Muhlen C, Schiffer E, Zuerbig P, Kellmann M, Brasse M, Meert N, et al. Evaluation of urine proteome pattern analysis for its potential to reflect coronary artery atherosclerosis in symptomatic patients. *J Proteome Res*. (2009) 8(1):335–45. doi: 10.1021/pr800615t

79. Jansen F, Yang X, Proebsting S, Hoelscher M, Przybilla D, Baumann K, et al. MicroRNA expression in circulating microvesicles predicts cardiovascular events in patients with coronary artery disease. *J Am Heart Assoc*. (2014) 3(6):e001249. doi: 10.1161/JAHA.114.001249

80. Kanhai DA, Visseren FLJ, van der Graaf Y, Schoneveld AH, Catanzariti LM, Timmers L, et al. Microvesicle protein levels are associated with increased risk for future vascular events and mortality in patients with clinically manifest vascular disease. *Int J Cardiol*. (2013) 168(3):2358–63. doi: 10.1016/j.ijcard.2013.01.231

81. Gidlöf O, Smith JG, Miyazu K, Gilje P, Spencer A, Blomquist S, et al. Circulating cardio-enriched microRNAs are associated with long-term prognosis following myocardial infarction. *BMC Cardiovasc Disord*. (2013) 13:12. doi: 10.1186/1471-2261-13-12

82. Matsumoto S, Sakata Y, Suna S, Nakatani D, Usami M, Hara M, et al. Circulating p53-responsive MicroRNAs are predictive indicators of heart failure after acute myocardial infarction. *Circ Res*. (2013) 113(3):322–6. doi: 10.1161/CIRCRESAHA.113.301209

83. Núñez E, Fuster V, Gómez-Serrano M, Valdivielso JM, Fernández-Alvira JM, Martínez-López D, et al. Unbiased plasma proteomics discovery of biomarkers for improved detection of subclinical atherosclerosis. *EBioMedicine*. (2022) 76 (103874):103874. doi: 10.1016/j.ebiom.2022.103874

84. Amabile N, Rautou PE, Tedgui A, Boulanger CM. Microparticles: key protagonists in cardiovascular disorders. *Semin Thromb Hemost*. (2010) 36 (8):907–16. doi: 10.1055/s-0030-1267044

85. Dickhout A, Koenen RR. Extracellular vesicles as biomarkers in cardiovascular disease; chances and Risks. *Front Cardiovasc Med*. (2018) 5:113. doi: 10.3389/fcvm.2018.00113

86. Xiao Y, Zheng L, Zou X, Wang J, Zhong J, Zhong T. Extracellular vesicles in type 2 diabetes mellitus: key roles in pathogenesis, complications, and therapy. *J Extracell Vesicles*. (2019) 8(1):1625677. doi: 10.1080/20013078.2019.1625677

87. Huang C, Fisher KP, Hammer SS, Navitskaya S, Blanchard GJ, Busik JV. Plasma exosomes contribute to microvascular damage in diabetic retinopathy by activating the classical complement pathway. *Diabetes*. (2018) 67(8):1639–49. doi: 10.2337/db17-1587

88. Guo SC, Tao SC, Yin WJ, Qi X, Yuan T, Zhang CQ. Exosomes derived from platelet-rich plasma promote the re-epithelization of chronic cutaneous wounds via activation of YAP in a diabetic rat model. *Theranostics*. (2017) 7(1):81–96. doi: 10.7150/thno.16803

89. Hwang HS, Kim H, Han G, Lee JW, Kim K, Kwon IC, et al. Extracellular vesicles as potential therapeutics for inflammatory diseases. *Int J Mol Sci*. (2021) 22(11):5487. doi: 10.3390/ijms22115487

90. Pasquali L, Svedbom A, Srivastava A, Rosén E, Lindqvist U, Ståhle M, et al. Circulating microRNAs in extracellular vesicles as potential biomarkers for psoriatic arthritis in patients with psoriasis. *J Eur Acad Dermatol Venereol JEADV*. (2020) 34 (6):1248–56. doi: 10.1111/jdv.16203

91. Wang ZY, Yan BX, Zhou Y, Chen XY, Zhang J, Cai SQ, et al. miRNA profiling of extracellular vesicles reveals biomarkers for psoriasis. *J Invest Dermatol*. (2021) 141 (1):185–9. e4. doi: 10.1016/j.jid.2020.04.021

92. Suades R, Greco MF, Padró T, Badimon L. Extracellular vesicles as drivers of immunoinflammation in atherothrombosis. *Cells*. (2022) 11(11):1845. doi: 10.3390/cells11111845

93. Badimon L, Suades R, Arderiu G, Peña E, Chiva-Blanch G, Padró T. Microvesicles in atherosclerosis and angiogenesis: from bench to bedside and reverse. *Front Cardiovasc Med*. (2017) 4:77. doi: 10.3389/fcvm.2017.00077

94. Suades R, Padró T, Crespo J, Sionis A, Alonso R, Mata P, et al. Liquid biopsy of extracellular microvesicles predicts future Major ischemic events in genetically characterized familial hypercholesterolemia patients. *Arterioscler Thromb Vasc Biol*. (2019) 39(6):1172–81. doi: 10.1161/ATVBAHA.119.312420

95. Chironi G, Simon A, Hugel B, Del Pino M, Gariepy J, Freyssinet JM, et al. Circulating leukocyte-derived microparticles predict subclinical atherosclerosis burden in asymptomatic subjects. *Arterioscler Thromb Vasc Biol*. (2006) 26 (12):2775–80. doi: 10.1161/01.ATV.0000249639.36915.04

96. Blood Task Force. (cited 2023 Mar 24). Available at: https://www.isev.org/blood-task-force

97. Badimon L, Padro T, Arderiu G, Vilahur G, Borrell-Pages M, Suades R. Extracellular vesicles in atherothrombosis: from biomarkers and precision medicine to therapeutic targets. *Immunol Rev*. (2022) 312(1):6–19. doi: 10.1111/imr.13127

98. Yang J, Shin TS, Kim JS, Jee YK, Kim YK. A new horizon of precision medicine: combination of the microbiome and extracellular vesicles. *Exp Mol Med*. (2022) 54 (4):466–82. doi: 10.1038/s12276-022-00748-6

99. Sluijter JPG, Davidson SM, Boulanger CM, Buzás EI, de Kleijn DPV, Engel FB, et al. Extracellular vesicles in diagnostics and therapy of the ischaemic heart: position

paper from the working group on cellular biology of the heart of the European society of cardiology. *Cardiovasc Res*. (2018) 114(1):19–34. doi: 10.1093/cvr/cvx211

100. Bobryshev YV, Killingsworth MC, Orekhov AN. Increased shedding of microvesicles from intimal smooth muscle cells in athero-prone areas of the human aorta: implications for understanding of the predisease stage. *Pathobiology*. (2013) 80(1):24–31. doi: 10.1159/000339430

101. Leroyer AS, Isobe H, Lesèche G, Castier Y, Wassef M, Mallat Z, et al. Cellular origins and thrombogenic activity of microparticles isolated from human atherosclerotic plaques. *J Am Coll Cardiol*. (2007) 49(7):772–7. doi: 10.1016/j.jacc.2006.10.053

102. Perrotta I, Aquila S. Exosomes in human atherosclerosis: an ultrastructural analysis study. *Ultrastruct Pathol*. (2016) 40(2):101–6. doi: 10.3109/01913123.2016.1154912

103. Goetzl EJ, Schwartz JB, Mustapic M, Lobach IV, Daneman R, Abner EL, et al. Altered cargo proteins of human plasma endothelial cell–derived exosomes in atherosclerotic cerebrovascular disease. *FASEB J*. (2017) 31(8):3689–94. doi: 10.1096/fj.201700149

104. Georgescu A, Simionescu M. Extracellular vesicles: versatile nanomediators, potential biomarkers and therapeutic agents in atherosclerosis and COVID-19-related thrombosis. *Int J Mol Sci*. (2021) 22(11):5967. doi: 10.3390/ijms22115967

105. Mayr M, Grainger D, Mayr U, Leroyer AS, Leseche G, Sidibe A, et al. Proteomics, metabolomics, and immunomics on microparticles derived from human atherosclerotic plaques. *Circ Cardiovasc Genet*. (2009) 2(4):379–88. doi: 10.1161/CIRCGENETICS.108.842849

106. Brodsky SV, Zhang F, Nasjletti A, Goligorsky MS. Endothelium-derived microparticles impair endothelial function in vitro. *Am J Physiol Heart Circ Physiol*. (2004) 286(5):H1910–1915. doi: 10.1152/ajpheart.01172.2003

107. Densmore JC, Signorino PR, Ou J, Hatoum OA, Rowe JJ, Shi Y, et al. Endothelium-derived microparticles induce endothelial dysfunction and acute lung injury. *Shock*. (2006) 26(5):464. doi: 10.1097/01.shk.0000228791.10550.36

108. Jansen F, Yang X, Franklin BS, Hoelscher M, Schmitz T, Bedorf J, et al. High glucose condition increases NADPH oxidase activity in endothelial microparticles that promote vascular inflammation. *Cardiovasc Res*. (2013) 98(1):94–106. doi: 10.1093/cvr/cvt013

109. He S, Wu C, Xiao J, Li D, Sun Z, Li M. Endothelial extracellular vesicles modulate the macrophage phenotype: potential implications in atherosclerosis. *Scand J Immunol*. (2018) 87(4):e12648. doi: 10.1111/sji.12648

110. Chang YJ, Li YS, Wu CC, Wang KC, Huang TC, Chen Z, et al. Extracellular MicroRNA-92a mediates endothelial cell-macrophage communication. *Arterioscler Thromb Vasc Biol*. (2019) 39(12):2492–504. doi: 10.1161/ATVBAHA.119.312707

111. Zheng B, Yin Wn, Suzuki T, Zhang Xh, Zhang Y, Song Ll, et al. Exosome-Mediated miR-155 transfer from smooth muscle cells to endothelial cells induces endothelial injury and promotes atherosclerosis. *Mol Ther*. (2017) 25(6):1279–94. doi: 10.1016/j.ymthe.2017.03.031

112. Hergenreider E, Heydt S, Tréguer K, Boettger T, Horrevoets AJG, Zeiher AM, et al. Atheroprotective communication between endothelial cells and smooth muscle cells through miRNAs. *Nat Cell Biol*. (2012) 14(3):249–56. doi: 10.1038/ncb2441

113. Zhao Y, Li Y, Luo P, Gao Y, Yang J, Lao KH, et al. XBP1 Splicing triggers miR-150 transfer from smooth muscle cells to endothelial cells via extracellular vesicles. *Sci Rep*. (2016) 6(1):28627. doi: 10.1038/srep28627

114. Tang N, Sun B, Gupta A, Rempel H, Pulliam L. Monocyte exosomes induce adhesion molecules and cytokines via activation of NF-κB in endothelial cells. *FASEB J Off Publ Fed Am Soc Exp Biol*. (2016) 30(9):3097–106. doi: 10.1096/fj.201600368RR

115. Aharon A, Tamari T, Brenner B. Monocyte-derived microparticles and exosomes induce procoagulant and apoptotic effects on endothelial cells. *Thromb Haemost*. (2008) 100(5):878–85. doi: 10.1160/TH07-11-0691

116. Wang JG, Williams JC, Davis BK, Jacobson K, Doerschuk CM, Ting JPY, et al. Monocytic microparticles activate endothelial cells in an IL-1β-dependent manner. *Blood*. (2011) 118(8):2366–74. doi: 10.1182/blood-2011-01-330878

117. Niu C, Wang X, Zhao M, Cai T, Liu P, Li J, et al. Macrophage foam cell–derived extracellular vesicles promote vascular smooth muscle cell migration and adhesion. *J Am Heart Assoc Cardiovasc Cerebrovasc Dis*. (2016) 5(10):e004099. doi: 10.1161/JAHA.116.004099

118. Distler JHW, Huber LC, Hueber AJ, Reich CF, Gay S, Distler O, et al. The release of microparticles by apoptotic cells and their effects on macrophages. *Apoptosis Int J Program Cell Death*. (2005) 10(4):731–41. doi: 10.1007/s10495-005-2941-5

119. Böing AN, Hau CM, Sturk A, Nieuwland R. Platelet microparticles contain active caspase 3. *Platelets*. (2008) 19(2):96–103. doi: 10.1080/09537100701777295

120. Abid Hussein MN, Nieuwland R, Hau CM, Evers LM, Meesters EW, Sturk A. Cell-derived microparticles contain caspase 3 in vitro and in vivo. *J Thromb Haemost JTH*. (2005) 3(5):888–96. doi: 10.1111/j.1538-7836.2005.01240.x

121. Pizzirani C, Ferrari D, Chiozzi P, Adinolfi E, Sandonà D, Savaglio E, et al. Stimulation of P2 receptors causes release of IL-1beta-loaded microvesicles from human dendritic cells. *Blood*. (2007) 109(9):3856–64. doi: 10.1182/blood-2005-06-031377

122. Sarkar A, Mitra S, Mehta S, Raices R, Wewers MD. Monocyte derived microvesicles deliver a cell death message via encapsulated caspase-1. *PLOS ONE*. (2009) 4(9):e7140. doi: 10.1371/journal.pone.0007140

123. Chatterjee V, Yang X, Ma Y, Cha B, Meegan JE, Wu M, et al. Endothelial microvesicles carrying src-rich cargo impair adherens junction integrity and cytoskeleton homeostasis. *Cardiovasc Res*. (2020) 116(8):1525–38. doi: 10.1093/cvr/cvz238

124. Mesri M, Altieri DC. Leukocyte microparticles stimulate endothelial cell cytokine release and tissue factor induction in a JNK1 signaling pathway. *J Biol Chem*. (1999) 274(33):23111–8. doi: 10.1074/jbc.274.33.23111

125. Robbins PD, Dorronsoro A, Booker CN. Regulation of chronic inflammatory and immune processes by extracellular vesicles. *J Clin Invest*. (2016) 126(4):1173–80. doi: 10.1172/JCI81131

126. Luquero A, Vilahur G, Crespo J, Badimon L, Borrell-Pages M. Microvesicles carrying LRP5 induce macrophage polarization to an anti-inflammatory phenotype. *J Cell Mol Med*. (2021) 25(16):7935–47. doi: 10.1111/jcmm.16723

127. Mause SF, von Hundelshausen P, Zernecke A, Koenen RR, Weber C. Platelet microparticles: a transcellular delivery system for RANTES promoting monocyte recruitment on endothelium. *Arterioscler Thromb Vasc Biol*. (2005) 25(7):1512–8. doi: 10.1161/01.ATV.0000170133.43608.37

128. Rautou PE, Leroyer AS, Ramkhelawon B, Devue C, Duflaut D, Vion AC, et al. Microparticles from human atherosclerotic plaques promote endothelial ICAM1-dependent monocyte adhesion and transendothelial migration. *Circ Res*. (2011) 108(3):335–43. doi: 10.1161/CIRCRESAHA.110.237420

129. Llorente-Cortés V, Otero-Viñas M, Camino-López S, Llampayas O, Badimon L. Aggregated low-density lipoprotein uptake induces membrane tissue factor procoagulant activity and microparticle release in human vascular smooth muscle cells. *Circulation*. (2004) 110(4):452–9. doi: 10.1161/01.CIR.0000136032.40666.3D

130. Vajen T, Benedikter BJ, Heinzmann ACA, Vasina EM, Henskens Y, Parsons M, et al. Platelet extracellular vesicles induce a pro-inflammatory smooth muscle cell phenotype. *J Extracell Vesicles*. (2017) 6(1):1322454. doi: 10.1080/20013078.2017.1322454

131. Furmanik M, Chatrou M, van Gorp R, Akbulut A, Willems B, Schmidt H, et al. Reactive oxygen-forming Nox5 links vascular smooth muscle cell phenotypic switching and extracellular vesicle-mediated vascular calcification. *Circ Res*. (2020) 127(7):911–27. doi: 10.1161/CIRCRESAHA.119.316159

132. Lozito TP, Tuan RS. Endothelial cell microparticles act as centers of matrix metalloproteinsase-2 (MMP-2) activation and vascular matrix remodeling. *J Cell Physiol*. (2012) 227(2):534–49. doi: 10.1002/jcp.22744

133. Vascotto SG, Beckham Y, Kelly GM. The zebrafish's swim to fame as an experimental model in biology. *Biochem Cell Biol*. (1997) 75(5):479–85. doi: 10.1139/o97-081

134. Grunwald DJ, Eisen JS. Headwaters of the zebrafish — emergence of a new model vertebrate. *Nat Rev Genet*. (2002) 3(9):717–24. doi: 10.1038/nrg892

135. Scott A, Sueiro Ballesteros L, Bradshaw M (辻千里), Tsuji C, Power A, Lorriman J, et al. In vivo characterization of endogenous cardiovascular extracellular vesicles in larval and adult zebrafish. *Arterioscler Thromb Vasc Biol*. (2021) 41(9):2454–68. doi: 10.1161/ATVBAHA.121.316539

136. Verweij FJ, Revenu C, Arras G, Dingli F, Loew D, Pegtel DM, et al. Live tracking of inter-organ communication by endogenous exosomes in vivo. *Dev Cell*. (2019) 48(4):573–89. e4. doi: 10.1016/j.devcel.2019.01.004

137. McCann JV, Liu A, Musante L, Erdbrügger U, Lannigan J, Dudley AC. A miRNA signature in endothelial cell-derived extracellular vesicles in tumor-bearing mice. *Sci Rep*. (2019) 9(1):16743. doi: 10.1038/s41598-019-52466-1

138. Barlin M, Erdmann-Gilmore P, Mudd JL, Zhang Q, Seymour RW, Guo Z, et al. Proteins in tumor-derived plasma extracellular vesicles indicate tumor origin. *Mol Cell Proteomics*. (2023) 22(1):100476. Available at: https://www.mcponline.org/article/S1535-9476(22)00284-5/abstract doi: 10.1016/j.mcpro.2022.100476

139. Delgado-Peraza F, Nogueras-Ortiz CJ, Volpert O, Liu D, Goetzl EJ, Mattson MP, et al. Neuronal and astrocytic extracellular vesicle biomarkers in blood reflect brain pathology in mouse models of Alzheimer's disease. *Cells*. (2021) 10(5):993. doi: 10.3390/cells10050993

140. Willis CM, Nicaise AM, Menoret A, Ryu JK, Mendiola AS, Jellison ER, et al. Extracellular vesicle fibrinogen induces encephalitogenic CD8+ T cells in a mouse model of multiple sclerosis. *Proc Natl Acad Sci*. (2019) 116(21):10488–93. doi: 10.1073/pnas.1816911116

141. Casella G, Colombo F, Finardi A, Descamps H, Ill-Raga G, Spinelli A, et al. Extracellular vesicles containing IL-4 modulate neuroinflammation in a mouse model of multiple sclerosis. *Mol Ther*. (2018) 26(9):2107–18. doi: 10.1016/j.ymthe.2018.06.024

142. Yang S, Liu P, Gao T, Song D, Zhao X, Li Y, et al. Every road leads to Rome: therapeutic effect and mechanism of the extracellular vesicles of human embryonic stem cell-derived immune and matrix regulatory cells administered to mouse

models of pulmonary fibrosis through different routes. *Stem Cell Res Ther*. (2022) 13 (1):163. doi: 10.1186/s13287-022-02839-7

143. Mohammed I, Ijaz S, Mokhtari T, Gholaminejhad M, Mahdavipour M, Jameie B, et al. Subventricular zone-derived extracellular vesicles promote functional recovery in rat model of spinal cord injury by inhibition of NLRP3 inflammasome complex formation. *Metab Brain Dis*. (2020) 35(5):809–18. doi: 10.1007/s11011-020-00563-w

144. Romanelli P, Bieler L, Heimel P, Škokić S, Jakubecova D, Kreutzer C, et al. Enhancing functional recovery through intralesional application of extracellular vesicles in a rat model of traumatic spinal cord injury. *Front Cell Neurosci*. (2022) 15:795008. doi: 10.3389/fncel.2021.795008

145. Gómez-Molina C, Sandoval M, Henzi R, Ramírez JP, Varas-Godoy M, Luarte A, et al. Small extracellular vesicles in rat Serum contain astrocyte-derived protein biomarkers of repetitive stress. *Int J Neuropsychopharmacol*. (2019) 22(3):232–46. doi: 10.1093/ijnp/pyy098

146. Guy R, Herman S, Benyamini H, Ben-Zur T, Kobo H, Pasmanik-Chor M, et al. Mesenchymal stem cell-derived extracellular vesicles as proposed therapy in a rat model of cerebral small vessel disease. *Int J Mol Sci*. (2022) 23(19):11211. doi: 10.3390/ijms231911211

147. Berger A, Araújo-Filho I, Piffoux M, Nicolás-Boluda A, Grangier A, Boucenna I, et al. Local administration of stem cell-derived extracellular vesicles in a thermoresponsive hydrogel promotes a pro-healing effect in a rat model of colo-cutaneous post-surgical fistula. *Nanoscale*. (2021) 13(1):218–32. doi: 10.1039/D0NR07349K

148. Khalaj K, Figueira RL, Antounians L, Gandhi S, Wales M, Montalva L, et al. Treatment with amniotic fluid stem cell extracellular vesicles promotes fetal lung branching and cell differentiation at canalicular and saccular stages in experimental pulmonary hypoplasia secondary to congenital diaphragmatic hernia. *Stem Cells Transl Med*. (2022) 11(10):1089–102. doi: 10.1093/stcltm/szac063

149. Ural EE, Toomajian V, Hoque Apu E, Veletic M, Balasingham I, Ashammakhi N, et al. Visualizing extracellular vesicles and their function in 3D tumor microenvironment models. *Int J Mol Sci*. (2021) 22(9):4784. doi: 10.3390/ijms22094784

150. Perez GI, Broadbent D, Zarea AA, Dolgikh B, Bernard MP, Withrow A, et al. In vitro and in vivo analysis of extracellular vesicle-mediated metastasis using a bright, red-shifted bioluminescent reporter protein. *Adv Genet*. (2022) 3(1):2100055. doi: 10.1002/ggn2.202100055

151. Ye Y, Shi Q, Yang T, Xie F, Zhang X, Xu B, et al. In vivo visualized tracking of tumor-derived extracellular vesicles using CRISPR-Cas9 system. *Technol Cancer Res Treat*. (2022) 21:15330338221085370. doi: 10.1177/15330338221085370

152. Nørgård MØ, Steffensen LB, Hansen DR, Füchtbauer EM, Engelund MB, Dimke H, et al. A new transgene mouse model using an extravesicular EGFP tag enables affinity isolation of cell-specific extracellular vesicles. *Sci Rep*. (2022) 12 (1):496. doi: 10.1038/s41598-021-04512-0

153. McCann JV, Bischoff SR, Zhang Y, Cowley DO, Sanchez-Gonzalez V, Daaboul GD, et al. Reporter mice for isolating and auditing cell type-specific extracellular vesicles in vivo. *Genes N Y N*. (2020) 58(7):e23369. doi: 10.1038/s41598-021-04512-0

154. Li W, Wang J, Yin X, Shi H, Sun B, Ji M, et al. Construction of a mouse model that can be used for tissue-specific EV screening and tracing in vivo. *Front Cell Dev Biol*. (2022) 10:2279. doi: 10.3389/fcell.2022.1015841

155. Yoshimura A, Kawamata M, Yoshioka Y, Katsuda T, Kikuchi H, Nagai Y, et al. Generation of a novel transgenic rat model for tracing extracellular vesicles in body fluids. *Sci Rep*. (2016) 6(1):31172. doi: 10.1038/srep31172

156. Angelillo-Scherrer A, Weber C, Mause S. Leukocyte-Derived microparticles in vascular homeostasis. *Circ Res*. (2012) 110(2):356–69. doi: 10.1161/CIRCRESAHA.110.233403

157. Sarlon-Bartoli G, Bennis Y, Lacroix R, Piercecchi-Marti MD, Bartoli MA, Arnaud L, et al. Plasmatic level of leukocyte-derived microparticles is associated with unstable plaque in asymptomatic patients with high-grade carotid stenosis. *J Am Coll Cardiol*. (2013) 62(16):1436–41. doi: 10.1016/j.jacc.2013.03.078

158. Chen W, Schilperoort M, Cao Y, Shi J, Tabas I, Tao W. Macrophage-targeted nanomedicine for the diagnosis and treatment of atherosclerosis. *Nat Rev Cardiol*. (2022) 19(4):228–49. doi: 10.1038/s41569-021-00629-x

159. Ma Q, Fan Q, Han X, Dong Z, Xu J, Bai J, et al. Platelet-derived extracellular vesicles to target plaque inflammation for effective anti-atherosclerotic therapy. *J Control Release Off J Control Release Soc*. (2021) 329:445–53. doi: 10.1016/j.jconrel.2020.11.064

Frontiers in
Cardiovascular Medicine

Innovations and improvements in cardiovascular treatment and practice

Focuses on research that challenges the status quo of cardiovascular care, or facilitates the translation of advances into new therapies and diagnostic tools.

Discover the latest Research Topics

See more →

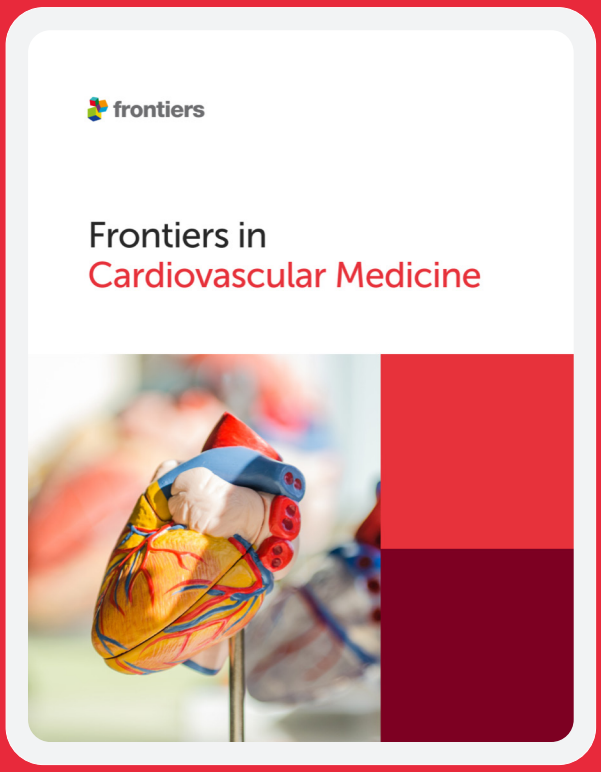

Frontiers

Avenue du Tribunal-Fédéral 34
1005 Lausanne, Switzerland
frontiersin.org

Contact us

+41 (0)21 510 17 00
frontiersin.org/about/contact